Pigments of My Imagination: Controlling Color and Redox Properties of Conjugated Organic Electrochromic Materials

A Dissertation
Presented to
The Academic Faculty

by

Dylan Thomas Christiansen

In Partial Fulfillment
of the Requirements for the Degree
Doctor of Philosophy in the
School of Chemistry and Biochemistry

Georgia Institute of Technology
August 2019

Pigments of My Imagination: Controlling Color and Redox Properties of Conjugated Organic Electrochromic Materials

Approved by:

Dr. John R. Reynolds, Advisor
School of Chemistry & Biochemistry
School of Materials Science & Engineering
Georgia Institute of Technology

Dr. Seung Soon Jang
School of Materials Science & Engineering
Georgia Institute of Technology

Dr. Seth Marder
School of Chemistry & Biochemistry
Georgia Institute of Technology

Dr. Paul Russo
School of Materials Science & Engineering
Georgia Institute of Technology

Dr. Stefan France
School of Chemistry & Biochemistry
Georgia Institute of Technology

Date Approved: [April 9, 2019]

“Things are only impossible until they’re not”

-Captain Jean-luc Picard

“Words are *important*. And when there is a critical mass of them, they change the nature of the universe.”

-Terry Pratchett, Going Postal

To my family, friends, and Martha

Acknowledgements

When I came to Georgia Tech as a new graduate student, I thought I had “it” figured out. I was proficient in the synthesis lab (mildly, in retrospect) and I thought I would just “crank out” molecules and polymers to get my Ph.D. done. I learned the hard way that there is more to it, as the pressures from funding sources, experimental failures, and deep scientific questions have driven me to explore and learn about new areas of chemistry and materials science. These difficulties acted as learning experiences for me. My time here was one of personal, professional, and scientific growth that I would not change. I have great fortune to have so many people to thank for my Ph.D. journey. Each person I have met has contributed a thread to my life and removing one would cause the tapestry to unravel.

I thank the professors at the University of West Florida for teaching, mentoring, and fostering my education and pursuit for higher education. They gave me opportunities in research, teaching, and leadership roles that have developed my love for chemistry. When I was the President of UWF’s Student Affiliates of the ACS we had the opportunity to host Dr. John Reynolds as an invited speaker. I did not know much about pi-conjugated materials, but I remember loving his seminar on electrochromism and color. I knew at that point that I would be applying to Georgia Tech.

When I joined the Reynolds group, I knew that JRR was a well-respected and diligent scientist. What I learned, and came to have a deep appreciation for, was that he is an outstanding mentor, an excellent manager, and virtuous human being. I want to thank him for his patience, guidance, and support in my journey. Together we have worked on five journal publications (and counting), two patents (and counting), and many grant proposals. From working together, I learned how to balance my passions for science and life. Additionally, I thank my committee members,

Dr. Seth Marder, Dr. Stefan France, Dr. Paul Russo, and Dr. Seung Soon Jang for their guidance and asking deep scientific questions that shaped my perception of my science along the way.

The culture of support in this research group extends beyond Dr. Reynolds, and I feel fortunate to have the support of many other graduate students, post docs, and research scientist. From discussing recent scientific literature to playing league kickball together our group does it best, and I have loved my time here. I want to give special thanks to Dr. James Ponder, who mentored me in the synthesis lab while I was a new graduate student. I also want to give special thanks to Dr. Anna Österholm and Dr. Eric Shen who have been instrumental in helping me work my way through challenges I have faced in projects through the years, including everything from how to set up a DPV experiment to deep discussions about the absorptions of odd electron systems. I would also like to thank Dr. Aimée Tomlinson for her support and contribution throughout my Ph.D. projects. While everyone in the group has contributed to my journey, I want to give special thanks to all of the fellow graduate students that have become good friends over the years: Brian Schmatz, Ian Pelse, Sandy Pittelli, Gus Lang, and Brandon Ditullio. We have shared good times that I will cherish fondly. All the aces played, lunches and drinks shared, and discussions about anything but science have made this experience richer.

On a more personal note, I want to thank my family. I thank my father for giving me the toughness necessary to endure and for my sense of humor. I was fortunate to have my mom in the Atlanta area when I chose to come to Georgia Tech. I thank her for giving me my passion for caring about others and for my passion for cooking. I am the youngest of three and have always looked up to my siblings, Jessica and Ian, for advice. We were each other's support system through the loss of our father, and I am forever grateful to them for their love and encouragement. I am

excited to be an uncle, as both my brother and sister are expecting. While I finish this dissertation and begin a new chapter in my life, there will be new lives to cherish and encourage.

I also want to thank my friends that have remained close to me through my life. Thomas Viele, who I introduce as my brother to everyone, has been my friend since kindergarten and I am grateful for these many years of friendship. His family took me in while my father and I were homeless, and I am indebted to them for their kindness. I want to thank Brandon Adams, who has been a fiercely loyal friend that always manages to keep in touch no matter how busy he is. I wish them both good luck in their futures.

Most importantly, I want to thank my life partner, Martha. We met in high school when I was sixteen and at the time, I had no idea how fortunate I was. She has been my rock, and her support has helped make me want to be a better person through it all. I feel as though I would not have made it through graduate school without her. Her warmth and care have made the good times incredible and made the hard time endurable.

Finally, I want to thank you, the reader, for taking the time to read my thesis.

-Dylan T. Christiansen 4/2019

Table of Contents

List of Tables

List of Figures

List of Schemes

List of Abbreviations and Symbols

a*	Green-red balance
AcDOT	Acyclic DOT; 3,4-(2-ethylhexyloxy)thiophene
b*	Blue-yellow balance
CB	Conduction band
CE	Counter electrode
CIE	International Commission on Illumination (Commission Internationale de l'Eclairage)
CV	Cyclic voltammetry
Đ	Dispersity
D50	Standard illuminant, white light at 5000 kelvin
DAT	3,4-dialkylthiophene
DCM	Dichloromethane
DHAP	Direct (hetero)arylation polymerization
DMAc	*N*,*N*-dimethylacetamide
DOT	3,4-dioxythiophene
DPV	Differential pulse voltammetry
$E_{g,\,opt}$	Optical band gap energy
E_{ox}	Oxidation potential
EA	Electron affinity
EC	Electrochromic
ECD	Electrochromic Device
ECP	Electrochromic Polymer
EDOT	3,4-ethylenedioxythiophene
EtOAc	Ethyl acetate

f	Oscillator strength
GPC	Gel permeation chromatography
HOMO	Highest occupied molecular orbital
IE	Ionization energy
ITO	Indium tin oxide
IR	Infrared
L*	Lightness
λ_{max}	Wavelength of maximum absorption
LUMO	Lowest unoccupied molecular orbital
M_n	Number average molecular weight
MCCP	Minimally color changing polymer
NBS	*N*-bromosuccinimide
NIR	Near infrared
NMR	Nuclear magnetic resonance
OTTLE	Optically transparent thin layer electrode
PC	Propylene carbonate
PEDOT	Poly(3,4-ethylenedioxythiophene)
PivOH	Pivalic acid
ProDOT	3,4-propylenedioxythiophene
RC	Random copolymer
RE	Reference electrode
SpecEchem	Spectroelectrochemistry
$TBAPF_6$	Tetrabutylammonium hexafluorophosphate
VB	Valence band
WE	Working Electrode

Summary

Electrochromism is the change in the color of a material as a result of an applied potential. This color change can be defined as switching when the charge states (oxidized and reduced) are alternately cycled. When color is generated upon reduction, the material is cathodically coloring, while color generation upon oxidation, is termed anodic coloration. In this dissertation, the properties of 3,4-dioxythiophene (DOT)- based π-conjugated electrochromic polymers (ECPs) and molecules are explored with a focus on controlling structure-property relationships to achieve desired light absorption across the visible region of the spectrum. This dissertation will have a focus on the target of attaining neutral colored and transmissive states and will examine both cathodic and anodic approaches to attaining this goal. Because of the electron rich nature of the DOT moieties, the cathodic polymers can switch to highly transmissive oxidized states, while UV absorbing anodic systems can still be effectively oxidized, giving these DOT materials the potential to be utilized in full color window or non-emissive display applications in either approach. This dissertation will have an emphasis on comparing and contrasting these two approaches.

Chapter 1 will serve as a general introduction to the development of color perception and electrochromic molecule and polymers, and it will describe the toolbox available to design and synthesize these materials. The chapter will chapter will discuss the history of cathodically coloring polymers and will then focus on the impact of anodically coloring electrochromics and their potential advantages over cathodically coloring polymers. There will also be a focus on how color neutral materials are created through both materials blending and random copolymerization. The chapter will culminate with the driving question of this dissertation, “How can electrochromic materials be designed to be color controlled, redox stable, and high-contrast?”

Chapter 2 will describe the molecular and polymer syntheses that have enabled the work discussed within this dissertation. Materials characterizations involving chemical structure, electrochemical, optical, and electronic properties will be reported with specific focus on techniques that are unique to the work in this dissertation. Electrochemical cell and device design, fabrication, and testing methods will be outlined. Specific detail will be given to the methodology surrounding the synthesis and processing of electrochromic polymers.

Chapter 3 describes a family of conjugated polymers that were designed and synthesized to yield wide-gap colored to transmissive switching ECPs with high redox stability based on a dialkylthiophene (DAT) monomer. Through subtle steric interactions between the arylene units, neutral polymer colors were tunable from yellow to deep reds while maintaining transmissive oxidized states. These DAT based polymers show increased redox switching stability compared to previous generations of wide-gap ECPs, with one polymer showing minimal contrast loss over 10,000 cycles. These polymers are also applied in subtractive color mixing with other ECPs in order to create black blends that are redox stable.

Chapter 4 will cover the breadth of color space accessible without the use of acceptors. In this study, eight random terpolymers were designed and synthesized where the ratios of the monomers are used to tune absorption. This project examines the advantages of using only three donor monomers to create broadly tunable materials and access a large portion of the color space with low oxidation potentials. Theoretical calculations helped guide the monomer choices and determine the range of absorption attainable in these systems. The limits of the all donor approach is examined using the materials as a platform for designing the next generation of electrochromic polymers.

Chapter 5 will delve deeper into the background of cathodically coloring polymers with an emphasis on their limits of contrast and discuss the theoretical contrast possibilities that are brought with the anodically coloring approach. This study focuses on examining the design principles of creating multi-heterocycle chromophores with a discrete conjugation length, which absorb ultraviolet light in the neutral state, and upon oxidation absorb throughout a broad spectral range in the visible. Three discrete-length chromophore polymers with alkylene linkers were examined via time dependent DFT, synthesized via direct heteroarylation polymerization, and the electrochromic properties of their thin films characterized. Using a tight feedback loop of theoretical calculations with design and synthesis, it is elucidated how steric interactions can be used to control the absorption of the neutral and oxidized states of these discrete chromophore polymers. It is shown that systems with high inter-ring strain can be used to increase the molar absorptivity of the charged state by forming multiple radical cation states on a single discrete chromophore. The challenges of electrochemical redox reversibility in the solid state in these systems, while they maintain their chemical redox reversibility is also demostrated.

Chapter 6 will present a new design paradigm that is established for anodically coloring molecules where the electronic energy levels of the radical cation state are controllably tuned independent of the neutral state. It is shown how the molecular structures of the chromophores can be altered to control the oscillator strengths of radical cation optical transitions, thus providing control over the color. This control ultimately allows for tuning the λ_{max} of the molecules' absorptions by over 400 nm. The neutral, colorless states of these molecules are UV absorbing, providing solutions that are colorless with L*a*b* values of 100,0,0. These molecules are oxidized to vibrantly colored radical cations that span the visible spectrum creating a variety of colors.

These molecules are also shown to mix to create transmissive, colorless blends that switch to opaque black solutions.

Finally, chapter 7 will discuss future steps for each of the sections covered in this dissertation. The first section will be on alternative monomers that can used to bring wide-gap cathodically coloring polymers. This will lead into what can be done to increase the broadness possible in all donor black electrochromics. This chapter will then change focus to the perspective on anodically coloring organic electrochromics beginning with the challenges of discrete chromophore polymers and lead into alternative methods for making films for increased processability. This section will ultimately cover what questions are left in terms of color and redox control in these systems and propose future directions in the endeavor to answer these questions.

Chapter 1 - Introduction

Electrochromism is the change in the light absorption/transmission of a material upon the application of an oxidizing or reducing potential. In order to design organic electrochromic molecules and polymers it is necessary to understand fundamental optics, how your eye perceives color, how conjugated organics manifest color, and the potential applications for electrochromism.

1.1 Fundamental Optics

In this dissertation, the passage of light through solutions and/or films of the materials is examined. Aside from a material's ability to absorb or transmit light, the nature of the film or solution can affect the measured spectra. In this section, some fundamental optics behind absorption, transmission, reflection, and scattering will be discussed. These are vital to how light behaves with respect to electrochromic materials in solutions and thin films.

1.1.1 Absorption, Transmission, Reflection, and Scattering

Transmission and absorption are interrelated, as they are opposite to one another (Figure 1.1.1.1). When all the light hitting the surface of the object is absorbed then the transmittance is 0% and the absorption is 100%, on the other hand, if all the light hitting the surface passes through the object then transmittance is 100% and absorption will be 0%. Transmittance values are mostly given as a percentage in accordance with total light passing through the object surface with respect to the total intensity of light falling on object. When the absorbance of the object is to be measured using a spectrophotometer, absorbance can be defined as Log_{10} (P_0/P), where I_0 is the intensity of the incident light ray, and P is the intensity of transmitted light. This dissertation will deal with how conjugated organic electrochromic materials absorb and transmit light.

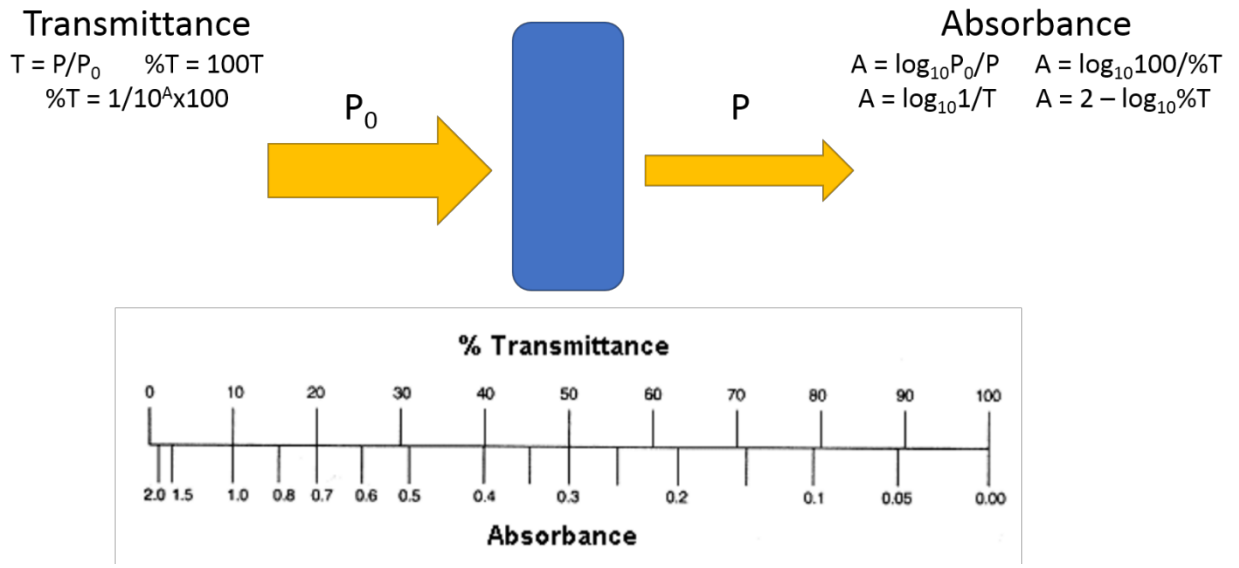

Figure 1.1.1.1: Illustration of the absorption of light in a sample and conversions between absorption and transmission. Concepts adapted from Tipler and Mosca's Physics for Scientists and Engineers.[1]

When light passes through a medium, it is transmitted, and the material is transparent. If a medium has no color, all the light has been transmitted except for the percentage of light that is reflected between the material of one medium and another. The refractive index of a material is a dimensionless quantity that describes how fast light propagates through a material relative to vacuum.[2] Figure 1.1.1.2 illustrates the concepts of light interactions at the interface of two media with differing refractive indices. The refractive index determines how much light is bent, or refracted, when entering a material. Refraction can only be avoided if the two media have the same refractive index or if the incident light is normal to the surface of the interface. The refractive indices also determine the amount of light that is reflected when reaching the interface of two media. The two types of reflection are specular reflection and diffuse reflection. In specular reflection all light is reflected at the same angle as the incident light and requires highly uniform

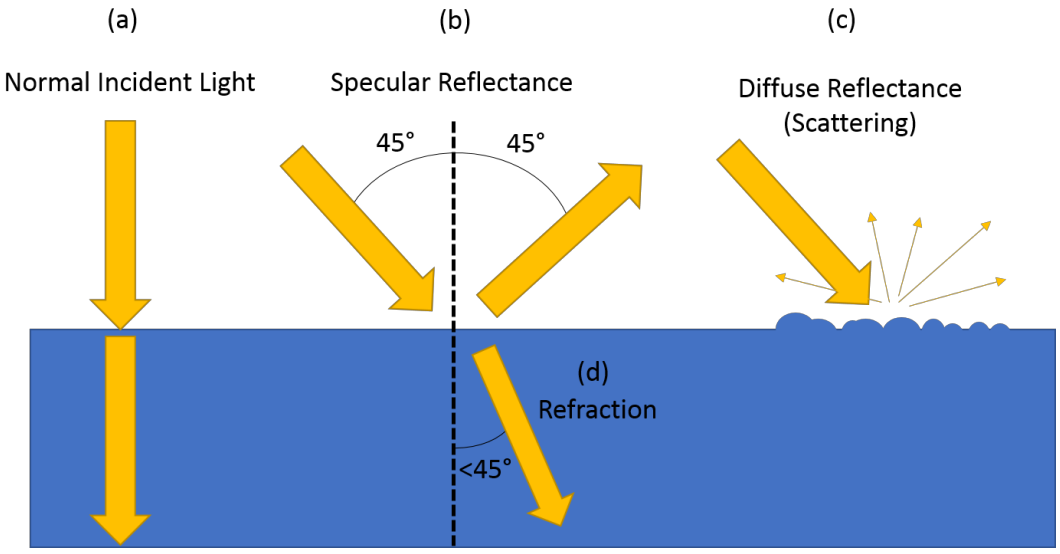

Figure 1.1.1.2. Interactions of light at the interface of two media with different refractive indices without absorption (a) normal light transmitting (b) specular reflectance (c) diffuse reflectance (d) refraction.[1]

and smooth surfaces. In contrast, diffuse reflectance occurs on rough surfaces where rays of light scatter in all directions and is often referred to as scattering.[3]

All these concepts are integral to examining how electrochromic materials behave in both solution and thin film. Between air, the cuvette, electrolyte, electrodes, and polymer films there are many interfaces where these interactions of light can occur. Scattering is a particularly difficult challenge to avoid as it can severely alter the measured data. In both solution and thin films, aggregates act to scatter light which can make the samples appear hazy which can be misinterpreted as absorption.

1.2 Colorimetry and Color Perception

When considering electrochromism and color change, it is important to understand where the eye can detect light (390-720 nm).[4] Here will be discussed how the eye perceives color and

how this color is quantified for the purposes of this dissertation. The science of this color quantification is colorimetry and was developed extensively by The International Commission on Illumination (CIE)[5] and explained at length by Billmeyer and Saltzman's Principles of Color Technology.[4]

1.2.1 Color Vision of the Human Eye

Perception of color begins with specialized retinal cells containing pigments with different spectral sensitivities, known as cone cells. In humans, there are three types of cones sensitive to three different regions in the visible, resulting in trichromatic color vision.[6,7] These cones are labeled according to the wavelength of the light to which they are sensitive: short/blue (B), medium/green (G), and long/red (R). Figure 1.2.1.1 details the normalized response spectra of human cones. The cones do not correspond well to colors as people know them, but the combined response from these cells are evaluated in the visual cortex of the brain to produce the colors people perceive. If the total light power spectrum is weighted by the individual spectral sensitivities of the three types of cone cells, one will get three effective stimulus values, and thus have formed the basis of the three values of tristimulus specification for the objective color of light.

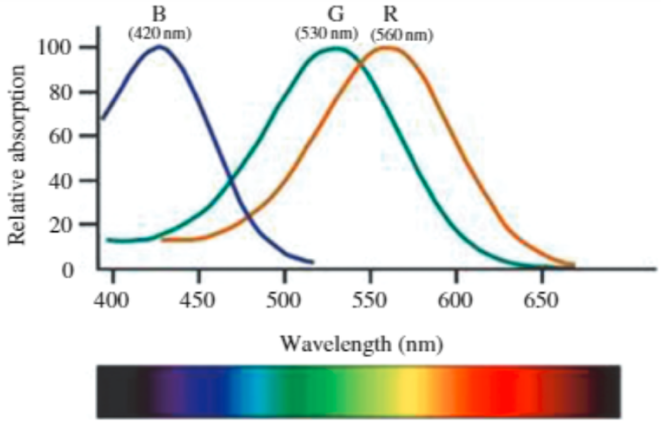

Figure 1.2.1.1: The normalized spectral sensitivities of human cone cells. Used with permission from Deeb et al.[8]

1.2.2 Quantification of Color (CIELAB color space)

The CIE 1976 L*a*b* color space was defined for color communication and is used in this dissertation for quantifying color (refer to Figure 1.2.2.1).[9,10] In this color space, the L* represents the brightness of a color with 0 being black and 100 being white, a* represents greens and reds while b* represents blues and yellows for negative and positive values respectively. The center represents colorless (achromatic) samples and as values of a* or b* progress farther from the origin, the greater the saturation (chroma). As values of a* or b* travel around the circumference of the sphere, hue changes in a uniform manner. The L*a*b* color space allows for 3-dimensional uniformity in color points.

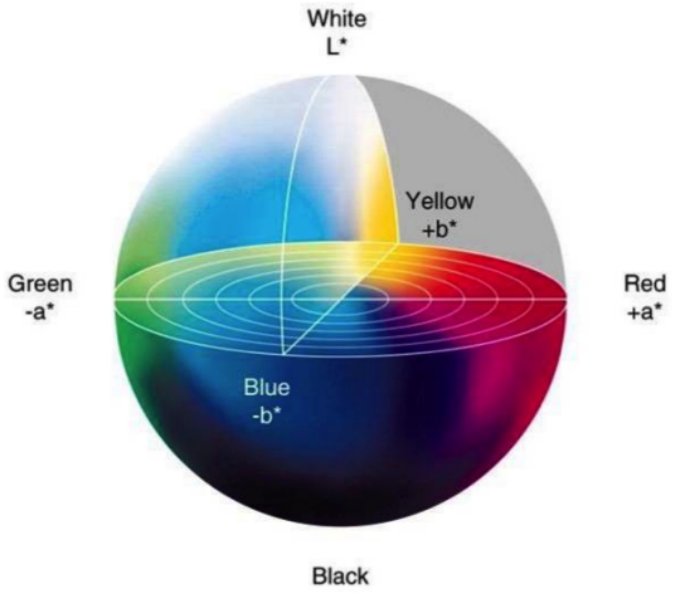

Figure 1.2.2.1. Artist rendition of the L*a*b* color space. Figure used with permission from Chiang et al.[11]

1.3 Controlling Properties of Conjugated Organic Materials

1.3.1 Structural Manifestation of Color in Conjugated Organic Materials

One attractive aspect of conjugated and conducting organic materials is the ability to fine-tune their optoelectronic properties with straightforward synthetic modifications. Because of this synthetic flexibility, seemingly related properties, such as redox potential and electronic band gap, can be decoupled and orthogonally modified without drastic adjustment of the fundamental materials synthesis process.[12–18] Thus, a new material with a desired set of properties can be realized by utilizing the current body of knowledge and tuning the chemical structure. To date, a large library of conjugated organic materials with extremely diverse materials properties has been published.[19–28] Fine-tuning and optimization of the properties for these systems is achieved by modification of the conjugated core or its pendant groups/side chains. The rest of this chapter will serve as a short tutorial on the basic concepts necessary to understand the field of electrochromism in conjugated organic materials. When considering how color is manifested in conjugated

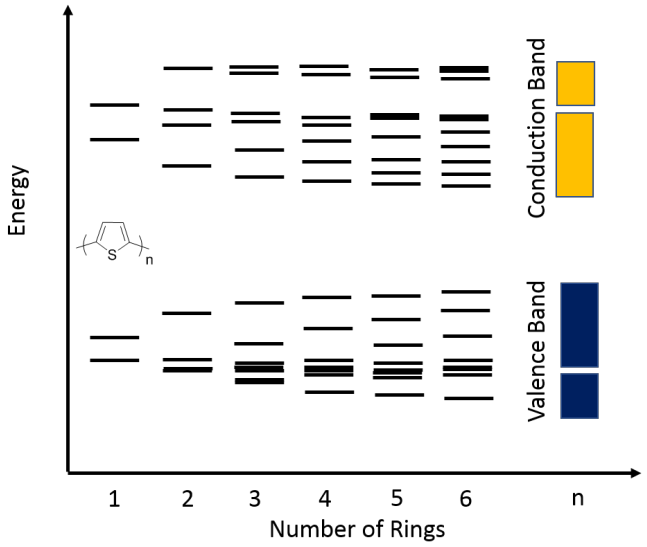

Figure 1.3.1.1 Evolution of the band structure for a polythiophene as the chain length grows. Figure was adapted with permission from Salzner et al.[30]

materials, it is important to consider π electron structure and how that leads to a band-like structure for polymers. Figure 1.3.1.1 shows how increasing conjugation leads to closing the HOMO-LUMO gap.[29]

Molecular orbital perturbation ultimately leads to a band structure, as the energy levels become so close that excitations can occur through thermal population. As the length of the polymer chain increases progressively from 1 to infinity, the occupied valence orbitals form continuous bands called the valence band, VB, and the empty orbitals coalesce into continuous bands called the conduction band, CB. For a polymer, the HOMO is thus defined as the highest occupied state in the valence band, and the LUMO is defined as the lowest unoccupied state in the conduction band. The difference in energy between the HOMO and the LUMO is defined as the band gap, E_g. The HOMO-LUMO energy difference is typically a good approximation of the optical gap, and thus tuning these energy levels can control color of the material being designed.

1.3.2 Charge States of Discrete Conjugated Molecules

When considering the oxidation or reduction of conjugated organic molecules, there has been significant research updating the model used to describe radical cation/radical anion states originally introduced by Bredas et al.[31–34] The updated model taking into account experimental ultraviolet photoelectron spectroscopy (UPS) and inverted photoelectron spectroscopy (IPES) measurements is examined in Figure 1.3.2.1.

From left to right: the reorganization energy λ corresponds to the difference between the initial ionization energy (IE) and the electron affinity (EA) of the newly charged species. The on-site Coulomb-interaction, U, causes a splitting into two HOMO-derived sub-levels, EA^+ and IE^+ (with respect to a common vacuum level $\phi_{el,\infty}$), while inter-site Coulomb- interaction causes a distance

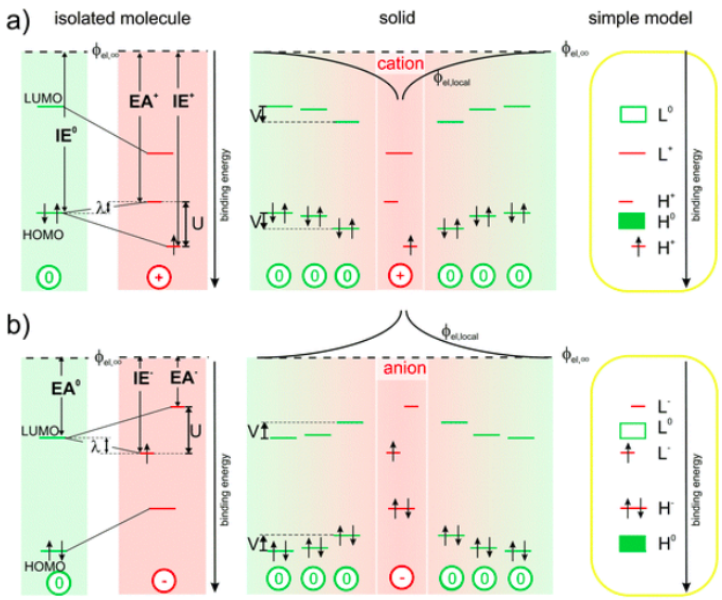

Figure 1.3.2.1. Revised energy levels in molecular semiconductors comprising radical charges: (a) origin of the experimentally observable spectral signature of cations (b) Analogous to (a) for radical anions. Figure used with permission from Winkler et al.[31]

dependent shift ($\phi_{el,local}$) to the energy levels of the neutral molecules in close vicinity of the cations. The right-most panel shows a simplified projection, correcting the traditional view. The energy required to remove an electron from a neutral molecule in the solid (IE^0) via UPS equals the energy gain upon returning it onto the relaxed cation (EA^+) via IPES plus the reorganization energy λ. Notably, the ionization energy IE^+ of the cation, i.e., the second ionization energy of a neutral molecule, is higher than the first ionization energy IE^0. This is related to the Coulombic interaction between electrons in the HOMO, commonly referred to as Hubbard *U* (peak-to-peak split between the occupied and unoccupied HOMO-derived levels of the cation obtained by UPS and IPES, respectively) for a valence hole in solid C60.[35,36] Accordingly, the upper unoccupied HOMO-derived energy level of the cation is shifted by λ into the gap of the semiconductor and, thereby, comes to lie above the HOMO of the neutral molecules in energy. The lower occupied HOMO-

derived sub-level appears at U–λ outside the gap of the semiconductor, that is, below the HOMO of the neutral molecules in energy. As shown in the center panel of Figure1.3.2.1a, the energy levels of neutral molecules residing in the Coulomb potential well ($\phi_{el,local)}$ of the cation are shifted by (up to) V, a quantity that can now, in analogy to U, be related to the inter-site Coulomb interaction.[37]

1.3.1 Charged States in Conjugated Polymers

As the discussion is extended to conjugated polymers, the charged state becomes more complicated with the inclusion of dications and multiple charges on a single chromophore/polymer chain, as explored in Figure 1.3.3.1.[38] In the charge neutral state (a) conjugated ECPs absorb in the visible approximated as a single π - π * transition (exceptions include donor-acceptor systems that have dual band absorbances and some random copolymers that have a manifold of absorbances).[39] The ideal oxidation states for a single polymer chain in solution consists of dual transition polarons and single transition bipolarons with discrete absorbances (b, c, and d respectively) at longer wavelengths than the neutral polymer. In the solid-state, charged states interact with one another creating a complex manifold of possible transitions. This leads to the characteristically broad profile for the oxidized states of fully conjugated ECPs (e). An asymmetric absorption throughout the visible region, absorbing more low energy red light and transmitting more of the higher energy blue light, manifests itself in such a way that highly oxidized states of conjugated ECPs exhibit a transmissive grey-blue hue. Due to this absorption, reaching a color neutral and fully transmissive oxidized state across the entire visible spectrum is difficult, if not impossible.

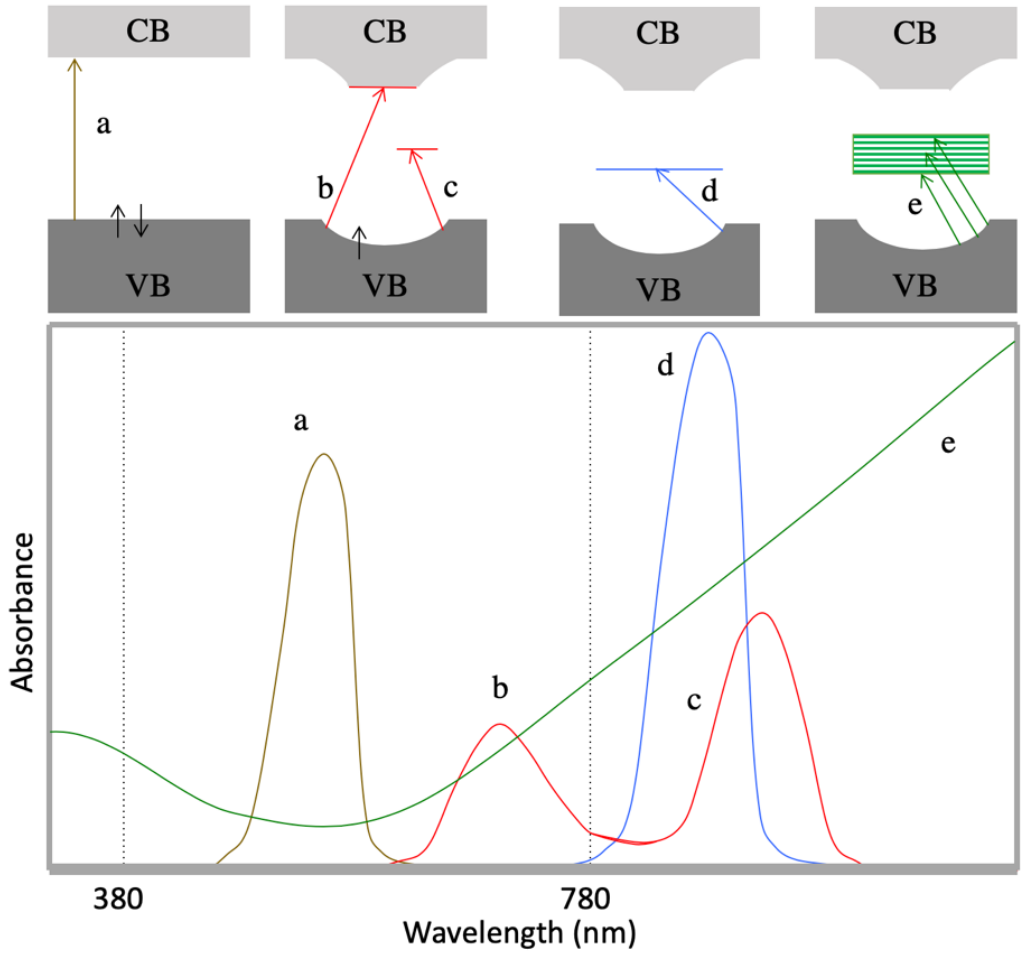

Figure 1.3.3.1. Electronic structures of allowed transitions in conjugated electrochromic polymer chains as a function of oxidation state: (a) a neutral polymer, (b and c) a polymer carrying a polaron, (d) a polymer carrying a bipolaron, (e) a polymer or assembly of polymer chains with a high concentration of polarons and bipolarons (intrachain or interchain polaron network), a chain or assembly of chains with a high concentration of bipolarons (intrachain or interchain bipolaron bands). A representation for absorbance spectra of these transitions is illustrated at the bottom. Figure adapted with permission from Bubnova et al. with considerations on radical cation band model from Png et al., Heimel et al., and Winkler et al.[31,32,38]

1.4 Electrochromism in Cathodically Coloring Conjugated Polymers

1.4.1 Discovery of PEDOT

In the 1980's Bayer's Central Research Department worked to commercialize polyacetylene and develop new conjugated polymers. While their research into polyacetylene did not result in a stable, commercializable material,[40] it did lead them to investigate new polymers composed of heterocycles, where the oxidized forms are stabilized by hetero atoms.[41] Dioxythiophenes (XDOTs) were ultimately invented by manipulation of the thiophene synthon into a bicyclic system containing a dioxane ring and a thiophene ring. It was found that 3,4-ethylenedioxythiophene (EDOT) could be prepared and oxidatively polymerized using ferric chloride.[42–45] After several years of research and development, polyEDOT (PEDOT), poly(3,4-propylenedioxythiophene) (PProDOT), and several other polymers were reported in the literature.[46] Aside from effectively blocking the β positions, protecting them during polymerizations, the oxygen atoms donate π-electron density into the heterocycle, making the ring electron rich and easier to oxidize. This effect raises the HOMO of the subsequent polymer, imparting these types of materials with low oxidation potentials (E_{ox}). This architecture can stabilize bipolarons to such a degree that they absorb energy far outside of the visible and into the NIR making them highly transmissive and nearly colorless when fully oxidized. This makes DOTs attractive to electrochromic applications as materials that can achieve vibrant colored states with high absorption in the visible and can switch to colorless, transmissive states with high absorptions outside of the visible.

1.4.2 Chemistry of Dioxythiophenes

Dioxythiophenes have been instrumental to the field of organic electrochromism due to them having low oxidation potentials, protection from β defects, and synthetically tunability. DOTs can be produced using straight forward synthesis starting from commercially available thiodiglycolic acid to produce a 3,4-dialkoxythiophene in Scheme 1.4.2.1a.[21,47] These first method requires multiple steps, but the chemistry is robust and cheap. In this route, esterification of thioglycolic acid is followed by reaction with diethyloxylate to form a 3,4-dihydroxy-thiophene, **3**. The reactive alcohols can be used as nucleophiles with an alkylbromide to add solubilizing side chains and give **4**. Subsequent saponification and decarboxylation give the desired 3,4dialkoythiophene, **6**. A second viable route starting from thiophene is also possible shown in Scheme **1.4.2.1b**. The thiophene is completely brominated to tetrabromothiophene[48] which is then subsequently and selectively dehalogenated with zinc metal in glacial acetic acid.[49] The final step utilizes Ullmann etherification with a copper (I) catalyst.[50] From dimethoxythiophene (DMOT) a transetherification with alcohols can lead to a variety of DOTs with various side chains and rings.[51,52]

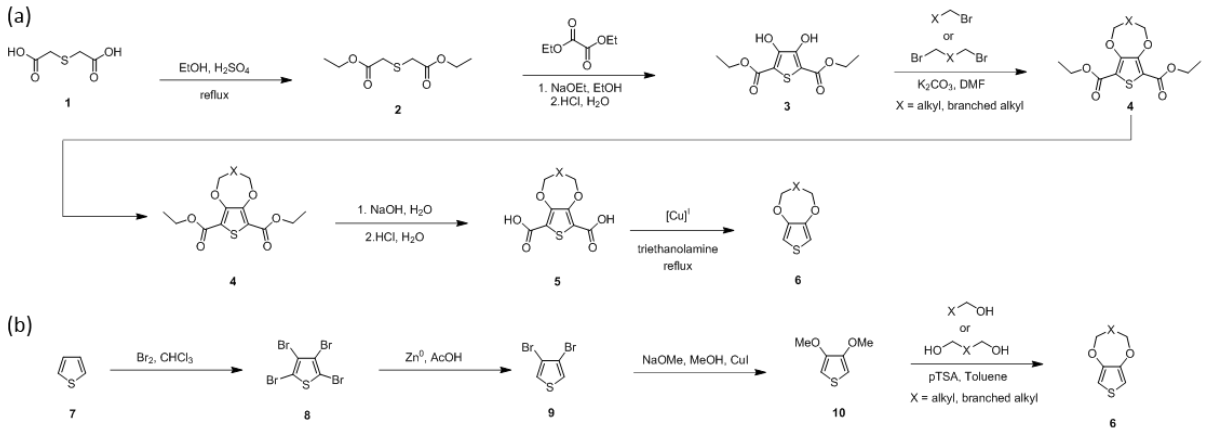

Scheme 1.4.2.1: (a) Total synthesis of 3,4-dialkoxythiophene starting from thiodiglycolic acid. (b) Alternate route starting from thiophene.

1.4.3 Redox and Color Switching

Of note is the use of two 2-ethylhexyloxymethyl ($EtHxOCH_2$-) side chains on the ProDOT unit (ProDOT-EH) to provide excellent solubility (>40 mg/mL) for the corresponding homopolymer with EC properties that are overall superior to electropolymerized PProDOT.[53] This section will discuss the redox switching of electrochromic polymer films using P(ProDOT-EH) as a model (refer to Figure 1.4.3.1). The material absorbs in the center of the visible with a λ_{max} at ~550 nm. This absorption allows red and blue light through making the material appear purple to the eye, as seen in the photography. Upon oxidation, radical cations begin to be formed along the polymer backbone. Spectral evidence of these species is seen at ~950 nm, but upon further oxidation to the dication state the peak attributed to these species decrease in intensity. In the dication state, this material absorbs in the NIR leaving an absorbance of 0.1-0.3 across the visible.

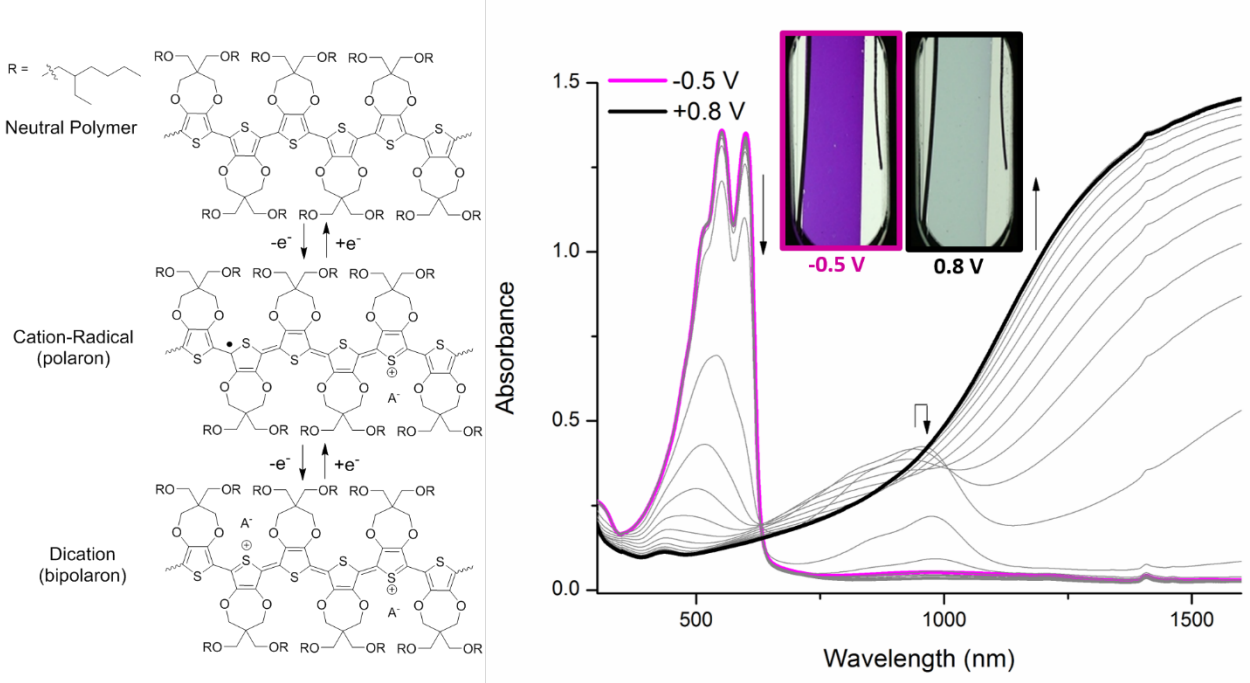

Figure 1.4.3.1. Oxidative spectroelectrochemistry of a P(ProDOT-EH) polymer showing exceptionally good contrast for a cathodically coloring ECP.

This small absorption in the visible is observed as a transmissive grey-blue, as seen in the photography.

1.4.4 Color Control in ECPs

The history of research in fully conjugated cathodically coloring ECPs has yielded materials that span the entire color palette while allowing the materials to be switched into their highly transmissive (bipolaron) forms, Figure 1.4.4.1.[54] The soluble P(ProDOT-EH), ECP-Magenta, has a seven-member dioxane ring with the side chains orthogonal to the plane of the backbone. The oxygens of the dioxane ring engage in non-bonding interactions with the sulfur atom of the adjacent thiophene ring that ultimately relaxes steric interactions along the conjugated chain and leads to a peak absorption near 550 nm, approximately in the middle of the visible spectrum. This polymer transmits both blue and green light making it appear purple to the eye.[53] In order to blueshift the absorbance an acyclic dioxythiophene (AcDOT) monomer can be used to increase interring strain to give ECP-Orange. This strain increases the dihedral angle between rings of the polymer, which decreases pi-overlap and widens the optical gap of the polymer resulting in the orange color.[55] This absorption can be slightly broadened when the AcDOT through random copolymerization with dimethoxythiophene (DMOT) and yield ECP-Red. Copolymerization of

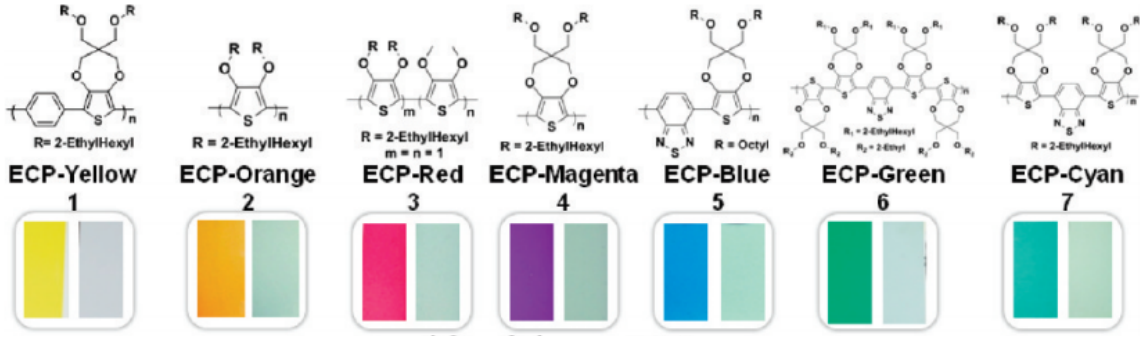

Figure 1.4.4.1. Structures and photography showing the resulting colors of the ECPs that cover the visible spectrum. Figure used with permission from Dyer et al.[54]

the ProDOT-EH with a 1,4-phenylene further twists the backbone and widens the gap to create ECP-Yellow.[56] In contrast, using electron poor units, like benzothiadiazole (BTD), with electron rich DOTs leads to low bandgap polymers with two absorption maxima, giving access to blue, cyan, and green ECPs.[39,57]

1.4.5 Challenges to Creating Yellow and Orange ECPs

One of the largest challenges to date with electrochromic polymers relates to the short switching lifetime of the yellow to clear switching polymer.[34,56,58–62] For an ECP to be yellow, it requires a high-energy optical absorption, between 380 and 550 nm in the colored state, refer to Figure 1.4.5.1. To then exhibit a high visible light contrast during switching, a cathodically coloring ECP then requires its oxidized state to absorb in the near infrared (> 700nm). ECPs that

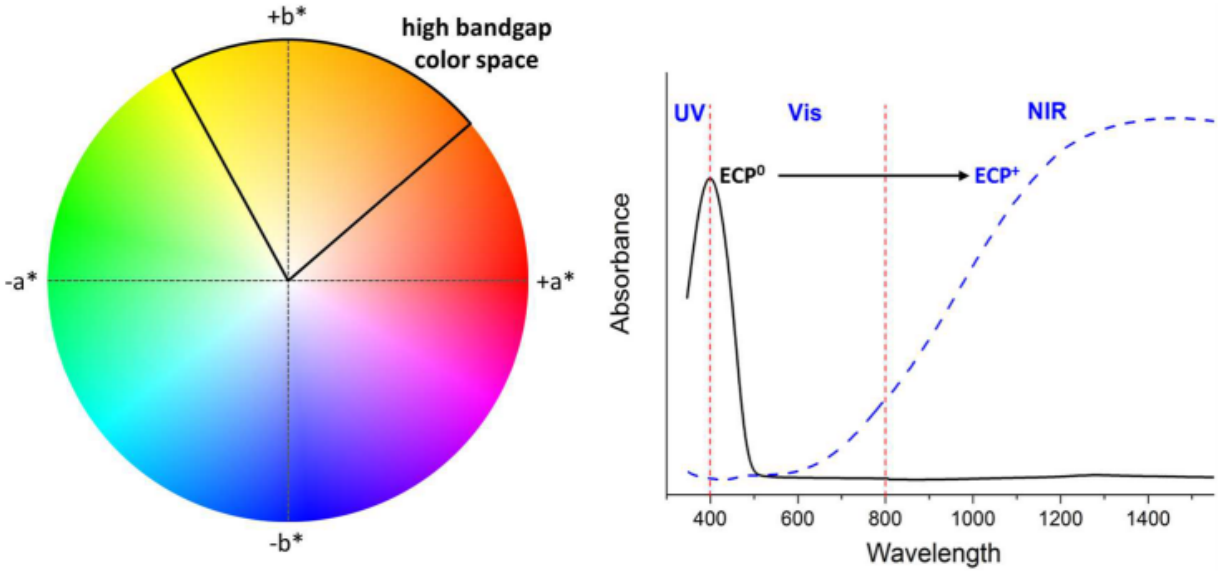

Figure 1.4.5.1. An L*a*b* color wheel with the high bandgap color space demarcated as well as representative UV−vis−NIR spectra of a high gap polymer in its charge neutral (ECP^0, black line) and oxidized (ECP^+, dashed blue line) states. Figure used with permission from Cao et al.[58]

have been developed with these optical properties have historically used phenylene units in the backbone of the polymer, which offer both a deep HOMO and a torsional strain that lowers pi-pi overlap along the backbone and widens the gap, relative to their all dioxythiophene counterparts. These phenylene-containing ECPs tend to have higher oxidation potentials than all thiophene polymers due to the larger energy of aromaticity relative to thiophene. These high oxidation potentials are hypothesized to be one of the causes of why yellow ECPs tend to have shorter switching lifetimes. Along with these high oxidation potentials there are open sites for reactivity of the radical cation states that leaves potential for nucleophilic attack and radical-radical coupling. Chapter 3 will discuss a new approach to creating wide-gap electrochromic polymers with increased redox stability.

1.5 Moving Towards Anodically Coloring Organic Molecules

1.5.1 Flipping the Spectrum to Achieve High Contrast

Although cathodically coloring polymers provide precise control of color and electrochemical properties, they have an inherent challenge when it comes to making improvements in contrast as discussed earlier. A class of materials that has potential to avoid this particular contrast issue is anodically coloring electrochromic (ACE) materials.[18,63–68] These materials have a neutral state absorption that is localized in the UV and, upon oxidation form broad charged-state absorptions that can be dominant across the visible. The most successful anodically coloring polymers prepared to date are made based on 3,4-dioxypyrroles or triphenylamines.[69–78] However, each of these materials have their own disadvantages. For 3,4-dioxypyrrole systems, the lack the facile chemistry for incorporation into alternating copolymers limits their synthetic flexibility. These polymers also contain charged states that mainly absorb in the near-IR with

minimal absorbance of blue light.[79] The triphenylamine polymers tend to undergo oxidation at potentials well over 1 V vs. Ag/Ag^+ which is higher than most fully conjugated, cathodically coloring electrochromic systems.[80,81] These issues detract from the ability to utilize these polymers in blends to create transmissive switching to broadly absorbing black mixtures.

Idealized spectra for an ACE material is detailed in Figure 1.5.2.1. As seen in the figure, anodic coloration has potential to be further explored as a methodology for designing electrochromic molecules/polymers where the NIR tailing observed in cathodically coloring ECPs is avoided. Materials need to be designed to have electron rich, conjugated chromophores of discrete length, which have wide optical gaps absorbing specifically in the UV in their neutral state and with minimal tailing into the visible in the colorless state. This can be seen by the solid curve in Figure 1.5.2.1. Upon oxidation to the radical cation state, short conjugation lengths maintain a high-energy absorption relative to fully conjugated polymer systems, moving the absorbance into the visible region (390-720 nm). This broad dual band absorbance is denoted by the dashed curve.

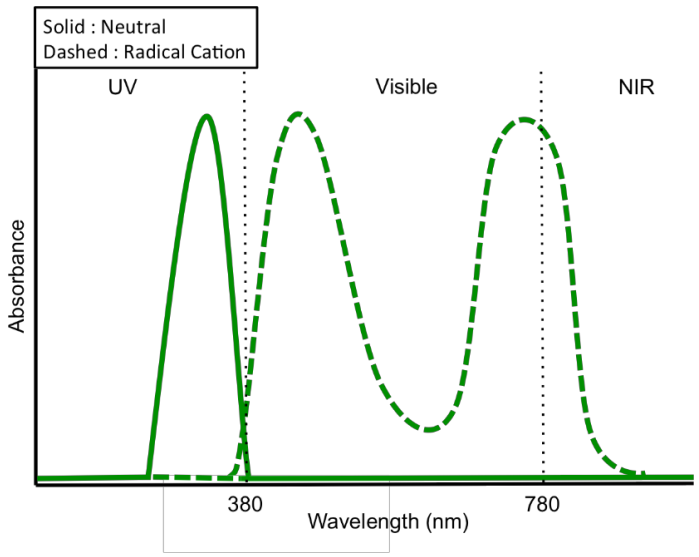

Figure 1.5.2.1. **Theoretical spectra for an ideal anodically coloring material with a UV absorbing neutral state and broadly absorbing radical cation state.**

1.5.2 Challenge of Controlling Color in Anodically Coloring Systems

In order to effectively design these materials as effective high contrast electrochromes, a fundamental understanding must be developed on how conjugation length, electron-rich character, and steric strain control the redox potential for switching to, and the absorption characteristics of, the radical cation state. Chapter 5 will examine these structure-property relationships. In the field of anodically coloring organic electrochromics there is a knowledge gap concerning how energy levels in the charged state are fundamentally controlled. [67,75,82–85] Manipulating the electronic energy levels of odd-electron organic systems is an area of research that has impacts well beyond electrochromism.[31,32] Chapter 6 will explore how electron rich/deficient moieties cross-conjugated into the chromophore can be utilized for manipulating radical cation energy levels and ultimately controlling absorption and color. Chapters 5 and 6 will deal with different approaches to creating anodically coloring materials as a means of overcoming the contrast barrier present in the field of electrochromism.

1.6 Electrochromic Devices and Applications

Here will be addressed electrochromic applications and general types of devices. There are several classifications of electrochromic materials: inorganic (Prussian blues and metal oxides), organic small molecule (viologens and dimethylterephthalates) and polymeric (based on polypyrrole and polythiophene). These materials have demonstrated the possibilities in a range of applications.

1.6.1 Film Based Devices

Film based devices are typically employed for metal oxides and polymeric electrochromic devices.[86,87] In the device schematic detailed in Figure 1.6.1.1, an ECP is the electrochromic layer.

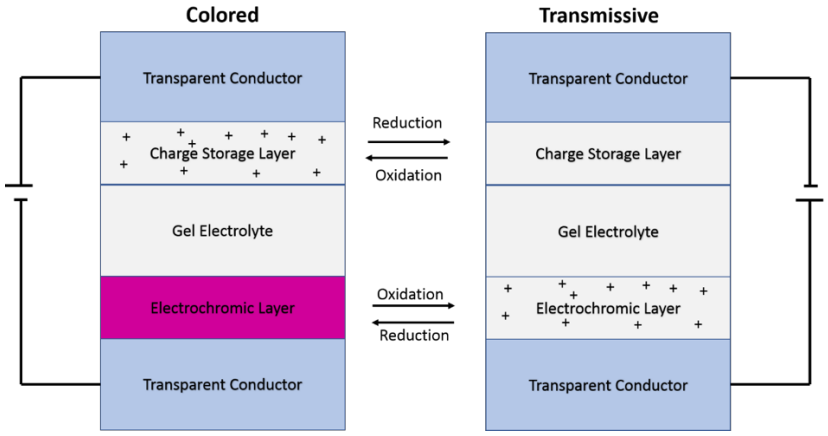

Figure 1.6.1.1. Film based electrochromic device architecture.

These types of devices act in a way similar to a battery in that there is a layered structure in which one layer holds the charge separated by an electrolyte bridge from the other electroactive layer. For this device to turn transmissive, an oxidizing potential is placed on the electrochromic layer and the charge storage layer is reduced. This process is reversed for the coloration of the device.

1.6.2 Solution Based Devices

Solution based devices are typically employed for discrete, molecular electrochromics, such as viologens.[88] A schematic showing the operation for a typical solution device based on a viologen is in Figure 1.6.2.1. In this device, an electrolyte solution or gel is sandwiched between two conductors. The solution/gel contains the electrochromic molecule as well as a molecule that can be oxidized at the counter electrode. The device is transmissive in the off state, and the viologen is in the dication form. Upon applying a reducing potential to the viologen, it turns to a vibrant blue. Once the device is turned off, the decolorization process relies on the redox active materials to diffuse to one another and oxidize/reduce one another. Returning to transmissive takes

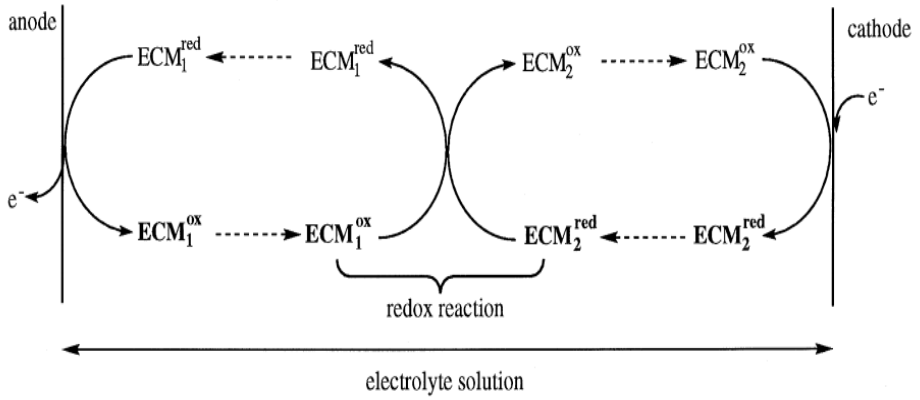

Figure 1.6.2.1. Principles of operation of a solution based electrochromic device. Figure used with permission from Mortimer et al.[89]

much longer than in film-based devices, leading to much research into designing devices and materials to facilitate this process.

1.6.3 Applications of Electrochromism

The first application to be discussed here is mirrors, or reflective ECDs. These types of devices are already seen in the automotive industry integrated in self-dimming rearview mirrors. In essence, these devices dim to prevent bright headlights from stunning the driver. This safety feature is accomplished by an electrochromic layer being installed over the mirror to modulate the amount of light reflecting off the mirror.[90–94]

Operating in either a reflective or transmissive mode, ECDs offer the ability to display full color information using a subtractive color mixing scheme. [95–100] These types of displays could be useful for advertising, data displays, and even watches.[101–103] Electrochromic displays are referred to as “passive” since they do not emit light and would not be subject to glare, making them much more readable in high light environments. Some materials are capable of electrochromic optical

memory meaning power only needs to be pulsed in short bursts over long periods of time, offering advantages over light emitting devices that require constant power. Though these ECDs do rely on an external light source, limiting their use to well-lit applications, to get around this, a white back light beneath the electrochromic layer can be utilized. However, EC materials have been shown to have potential to be utilized in dual use emissive/non-emissive systems, allowing day and night applications.[104,105] Researchers has been rather imaginative in the use of substrate for these displays, giving rise to ECDs based on paper or cloth which could lead to dynamic clothing and camouflage applications.[106–109] These and various niche applications are discussed at length by Monk *et al.*[110]

In 1985 the term "smart window" was coined by Svensson and Granqvist as a term for electrochromic windows.[111] These devices are very similar the display applications, but require all components to have a transmissive state. In large buildings with many windows, these devices actually carry the ability to eliminate a significant amount of cost and energy associated with heating/cooling the building.[112–116] View Inc., Sage Glass, and Kinestral are companies have installed electrochromic windows in buildings across North America and parts of the world.

These types of devices are also of particular interest for aircraft applications. Through cooperation between the Gentex Corporation, PPG Aerospace, and Boeing, electrochromic windows have been installed on the Boeing 787 "Dreamliner".[117] My research in particular was funded for military applications where either a pilot's helmet visor or cockpit canopy would darken when a fighter rises above clouds and then becomes transmissive when it flies below clouds, relieving the pilot's eyes and concentration during operations as they would no longer need manually lift or lower the current tinted visors. This same principle applies to ground troops who must breach dark rooms from high light environments, such as deserts. This same idea for

electrochromic visors has been attempted for generic eyewear. Electrochromic eyewear is different from photochromic as photochromic materials change color based on the intensity and wavelength of ambient light, thus taking several seconds to minutes to switch states. EC eyewear is currently under exploration and shows promise in the coming future.[118,119]

1.7 Dissertation Thesis

In this dissertation, the properties of 3,4-dioxythiophene (DOT)-based π-conjugated electrochromic polymers (ECPs) and molecules are explored with a focus on controlling structure-property relationships to achieve desired light absorption across the visible region of the spectrum. This dissertation will have a focus on the target of attaining color neutral colored and transmissive states and will examine both cathodic and anodic approaches to attaining this goal. Because of the electron rich nature of the DOT moieties, the cathodic polymers can switch to highly transmissive oxidized states, while UV absorbing anodic systems can still be effectively oxidized, giving these DOT materials the potential to be utilized in full color window or non-emissive display applications in either approach. This dissertation will have an emphasis on comparing these two approaches.

Chapter 1 will introduce the design, fundamental properties, and methods of processing conjugated, cathodically coloring electrochromic polymers, placing specific emphasis on the interplay between molecular structure, electrochromic properties, and redox stability. This chapter will examine the limits of the cathodic coloration approach and examine anodically coloring molecules and materials as an alternative method. Polymer and molecular synthesis, characterization, and processing methodology unique to this dissertation will be presented in detail in Chapter 2. Chapter 3 describes the use dialkylthiophenes to increase redox stability while

maintaining a wide optical gap. Chapter 4 explores using random all donor polymers to create broadly absorbing polymers with low oxidation potentials and improved optical memory. Chapter 5 delves into anodically coloring materials as an alternative method for high contrast in electrochromic materials. It will examine conjugation broken polymers and the advantages and drawback to the approach. Chapter 6 will examine how color is controlled in anodically coloring molecular systems where the radical cation state is being directly manipulated thorough the design of the molecular structure. Finally, Chapter 7 will give perspective on the projects in this dissertation and what can be taken away from each one to give alternative approaches to be explored in designing and synthesizing the next generation of conjugated organic electrochromic materials.

Chapter 2 - Experimental Methods

2.1 Synthesis of Conjugated Molecules and Polymers

2.1.1 Conjugated Materials Synthesis and Metal Catalyzed Cross Coupling

The synthesis of conjugated polymers has changed a lot in the last fifty years. Electrochemical polymerization is a means of making typically insoluble polymer films directly onto electrodes from solutions of monomer in electrolyte.[120,121] This method employs oxidation of the monomer to a radical cation whereby radical-radical coupling occurs to form dimers and protons are eliminated to form a neutral dimer. These dimers are subsequently oxidized and couple with nearby monomers or dimers. This process continues to as polymer precipitates onto the electrode. As the focus in the field has turned towards being able to coat films using high throughput techniques, and as metal-mediated cross-coupling reactions have grown more sophisticated, the focus of this thesis is the preparation and properties of soluble polymers prepared via a Pd catalyzed cross-coupling reaction.

Reactions such as Suzuki-Miyaura (Suzuki), Negishi, and Migita-Kosugi-Stille (Stille) couplings became common methods to form discrete chromophores and conjugated polymers.[122–126] These reaction mechanisms share many similar steps to create carbon-caron bonds between aryl units. These coupling reactions typically use palladium (Pd) in the zero-oxidation state as the catalyst with ligands to provide solubility and tune catalyst reactivity. The catalytic cycle for a Stille reaction of a trimethylstannyl-EDOT and bromobenzene can be seen in Figure 2.1.1.1 as a specific example of this catalytic cycle. The Pd(0) ligand complex undergoes oxidative addition with a carbon halide bond to form a Pd(II) species with negative charges on the halide and carbon species. The Pd then undergoes transmetalation with the organometallic species (the trimethyltin

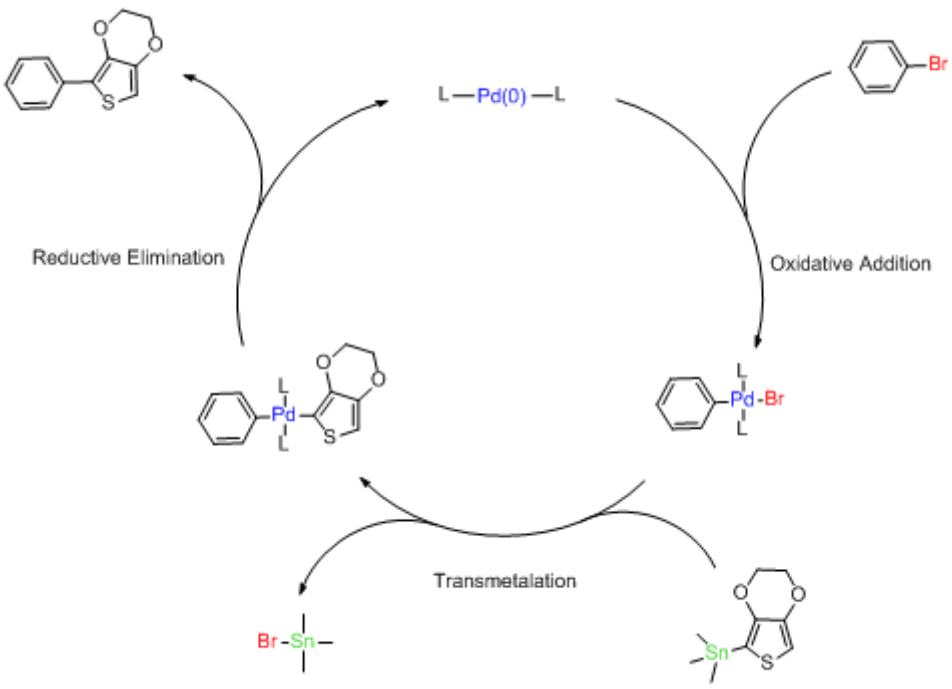

Figure 2.1.1.1. Catalytic cycle for the Stille reaction to form a carbon to carbon bond between EDOT and benzene with the typical steps seen in Pd catalyzed cross-couplings outlined.

in this case) so that both carbon species are bonded to the Pd and the halide and metal/organometallic species leave the cycle. The Pd then undergoes reductive elimination to form a carbon-carbon bond and restore the catalyst to the zero-oxidation state. This reaction is heavily used in the formation of discrete conjugated chromophores in Chapter 6 of this dissertation.

2.1.2 Direct (Hetero)Arylation Polymerization (DHAP)

Direct arylation has been used for the synthesis of discrete conjugated molecules for decades.[127–129] A host of metals have been used to catalyze the C-H activation, including Ir, Ru, Rh, and Pd.[130–133] The conditions for the reactions are not nearly as universal compared to Suzuki and Stille, as the conditions for each aryl system must be individually optimized, making the scope

of the syntheses much more focused in many cases. Direct arylation does however reduce the number of synthetic steps and avoids the creation of potentially hazardous intermediates, such as organo-tin compounds. Direct arylation is a specific example of C-H activation that has become increasingly important to build discrete molecules, oligomers, and polymers.[134]

Over recent years C-H activation has become a common method for the synthesis of conjugated polymers and is typically referred to as direct (hetero)arylation polymerization (DHAP). The first reported synthesis of a high weight conjugated polymer via DHAP was in 2010 using a Pd based catalyst to prepare regioregular poly(3-hexylthiophene) (P3HT).[135] Other reports of homopolymers and copolymers prepared via DHAP appeared the following year. Mario Leclerc, Barry Thompson, Takaki Kanbara, and Michael Sommer stand out as pioneers of this field, with each offering unique approaches to understanding and/or optimizing DHAP for various systems.[136–143] The Reynolds group has demonstrated the synthesis of various ECPs via DHAP and that the resulting polymers have lower residual metal content than the same materials prepared via oxidative or Grignard metathesis (GRIM) polymerization.[144]

The mechanism of DHAP, as proposed in the literature, shares many common steps with the previously discussed Pd catalyzed cross-coupling reactions.[145] This mechanism is detailed in Figure 2.1.2.1, where an alternating copolymer of EDOT and a 3,4-dialkylthiophene (DAT) is used as an example. Oxidative addition occurs in the same fashion as in the Stille mechanism. After oxidative addition the halide is displaced from the Pd species by a carboxylate or carbonate anion. The C-H activation step that follows has had several mechanisms proposed, but a generally accepted pathway involves a concerted metalation and deprotonation.[142,145] This is followed by a reductive elimination in the same manner as in the Stille mechanism. This reaction pathway is used extensively as a polymerization technique in Chapters 3, 4, and 5 for creating ECPs.

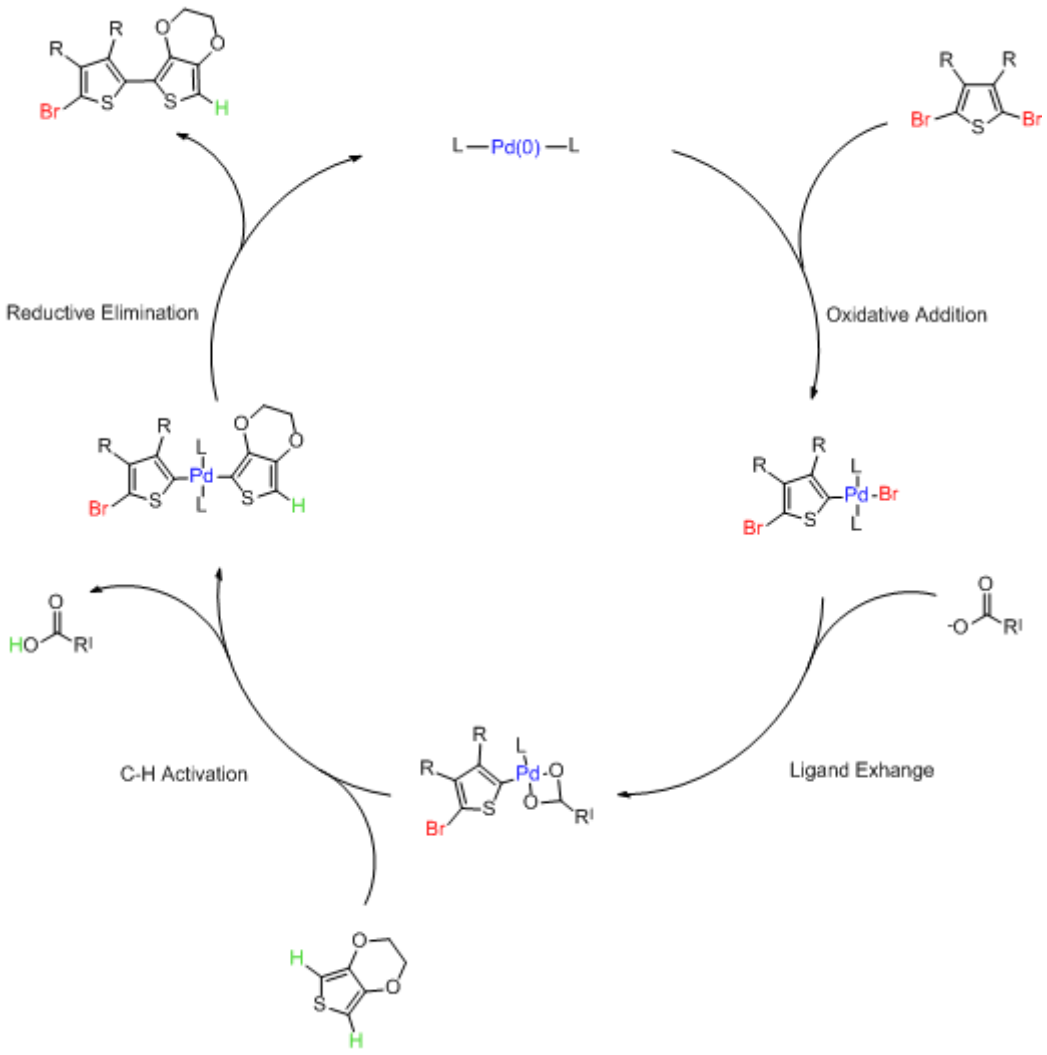

Figure 2.1.2.1. A proposed catalytic cycle for DHAP to form an EDOT-DAT copolymer with the various steps of the cycle outlined. Based on a reported cycle in the literature.[76]

2.2 Characterization of Electrochromic Polymers

Having discussed the background, theory, and synthesis of electrochromic polymers and molecules, a major portion of this chapter will focus on general considerations for how they were characterized. The structural and optoelectronic characterization of these materials must be done rigorously and consistently in order to draw accurate conclusions from the comparisons. Herein will be outlined the methods and experiments that were employed in characterization. To initially

characterize the properties of ECPs the following experiments must be performed: electrochemistry (cyclic voltammetry (CV) and differential pulse voltammetry (DPV)), spectroelectrochemistry (SpecEchem), chronoabsorptometry (kinetics), photography, and colorimetry. With these properties in mind more advanced studies can be taken underway, such as redox stability testing and device construction/testing. This section will outline how all these experiments are set up and describe some practical considerations for how the materials are handled

2.2.1 Practical Considerations for Solubility, Stability, and Storage

As these ECPs are purified by Soxhlet extraction, some inherent knowledge about the solubility of the polymer is gained before a dried sample is obtained. If the polymer is extracted in the methanol or acetone fraction, then it will likely dissolve in the propylene carbonate (PC)/electrolyte solution or delaminate from the electrode. If the material is extracted in the hexanes fraction, then it is highly soluble for casting purposes, but will not dissolve in the electrolyte. If the material comes out in the chloroform fraction, then further solubility testing will be necessary. It is wise to take small portions (~5 mg or spatula tips worth) and experiment with the solubility as it will aid in the selection of solvents for film casting. These materials are generally stable in the bulk, but recent studies have shown that they are light and air sensitive and will photoxidize or bleach while standing in air under illumination over prolonged periods of exposure.[146] Therefore, it is best to store bulk polymers in the dark and film samples under inert atmosphere without exposure to light.

2.2.2 Procedures for Making Polymers Solutions and Preparing Films

The polymers were spray cast into films using Anest Iwata airbrushes. These are compatible with many organic solvents at room temperature. Small volumes of polymer solutions are required with 15 mg of polymer in 5 mL of toluene or chloroform. This amount is more than enough to cast five or six films of an area of ~2 cm^2 on ITO coated glass. Films for optical measurements are sprayed to an absorbance of 1.0 ± 0.1 to create accurate comparisons between polymers. The ITO electrodes were purchased from Delta Technologies, Ltd. (7 x 50 x 0.7 mm, sheet resistance, Rs 8-12 Ω/sq). Prior to spraying, the solution is filtered through a 0.45 μm PTFE syringe filter to ensure that the spraying solution is free of particulates, and to prevent clogging of the airbrush. To achieve films with clarity, the best conditions for flow pressure and solvent is 15 psi for toluene and 10 psi for chloroform. Quick passes over the electrode help prevent pooling of the solution, which will lead to rough and hazy films. Solutions that must be continually heated to maintain solubility will be unsuitable for spray casting, if this is the case use spin casting or blade coating methods.

Before spraying, fresh ITO/glass slides must be cleaned; this is done by first removing the plastic film binding the slides together then identifying the conductive side. Clean the slide by sonicating with acetonitrile, isopropyl alcohol (IPA), acetone, and finally chloroform. If you are recycling slides, wipe clean the used polymer films with chloroform and repeat the above cleaning procedure. Delamination may occur for some polymers during electrochemical measurements. This can be avoided by dipping cleaned slides into 0.1M dodecyl-1-phosphonic acid/IPA and rinsing with IPA. The treated slides allow for better adhesion of the polymer and reduce delamination.

2.2.3 Polymer Film Electrochemistry

Electrochemical measurements were carried out using an EG&G Princeton Applied Research model 273A potentiostat/galvanostat used under the control of Corrware II in a 3-electrode cell configuration. An example electrode set up is shown below in Figure 2.2.3.1. The oxidation is evident in the CV. Due to slow relaxation effects in neutral conjugated polymers from intercalation of solvent and ions, the properties of films such as redox potentials and absorption spectra can change upon doping and dedoping.[147–149] Thus, cyclic voltammetry is utilized to electrochemically condition electrochromic polymer films.

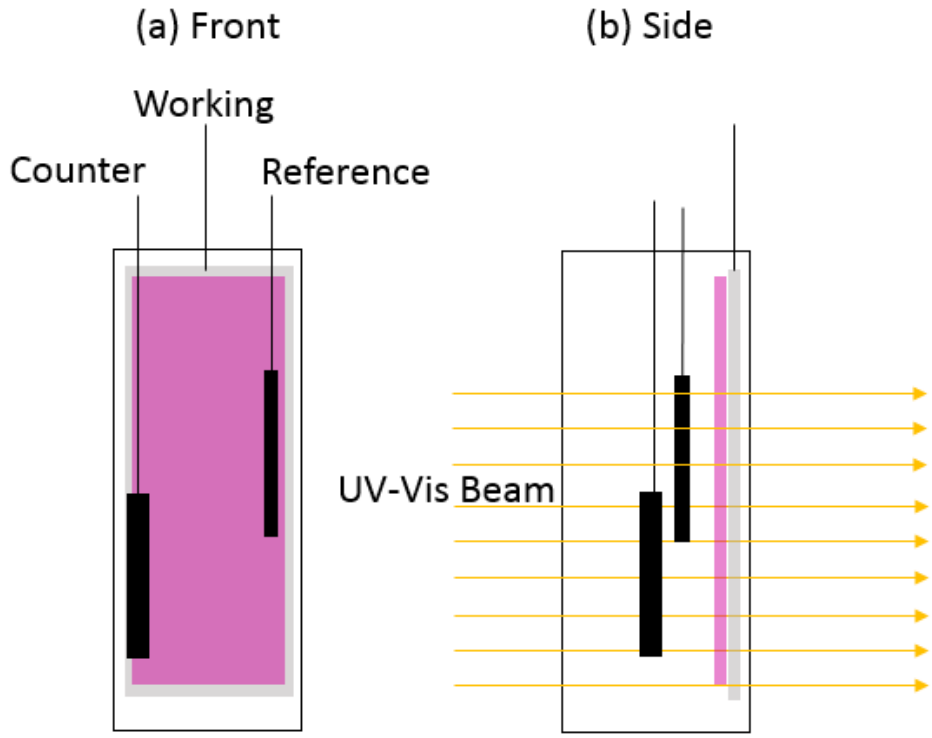

Figure 2.2.3.1. Cartoon of three-electrode setup in a cuvette (a) front view (b) side view

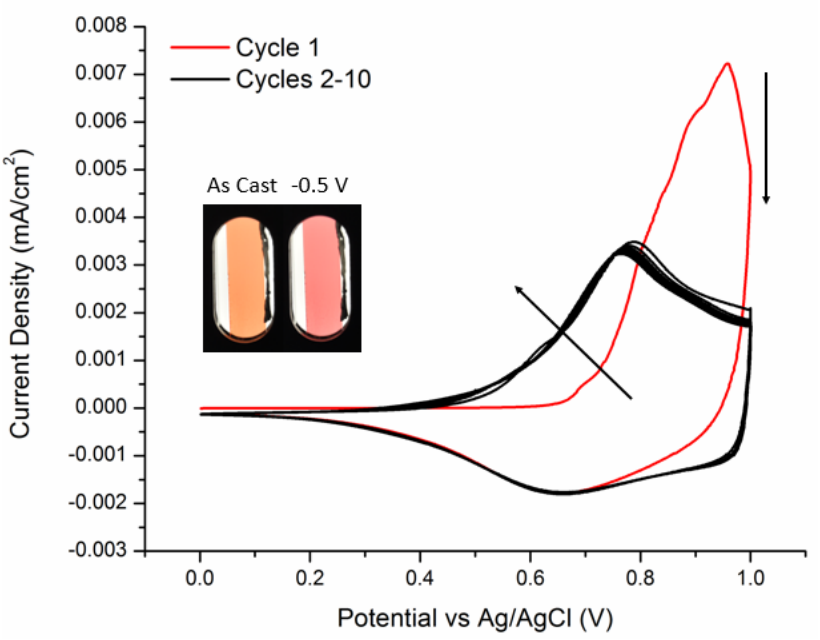

Figure 2.2.3.2. Break-in CV curves and photographs of DAT-ProDOT

In Figure 2.2.3.2, the electrochemical and optical changes upon break-in are particularly evident using **DAT-ProDOT** as an example. This example demonstrates that the oxidation potential of a conditioned film is lower than that of the as cast film. The electrochemical conditioning is performed in the materials most stable electrochromic switching window at a rate of 50 mV/s over 10 cycles where a stable and reproducible CV curve is achieved. Often, the optical properties of a polymer can change drastically upon break-in, the greatest being observed between the first and second potential sweep.

Differential pulse voltammetry (DPV) is used to determine the oxidation potential of a polymer/molecule where the setup is the same for CV. Polymer films are drop cast from (~3 mg/mL) onto Pt button electrodes with an area of 0.02 cm^2 and immersed into 0.5M $TBAPF_6$/PC. The polymer film is held at the neutral state potential for one minute and then swept to the oxidized state voltage. Experiments performed in this dissertation used a potential step of 50 mV with

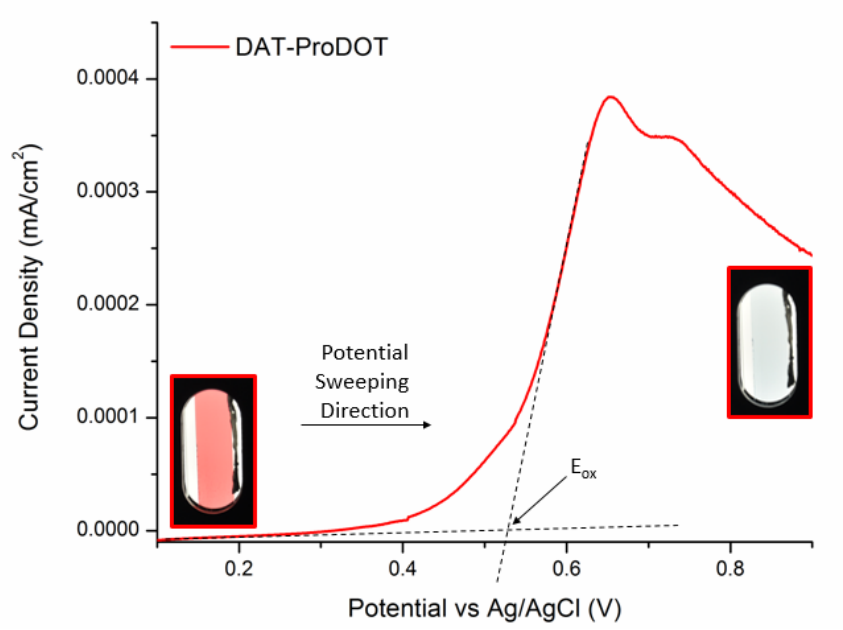

Figure 2.2.3.3. DPV curve of DAT-ProDOT where the Eox is indicated by the onset.

measurements intervals of 5 ms over the range of potentials dictated by the CV. The oxidation potential (Eox) is determined as the onset for an increase in current as illustrated in Figure 2.2.3.3 for DAT-ProDOT. This method has the advantage over CV because the sampling of the current before a potential change minimizes the effect of the charging/capacitive current. The films should be broken-in using the same conditions as for CV. If you are performing reduction the DPV must be done in a glovebox or under an argon atmosphere with degassed electrolyte to protect the radical anions and dianions from exposure to water or oxygen.

2.2.4 Photography

Photographs are taken to aid in the illustration of color properties. As an example, Figure 2.2.4.1 shows photographs of the random copolymers examined in Chapter 4 in the neutral (broken in) and oxidized states. It can be seen that neutral states of the polymers here show a wide range of colors. Below each neutral polymer film is the oxidized state of the same polymer, as the

Figure 2.2.4.1. Photographs of the random copolymers examined in Chapter 4 in the neutral (electrochemically conditioned) and oxidized states.

polymer is held at an oxidizing potential. When taking photographs, particularly with a digital camera, the setup and execution must be considered to ensure that the photographs are objectively comparable. The light source in this work is a D50 bulb to accurately compare the photographs to the calculated colorimetry. The lighting needs to be the same in all instances, with the source coming from the same angle to the objective to avoid scattering and stray lighting being mitigated by a curtain. The photography in this dissertation was performed on a Nikon D90 camera with a 18-105 mm lens. The ISO sensitivity was 200 -0.3 EV, white balance was 5000K, aperture was f/3.5 when zoomed all the way out, and the shutter speed was 1/80 s for all photographs. As the polymer films in an electrochemical cell are placed in a cell holder in the light booth, a photo is taken. The film then undergoes electrochemical conditioning via CV followed by a potentiostatic hold at a reducing potential. A photograph is then taken of the now broken in polymer film. The film is then held at an oxidizing potential for a photograph of the transmissive state. For some systems, photographs of the intermediate states are taken to show the progression of color change as a function of applied potential.

2.2.5 Spectroelectrochemistry

Once the electrochemistry of a polymer is well understood, then spectroelectrochemistry can be performed. This experiment monitors the spectra as a function of the applied potential. These experiments were all performed using an Agilent Cary 5000 UV-vis / NIR spectrophotometer. For new materials the entire spectrum needs to be collected across the near infrared (NIR) to visible to the ultra violet (UV), from 2000-300 nm. This range enables you to observe polaron or bipolaron oxidized states, D-A or π to π* effects, or over oxidation in a conjugated polymer. When data is collected, it is typically plotted from 1600-300 nm, from the NIR the edge of the UV. An example of the collected data is detailed in Figure 2.2.5.1.

An electrochemical cell containing the polymers on ITO/glass in electrolyte solution are placed into the UV-Vis (same cell as described in Figure 2.2.3.1). A photograph is taken before any potential is applied, then the film is electrochemically conditioned. Using the potentiostatic

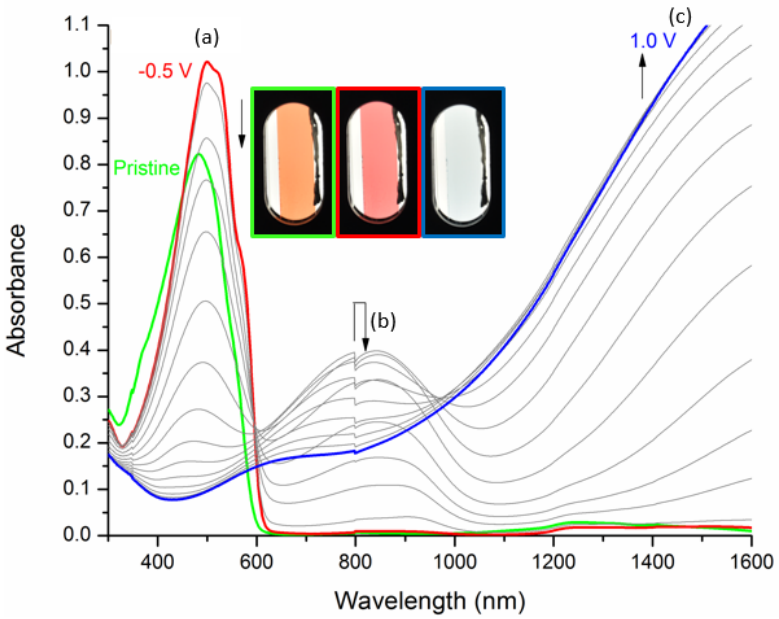

Figure 2.2.5.1. Full spectroelectrochemistry for a film of DAT-ProDOT including as cast spectra and photography (a). Neutral (b) polaron, and bipolaron absorptions

experiment a reducing potential is applied, and the spectrum is measured. This is repeated in 50 mV steps until the highest stable potential is reached. In the example of the collected data in Figure 2.2.5.1 the potential increases and there is a loss in absorbance at the π to π* with a λ_{max} at ~500 nm (a) coupled with simultaneous growth and then loss of a polaron band at ~850 nm (b) and overall increase in a bipolaron band in the NIR (c). The band gap is taken as the onset of absorption. The small notch at 800 nm is the detector change-over from NIR to UV-Vis. Such artifacts should not be electronically smoothed away.

2.2.6 Colorimetry

In Chapter 1 colorimetry and how the eye perceives color was discussed. Here colorimetry was calculated using Star-Tek colorimetry software using settings of a D50 illuminant, 2 degree observer, and L*a*b* color space. After spectroelectrochemistry, the spectra attained at progressive voltage levels were converted using this software. The method utilizing the Star-Tek package can take all of the spectra and directly convert them into color values in a variety of spaces

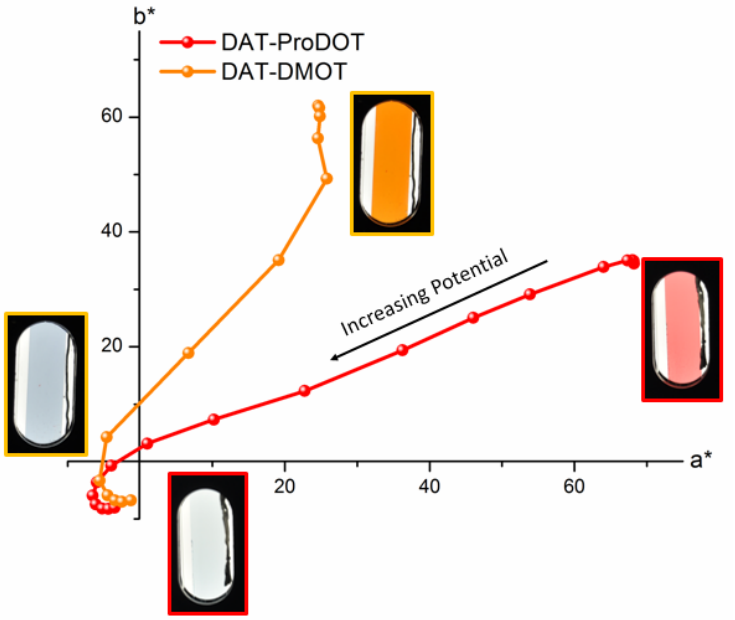

Figure 2.2.6.1: Colorimetry in a*b* and photography of DAT-ProDOT and DAT-DMOT

with different illuminants in a very efficient time frame. With color values calculated, photographs help correlate and visualize the colorimetry of ECPs as shown in Figure 2.2.6.1 for DAT-ProDOT and DAT-DMOT.

2.2.7 Device Construction and Redox Stability Testing

A schematic showing a cross section of an ECD can be seen in Figure 2.2.8.1. Device construction involves air-brush spraying a film of ECP from 3 mg/mL toluene solution onto glass/ITO with dimensions of 5 cm x 6 cm to an absorbance of 1.0 and using poly(isobutylene) tape create a double seal around the polymer active area and around the edge the slide. On another glass/ITO slide another film of minimally color changing polymer (MCCP) is air-brush sprayed to the same dimensions to act as a charge storage layer but with a thickness dictated by balancing the amount of charge stored by the electrochromic polymer.[150] The MCCP slide is then immersed into 0.5 M $TBAPF_6$/PC electrolyte solution in a three-electrode cell and oxidized for 10 seconds at 0.8 V relative to Ag/AgCl. Both slides are then brought into a glove box with an argon atmosphere

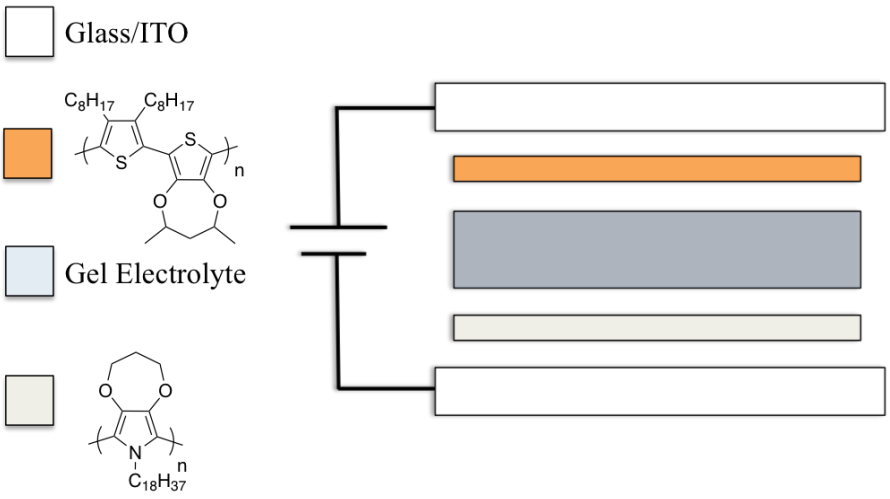

Figure 2.2.8.1. Architecture for an ECD with MCCP as charge storage layer showing the layers in the device

and a gel electrolyte (0.5 M $TBAPF_6$ in 5% w/w PMMA in PC) is drop cast over the active area of the electrochromic polymer. The slide coated with the MCCP film is placed on top and the stack is placed on a hot plate set to 90 °C to allow for the poly(isobutylene) sealant to adhere. The device is cooled to room temperature before removal from the glove box.

In order to examine the redox stability of an ECP or device, the %T at λ_{max} is monitored as the film/device is redox cycled through wave pulse voltammetry. The contrast is calculated between the neutral and oxidized state at every one hundred cycles for a film in electrolyte and at every one thousand cycles for a device. Figure 2.2.8.2 shows spectra of both the colored and transmissive state of an ECD over the course of 10,000 cycles. The loss in the contrast between these states can be seen as changes in the transmittance spectra detailed by the arrows.

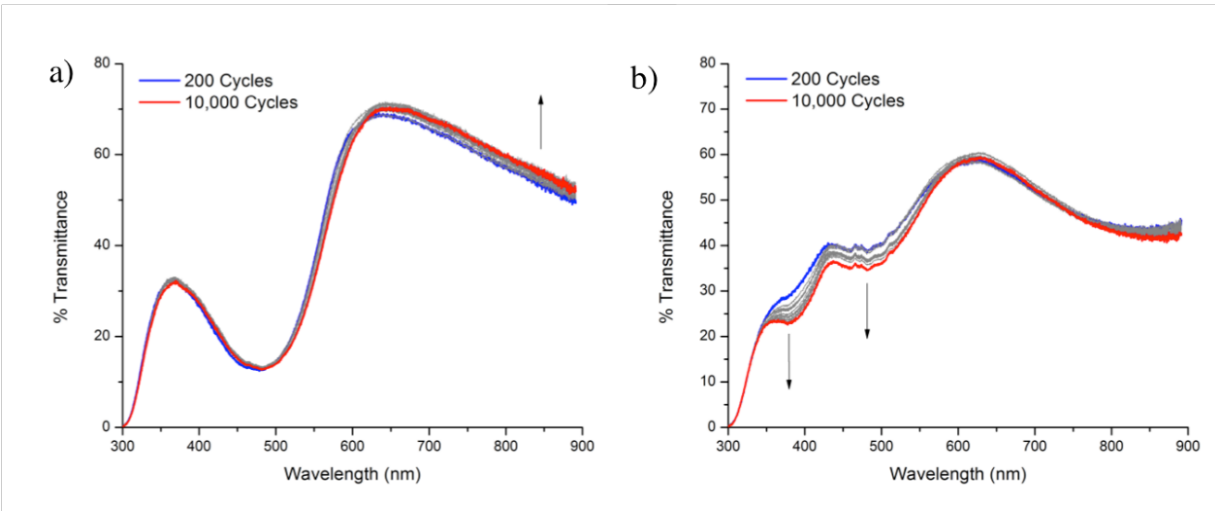

Figure 2.2.8.2. Evolution of transmittance spectra of an ECP device over 10,000 cycles for the (a) colored and (b) transmissive states. Each spectrum is a step of 200 cycles up to 1000 switches, and every 1,000 cycles up to 10,000 switches.

2.3 Characterization of Electrochromic Molecules

While there are a lot of similarities between the electrochromic characterizations of polymers and molecules, there are differences to consider that will impact how the techniques are performed. The rest of this chapter will highlight these differences and discuss the methods for making measurements on small molecule electrochromes.

2.3.1 Practical Considerations for Solubility, Stability, and Storage

While polymers require selective solubility for casting solvents over electrolyte solutions, electrochromic molecules are characterized in solution and therefor need to be soluble in the electrolyte solution. For the purposes of these characterizations, the solvent used is dichloromethane (DCM) as it is a good solvent for both organics and soft electrolytes. As the electrochromic molecules in this dissertation are designed to be extremely electron rich, they are susceptible to being oxidized in air/light. These molecules kept under inert gas in sealed vials and stored in the dark in a freezer. They are stable enough to have out during the day for characterization without any observable degradation but should be kept as described if stored for long periods.

2.3.2 Solution Electrochemistry

All electrochemical measurements performed on these molecules are done in solution at 250 μM and were carried out using an EG&G Princeton Applied Research model 273A potentiostat/galvanostat under CorrWare control in a three-electrode cell configuration. CV and DPV were carried out with Pt button electrodes with a surface area of 0.02 cm^2 as a working electrode, a Ag/AgCl reference electrode, and a Pt flag as the counter electrode. An electrolyte solution of 0.5 M tetrabutylammonium hexafluorophosphate ($TBAPF_6$, 98%, purified via

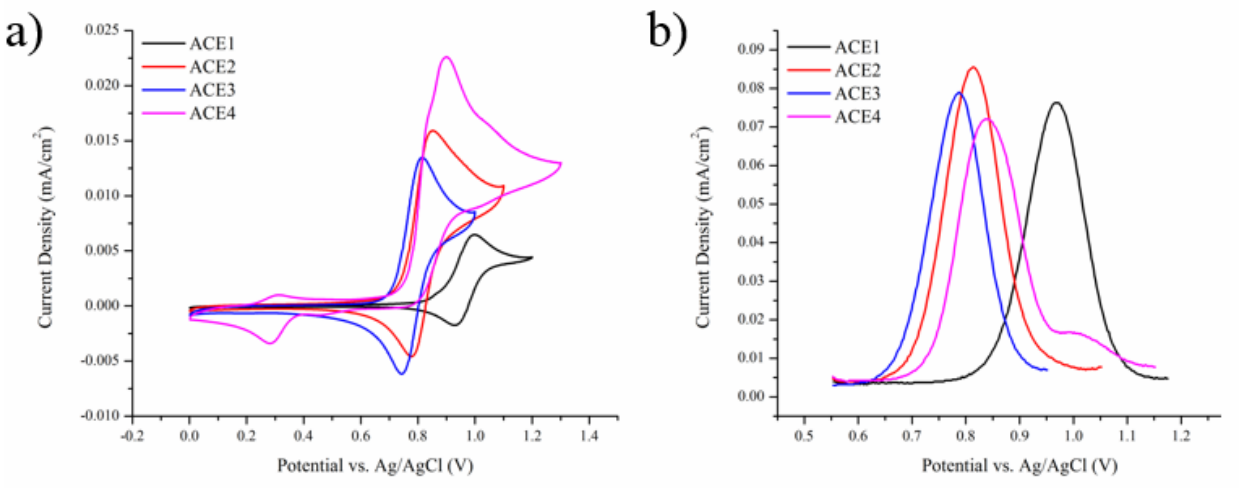

Figure 2.3.2.1. Cyclic (a) and differential pulse (b) voltammograms of 250 µM of electrochromic molecules in 0.5M TBAPF$_6$/DCM solution.

recrystallization from hot ethanol) in dichloromethane (DCM) was used in all electrochemical measurements. Figure 2.3.2.1 details example CV and DPV traces. In contrast to polymers, the peak of the DPV is measured to be the oxidation potential of a molecule in solution.

2.3.3 Optically Transparent Thin Layer Electrode (OTTLE) Spectroelectrochemistry

Spectroelectrochemistry of discrete molecules is performed in an optically transparent thin layer electrode (OTTLE). Figure 2.3.3.1 details a schematic of the OTTLE used in this dissertation and photographs showing the nature of cropping the figures is detailed. In this set up, the working electrode is a platinum mesh with a platinum counter electrode and Ag/AgCl reference electrode. The electrochromic molecules are dissolved at 250 µM in 0.5 M TBAPF$_6$/DCM. The spectroelectrochemistry set up is the same as with polymers. A photograph is taken before any potential is applied. Using the potentiostatic experiment a reducing potential is applied, and the spectra is measured. This is repeated in 50 mV steps until the highest stable potential is reached.

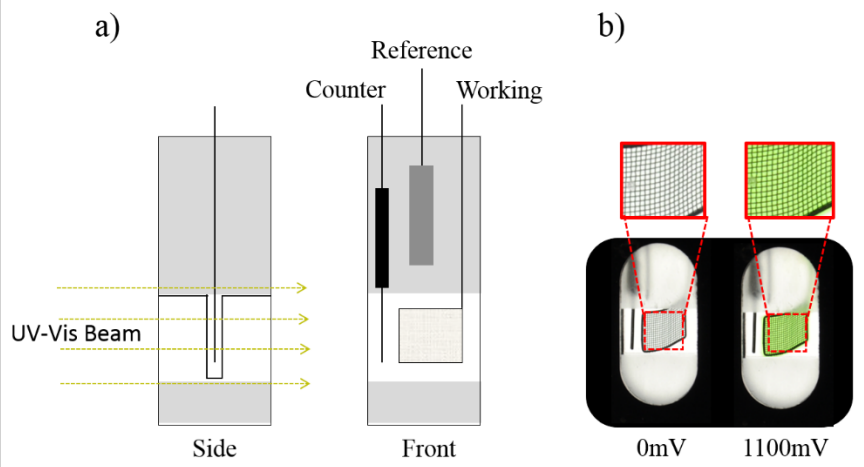

Figure 2.3.3.1. (a) Schematic of OTTLE (b) Photograph showing the nature of the beam path and cropping for purposes of showing color.

When the data is processed for these measurements, the OTTLE can cause a considerable amount of noise. This noise can be mitigated by subtracting the neutral spectrum as a baseline.

2.3.4 Solution Oxidative Doping

Solution doping of these material helps show the color and can help probe materials in higher oxidation states. To perform the experiment, the molecules are dissolved at 250 µM in dry DCM in an argon filled glovebox. The solutions are portioned into ten 5 mL small batches in borosilicate vials and stoichiometric amounts of a 250 mM solution of $Fe(OTf)_3$ are added between 0 equivalents and 4 equivalents at 0.5 eq increments. Clean DCM is used to make all the volumes equivalent. The vials are sealed and brought out of the glovebox and photographs are taken the vials are opened. UV-Vis Spectra is taken for each sample relative to a standard of DCM. The spectra, Figure 2.3.4.1, show the evolution of the absorbance as a function of doping. These absorbance peaks and relative intensities should correlate with the OTTLE spectroelectrochemistry.

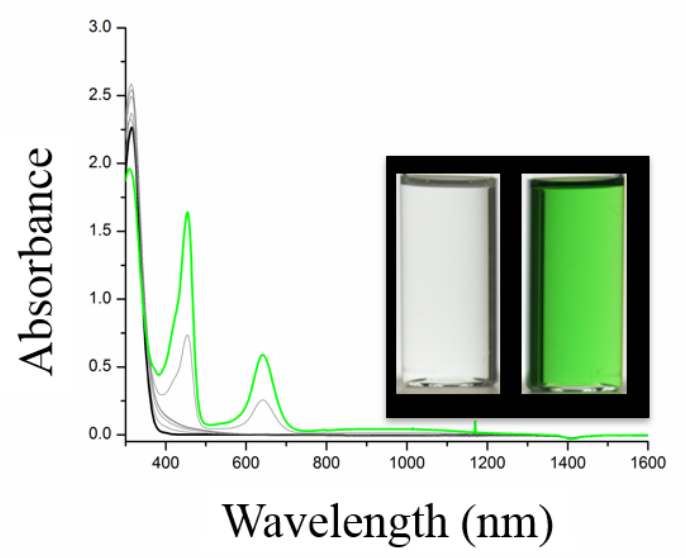

Figure 2.3.4.1. Evolution of UV-Vis spectra of oxidatively doped solutions of an anodically coloring molecule. Inset photograph shows the extreme states. The solutions are 250 µM of each compound and $Fe(OTf)_3$ is the dopant.

Chapter 3 - A Dialkylthiophene (DAT) as a Monomer for Wide-Gap Cathodically Coloring Electrochromic Polymers.

Adapted from:

Christiansen, Dylan T. and Reynolds, John R. Fruitful Usage of a Dialkylthiophene for Redox Stable Switching in Wide-Gap Cathodically Coloring Electrochromic Polymers Macromolecules; **2018**, 51 (22), 9250-9258

&

Savagian, Lisa. R.; Österholm, Anna. M.; Shen, D. Eric; Christiansen, Dylan T.; Kuepfert, Michael; Reynolds, John R. Conjugated Polymer Blends for High Contrast Black-to-Transmissive Electrochromism. Adv. Opt. Mater. **2018**,1800594.

A series of conjugated polymers are prepared via direct hetero arylation polymerization with the goal of yielding wide-gap yellow and orange colored switching to transmissive cathodically coloring electrochromic polymers (ECPs). The polymers are based on repeat units of dialkylthiophene (DAT) in alternation with dioxythiophenes (DOTs) with various side chains to induce differing levels of interring strain yielding 3,4-ethylenedioxythiophene (DAT-EDOT), 3,4-propylenedioxythiophene (DAT-ProDOT), 3,4-(1,3-dimethylpropylene) dioxythiophene (DAT-DMP), and 3,4-dimethoxythiophene (DAT-DMOT) structured polymers. Examination of the optoelectronic properties via UV−Vis−NIR spectroscopy, differential pulse voltammetry, and spectroelectrochemistry show that, while increasing the interring strain induced by the side chain of the DOT unit leads to an increased oxidation potential ranging from -122 to +288 mV relative to Fc/Fc^+, this does not decrease the accessibility of the extreme charge states. Through subtle steric interactions between the arylene units, neutral polymer colors were tunable from yellow to deep reds while maintaining transmissive oxidized states. These DAT based polymers also show

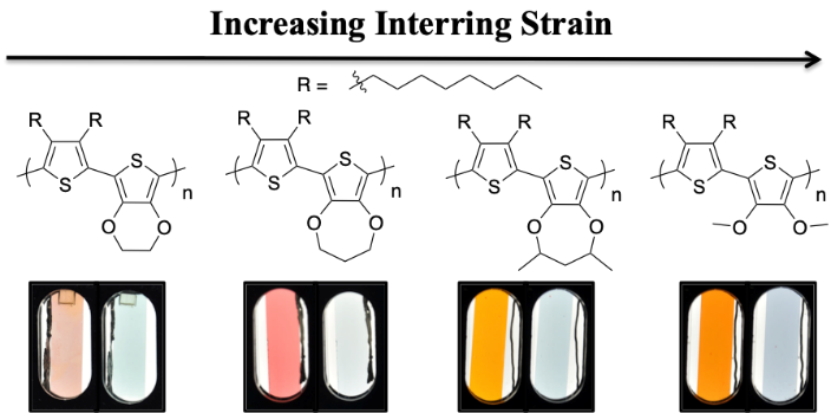

Figure 3.1. Design scheme of the DAT-XDOT systems arranged in order of blue-shifting absorbance

increased redox switching stability compared to that of previous generations of high gap cathodically coloring ECPs that incorporate phenylene units as the wide gap comonomer with DAT-ProDOT and DAT-DMP films showing minimal loss of electrochromic contrast over 1,000 switches and a DAT-DMP device showing minimal contrast loss over 10,000 cycles. With these properties, these polymers have the ability for subtractive color mixing with other ECPs in order to create broadly absorbing, color neutral (black and brown) blends that are redox stable.

3.1 Design Approach

Figure 3.1.1 shows some key polymers in the progression of designing soluble, yellow electrochromic polymers leading to the design of the current generation. Starting with generation 1, ProDOT-Ph was the first successful synthesis of a yellow to clear ECP using the phenylenes. When this material is sprayed into a film onto an ITO working electrode and subjected to repeated potential square waves that oxidize and reduce the polymer it shows instability to switching within the first 10-20 cycles due to the high oxidation potential required to switch and the potential reactivity of the phenylene unit itself in the charged state.[151] The design rationale for $AcDOT_2$-Ph

was to increase the electron rich dioxythiophene content of the polymer to lower the oxidation potential and maintain the wide gap by using the increased interring strain provided by the acyclic nature of the AcDOT unit. This polymer's is only slightly more stable than ProDOT-Ph showing significant drops in contrast within the first one-hundred redox cycles. The second generation polymers were synthesized to attempt to address these issues by incorporating methoxy groups on the phenylene portion of the polymer in order to simultaneously lower the oxidation potential to switch and sterically block the open sites from nucleophilic attack and radical coupling.[58] While $AcDOT_2$-$Ph(OMe)_2$ maintains a vibrant yellow color, the increased strain imparted by the $Ph(Ome)_2$ unit causes the polymer to have a high oxidation potential and only a marginal increase in redox stability. During redox switching, $ProDOT_2$-$Ph(Ome)_2$ lasts over 100 cycles with no drop in contrast, but the decrease in strain redshifts the absorbance λ_{max} by 54 nm leading to a red-orange polymer.

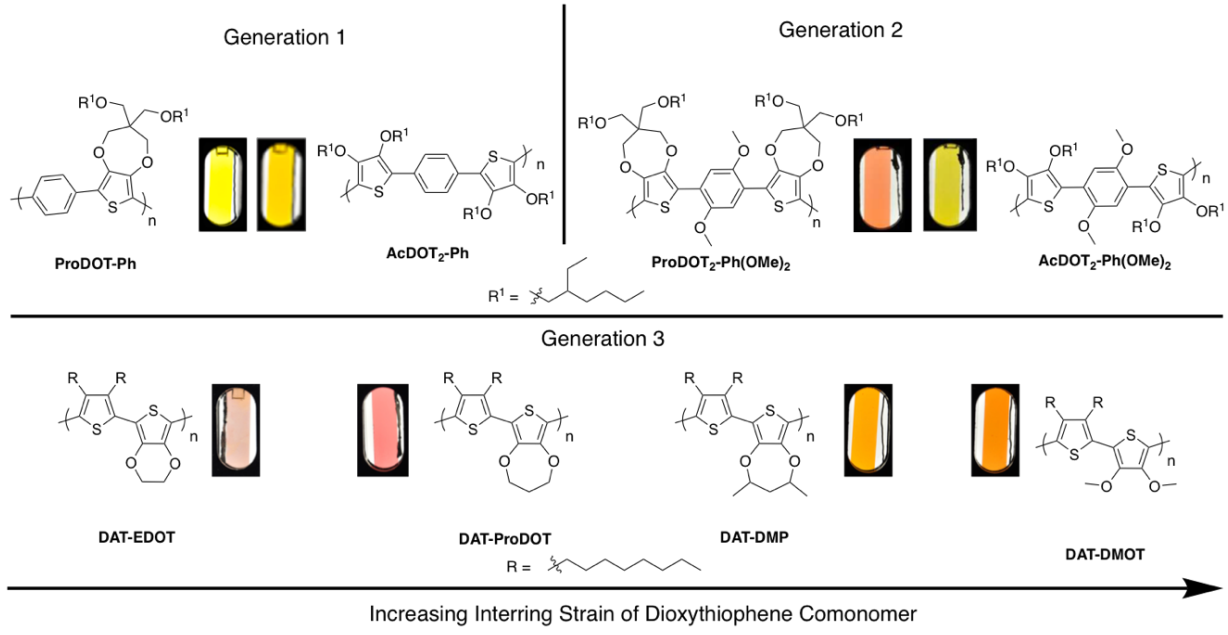

Figure 3.1.1. Key polymers in the progression of designing soluble, wide-gap electrochromic polymers.

In order to overcome the issues with the redox switching stability in high gap phenylene-containing ECPs, here the use of a dialkylthiophene (DAT) incorporated into alternating copolymers with dioxythiophenes to achieve a wide optical gap is reported. The DAT monomer synthesized and used for the generation 3 study, specifically 3,4-dioctylthiophene, provides interring strain with alkyl chains directly appended to the backbone helping the copolymers to reach wide optical gaps while blocking possible reactive sites for the radical cations. The octyl groups allow for the use of DOT monomers that do not have side chains and still yield soluble polymers than can be spray processed into thin films for characterization and use. The DOT comonomers were designed to vary in the interring strain they provide to the pi-conjugated backbone of the system. It is shown that increasing interring strain can be used to blue-shift the absorption of the polymers by over 70 nm to tune color between yellows, oranges, and reds. It is also shown that three of the copolymers show increased redox switching stability as films in solution compared to previous high gap ECPs with minimal drops in contrast over 1000 cycles in electrolyte solution. Due to its lack of color shifting upon repeated redox cycling the redox stability of DAT-DMP is investigated further in the construction of an encapsulated device containing DAT-DMP and a charge-storing polymer separated by a gel electrolyte. After an initial equilibration period of 200 switches, this device shows a contrast loss of <5 Δ%T after 10,000 cycles, which indicates a >81% retention of contrast overall.

3.2 Synthesis of DAT Copolymers *via* Direct Arylation

The synthetic approach to the monomer and polymer syntheses is shown in Scheme 3.2.1. Synthetic procedures, NMR spectra, and elemental analyses are located in the Experimental Section (3.8) and the GPC traces for all polymers are collated in supplementary Figure 3.7.1. Starting with commercially available 3,4-dibromothiophene a Kumada coupling afforded 3,4-

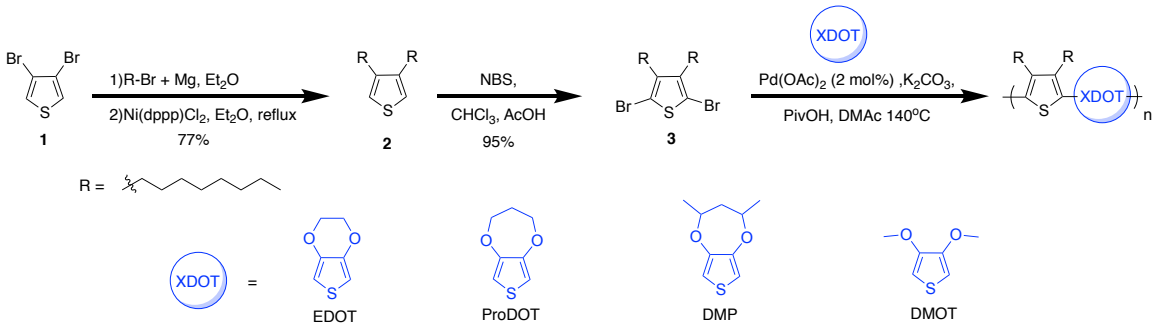

Scheme 3.2.1. Synthetic Approach to a Dialkylthiophene Monomer and Subsequent Direct Hetero Arylation Polymerization

dioctylthiophene, followed by subsequent bromination with NBS to form the desired 2,5-dibromo-3,4-dioctylthiophene. The synthetic scheme diverges from here where this compound can be used for direct hetero arylation polymerization with a dioxythiophene monomer to prepare the alternating copolymers **DAT-EDOT**, **DAT-ProDOT**, **DAT-DMP**, and **DAT-DMOT**.[144,152,153]

A comparison of polymerization yields and GPC estimated molecular weights are collated in Table 3.2.1. All of the polymers are soluble in toluene to at least 20 mg/mL allowing for airbrush spray processing and drop casting for film formation.

Table 3.2.1. GPC Estimated Polymer Molecular Weights and Polymerization Yields of DAT-XDOT Polymers

Polymer	Yield (%)	M_n (kDa)	M_w (kDa)	Đ
DAT-EDOT	79	61	143	2.3
DAT-ProDOT	81	32	81	2.6
DAT-DMP	77	25	56	2.2
DAT-DMOT	64	37	150	4.1

3.3 Electrochemical and Optical Properties

For electrochemical characterization, polymer films were drop cast onto Pt button electrodes from 3 mg/mL solutions in $CHCl_3$ to cover the electrode. Cyclic voltammetry (CV) and differential pulse voltammetry (DPV) were measured on films of the polymers in order to gain insight into how the different DOT comonomers affected the electrochemical properties of the resulting polymer (CV data is in supplementary Figure 3.7.2). Upon examining the electrochemical oxidation of the materials via DPV, Figure 3.3.1a, it can be seen that the onset of oxidation follows the trend of interring strain imposed by the DOT comonomer. As interring strain is increased from the least strained EDOT to the most strained DMOT, the resultant onset of oxidation (E_{ox}) ranges from -122 mV to +288 mV relative to Fc/Fc^+ giving a large window for tuning the desired optical switching potential (E_{ox} values are collated in Table 3.3.1). These polymers all have E_{ox} values below the polymers in the generation one high gap polymers (ProDOT-Ph and $AcDOT_2$-Ph). Both DAT-EDOT and DAT-ProDOT have E_{ox} values below that of the generation two polymers

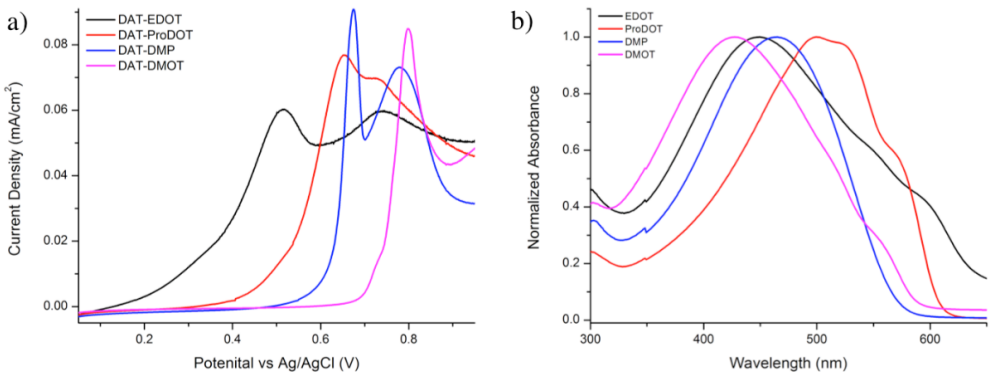

Figure 3.3.1. (a) Comparison of E_{ox} acquired via DPV for polymers on Pt button electrode in 0.5 M $TBAPF_6$/PC. Reference: -450 mV vs Fc/Fc^+. (b) Neutral state spectra of DAT-EDOT, DAT-ProDOT, DAT-DMP, and DAT-DMOT on ITO-coated glass in 0.5 M $TBAPF_6$/PC electrolyte solution after 10 CV electrochemical conditioning cycles.

(ProDOT$_2$-Ph(OMe)$_2$ and AcDOT$_2$-Ph(OMe)$_2$) at -122 mV and 74 mV respectively. The DAT-DMP and DAT-DMOT polymers' E_{ox} values fall between ProDOT$_2$-Ph(OMe)$_2$ and AcDOT$_2$-Ph(OMe)$_2$ with 180 mV and 288 mV respectively.

For optical characterization, polymer films were airbrush sprayed onto glass/ITO electrodes from 3 mg/mL solutions in toluene, and the films subjected to 10 CV cycles before UV/Vis was measured (as cast film spectra are in Supplementary Figure 3.7.3). While DAT-ProDOT, DAT-DMP, and DAT-DMOT all formed nice smooth films from this method, DAT-EDOT films were consistently hazy which is indicative of induced order during film formation. Figure 3.3.1b shows the UV-Vis spectra of the films of the polymers after electrochemical conditioning. The UV/Vis absorption data is collated in Table 3.3.1 in order of increasing λ_{max} including the previous generation polymers. It is important to note that the λ_{max} and E_g do not follow the same trend as there is varying absorption broadness between the different polymers. This varying broadness manifests itself in the color of the polymer films not correlating with λ_{max}, as these polymers span the yellow-orange-red region. It should be noted that when comparing as cast films to conditioned films the polymers' absorbances typically exhibit varying degrees of red-shifting and broadening. When a polymer film is sprayed from a high vapor pressure solvent it is deposited in a kinetically determined morphology as the solvent evaporates.[154] Upon electrochemical oxidation, the conjugated polymer must enter a more quinoid like structure that causes its backbone to planarize and extend the effective conjugation length of the chromophore. Upon reduction back to the neutral state, the polymer geometry retains a more planar geometry (relative to the as cast film) leading to a longer effective conjugation length and red-shifted absorbance. This typical red-shifting upon cycling was not observed for DAT-DMP as its absorbance exhibited a small blue-shift of its onset of ~5 nm.

Table 3.3.1. Optical and Electrochemical Properties of DAT-XDOT Polymers

Polymer	E_{ox}[a] (mV) vs Fc/Fc^+	λ_{max} (nm)[b]	E_g[b,c] (eV)
DAT-DMOT	288	427	2.10
$AcDOT_2$-$Ph(OMe)_2$[d]	330	446	2.38
ProDOT-Ph[d]	451	448	2.44
DAT-EDOT	-122	448	1.88
$AcDOT_2$-Ph[d]	438	464	2.30
DAT-DMP	180	466	2.19
DAT-ProDOT	74	500	2.03
$ProDOT_2$-$Ph(OMe)_2$[d]	126	500	2.18

[a] As determined by DPV as the onset of the current for oxidation. [b] For films cast onto ITO-coated glass measured after 10 CV cycles listed in order of increasing wavelength. [c] Bandgap determined by onset of light absorption. [d] Values from reference 58.

3.4 Spectroelectrochemistry and Color Properties

Spectroelectrochemical measurements were performed on polymer films sprayed on ITO-glass in 0.5 M $TBAPF_6$ in propylene carbonate with a platinum counter electrode and a Ag/AgCl reference electrode with results shown in Figure 3.4.1 along with photographs of the films held at potential extremes dictated by the CV results. Optical contrast at λ_{max} and the L*a*b* values are collated in Table 3.4.1. Upon electrochemical conditioning of electrochromic polymers the UV-Vis absorption typically exhibits a characteristic red-shift of the absorbance as the polymer extends its effective conjugation in the charge neutral state.

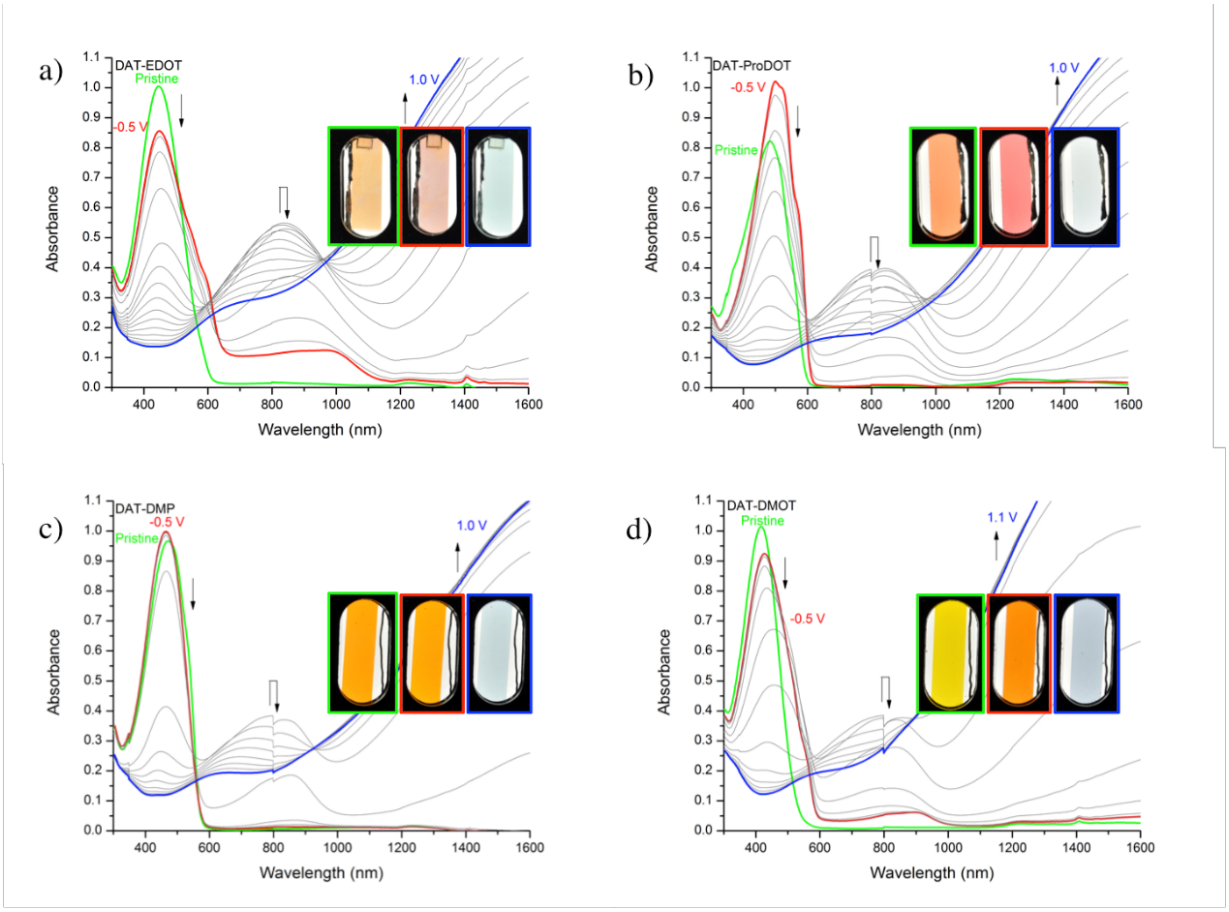

Figure 3.4.1. Spectroelectrochemistry and photographs of (a) DAT-EDOT, (b) DAT-ProDOT, (c) DAT-DMP, and (d) DAT-DMOT. The applied potential was increased in 50 mV steps between the fully colored and bleached states in 0.5 M $TBAPF_6$/PC. The arrows show the progression of the peak evolution as a function of increasing potential.

As a pristine film, DAT-EDOT shown in Figure 3.4.1a absorbs with a λ_{max} of 448 nm giving rise to the orange color of the material. As can be seen in the photography it can be noted that this polymer forms relatively hazy films. Upon electrochemical break in there is a red-shifting of the onset of absorbance with the appearance of a shoulder at 650 nm, but there is a drop in absorbance at λ_{max} and a low intensity, broad absorbance between 600 nm and 1100 nm indicative of polaron trapping. This broad absorption gives rise to the observed muted pink color of the

material. It in unknown whether this phenomenon is caused by either chemical or morphological differences from the other polymers. The trapping in DAT-EDOT is hypothesized to be due to the oxidation of this polymer causing the formation of local potential wells where the polaron is energetically trapped. Upon oxidation, the polaronic peak is still present, and leads to a fairly asymmetric tailing across the visible and a slightly blue hue remains compared to the other polymers. The as cast film of DAT-ProDOT shown in Figure 3.4.1b absorbs with a λ_{max} of 491 nm, thus giving rise to a vibrant orange color. Upon break in, this polymer exhibits an increase in absorbance along with the characteristic red-shifting to a λ_{max} of 500 nm leading to a red colored polymer with no peaks indicating trapped polarons. Upon oxidation, this polymer's spectrum is flat across the visible giving a highly color neutral and transmissive state. DAT-DMP as a pristine film, shown in Figure 3.4.1c, absorbs with a λ_{max} of 466 nm. Upon break in, this spectrum exhibits a slight blue-shift in onset with a λ_{max} and observable color that remained unchanged as a vibrant orange is observed in both states. Note that this polymer also does not show any indication of trapped polarons. In the oxidized state this polymer shows the highest color neutrality with a spectrum that is flat across the visible region. The as cast film of DAT-DMOT, shown in Figure 3.4.1d, has the highest energy λ_{max} of 421 nm and a vibrant yellow color, which was expected due to the increased interring strain compared to the other polymers. Upon break in the red-shift caused by relief of ring strain can be observed with the color shifting to an orange. There is also a small amount of absorbance between 600 nm and 1000 nm indicative of slight polaron trapping. This polaronic absorption can be seen again in the oxidized state with slight increased tailing into the visible from the NIR similar to that of DAT-EDOT and leading to a slightly blue hued transmissive state.

Table 3.4.1. Color and Switching Properties of DAT-XDOT Polymers

Polymer	Δ%T[a, b] ($at\lambda_{max}$)	Neutral State L*, a*, b* color coordinates[b]	Oxidized State L*, a*, b* color coordinates[b]
DAT-EDOT	58	65, 24, 36	83, -5, -8
DAT-ProDOT	63	60, 68, 34	86, -4, -8
DAT-DMP	65	87, 23, 59	90, -2, -4
DAT-DMOT	60	82, 25, 62	85, -1, -7
ProDOT-Ph[c]	67	87, 21, 73	88, -1, -3
$AcDOT_2$-Ph[c]	51	87, 9, 76	87, 2, 4
$ProDOT_2$-$Ph(OMe)_2$[c]	70	80, 47, 36	91, -1, -1
$AcDOT_2$-$Ph(OMe)_2$[c]	59	89, -4, 85	81, -1, -1

[a] Difference between steady-state transmittance measured at fully oxidized and fully neutral states (all films sprayed to 10%T at λ_{max}). [b] For a film cast onto ITO-coated glass. [c] Values from reference 39.

Colorimetry utilizing the L*a*b* color space, where a*b* values correlate to the chroma or saturation of a color (note: −a* and +a* correspond to green and red and −b* and +b* correspond to blue and yellow, respectively) and L* depicts the lightness (a value of 0 would be black and 100 would be white.), was used to demonstrate the control over colors in the neutral states. The a*b* color space results for the polymer films under study are presented graphically in Figure 3.4.2. In the neutral state, after electrochemical break-in, the polymers had L* values ranging from 60 to 87, a* values ranging from 23 to 68, and b* values ranging from 34 to 62, thus remaining in the yellow-orange-red color space similar to the color coordinates for the previous generations' ECPs

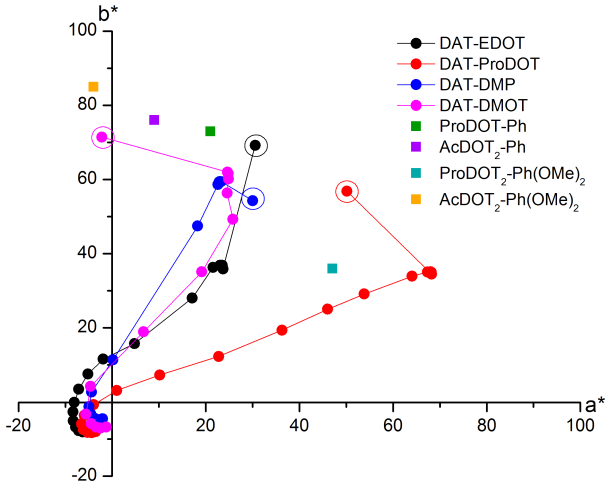

Figure 3.4.2. Colorimetric analysis of all the polymers. Plots of a*b* color coordinates at increasing applied potentials in 0.1 V steps from neutral (0 V vs. Ag/AgCl) to fully oxidized states (1.0 V for DAT-EDOT, 1.0 V for DAT-ProDOT, 1.0 V for DAT-DMP, and 1.1 V for DAT-DMOT).

also shown in Figure 4. In the oxidized states, the transmissive forms had L* values increased to range from 83 to 90, with low a* values ranging from −5 to -1, and b* values ranging from −8 to -4.As the magnitudes of a* and b* increase, the colors become more saturated, and as one traverses between color points, the hue changes.

In this figure, measurements were performed in 0.5 M $TBAPF_6$/PC of films spray-cast onto ITO/glass electrodes. The polymer neutral states are furthest from the origin and the values track toward the origin as the polymer is oxidized to the bleached state. The encircled points indicate the a*b* coordinates of the as cast/pristine polymer before electrochemical cycling. The points not connected by lines are the neutral state a*b* coordinates of the previous generations' polymers. It can be seen that, upon break in, the change in color coordinates are greatest for DAT-ProDOT and DAT-DMOT with a decrease in a* and increase in b* indicating a red-shifting absorbance, while

DAT-EDOT and DAT-DMP do not exhibit this characteristic change in color coordinates. DAT-EDOT's color coordinates move towards the origin upon break in showing a drastic decrease in color vibrancy caused by the apparent polaron trapping seen in the spectroelectrochemistry. DAT-DMP's color coordinates actually show a slight increase in a* and decrease in b* which can be explained by the slight blue-shift in the onset of absorbance of the film upon break in. This is observed as only a small shift in color of the material upon break-in (remaining orange), which allows for ease of predicting the polymer's usefulness in color mixing.

After the initial electrochemical break in all of the polymers lie within the desired yellow-orange-red color space (positive a* and positive b*) and upon electrochemical oxidation the color coordinates are shifted close to the origin indicating color neutrality. In the neutral state, DAT-EDOT shows the least saturation of color with an L*a*b* of 65, 24, 36 but does reach a highly transmissive oxidized state with an L*a*b* of 83, -5, -8 further evidence that polaron trapping is the cause of the loss of contrast as the oxidized state of the material is still highly transmissive. DAT-DMOT and DAT-DMP both show similar neutral state color coordinates of 82, 25, 62 and 87, 23, 59 respectively. DAT-DMP does show a slightly more color neutral and transmissive oxidized state with color coordinates of 90, -2, -4 compared to 85, -1, -7 for DAT-DMOT. The polymer film of DAT-ProDOT has a high b* with color coordinates at 60, 68, 34 giving rise to its vibrant orange-red color. This polymer still oxidizes to a highly transmissive and color neutral state with color coordinates of 86, -4, -8.

The small structural changes allowed for varying interring steric strain between these polymers and led to small yet distinct changes in color. The human eye is sensitive to small changes in absorption, making this approach to color tuning advantageous. Increasing interring steric strain

causes blue-shifting absorbance at the cost of increasing oxidation potential. This trade off must be balanced when attempting to control color and redox activity.

3.5 Film Switching Stability

Redox switching stability of these wide gap systems has been one of the larger hurdles for obtaining useable materials, both as vibrant color switching ECPs and for creating high contrast black to transmissive polymer blends. To this end examining the contrast as a function of the number of switches gives a platform to compare materials, Figure 3.5.1. In order to examine the

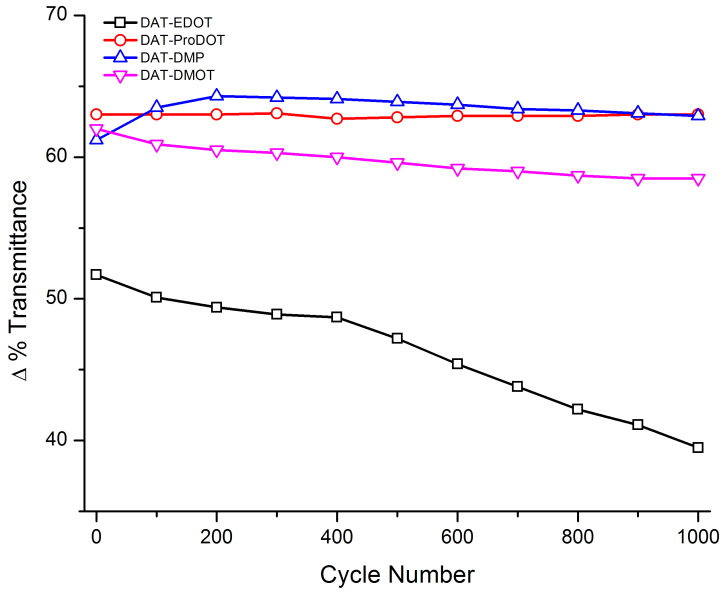

Figure 3.5.1. Contrast loss of ECP films measured relative to a glass/ITO background at λ_{max} as a function of number of switches in 0.5 M $TBAPF_6$/PC electrolyte solution with repeated square-wave potential steps for 1000 cycles. DAT-EDOT measured -0.5 to 1.0 V at 5 second steps, DAT-ProDOT measured from -0.5 to 1.0 V at 5 second steps, DAT-DMP measured from -0.5 to 1.0 V at 5 second steps, and DAT-DMOT measured from -0.5 to 1.1 V at 7 second steps.

electrochemical redox stability of these polymers, films of each were sprayed to 10 %T on ITO glass and the transmittance at λ_{max} was monitored over the course of 1000 repeated square-wave potential steps for 1000 cycles in 0.5 M $TBAPF_6$/PC electrolyte solution that had been thoroughly dried and degassed with argon. Figure 3.5.1 details the relationship between optical contrasts of the polymer films as a function of the number of electrochemical switches (% transmittance vs time data is available in supplementary Figure 3.7.4). It should be noted that the experiment was started after an electrochemical break in of 10 CV cycles in order to monitor the proper peak maxima.

This break in explains why DAT-EDOT has an initial contrast of only 53 Δ%T. The polymer shows signs of a large amount of polaron trapping after the first electrochemical switch, as seen in the spectroelectrochemistry. The film only loses more contrast over the course of the 1000 electrochemical switches, ultimately dropping below 40 Δ%T. This polymer shows the most rapid decrease in contrast, which is attributed to the observations of polaron trapping, which becomes more pronounced over the course of repeated electrochemical cycling. The other polymers all show initial contrasts above 60 Δ%T. DAT-DMOT shows an initial contrast of 64 Δ%T and over the course of the experiment only sees a slight drop in contrast to 59 Δ%T on the final switch. DAT-ProDOT shows an initial contrast of 65 Δ%T and maintains this contrast over the course of the experiment with no measurable loss. DAT-DMP shows an initial contrast of 63 Δ%T and over the course of the experiment there is a slight increase in contrast in the first few hundred switches that levels off at 65 Δ%T. This indicates that there is a larger break in period required for this polymer to reach an equilibrium state, but the films retain a high contrast with minimal color change throughout. Especially important DAT-ProDOT, DAT-DMP, and DAT-DMOT all show significant increases in film switching stability compared to previous generations of wide gap

electrochromic polymers, with only $ProDOT_2$-$Ph(OMe)_2$ showing redox stability for up to 100 switches.

3.6 Device Switching Stability

With the results obtained and discussed above, DAT-DMP was identified as the best candidate for further examination when considering the use of these polymers as the high-energy absorption component to create black to transmissive switching films.[156] DAT-EDOT is not as redox stable as the other materials and DAT-ProDOT absorbs at too low an energy to serve this purpose. While both DAT-DMOT and DAT-DMP absorb the high energy portion of the spectrum, DAT-DMP does not shift in absorbance after redox cycling making it the best candidate for further examination. In order to further probe the material's redox stability, an electrochromic device was fabricated and switching stability was tested over 10,000 cycles.

Figure 3.6.1 details the evolution of the transmittance at λ_{max} in both the neutral and oxidized states every 1000 cycles (The measured spectra are located in supplementary Figure 3.7.5). There is an initial 200 cycles for device equilibration of the MCCP and ECP charge storages. It can be seen that there is minimal change in the neutral state over the course of the experiment indicating the color is not changing over the course of the cycles. The oxidized state does show small decreases in transmittance indicative of charge imbalance in the device and/or degradation of the MCCP as the decrease in absorbance corresponds to absorbance from the DAT-DMP film. A lack of charge in the charge storage layer, by either degradation or imbalance relative to the amount of DAT-DMP, would cause the DAT-DMP layer to retain absorbance. The disappearance of the peak at 380 nm upon reduction indicates that the MCCP is not degrading to give rise to this peak. This peak is likely due to imbalance in the device. After this device's electrochemical conditioning the oxidized state the device remains consistent over the course of 10,000 switches showing a drop in

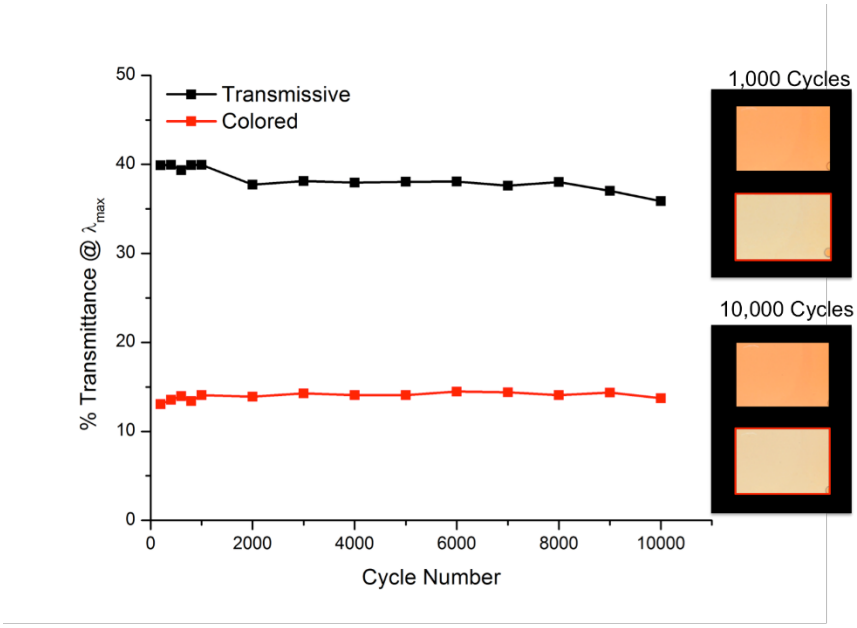

Figure 3.6.1. Transmittance of the transmissive and colored states measured relative to an air background at λ_{max} versus number of switching cycles in DAT-DMP device with repeated square-wave potential steps for 10,000 cycles measured -0.5 V to +0.6 V at 5 second steps and pictures at 1,000 and 10,000 cycles.

contrast of 4.7 Δ%T. Most noteworthy is that the %T in the colored state remains consistent over the course of the entire cycling period indicating that the polymer electrochrome is redox stable in the encapsulated device over this cycling range.

3.7 Conclusions and Perspective

The structure−property relationships of wide-gap electrochromic polymers based on repeat units of electron-rich dioxythiophenes of varying steric bulk in alternation with dioctylthiophene were examined. ECPs were obtained with yellow, orange, and red neutral states that switch to colorless oxidized states. The understanding of how small changes in structure allows control of

absorption properties in this color space allows for a more informed approach to accessing yellow, orange, and red ECPs with a specific target hue in mind.

It is shown that the synthetic effort of incorporating dioctylthiophene units in place of the phenylenes improves redox stabilities, lowers oxidation potentials, and allows for the use of DOTs without long side chains as comonomers while maintaining a wide optical gap and solution processability. However, with the EDOT system, the presence of trapped polarons cause a fast degradation of the colored state in an electrochemical cell. Moving to more strained systems allowed for tuning the color to a more orange hue, while maintaining low oxidation potentials and redox stabilities that last over 1,000 switches as a film in electrolyte solution. From this understanding, an absorptive/transmissive electrochromic device with DAT-DMP was made to show that there is minimal contrast loss over 10,000 switches. This redox cycling stability is enhanced by two orders of magnitude in number of cycles than previous generation wide gap ECP based devices. This approach could be adapted to other systems by incorporating moieties that block potential reactive sites on the polymer backbone to improve redox stability. The incorporation of the dioctylthiophenes in place of phenylene rings improved upon previous designs of high bandgap ECPs, bringing the field closer to having a full color palette of stable, high-performance ECPs.

3.8 Supplementary Figures

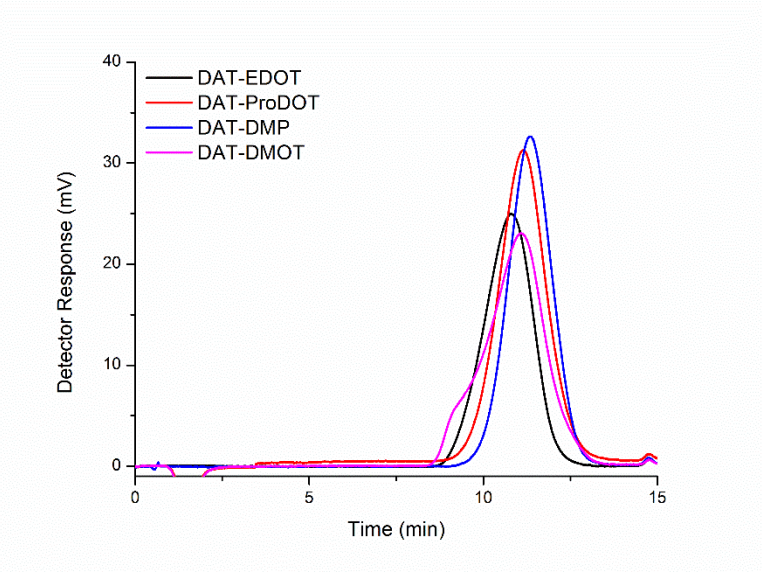

Figure 3.7.1. GPC traces of DAT-EDOT, DAT-ProDOT, DAT-DMP, DAT-DMOT in $CHCl_3$ at 40 ^oC.

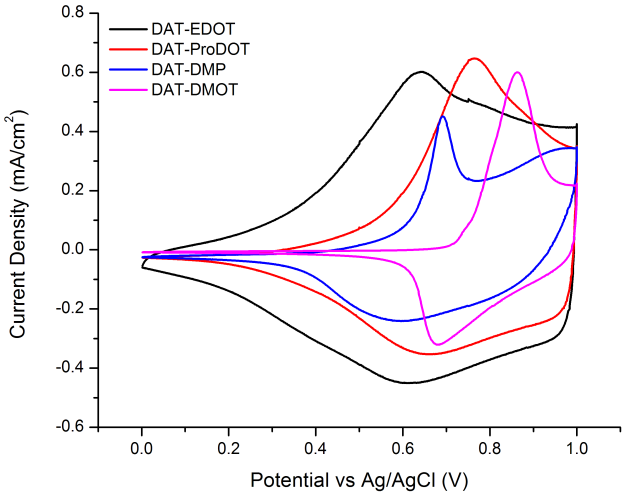

Figure 3.7.2. Comparison of CV of DAT-EDOT, DAT-ProDOT, DAT-DMP, DAT-DMOT on Pt button electrode in 0.5 M $TBAPF_6$ /PC. Reference: -450 mV vs Fc/Fc^+.

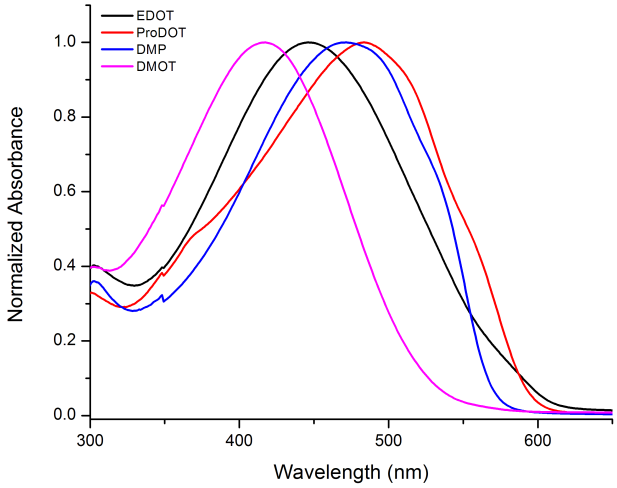

Figure 3.7.3. Neutral state as cast UV-Vis spectra of DAT-EDOT, DAT-ProDOT, DAT-DMP, DAT-DMOT on ITO-coated glass in 0.5 M TBAPF$_6$/PC electrolyte solution.

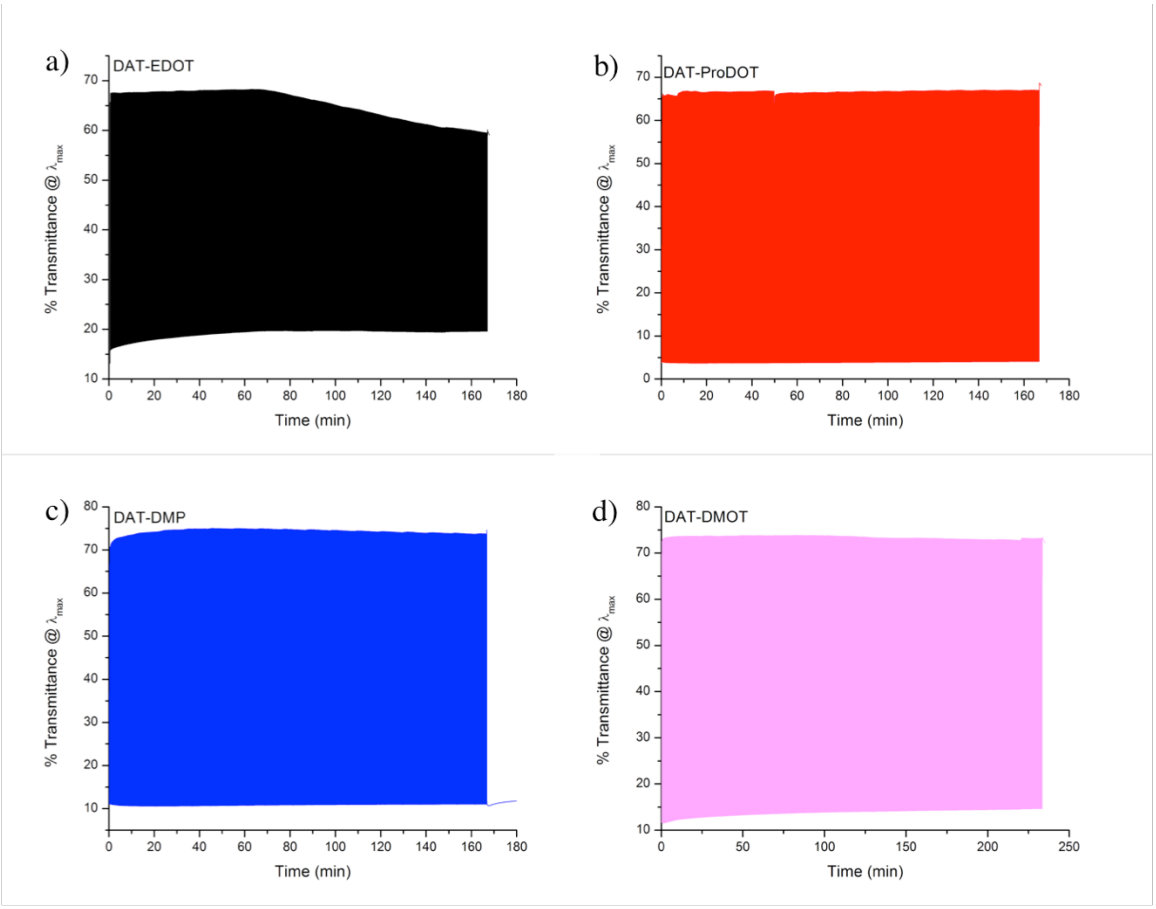

Figure 3.7.4. Long-term stability study of all polymers in 0.5 M $TBAPF_6$/PC electrolyte solution for 1000 cycles. (a) DAT-EDOT measured at 448 nm from -0.5 to 1.0 V at 5 second steps, (b) DAT-ProDOT measured at 500 nm from -0.5 to 1.0 V at 5 second steps, (c) DAT-DMP measured at 466 nm from -0.5 to 1.0 V at 5 second steps, and (d) DAT-DMOT measured at 427 nm from -0.5 to 1.1 V at 7 second steps.

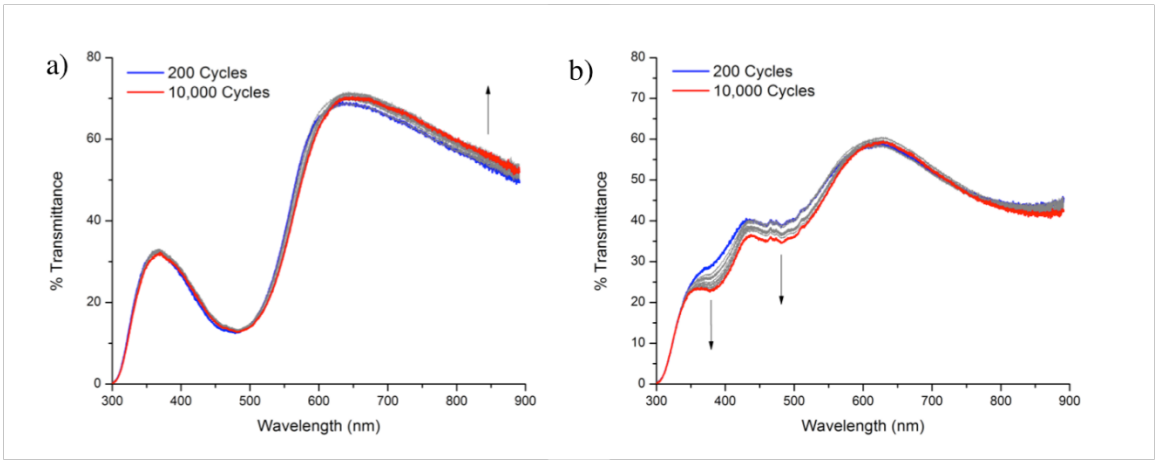

Figure 3.7.5. Evolution of transmittance spectra of DAT-DMP device with repeated over 10,000 cycles for the (a) colored and (b) transmissive states. Each spectrum is a step of 200 cycles up to 1000 switches, and every 1,000 cycles up to 10,000 switches.

3.9 Synthetic Procedures

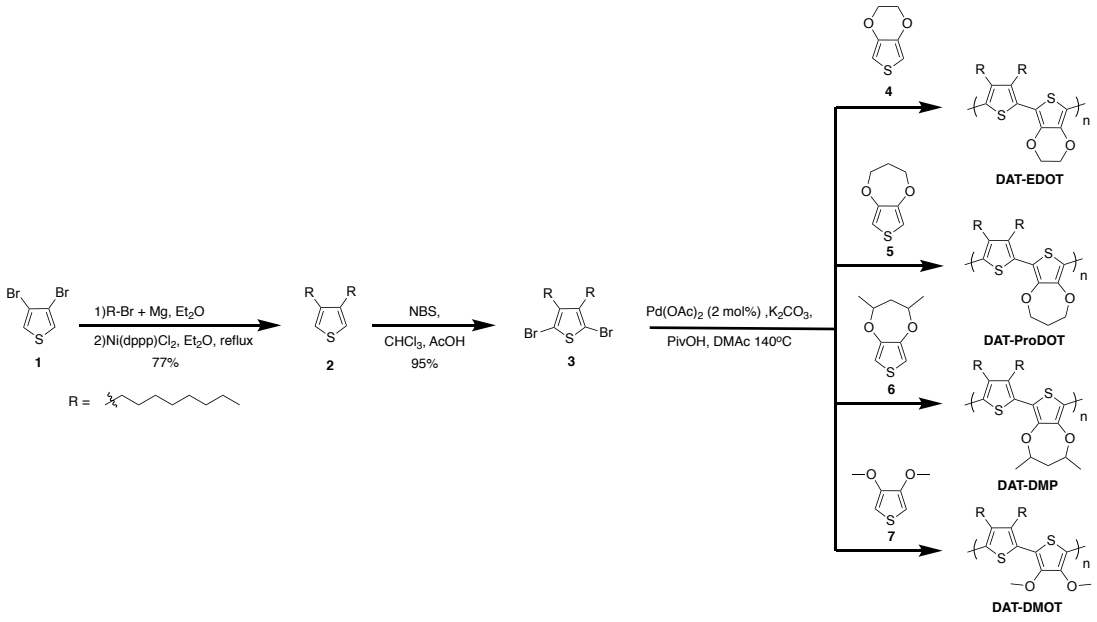

Scheme 3.8.1. Synthetic Outline of DAT-XDOT Polymers

3,4-dioctylthiophene (2): Into a 1000 mL 3-neck round bottom flask with a stir bar, addition funnel, and condenser was added **1** (20.0 g, 82.7 mmol), Ni(dppp)Cl_2 (672 mg, 1.24 mmol), and 600 mL dry Et_2O. This mixture was cooled on ice while Mg (4.825 g, 198.4 mmol) was flame dried under vacuum in a 250 mL, 2-neck round bottom flask with a condenser attached. Et_2O (100 mL) was transferred to the 250 mL flask via a cannula. 1-bromooctane (38.33 g, 198.4 mmol) was added drop-wise to the 250 mL flask via a syringe as the reaction was maintained at mild reflux, and then the reaction was heated to reflux for another 30 minutes upon completion of addition. The mixture was transferred to a pressure equalizing addition funnel via cannula and added to the 600 mL flask drop-wise over 1 hour. The mixture was heated to reflux for 24 hours then cooled to room temperature and placed in an ice bath. Another addition funnel was charged with 125 mL of 0.2 M HCl and the reaction was quenched drop-wise until a pH of 6 was reached. The mixture was poured into 300 mL of 0.2 M HCl and extracted with Et_2O (3 x 100 mL). The organic fractions were combined, dried over $MgSO_4$, and solvent was removed in vacuo to form a orange oil. The oil was passed through a silica plug with hexanes to yield yellow oil. The product was purified by vacuum distillation (bp 170 ^oC at 10 mbar) to give a clear oil with a yield of 77%. ^1H NMR ($CDCl_3$, ppm): δ 6.90 (s, 2H), 2.54-2.49 (t, 4H, J=7.8 Hz), 1.68-1.58 (p, 4H, J=7.2 Hz), 1.46-1.22 (br, m, 20H), 0.93-0.88 (t, 6H, J=6.3 Hz); $^{13}C\{^1H\}$ NMR ($CDCl_3$, ppm): δ 142.10, 119.86, 31.92, 29.68, 29.64, 29.51, 29.31, 28.88, 22.70, 14.13.

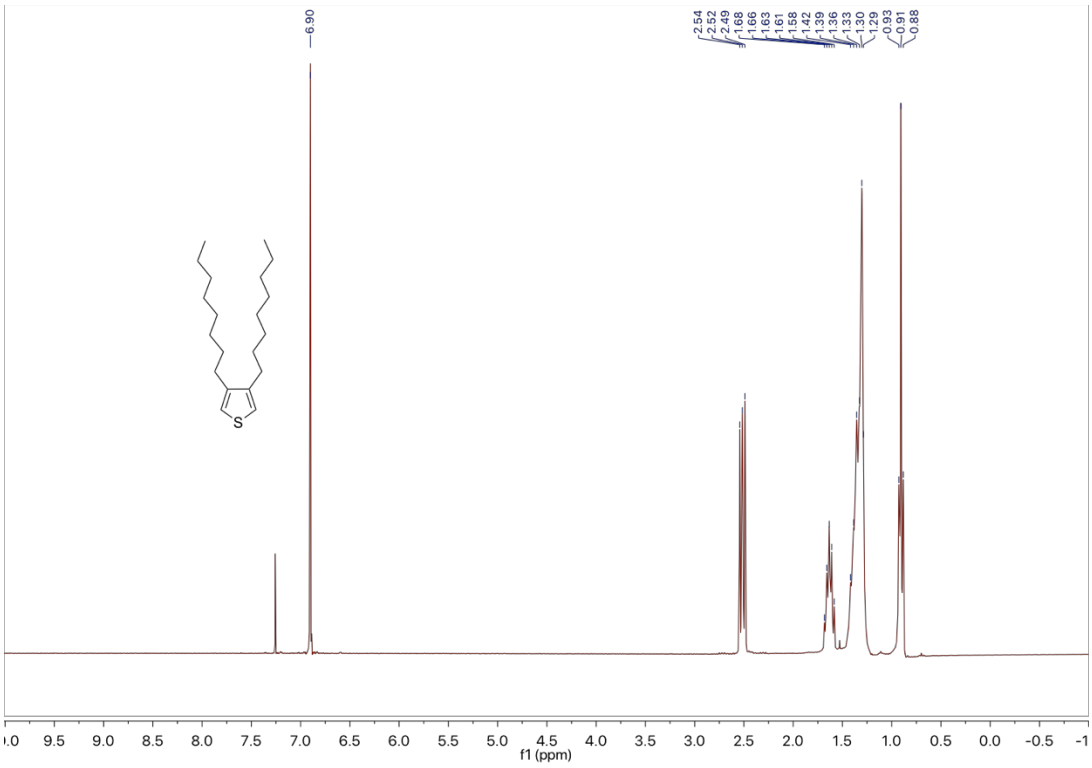

^{1}H NMR for **3,4-dioctylthiophene (2)**

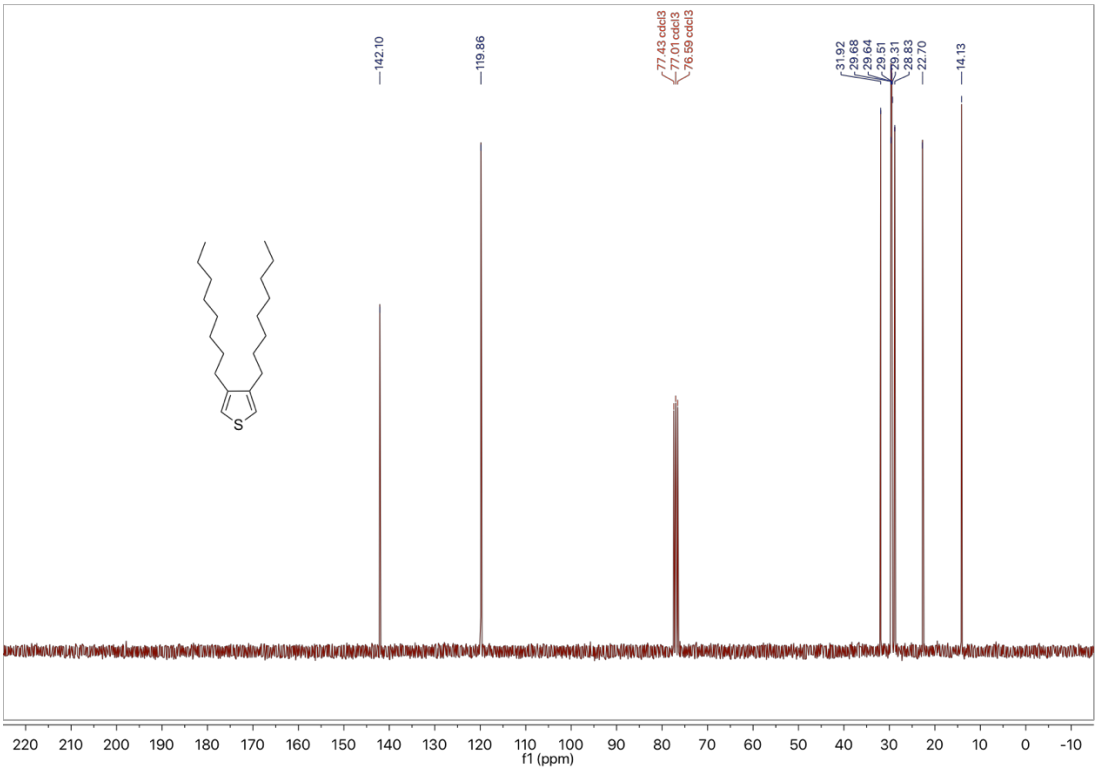

^{13}C{^{1}H} NMR for **3,4-dioctylthiophene (2)**

2,5-dibromo-3,4-dioctylthiophene (3): Into a 250 mL round bottom flask with a stir bar was added **2** (4.00 g, 13.0 mmol), $CHCl_3$ (40 mL), and AcOH (20 mL). The solution was cooled in an ice water bath to 0 ˚C. NBS (5.30 g, 29.8 mmol) was added in two portions and then the mixture was refluxed for two hours. The reaction was cooled to room temperature and 150 mL of H_2O was added. The reaction was extracted with DCM (3 x 40 mL) and the combined organic extracts were washed with H_2O (2 x 100 mL) and brine (50 mL). Solvent was removed from the organic layer. The compound was purified by column chromatography with hexanes as the eluent to afford a clear oil with a yield of 95%. ^{1}H NMR ($CDCl_3$, ppm): δ 2.53-2.48 (t, 4H, J=7.5 Hz), 1.53-1.41 (p, 4H, J=7.2 Hz), 1.40-1.24 (br, m, 20H), 0.93-0.85 (t, 6H, J=6.6 Hz); ^{13}C{^{1}H} NMR ($CDCl_3$, ppm): δ 141.44, 107.78, 31.87, 29.54, 29.53, 29.31, 29.22, 28.95, 22.67, 14.11.

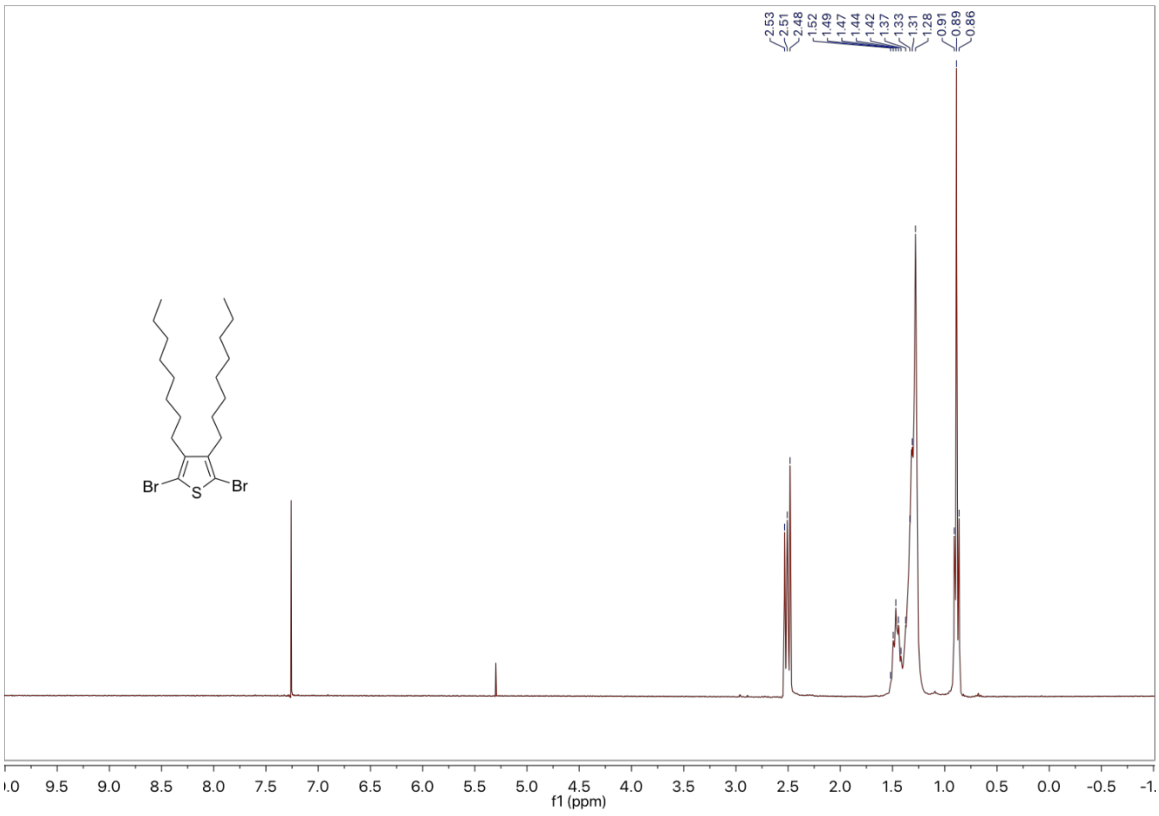

^{1}H NMR for **2,5-dibromo-3,4-dioctylthiophene (3)**

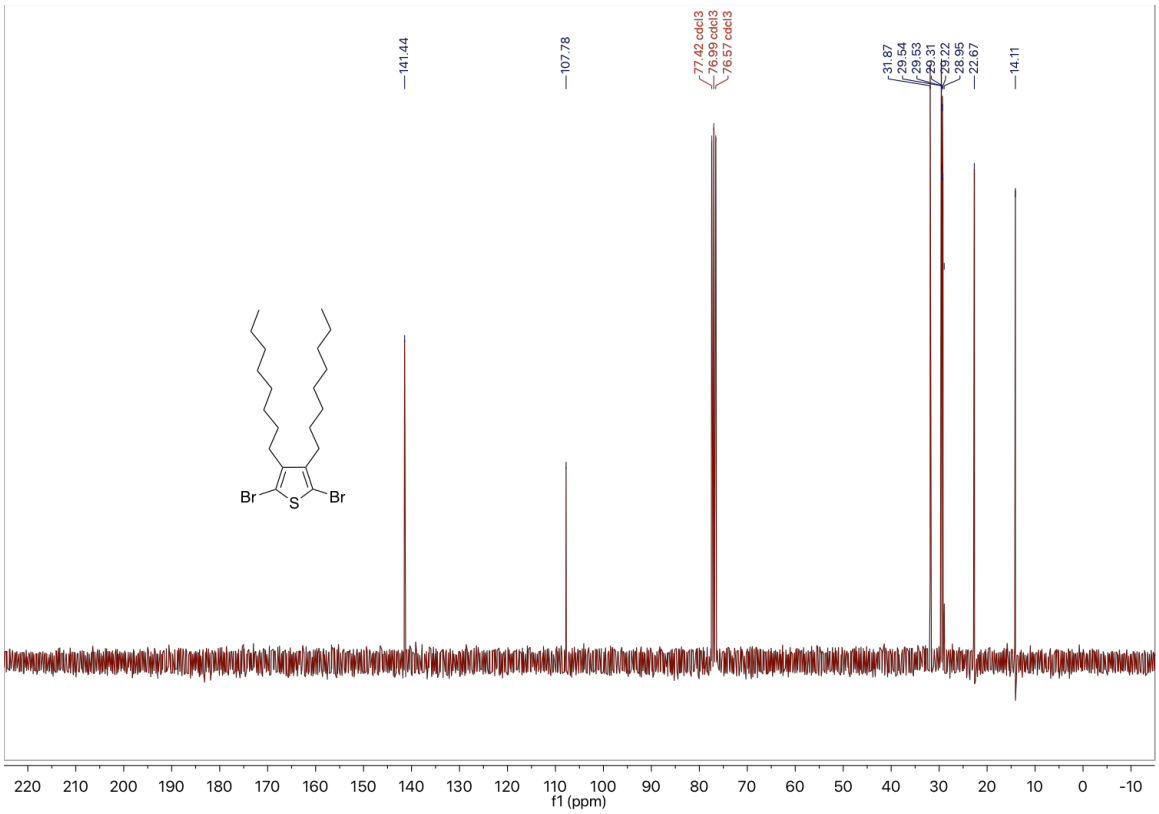

$^{13}C\{^{1}H\}$ NMR for **2,5-dibromo-3,4-dioctylthiophene (3)**

General Polymerization Procedure: To a 50 mL schlenk tube equipped with a stir bar, the dibromide monomer **3** (0.500 g, 1.07 mmol), dihydrin monomer (**4**, **5**, **6**, or **7**) (1.07 mmol), 2 mol% palladium acetate (4.8 mg, 0.021 mmol), pivalic acid (0.109 g, 1.07 mmol), and potassium carbonate (0.445 g, 3.21 mmol) were added. The mixture was then vacuum purged for 45 minutes followed by three purge and argon back-fill cycles. N,N-dimethylacetamide (10.8 mL) was degassed by bubbling with argon for 45 minutes and then injected into the flask to dissolve the contents. The reaction mixture was stirred at 140 ˚C for 24 hours and then removed from the heat and allowed to cool to r.t. The polymer dispersion was dissolved with $CHCl_3$ and precipitated into methanol and stirred for 45 minutes. The precipitate was filtered into a soxhlet extraction thimble and washed with methanol, acetone, hexanes, and chloroform respectively. The washings were conducted until color was no longer observed during extraction. After dissolution from the soxhlet

thimble, the solvent was removed via rotovap and then 20 mL of chloroform was added followed by 100 mg of the palladium scavenger diethylammonium diethyldithiocarbamate, 150 mg of 18-crown-6 and then stirred for 6 hours at 50 ◦C. The polymer was then precipitated into 300 mL of methanol. The precipitate was filtered over a 0.45 μm Nylon pad and washed with 300 mL of pure methanol and allowed to dry. The dried material was collected into a tared vial and vacuum dried.

Poly(3,4-dioctylthiophene-co-2,3-dihydrothieno[3,4-*b*][1,4]dioxine) (DAT-EDOT): Orange-red solid in 79% yield (572 mg). ^{1}H NMR (300 MHz, CHCl3) δ 4.31 (br s, 4H), 2.69 (br s, 4H), 1.56 (br s, 4H), 1.46-1.19 (br, m, 20H), 0.93-0.78 (br t, 6H). Anal. calcd. for $C_{26}H_{38}O_2S_2$ C 69.91, H 8.57, S 14.35 Found C 69.76, H 8.41, S 14.07. GPC: Mn: 61.3 kDa, Mw: 142.9 kDa, Đ: 2.33, in $CHCl_3$ vs PS.

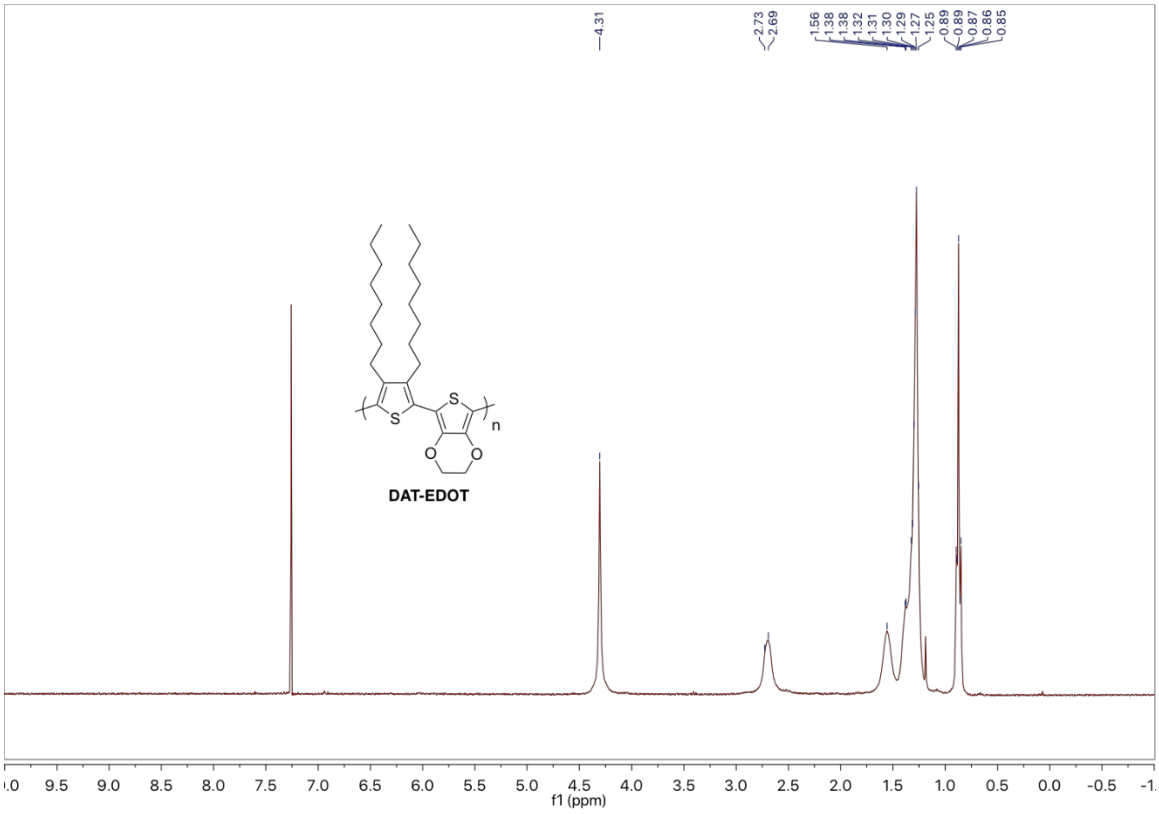

^{1}H NMR for **DAT-EDOT**

Poly(3,4-dioctylthiophene-co-3,4-dihydro-2*H*-thieno[3,4-*b*][1,4]dioxepine) (DAT-ProDOT): Orange-red solid in 81% yield (586 mg). ^{1}H NMR (300 MHz, CHCl3) δ 4.21 (br t, 4H), 2.71 (br s, 4H), 2.27 (br t, 2H), 1.56 (br s, 4H), 1.45-1.20 (br, m, 20H), 0.92-0.80 (br t, 6H). Anal. calcd. for $C_{27}H_{40}O_2S_2$ C 70.39, H 8.75, S 13.92 Found C 70.10, H 8.57, S 13.62. GPC: Mn: 31.7 kDa, Mw: 81.1 kDa, Đ: 2.56, in $CHCl_3$ vs PS.

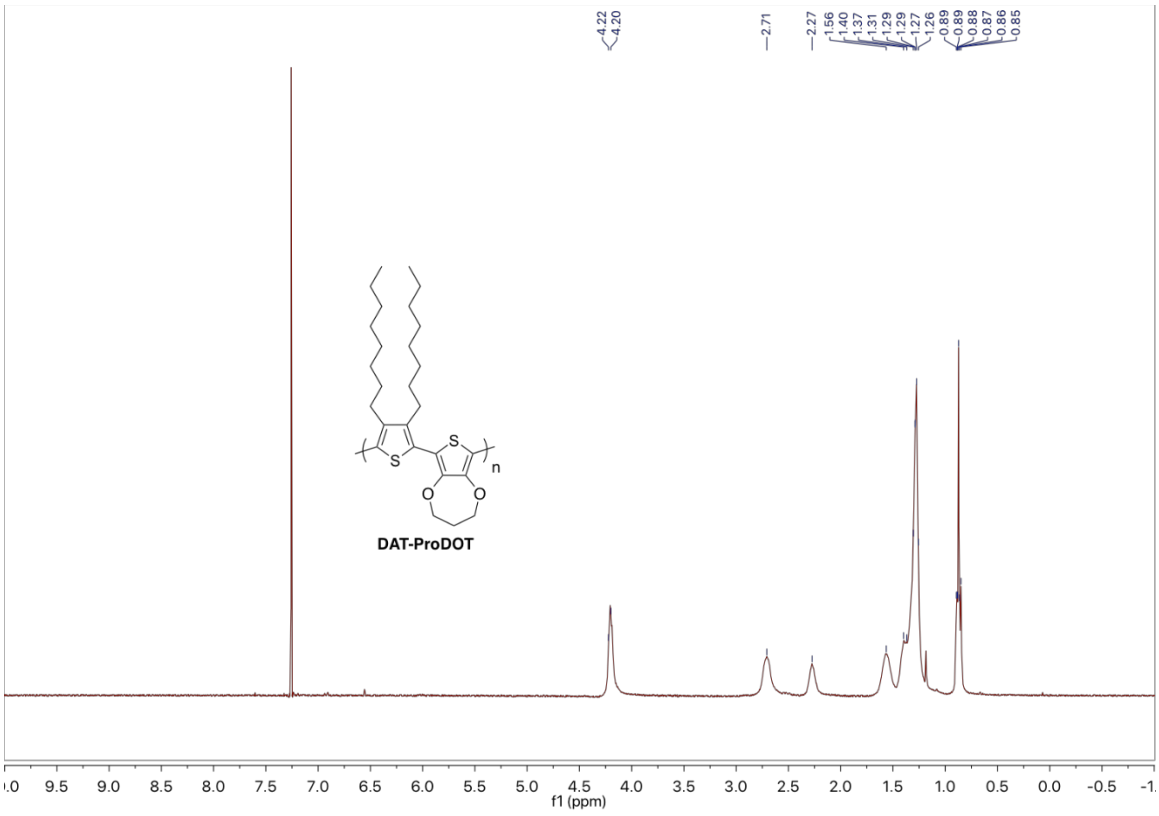

^{1}H NMR for **DAT-ProDOT**

Poly(3,4-dioctylthiophene-co-2,4-dimethyl-3,4-dihydro-2*H*-thieno[3,4-*b*][1,4]dioxepine) (DAT-DMP): Orange solid in 77% yield (610 mg). ^{1}H NMR (300 MHz, CHCl3) δ 4.69-4.55 (br, 1H), 4.13-3.96 (br, 1H), 2.85-2.61 (br, 4H), 2.22-1.90 (br, 2H), 1.74-1.12 (br m, 30H), 0.94-0.79 (br t, 6H). Anal. calcd. for $C_{29}H_{44}O_2S_2$ C 71.26, H 9.07 S 13.12 Found C 70.99, H 8.93, S 12.96. GPC: Mn: 25.2 kDa, Mw: 56.2 kDa, Đ: 2.23, in $CHCl_3$ vs PS.

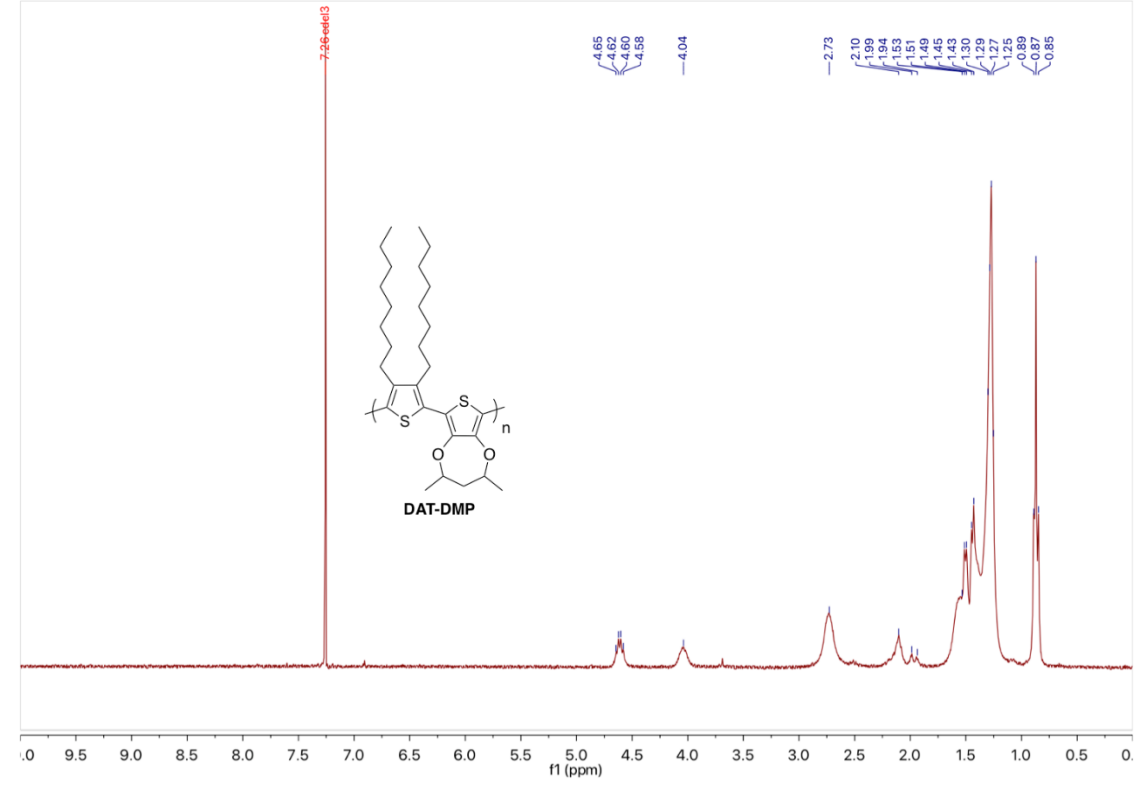

^{1}H NMR for **DAT-DMP**

Poly(3,4-dioctylthiophene-co-3,4-dimethoxythiophene) (DAT-DMOT): Orange solid in 64% yield (465 mg). ^{1}H NMR (300 MHz, CHCl3) δ 3.87 (br s, 6H), 2.71 (br s, 4H), 1.56 (br s, 4H), 1.44-1.20 (br, m, 20H), 0.92-0.82 (br t, 6H). Anal. calcd. for $C_{26}H_{40}O_2S_2$ C 69.59, H 8.99, S 14.29 Found C 69.34, H 8.78, S 14.02. GPC: Mn: 36.9 kDa, Mw: 149.8 kDa, Đ: 4.05, in $CHCl_3$ vs PS.

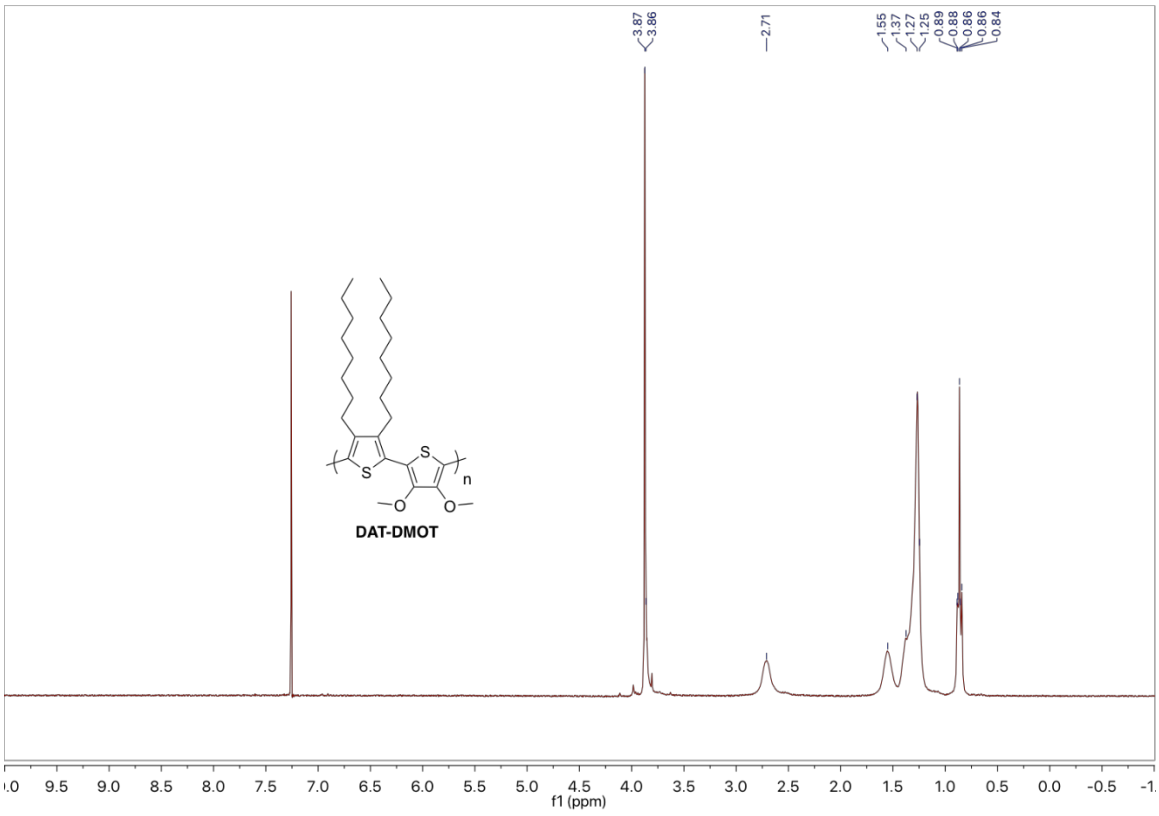

^{1}H NMR for **DAT-DMOT**

Chapter 4 - All Donor Electrochromic Polymers that are Tunable Across the Visible Spectrum via Random Copolymerization.

A series of conjugated, random terpolymers are prepared via direct (hetero)arylation polymerization yielding cathodically coloring electrochromic polymers (ECPs) that span the visible spectrum. The polymers are based on repeat units of a dialkylthiophene (DAT), a 3,4-propylenedioxythiophene (ProDOT), and dimers of 3,4-ethylenedioxythiophene (biEDOT). Using a tight feedback loop between computational and experimental chemistry, the colors of these polymers are controllably tuned to cover the visible spectrum through controlling the monomer ratios. Examinations via UV−Vis−NIR spectroscopy, differential pulse voltammetry, spectroelectrochemistry, and colorimetry show that while these systems can vary greatly in their spectral properties, their oxidation potentials are all below 0.48 V vs Ag/AgCl. The color tunability allows for access to neutral state orange, red, pink, magenta, purple, and blue polymers of various hues with a* ranging from 22 to 35 and b* values ranging from -44 to 45, while maintaining highly transmissive oxidized states. This approach allows access to a wide gamut of colors with only three monomers while affording materials with low oxidation potentials and high contrast.

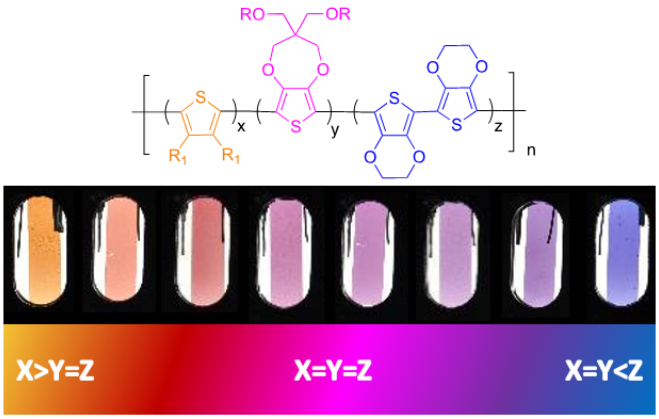

Figure 4.1. Random copolymer structure and photography showing breadth of color control

4.1 Design Approach

Random copolymerization has been used in many approaches as a means of accessing secondary colors such as red, brown, and black in electrochromic polymers.[9–13] With random copolymerization broad, low energy absorbances can be achieved when an accepting moiety is in the polymer backbone. The drawback of donor-acceptor systems is that they tend to have higher oxidation potentials brought on by the accepting moiety, thus making their usefulness in devices limited. A new approach that circumvents the challenges brought on by incorporating electron acceptors into the main chain is developed in this work. When considering how to make color tunable systems without acceptors, it is important to understand how one can design materials for specific regions of the color space, Figure 4.1.1a. All donor systems can cover three of the four regions shown here, as green materials, having a highly negative b*, require dual absorption. The current state of the art all-donor polymers was examined to develop an approach to make a color-tunable system, Figure 4.1.1b.

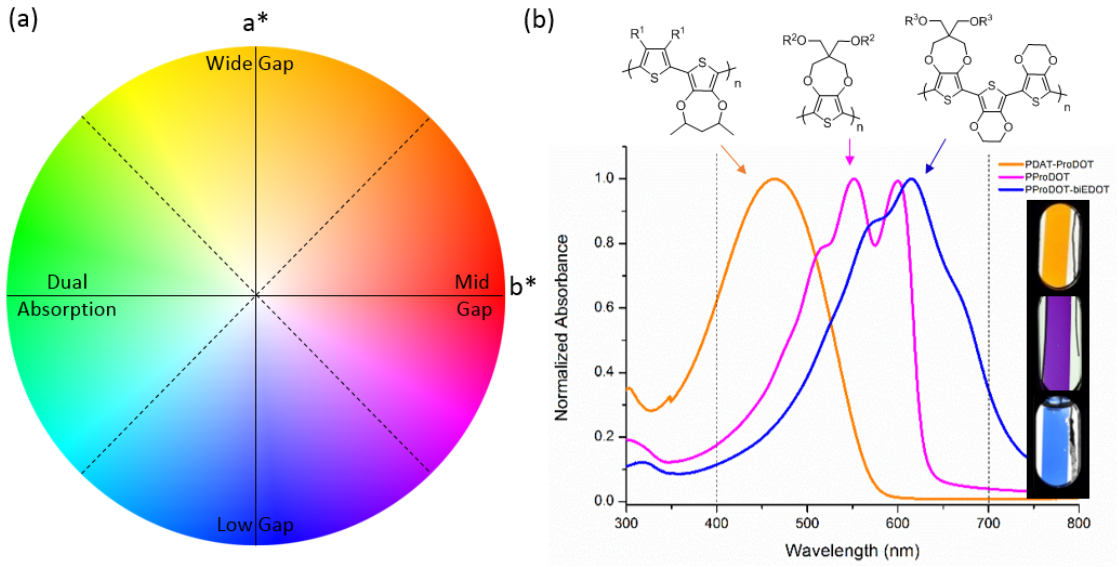

Figure 4.1.1. (a) An L*a*b* color space cross section and (b) the all donor polymers used for inspiration that show tunability across the visible spectrum.

Yellow electrochromic polymers have historically suffered from high oxidation potentials and low redox stability over one hundred switches, which is attributed to the open sites on the phenylene leaving the materials susceptible to nucleophilic attack or radical-radical coupling. The incorporation of a dialkylthiophene (DAT) as a monomer of high redox stability in wide-gap electrochromic polymers has helped to overcome this challenge.[14] For absorbing the middle of the spectrum, the homopolymer of 3,4-propylenedioxythiopohene (ProDOT) with 2-ethyl-hexyloxy side chains offers a high solubility, low oxidation potential for switching, as well as high contrast.[15] This purple polymer also shows exemplary contrast, redox stability, and switching speed. For narrow gap polymers, typically donor-acceptor systems are used. The drawbacks to these systems, as previously discussed, have been circumvented with the advent of a soluble poly(3,4-ethylene-dioxythiophene) (PEDOT) analog that covers the narrow gap portion of the visible spectrum.[16] In this polymer the biEDOT portion of the polymer brings electron richness and planarity, narrowing the optical gap and covering the low energy portion of the visible region.

In this work, the combination of DAT, ProDOT, and biEDOT into random copolymers was demonstrated to give broadly tunable electrochromic materials that span the visible spectrum, Figure 4.1.2. Using a tight feedback loop between theory and experiment, the ratios of these monomers are demonstrated to tune the absorbance of the resulting polymer, thus giving access to a wide range of colors. Utilizing only these three monomers in different ratios provides access to polymers that are orange, red, pink, magenta, purple, and blue, all of which can be oxidized to a highly transmissive form. Increased DAT content blue shifts the absorbance of the polymer and increased biEDOT content redshifts the absorbance, relative to the 1:1:1 ratio, while ProDOT brings high solubility and low oxidation potential. As detailed in Figure 4.1.2, the nomenclature of the polymers discussed in this work will be determined by the ratio of the monomers in the

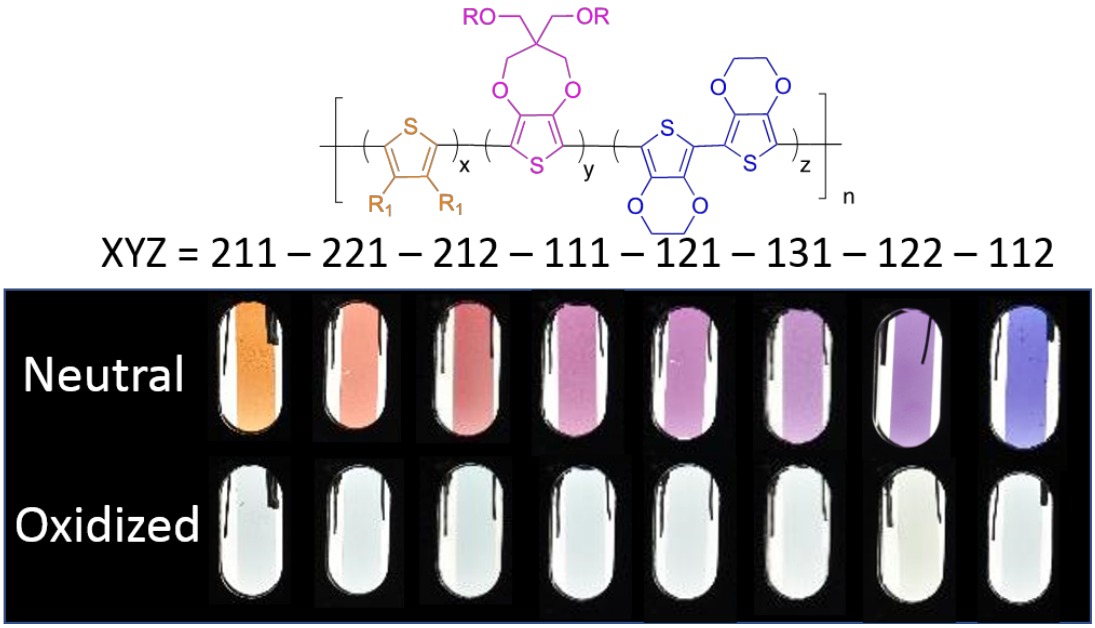

Figure 4.1.2. Repeat unit structure of random copolymers and target polymer ratios that allow access to an array of colors that span the visible spectrum and oxidize to transmissive.

backbone. For example, a random copolymer that is two parts DAT and one part each of ProDOT and biEDOT would be RC211.

4.2 Quantum Chemical Calculations (Dr. Aimée Tomlinson)

The quantum chemical calculations for this project were executed by Dr. Aimee Tomlinson. I was involved with the design of the experiments, data processing, and writing of this section of the publication that came from this body of work.

To elucidate the impact on the number and identity of aryl ring incorporation on the color of these systems, density functional theory (DFT) is utilized. It was found that pairing the mPW1PBE functional with the cc-PVDZ basis set while including dichloromethane through the conductor polarizable calculation model (CPCM), provides excellent correlation to experimental data.[17,18] A set of small oligomers is chosen to model possible random copolymers with varying degrees of

conjugation and ring strain, as well as assess their influence on the predicted color (a complete list of the structures is given in Supplementary Figure 4.6.1 and their calculated frontier molecular orbitals are provided in Supplementary Figure 4.6.2). For each system, the neutral geometry is optimized followed by a frequency calculation in order to ensure the most stable configuration is

Table 4.2.1. First excited state gaps, dihedral angles and visible excited state wavelengths and oscillator strengths for the target oligomers. The legend indicates how the structures and their corresponding dihedral angles are defined.

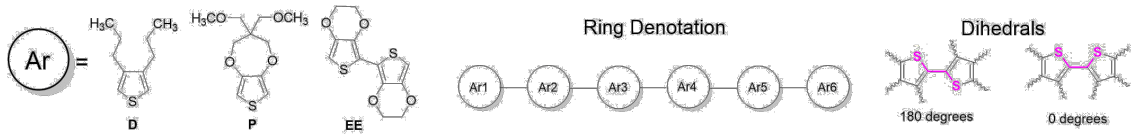

Oligomer	E_g (eV)	Dihedral Angles					Peak Maximum	
		Ar1-Ar2	Ar2-Ar3	Ar3-Ar4	Ar4-Ar5	Ar5-Ar6	λ (nm)	*f*
PEEP	2.62	179.7	178.1	179.7			473.3	1.6005
EEPEE	2.38	176.4	178.7	178.7	176.4		521.1	2.0269
PEEPEE	2.22	179.3	177.9	179.0	179.7	178.5	559.6	2.4779
DEED	2.72	156.9	179.7	156.9			456.6	1.5363
EEDEE	2.45	178.3	168.4	168.4	178.3		506.4	1.9432
EEPPEE	2.23	178.4	179.2	175.9	179.2	178.4	556.7	2.4360
DPPD	3.09	46.8	175.6	48.9			401.3	1.2749
PDPDP	2.49	169.1	176.9	176.9	169.1		497.4	1.7931
PDEEDP	2.35	163.7	163.0	179.6	163.0	163.7	528.6	2.2510
DPDP	2.98	137.2	160.9	136.9			416.2	1.1896
DPDPD	2.48	178.6	179.9	179.9	178.6		500.8	1.9028
DPDPDP	2.53	166.2	179.1	178.2	169.9	128.3	489.9	2.5072

produced. Time-dependent density functional theory (TD-DFT) calculations are then applied to these structures in order to simulate the UV-Vis spectra and predict the color of these oligomers.

An examination of the calculated HOMO-LUMO gaps will provide direction with respect to the potential spectral breath, or the absorption tunability limits which may be attained by the copolymers. As the strain along the backbone is increased by adding DAT units, the HOMO-LUMO gap is widened. Oligomers possessing the most DAT are particularly influenced by distortion from planarity causing a gap increase. The most twisted species (those which are most deviated from the defined 180° trans planar geometry) are DPPD, DPDP, DEED and DPDPDP with values as low as 128.3°, 156.9°, 136.9° and 46.8°, and corresponding first excited state gaps of 3.09 eV, 2.98 eV, 2,72 eV, and 2.53 eV, respectively (see Table 4.2.1). DPDPDP is the only 6-aryl group oligomer to be greatly impacted by inclusion of DAT as compared to PDEEDP which possesses a first excited state gap that is nearly 0.2 eV smaller. The remaining oligomers demonstrate that as the conjugation is extended the first excited state gap is reduced as seen in EEPPEE and PEEPEE.

The calculated UV-Vis spectra of these systems provide visible peak maxima that vary from 401 nm to 560 nm, spanning a difference of nearly 160 nm. Of the 15 generated excited states, only 3 or 4 possess oscillator strengths of 0.1 or higher (see Supplementary Table 4.6.1). Aside from the peak maxima location there are no differences in the predicted peak shapes in the visible range as shown in Figure 4.2.1 (For more detailed comparisons see Supplementary Figure 4.6.3 and Supplementary Figure 4.6.4). In fact, the set of oligomers possessing 5 aryl groups produce nearly identical spectra and have peak maxima which differ by only 24 nm. The 4 and 6 aryl group structures are more impacted by torsion along the backbone and have ranges of 72 nm and 70 nm, respectively.

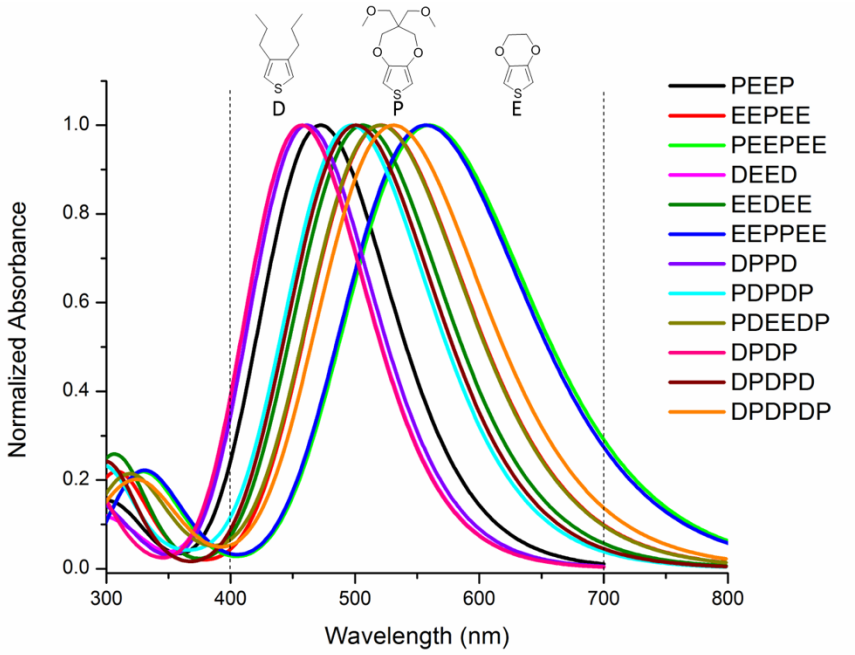

Figure 4.2.1. The calculated absorbance of the model chromophores showing the limits of spectral breadth accessible for this approach. The side chains for each monomer have been reduced to avoid local energy minima caused by many degrees of free rotation of the alkyl chains.

The simulated UV-Vis of these molecules also provides a means to estimate the color which may be producedin the CIE L*a*b* color space.[19–21] Positive a*and b* values represent red and yellow while the negative values indicate blue and green, respectively. As the magnitudes of a* and b* increase, the color becomes more saturated, and as one traverses between color points, the hue changes. L* depicts the lightness: a value of 0 would be black and 100 would be white. The L*, a*, and b* coordinates are translated to the RGB color space to display the predicted color of the oligomers (both sets of coordinates are given in Supplementary Table 4.6.2) and are indicated in Figure 4.2.2 along with their corresponding HOMO, LUMO and first excited state gap values. The predicted colors give a range of the color space that could be reached.

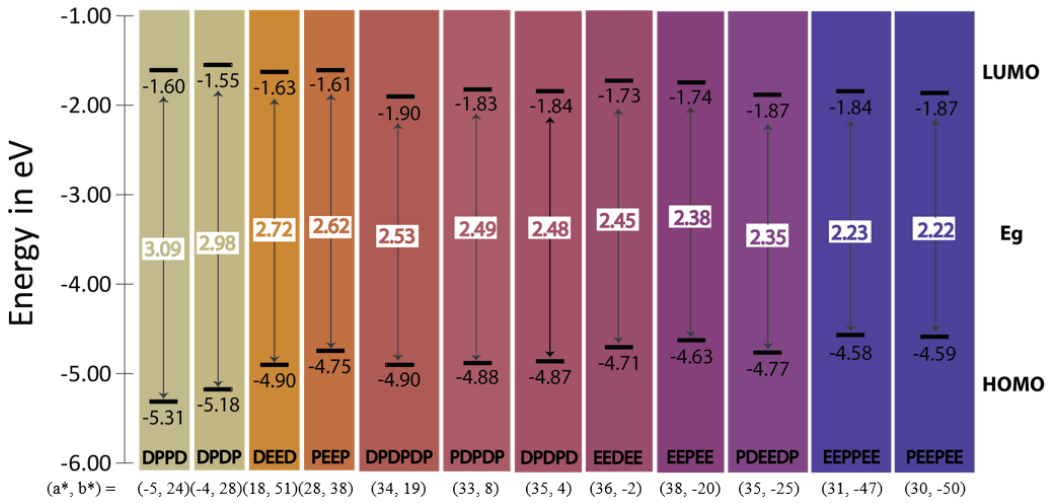

Figure 4.2.2. Oligomers are arranged in order of decreasing first excited state gap. The corresponding HOMO, LUMO and RGB color are provided. The corresponding (a*, b*) values are given below the corresponding energy level diagram.

4.3 Synthesis of Random Copolymers via Direct Arylation

The approach to the polymer syntheses is shown in Scheme 4.3. The polymers were prepared via direct (hetero)arylation polymerization where the ratios of the monomers allow for tuning the color. The stoichiometry is balanced by using the proper proportions of ProDOT and ProDOT-Br_2 such that the bromide:hyride ratio is equal to one. The polymerizations were carried out under an argon atmosphere over 24 hours followed by precipitation into methanol. The polymers were purified via Soxhelet extraction, during which they were washed with methanol, acetone, hexanes, and chloroform. The chloroform fraction was retained and underwent palladium and potassium scavenging before reprecipitation, filtering, and drying to afford the desired product. Polymerization yields were all ≥ 67 % and GPC estimated molecular weights were all ≥ 10 kDa, relative to a polystyrene standard. These molecular weights show that the polymers are above the effective conjugation length and would not change in color if they were a greater length. A

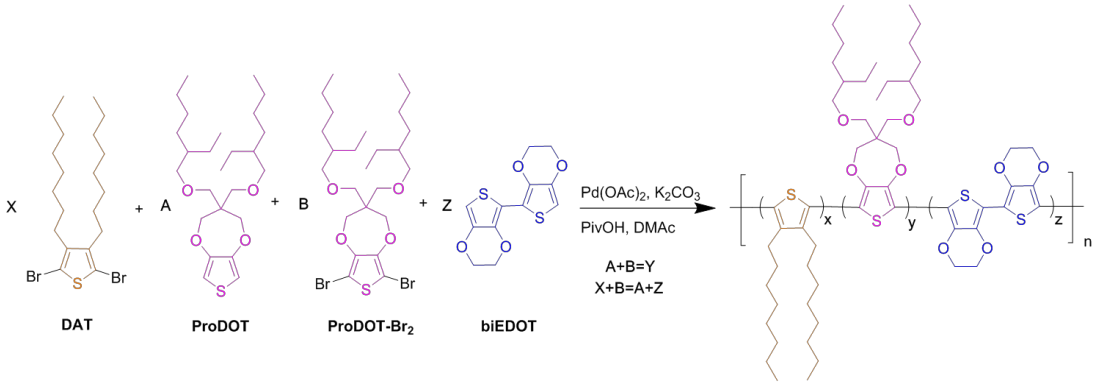

Scheme 4.3. Synthetic Approach to Random Copolymerization through Direct Arylation

comparison of polymerization yields and GPC estimated molecular weights are collated in Table 4.3.1 and all GPC traces are shown in Supplementary Figure 4.6.5. Synthetic procedures, NMR spectra, and elemental analyses are also in the Supporting Information. All polymers are soluble in in $CHCl_3$ upwards of 5 mg/ml allowing for airbrush spray processing and drop casting for film formation.

Table 4.3.1. GPC Estimated Molecular Weights and Polymerization Yields for RCs

Polymer	Yield (%)	M_n (kDa)	Đ
RC211	77	13	1.4
RC221	72	33	2.0
RC212	69	15	1.8
RC111	75	22	2.4
RC121	81	26	3.4
RC131	69	17	2.3
RC122	67	15	1.7
RC112	70	10	1.5

4.4 Tuning Oxidation and Absorption through Monomer Ratios

4.4.1 Electrochemical and Optical Properties

For electrochemical characterization polymer films are drop cast onto Pt button electrodes from 2 mg/mL solutions (3 µL) in $CHCl_3$ to cover the electrode. Cyclic voltammetry (CV) and differential pulse voltammetry (DPV) were measured on films of the polymers in order to gain insight into how the different comonomers affected the electrochemical properties of the resulting polymer. Representative CV and DPV are provided in Figure 4.4.1.1 for RC211 and RC112. Upon examining the electrochemical oxidation of the materials via DPV, the onset of oxidation follows the expected trend of polymers containing more DAT have higher oxidation potentials (CV and DPV for polymers can be found in Supplementary Figure 4.6.6). As monomer ratios are tuned, the resultant onsets of oxidation (E_{ox}) as determined by DPV range from -81 mV to +476 mV relative to Ag/AgCl giving a large window for tuning the desired electrochemical switching potential (E_{ox} values are collated in Table 4.4.1.1).

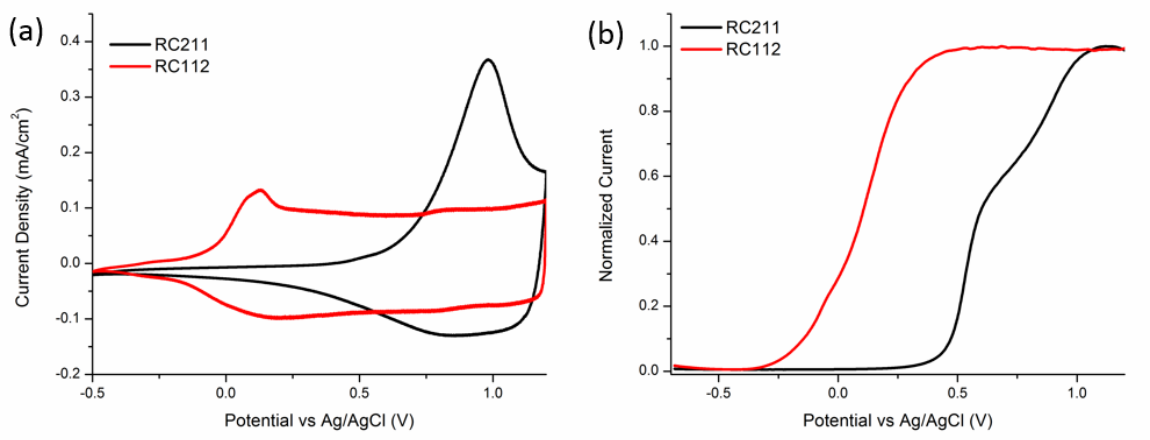

Figure 4.4.1.1. Comparison of (a) CV and (b) DPV of RC211 and RC112 on Pt button electrode in 0.5 M $TBAPF_6$ /PC. Reference: 450 mV vs Fc/Fc^+.

Table 4.4.1.1. Optical and Electrochemical Properties of RCs

Polymer	E_{ox}[a] (mV) vs Ag/AgCl	λ_{max} (nm)[b]	E_g[b,c] (eV)
RC211	476	458	2.04
RC221	444	495	1.88
RC212	163	512	1.83
RC111	141	539	1.82
RC121	101	550	1.81
RC131	105	553	1.77
RC122	-46	568	1.75
RC112	-81	586	1.70

[a] As determined by DPV as the onset of the current for oxidation [b] For films cast onto ITO-coated glass measured after 10 CV cycles [c] Bandgap determined by onset of light absorption

The E_{ox} for RC111 as a reference point at +141 mV, as more DAT is added to the polymer structure and the E_{ox} increases. RC221 has an E_{ox} measured to be +444 mV, and the highest E_{ox} was measured to be +476 mV for RC211. This observation is due to DAT being the least electron rich of the monomers and provides the most interring strain. More interring strain causes a higher energy barrier to planarize the conjugated backbone upon oxidation. Conversely, biEDOT provides more planarity and electron richness to the polymer compared to DAT, increasing the ratio of biEDOT in the structure lowers the oxidation potential. This is seen in the E_{ox} with RC122 having an E_{ox} of -46 mV and RC112 being the polymer with the lowest E_{ox} at -81 mV.

For optical characterization, polymer films are airbrush sprayed onto glass/ITO electrodes from 3 mg/ml solutions in 1:1mixtures of toluene:chloroform. All of these polymers form smooth films with little scattering. Films are sprayed to an absorbance of 1.00 ± 0.05 in the as-cast state.

UV-Vis spectra are measured in 0.5 M $TBAPF_6$/PC electrolyte solution after 10 CV cycles, as the polymers will swell with electrolyte upon oxidation and their absorbance intensities and λ_{max} may change. Upon electrochemical conditioning of electrochromic polymers, the UV-Vis absorption typically exhibits a characteristic red-shift of the absorbance as the polymer's conjugation in the charge neutral state is extended compared to the as cast film. Absorbance values are normalized due to the increase/decrease of absorbance upon redox cycling. Figure 4.4.1.2 shows the UV-Vis spectra of the films of the polymers after break-in. These polymers' absorptions show a range of λ_{max} from 458 nm to 586 nm and optical gaps measured to be 1.70 to 2.04 eV, which covers a large portion of the visible spectrum.

Using RC111 as a refence point for each case the λ_{max} is measured to be 539 nm. It is evident that the amount of DAT in the polymer has a profound effect on both the λ_{max}, as evidenced in Figure 4.4.1.2a. This monomer causes the most interring strain, so for every monomer inserted into the backbone there is a point of torsion that decreases pi-pi overlap between rings, lowering the effective conjugation length, and widening the optical gap. With RC211 having the highest ratio of DAT, it has the highest energy and broadest absorption with the λ_{max} measured to be 458

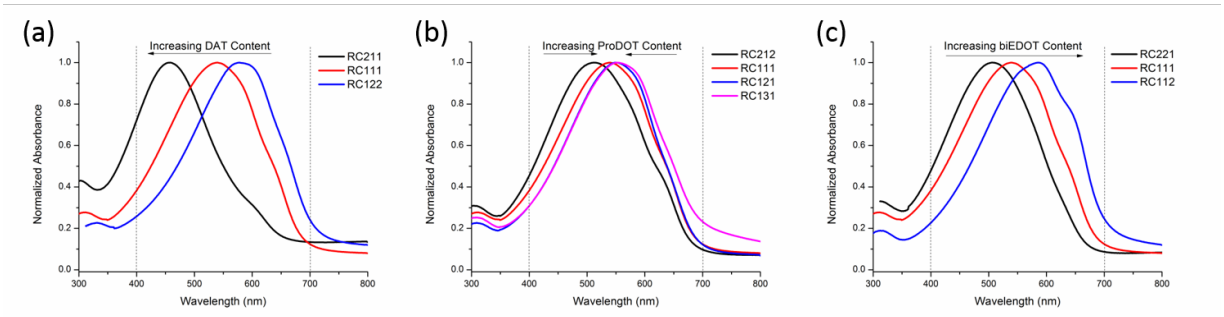

Figure 4.4.1.2. Neutral state spectra on ITO-coated glass comparing the effects of varying the amount of (a) DAT, (b) ProDOT, and (c) biEDOT while holding the ratios of the other monomer constant.

nm. As the DAT content is reduced compared to RC111 for RC122, there is a red-shifting in the λ_{max} to 568 nm. The ratio of biEDOT has an analogous, but opposite, trend as what is seen for DAT, Figure 4.4.1.2c. As the biEDOT ratio is increased, there is a red-shifting of the λ_{max} with measurements of 495 nm, 539 nm, and 586 nm for RC221, RC111, and RC112, respectively.

ProDOT content has the smallest effect on controlling the absorption, Figure 4.4.1.2b, which is expected since it lies in between the other monomers in terms of electron richness and interring planarity. As the ProDOT ratio is increased, there is a red-shifting of the λ_{max} with measurements of 512 nm, 539 nm, 550 nm, and 553 nm for RC212, RC111, RC121, and RC131, respectively. The high energy absorption of RC212 is likely due to the high content of DAT and as the ProDOT content is further increased there is much smaller red-shifting effect that becomes only a 3 nm shift between RC121 and RC131.

4.4.2 Color and Switching Properties

Spectroelectrochemical measurements were performed on polymer films sprayed on ITO-glass in 0.5 M $TBAPF_6$/PC with a platinum counter electrode and a Ag/AgCl reference electrode. Representative results for RC211 and RC112 are detailed in Figure 4.4.2.1 along with photographs of the films held at potential extremes dictated by the CV results (spectroelectrochemistry results for all polymers are shown in Supplementary Figure 4.6.7 and Supplementary Figure 4.6.8). In these experiments, a three-electrode cell is set up in a cuvette where the polymer film acts as the working electrode. The UV-Vis spectrum is then monitored as a function of the applied potential to the film. As seen in the figure, the neutral state absorption in the visible is depleted upon oxidation, and there is an increase of the charged state absorption in the NIR. After complete oxidation, all the materials show high transmissivity across the visible. This transition between

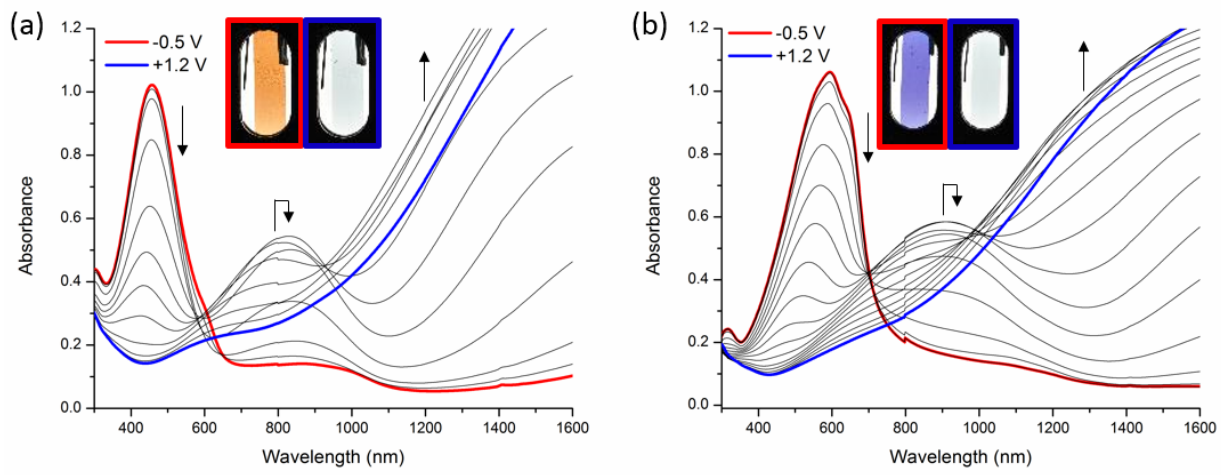

Figure 4.4.2.1. Spectroelectrochemistry and photographs of (a) RC211 and (b) RC112. The applied potential was increased in 100 mV steps between the fully colored and bleached states in 0.5 M $TBAPF_6$/PC.

colored and transmissive can also be observed in the photography.

In this work the color is quantified using the L*a*b* color space. Colorimetry is used to demonstrate the control over color with this materials design approach. The a*b* color space results for the polymer films are presented graphically in Figure 4.4.2.2 with the L*a*b* values collated in Table 4.4.2.1. In this figure, the polymer neutral states are circled, and the lines are to guide the eye to each measurement. Neutral state values for PDAT-ProDOT, PProDOT, and PProDOT-biEDOT are provided in the figure for comparison. All of the new random copolymers show lower saturation than these systems, as they are broader in absorbance. In the neutral state, after a redox switching equilibration, the polymers had L* values ranging from 32 to 66, a* values ranging from 22 to 35, and b* values ranging from -44 to 45, thus traversing across the wide-gap, mid-gap, and low-gap color spaces. In the oxidized states, the polymers had L* values ranging

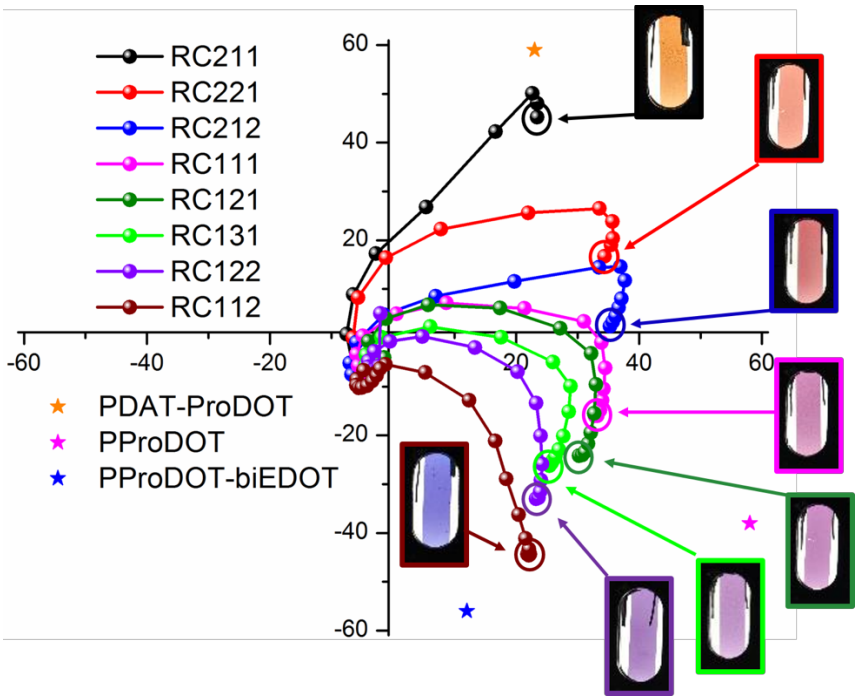

Figure 4.4.2.2. Colorimetric analysis and neutral state photographs of all the polymers. Plots of a*b* color coordinates at increasing applied potentials in 0.1 V steps from neutral (-0.5 V vs. Ag/AgCl) to fully oxidized states (1.2 V vs. Ag/AgCl). Measurements were performed in 0.5 M $TBAPF_6$/PC of films spray-cast onto ITO/glass electrodes.

from 86 to 91, a* values ranging from −3 to -1, and b* values ranging from −7 to -4, thus giving forms that are both highly transmissive and color neutral.

In Figure 4.4.2.2, the color coordinates of the neutral films are circled, and the lines follow to each measurement, as the oxidation potential is increased by 100 mV at each step. For all the polymer films, there is an observed increase in a* as the film begins to be oxidized. As the polymers are random in repeat pattern, the individual chromophores along the chain will have varying oxidation potentials. The chromophores with the lowest oxidation potential would be those containing the most DOT/least DAT and would therefore have the most red-shifted absorptions.

As the chromophore is oxidized, these portions of the polymer oxidize first leaving the highest oxidation potential and widest gap chromophores, consisting of the portions with the most DAT incorporated into the chain. The polymers with the most DOT in their structure have more gradual increases in a* as they begin to oxidize, while the polymers with the least DOT have small sharp jumps in a* at the beginning of oxidation.

Table 4.4.2.1. Color and Switching Properties of RCs

Polymer	Δ%T[a, b] ($at\lambda_{max}$)	Neutral State L*, a*, b* color coordinates[b]	Oxidized State L*, a*, b* color coordinates[b]
RC211	62	66, 23, 45	84, -2, -6
RC221	70	62, 34, 16	91, -2, -7
RC212	67	44, 35, 2	86, -2, -6
RC111	64	40, 33, -16	87, -2, -5
RC121	66	47, 30, -24	90, -1, -4
RC131	62	46, 25, -26	89, -3, -5
RC122	60	42, 23, -33	88, -2, -5
RC112	58	32, 22, -44	88, -2, -6
PDAT-ProDOT[c]	65	87, 23, 59	90, -2, -4
PProDOT[c]	71	42, 58, -38	89, -3, -3
PProDOT-biEDOT[c]	71	34, 10, -56	83, -3, -5

[a] Difference between steady-state transmittance measured at fully oxidized and fully neutral states (all films sprayed to 10%T at λ_{max}) [b] For a film cast onto ITO-coated glass. [c] Values from references 156 and 157.

When examining the breadth of the color space obtainable through this approach the most logical reference point is the polymer containing equal parts of each monomer. The neutral state for RC111 has a*, b* values of 33, -16, which is observed as a purple-pink color in the photography. As more ProDOT is added to the structure, there is a decrease in both the a* and b* values for RC121 (30, -24) and continues to RC131 (25, 26). This shift in values indicates an increase in the blueness and decrease in the redness of the film, which is observed in the photography as the films appearing less pink and more purple relative to RC111. As more biEDOT is added to the polymer structures, there is less interring strain, further red-shifting absorbance, and more blue light being transmitted. For RC122 (23, -33) and RC112 (22, -44), there is a large decrease in b* values leading to very blue films seen in the photography. Similar to the electrochemistry, the incorporation of DAT has the largest effect on the colorimetry. As more DAT is added to the structure, there is more interring strain, further blue-shifting absorbance, and more red light being transmitted. This causes a rise in the b* value, indicating that the color is becoming less blue. The colorimetry values for RC212 (35, 2) are near the positive a* axis, observed as a red color in the photography. Replacing the biEDOT with the slightly more strained ProDOT in RC221 (34, 16), leads to an increase in a* values leading to light red film. For RC211 (23, 45), there is a large increase in a* values, as the polymer structure is dominated by the high strain monomer, leading to an orange film.

4.4.3 Color Mixing

To further examine the spectral range of these systems and to gain perspective on how they can be applied, these polymers were combined to create broadly absorbing blends, Figure 4.4.3.1. The spectroelectrochemistry and photography show the potential for solution phase color mixing

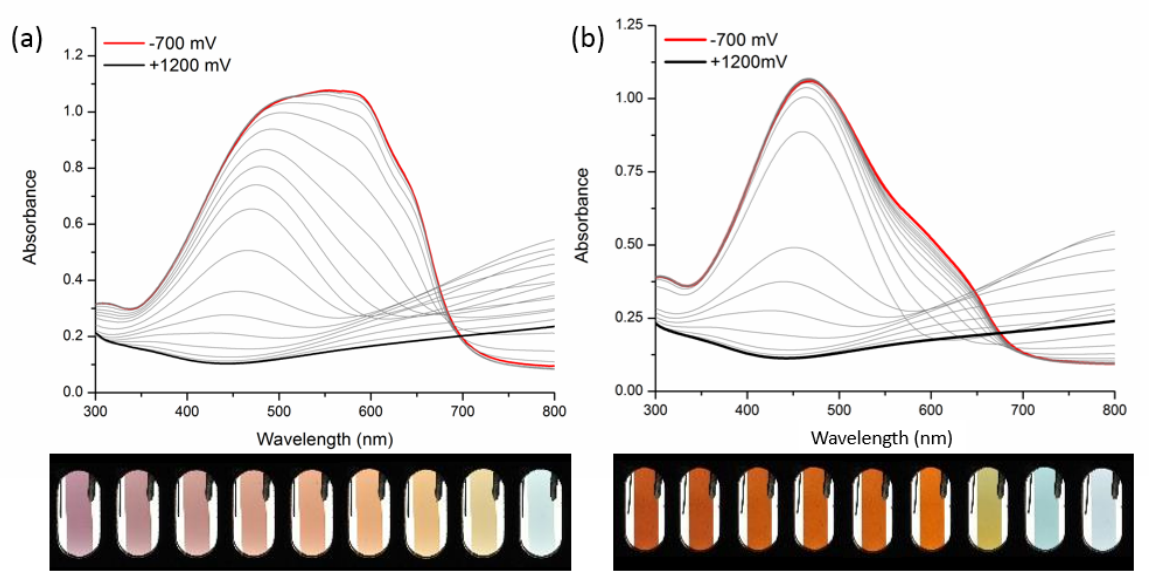

Figure 4.4.3.1. Spectroelectrochemistry and photography of mixtures of RC211 and RC122 at ratios of (a) 1:1 and (b) 2:1. The photographs are taken at potential steps of 200 mV to show the progression of the color change as a function of applied potential.

of these polymers, similar to inks, to create films of low color saturation, which are of interest for eyewear and tinting application. In this experiment, solution mixtures of RC211 and RC112 at 3 mg/mL in ratios of 1:1 and 2:1 were created and films were cast via airbrush spraying. The limitations of the all donor approach to creating black-to-clear switching electrochromics is evident in Figure 4.4.3.1a. This 1:1 mixture of polymers gives a conformal absorption between ~450-650 nm, but some red and blue light transmit making the material purple. Without the donor-acceptor absorption to aid with the low energy wavelengths, a flat absorption across the visible is not feasible. Turning attention to Figure 4.4.3.1b, the 2:1 ratio of RC211 and RC112 affords an aesthetically pleasing brown-to-transmissive switching blend. Considering eyewear and tinting applications of electrochromism, secondary colors like browns and reds are desirable.

Black and brown electrochromic systems containing donor-acceptor moieties have a

challenge where the portion with large amounts of donor bleaches well before the other portions, leaving a green intermediate state that is not desirable for eyewear and tinting applications. The materials and mixtures in this study do not go through this same transition. As seen in the photography, these materials go through an orange/brown intermediate which is more desirable for these applications.

4.5 Conclusions and Perspective

Electrochromism is a field where small changes in color can have large ramifications on the applicability of the material into devices. In this work, a tight feedback loop of calculations and experiments guided the design of electrochromic polymers that cover the visible spectrum with only three monomers. TDDFT was used to predict the spectral breadth that was attainable with these systems and guided the synthesis. The synthesized materials allowed for a large portion of the color space to be covered while maintaining low oxidation potentials, high contrast, and long-lasting optical memory. These properties allow the materials to function with low power consumption and offer. Their mixture and subsequent processing into broadly absorbing blends have potential in applications where muted and secondary colors are beneficial.

4.6 Supplementary Figures and Tables

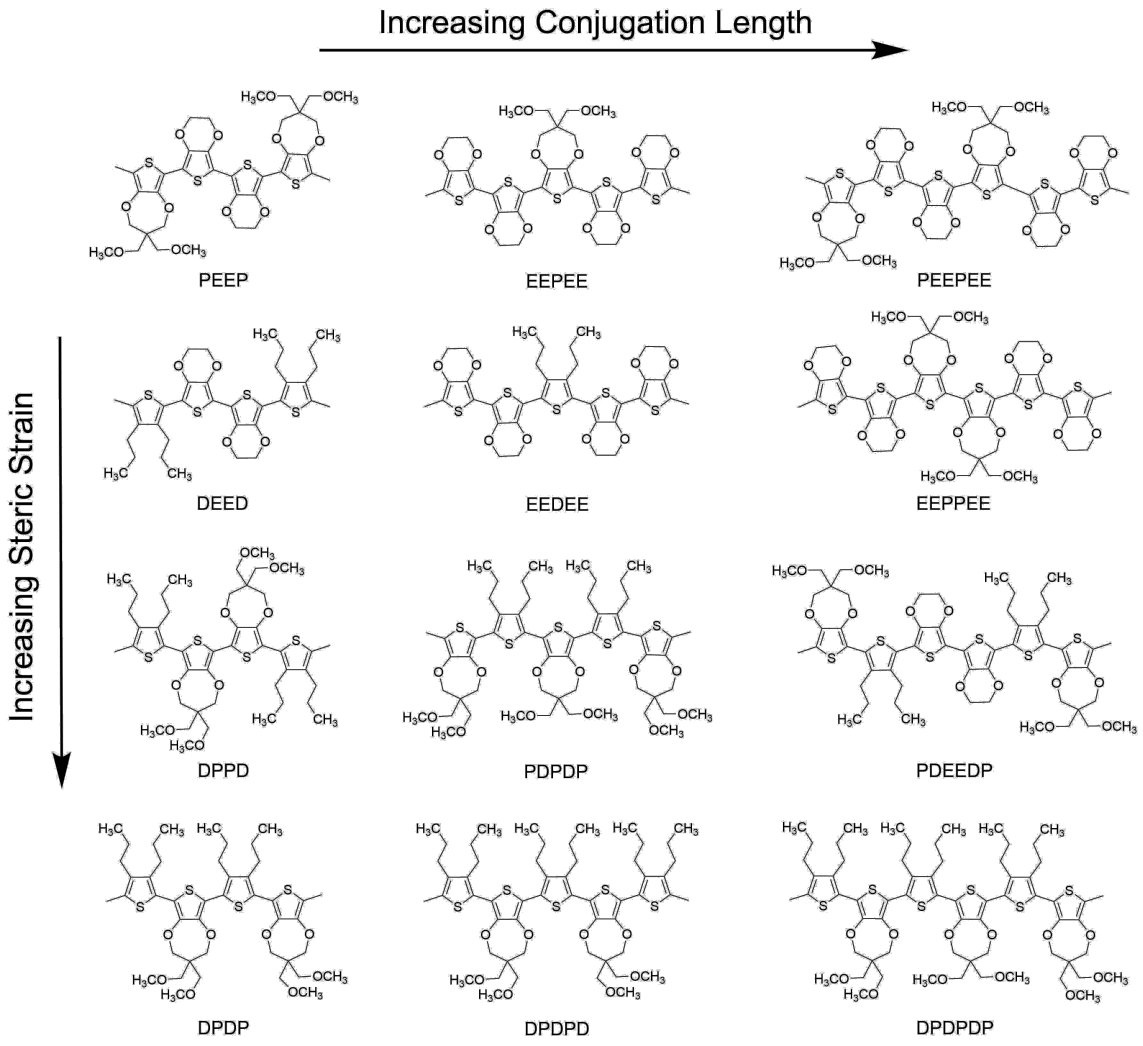

Figure 4.6.1. Set of oligomers used for RC computational study.

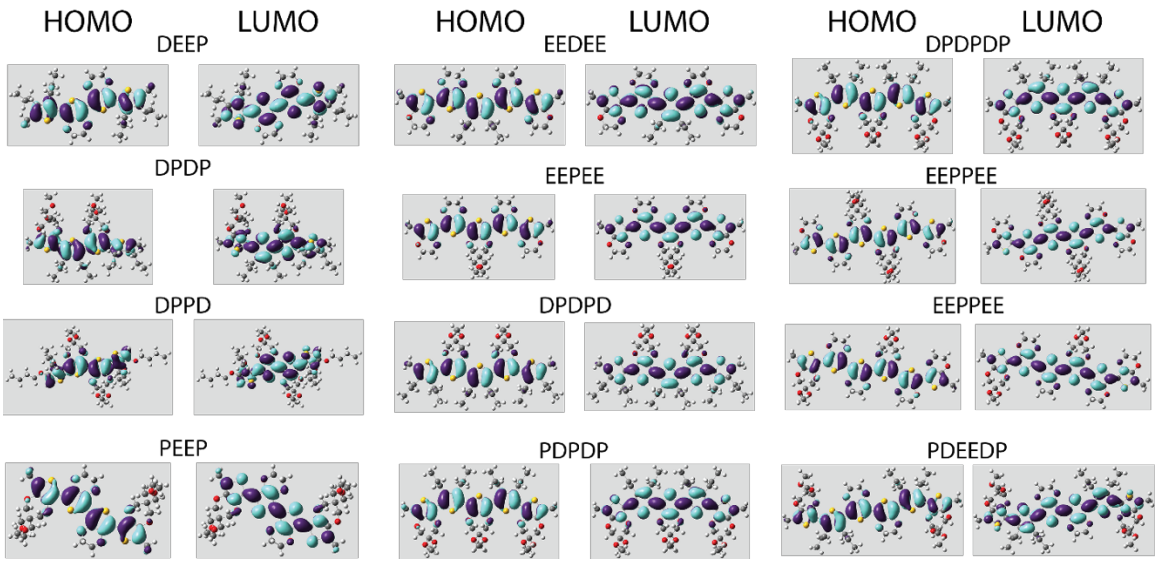

Figure 4.6.2. Frontier molecular orbitals for each RC oligomer

Table 4.6.1. Excited State Analysis for RC Oligomers for All States with Oscillator Strengths Above 0.1

Oligomer	λ (nm)	*f*	λ (nm)	*f*	λ (nm)	*f*	λ (nm)	*f*
PEEP	473.3	1.6005	312.2	0.132	265.4	0.1471		
EEPEE	314.9	2.0269	314.9	0.1937	303.8	0.1338	262.6	0.1617
PEEPEE	559.6	2.4779	340.0	0.2461	319.9	0.1562		
DEED	456.6	1.5363	311.3	0.1291	261.1	0.1015		
EEDEE	506.4	1.9432	311.5	0.2068	309.4	0.1718	265.4	0.1340
EEPPEE	556.7	2.4360	341.9	0.2701	318.3	0.2271		
DPPD	401.3	1.2749	300.5	0.1003	246.7	0.1120		
PDPDP	497.4	1.7931	304.2	0.1264	268.6	0.1143		
PDEEDP	528.6	2.2510	327.1	0.1737	314.2	0.1221		
DPDP	416.2	1.1896	267.8	0.2056	262.3	0.1281		
DPDPD	500.8	1.9028	303.9	0.2036	303.7	0.1371	259.8	0.1576
DPDPDP	489.9	2.5072	311.7	0.3270	302.9	0.1208		

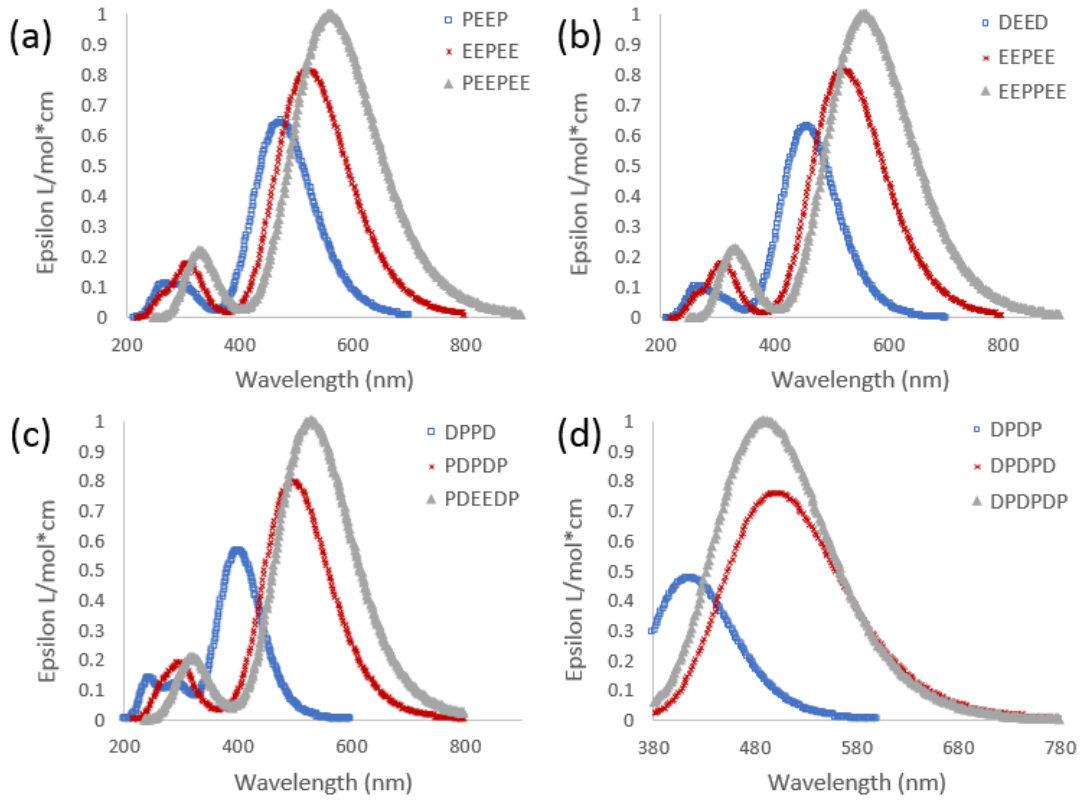

Figure 4.6.3. Contrasting Sets by Increasing Conjugations (by rows in Figure 4.6.1)

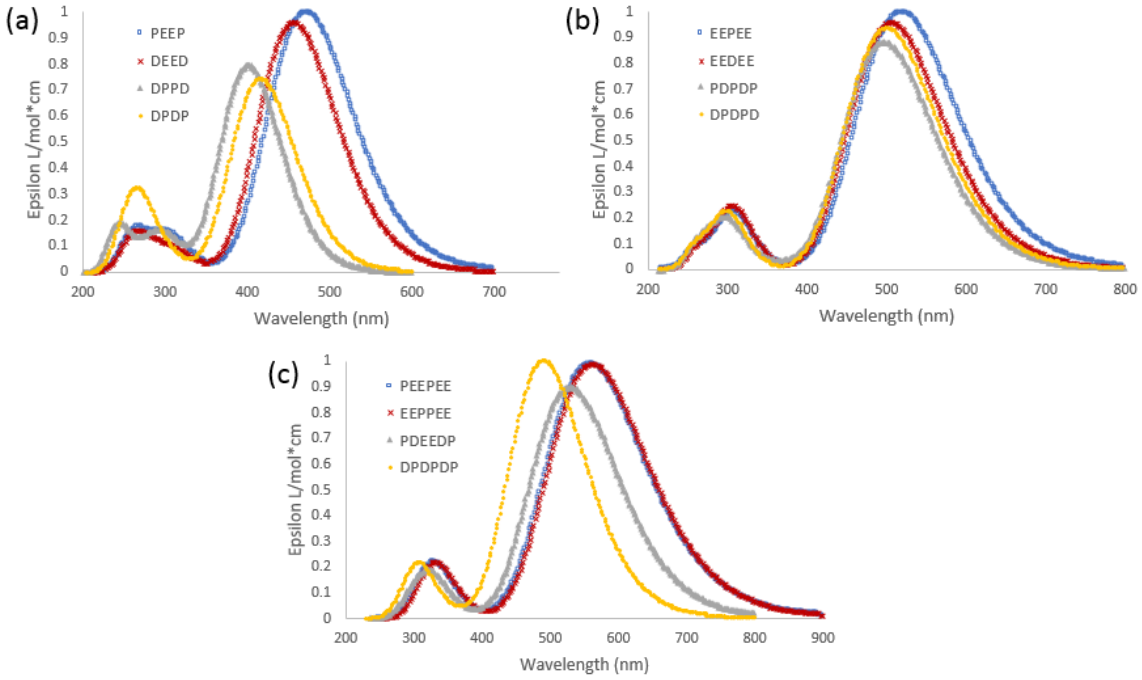

Figure 4.6.4. Contrasting Sets by Increasing Ring Strain (by columns in Figure 4.6.1)

Table 4.6.2. Calculated Color Coordinates of RC Oligomers

Oligomer	L*	a*	b*	R	G	B
DPPD	75.01	-5.00	24.08	192.4	186.0	140.2
DPDP	74.09	-3.73	27.87	194.3	182.6	130.9
DEED	61.86	18.27	51.24	201.6	135.4	55.8
PEEP	54.96	27.69	38.37	191.2	111.1	65.8
DPDPDP	48.29	33.74	18.79	174.4	90.1	84.7
PDPDP	47.96	33.25	8.43	169.1	90.4	101.0
DPDPD	45.51	35.11	4.31	163.0	82.9	101.9
EEDEE	43.13	36.33	-2.49	155.0	76.4	107.1
EEPEE	37.67	37.96	-19.89	132.5	63.2	121.4
PDEEDP	38.81	35.27	-25.46	127.5	69.4	133.2
EEPPEE	33.65	30.92	-47.75	80.2	64.6	155.8
PEEPEE	33.16	30.32	-49.51	74.2	64.3	157.3

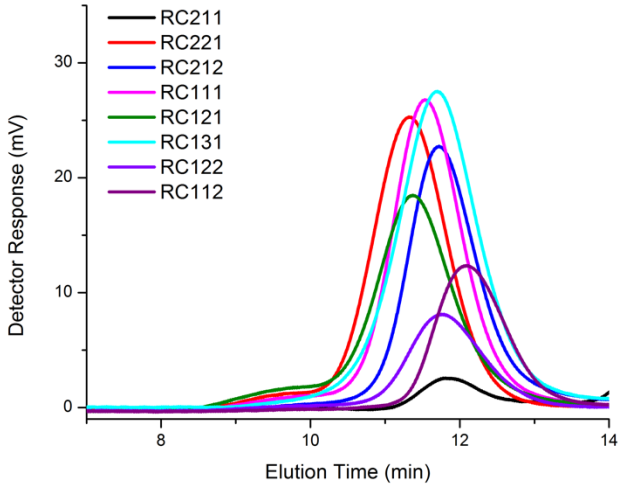

Figure 4.6.5. GPC traces of RCs in $CHCl_3$ at 40 °C.

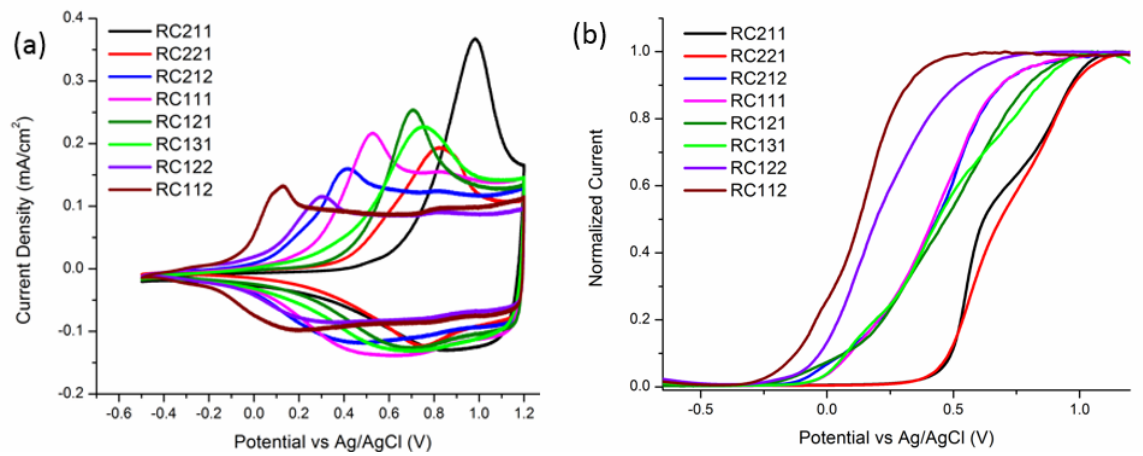

Figure 4.6.6. Comparison of (a) CV and (b) DPV of polymer films on Pt button electrode in 0.5 M $TBAPF_6$ /PC. Reference: 450 mV vs Fc/Fc^+.

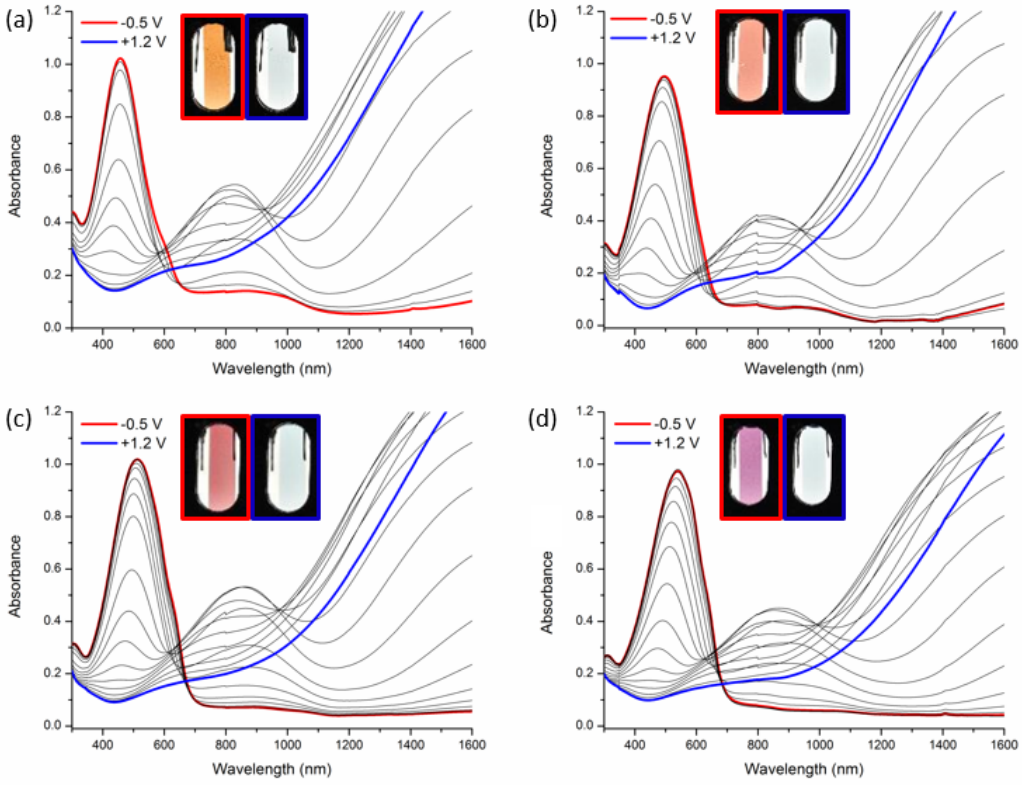

Figure 4.6.7. Spectroelectrochemistry and photographs of (a) RC211, (b) RC221, (c) RC212, and (d) RC111. The applied potential was increased in 100 mV steps between the fully colored and bleached states in 0.5 M $TBAPF_6$/PC.

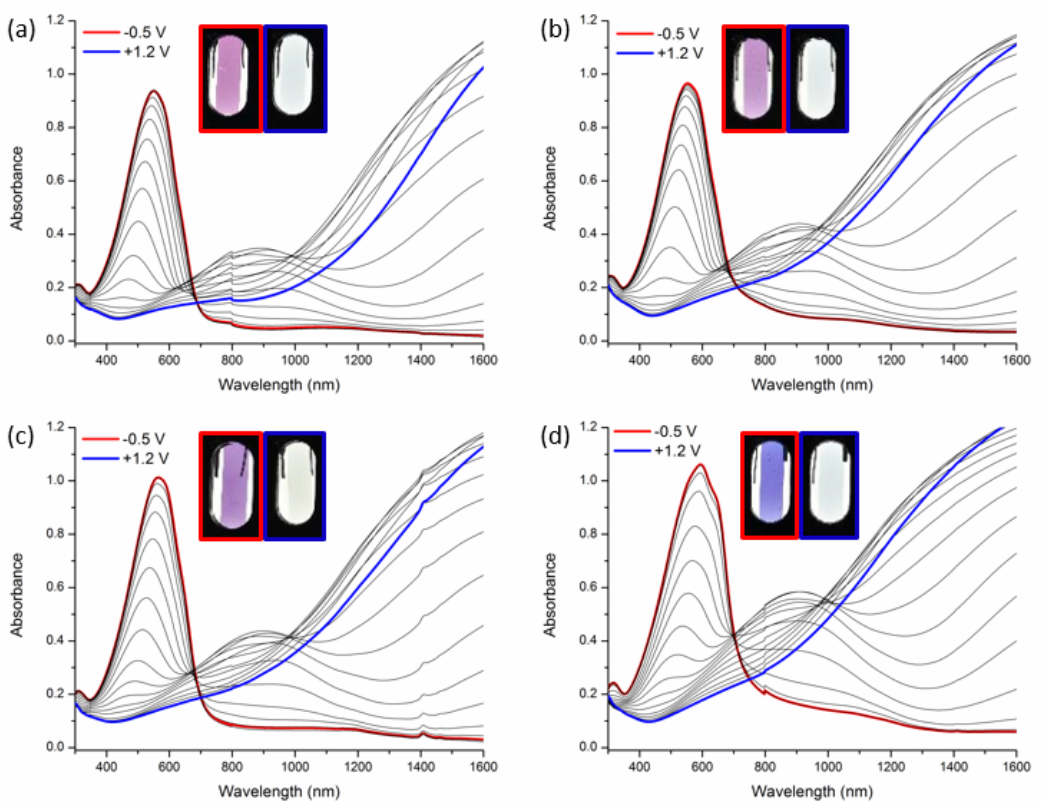

Figure 4.6.8. Spectroelectrochemistry and photographs of (a) RC121, (b) RC131, (c) RC122, and (d) RC112. The applied potential was increased in 100 mV steps between the fully colored and bleached states in 0.5 M $TBAPF_6$/PC.

4.7 Synthetic Procedures

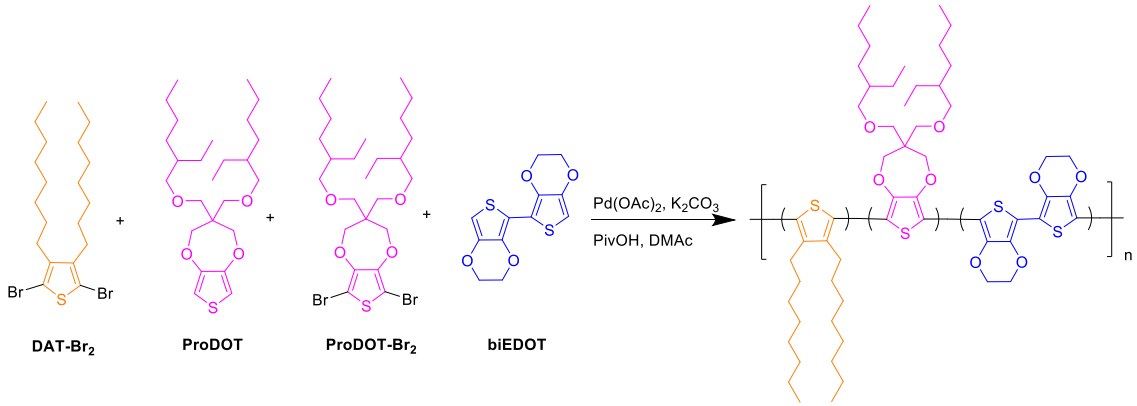

General Polymerization Procedure using RC111 as an Example: To a 25 ml schlenk flask equipped with a stir bar was added **DAT-Br$_2$** (100.0 mg, 0.21 mmol), **ProDOT** (47.2 mg, 0.11 mmol), **ProDOT-Br$_2$** (64.2 mg, 0.11 mmol), **biEDOT** (60.5 mg, 0.21 mmol), 2 mol% palladium acetate (1.5 mg), pivalic acid (32.8 mg, 32 mmol), and potassium carbonate (133.4 mg, 0.97 mmol). The mixture was then vacuum purged for 45 minutes followed by three purge and argon back-fill cycles. N,N-dimethylacetamide (6.4 mL) was degassed by bubbling with argon for 45 minutes and then injected into the flask to dissolve the contents. The reaction mixture was stirred at 140 °C for 24 hours and then removed from the oil bath and allowed to cool to room temperature. The polymer dispersion was dissolved with $CHCl_3$ and precipitated into methanol and stirred for 45 minutes. The precipitate was filtered into a soxhlet extraction thimble and washed with methanol, acetone, hexanes, and chloroform respectively. The washings were conducted until color was no longer observed during extraction. After dissolution from the soxhlet thimble, the solvent was removed via rotovap and then 20 ml of chloroform was added followed by 100 mg of the palladium scavenger diethylammonium diethyldithiocarbamate, 150 mg of 18-crown-6 and then stirred for 6 hours at 50 ◦C. The polymer was then precipitated into 300 ml of methanol. The precipitate was filtered over a 20 µm Nylon pad and washed with 300 ml of pure methanol and

allowed to dry. The dried material was collected into a tared vial and vacuum dried. Purple powder in 75% yield (165 mg). ^{1}H NMR (300 MHz, $CDCl_3$) δ 4.48-4.22 (br, 8H), 4.19-3.99 (br, 4H), 3.64-3.40 (br, 4H), 3.36-3.18 (br, 4H), 2.82-2.50 (br, 4H), 1.67-1.14 (br, 42H), 0.98-0.72 (br, 18H). Elemental Analysis Calculated: C 66.88, H 8.52, S 12.31; Found: C 66.02, H 7.88, S 12.95. GPC: Mn: 22 kDa, Đ: 2.4, in $CHCl_3$ vs PS.

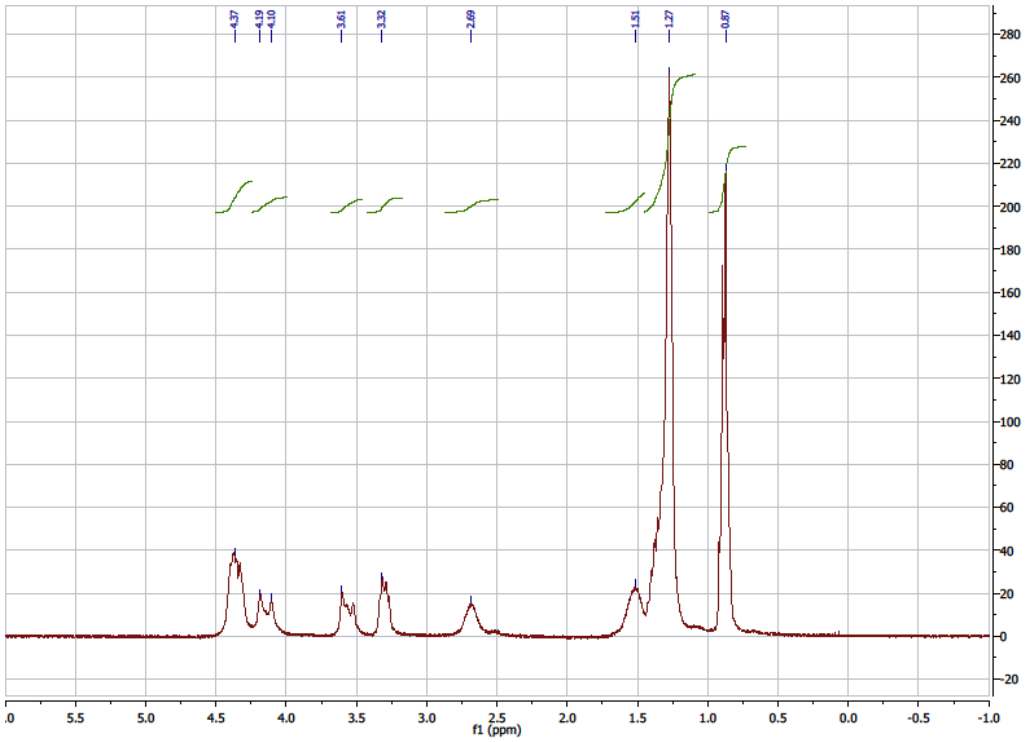

^{1}H NMR for **RC111**

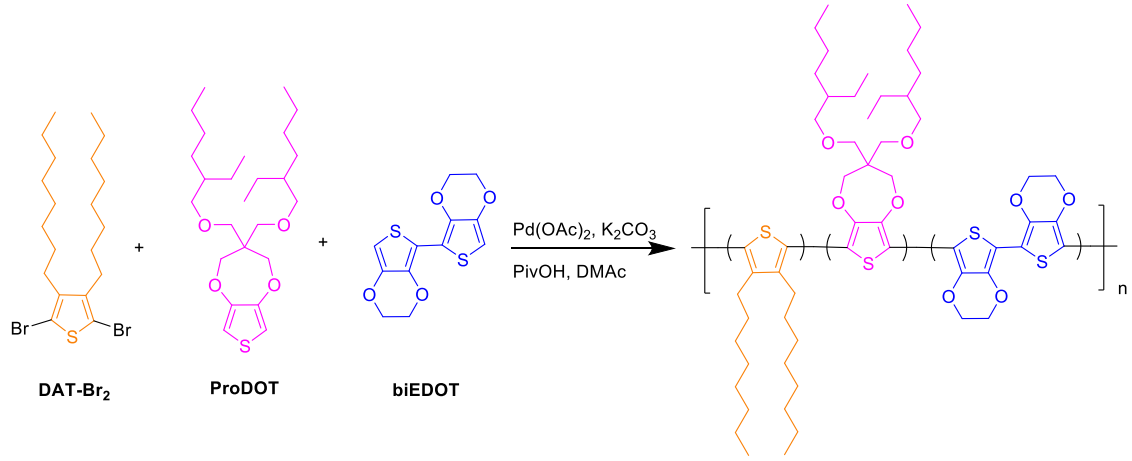

RC211: Orange solid in 77% yield (110 mg). ^{1}H NMR (300 MHz, $CDCl_3$) δ 4.48-4.22 (br, 8H), 4.19-3.99 (br, 4H), 3.64-3.40 (br, 4H), 3.36-3.18 (br, 4H), 2.82-2.50 (br, 8H), 1.67-1.14 (br, 66H), 0.98-0.72 (br, 24H). Elemental Analysis Calculated: C 69.49, H 9.12, S 11.89; Found: C 68.08, H 8.53, S 12.55. GPC: Mn: 13 kDa, Đ: 1.4, in $CHCl_3$ vs PS.

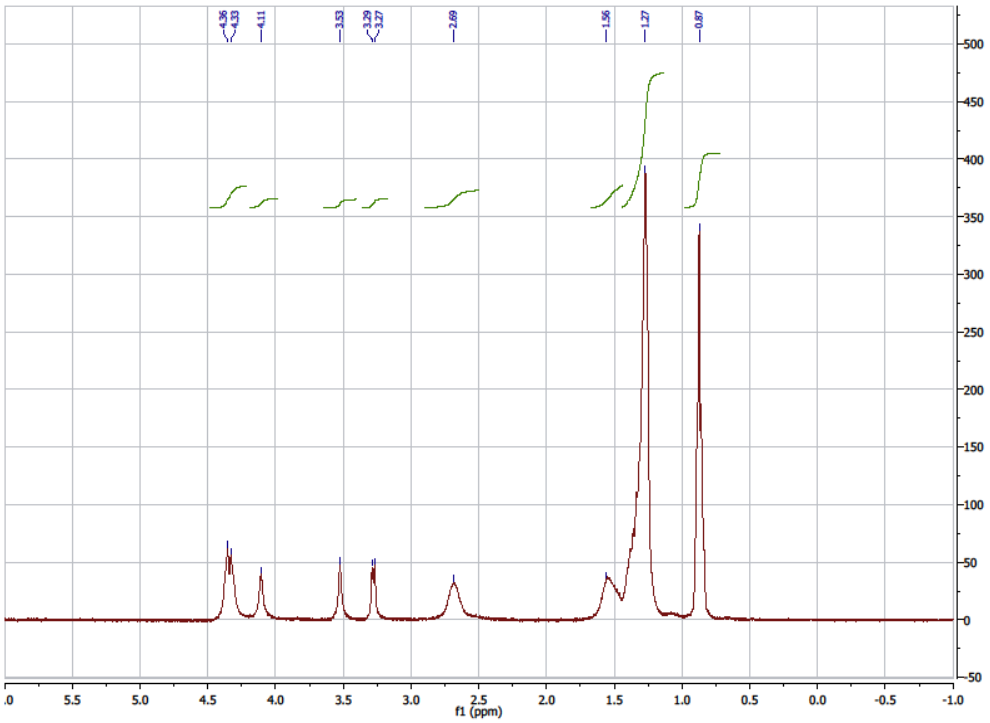

^{1}H NMR for **RC211**

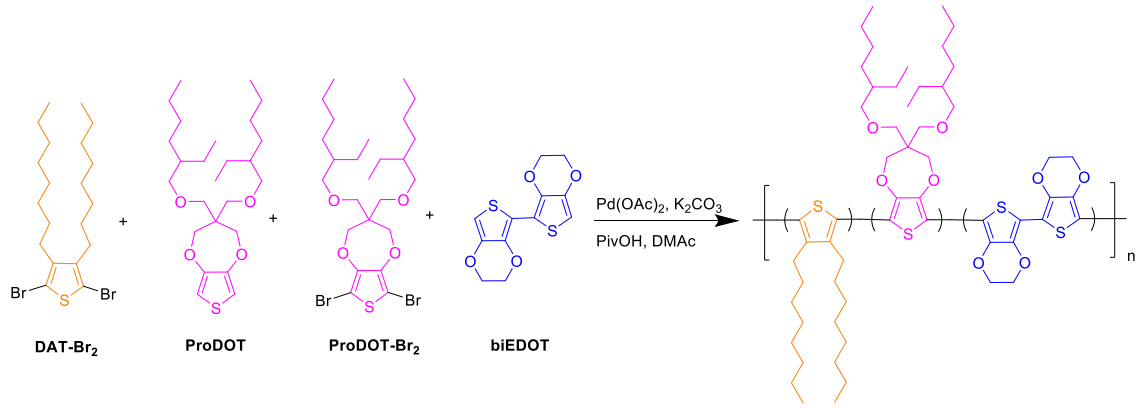

RC221: Red lustrous solid in 72% yield (137 mg). ^{1}H NMR (300 MHz, $CDCl_3$) δ 4.48-4.22 (br, 8H), 4.19-3.99 (br, 8H), 3.64-3.40 (br, 8H), 3.36-3.18 (br, 8H), 2.82-2.50 (br, 8H), 1.67-1.14 (br, 84H), 0.98-0.72 (br, 36H). Elemental Analysis Calculated: C 69.24, H 9.25, S 10.77; Found: C 68.19, H 8.72, S 11.05. GPC: Mn: 33 kDa, Đ: 2.0, in $CHCl_3$ vs PS.

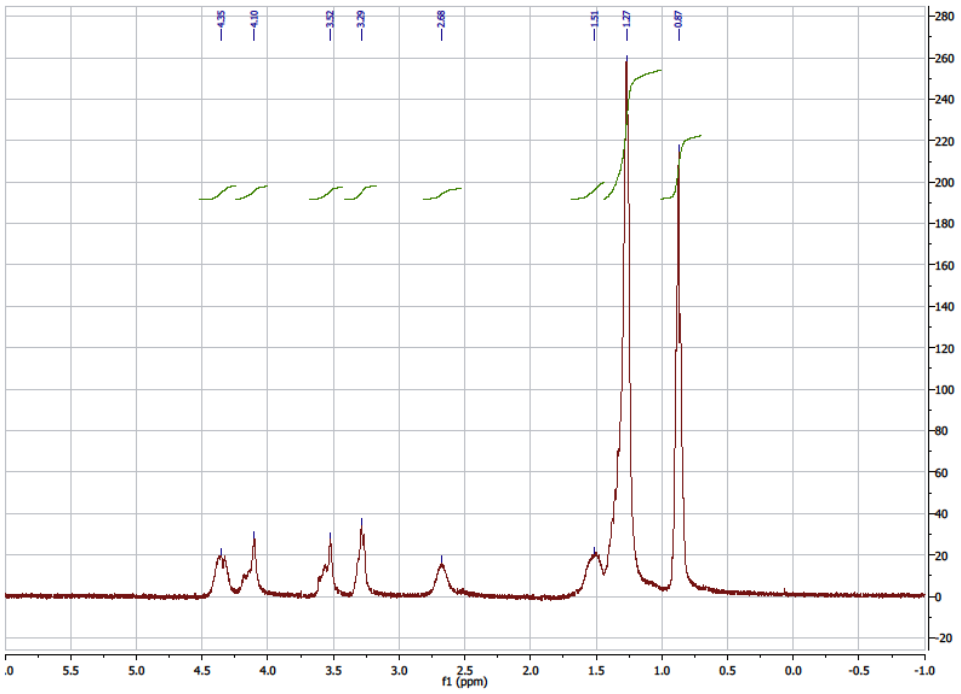

^{1}H NMR for **RC221**

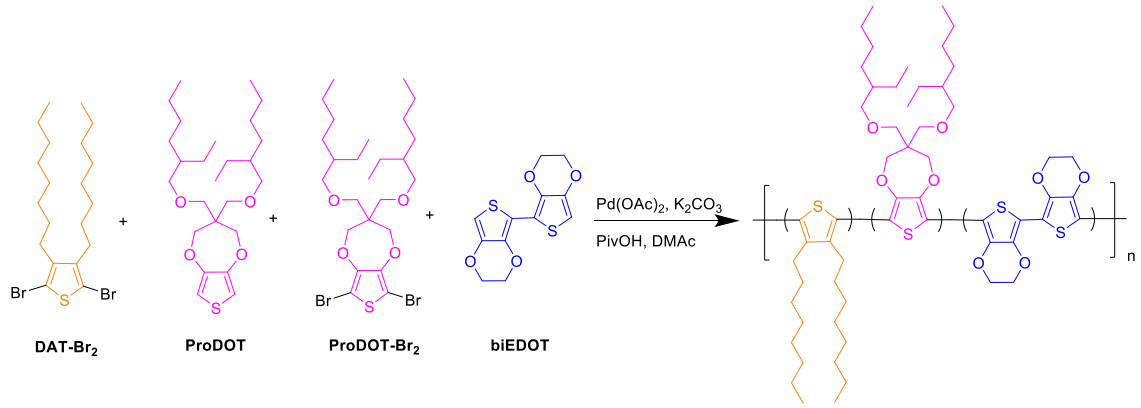

RC212: Dark red solid in 69% yield (120 mg). ^{1}H NMR (300 MHz, $CDCl_3$) δ 4.48-4.22 (br, 16H), 4.19-3.99 (br, 4H), 3.64-3.40 (br, 4H), 3.36-3.18 (br, 4H), 2.82-2.50 (br, 8H), 1.67-1.14 (br, 66H), 0.98-0.72 (br, 24H). Elemental Analysis Calculated: C 66.46, H 8.21, S 13.65; Found: C 65.20, H 7.43, S 13.93. GPC: Mn: 15 kDa, Đ: 1.8, in $CHCl_3$ vs PS.

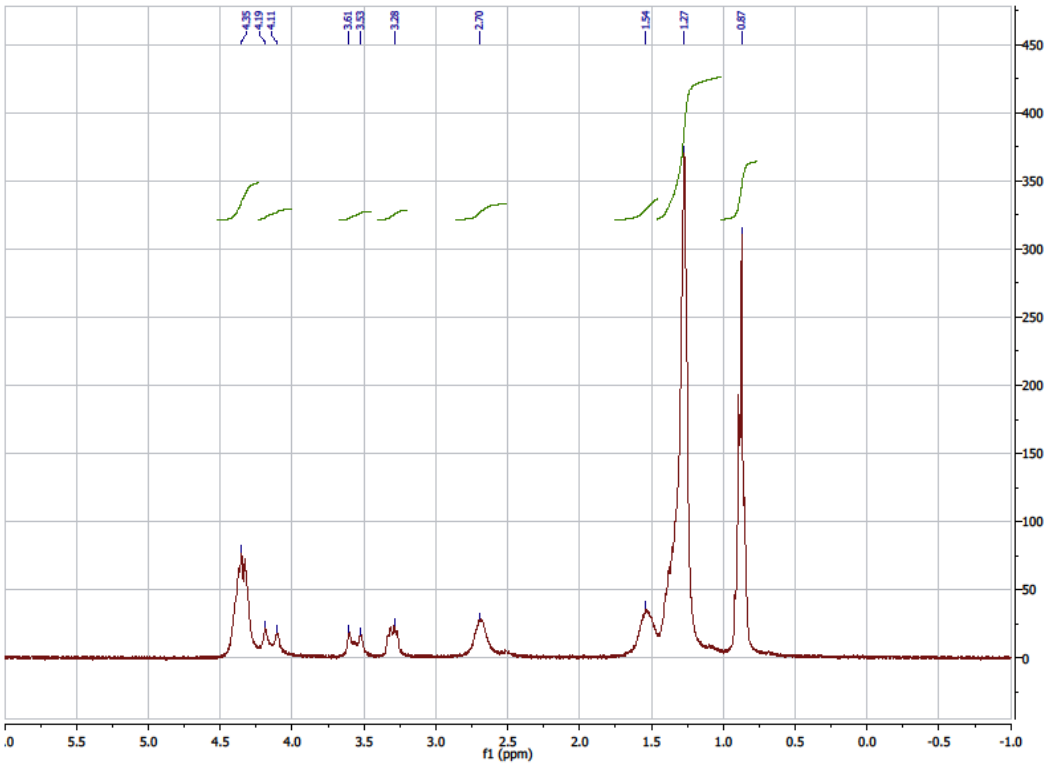

^{1}H NMR for **RC212**

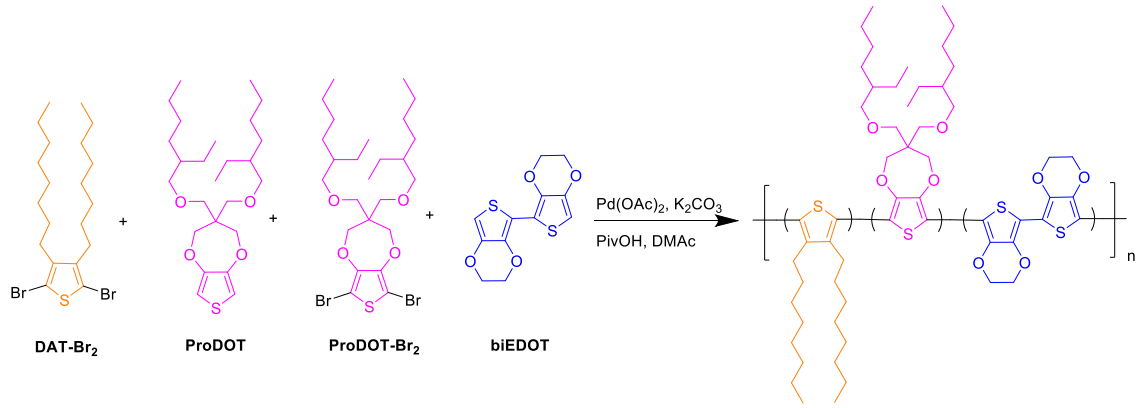

RC121: Purple solid in 81% yield (255 mg). ^{1}H NMR (300 MHz, $CDCl_3$) δ 4.48-4.22 (br, 8H), 4.19-3.99 (br, 8H), 3.64-3.40 (br, 8H), 3.36-3.18 (br, 8H), 2.82-2.50 (br, 4H), 1.67-1.14 (br, 60H), 0.98-0.72 (br, 30H). Elemental Analysis Calculated: C 67.35, H 8.85, S 10.83; Found: C 66.90, H 8.39, S 11.34. GPC: Mn: 26 kDa, Đ: 3.4, in $CHCl_3$ vs PS.

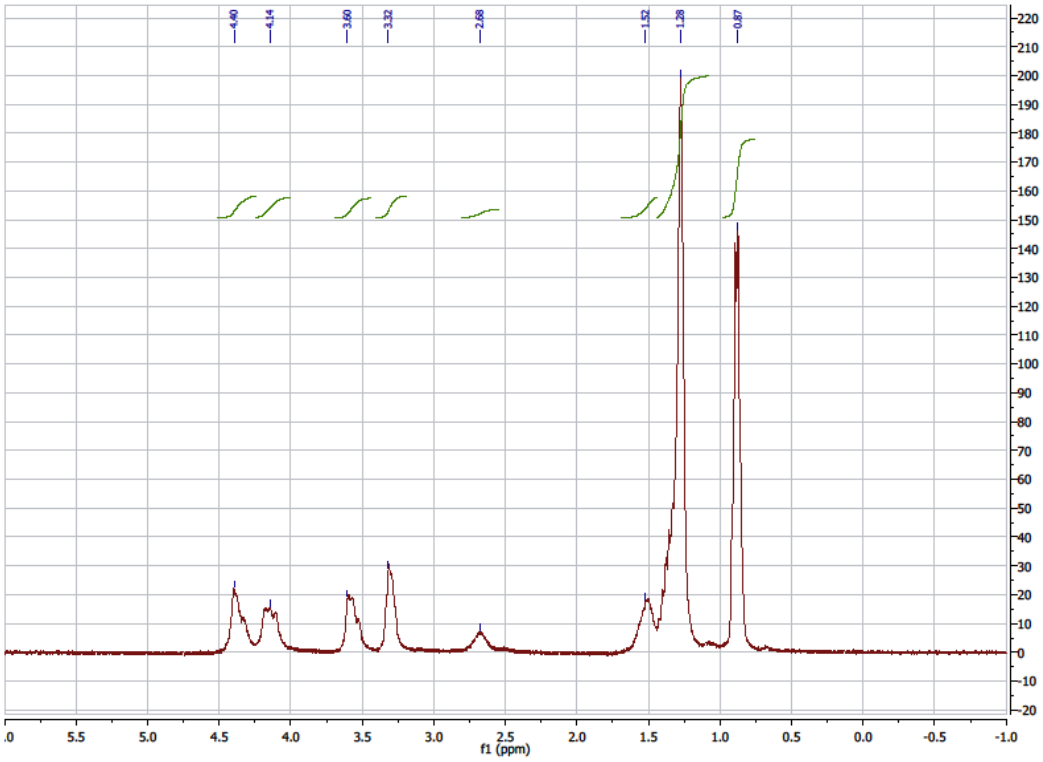

^{1}H NMR for **RC121**

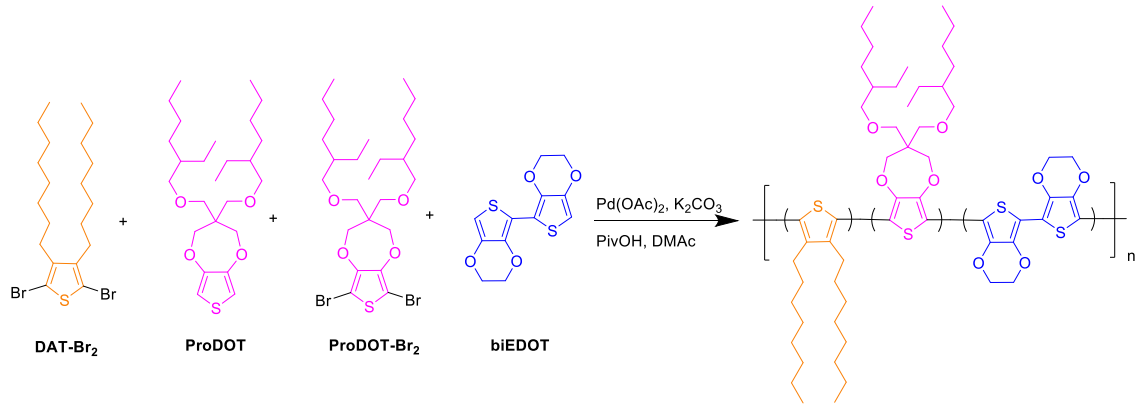

RC131: Purple solid in 69% yield (282 mg). ^{1}H NMR (300 MHz, $CDCl_3$) δ 4.48-4.22 (br, 8H), 4.19-3.99 (br, 12H), 3.64-3.40 (br, 12H), 3.36-3.18 (br, 12H), 2.82-2.50 (br, 4H), 1.67-1.14 (br, 78H), 0.98-0.72 (br, 42H). Elemental Analysis Calculated: C 67.60, H 9.04, S 10.02; Found: C 65.00, H 8.39, S 10.94. GPC: Mn: 17 kDa, Đ: 2.3, in $CHCl_3$ vs PS.

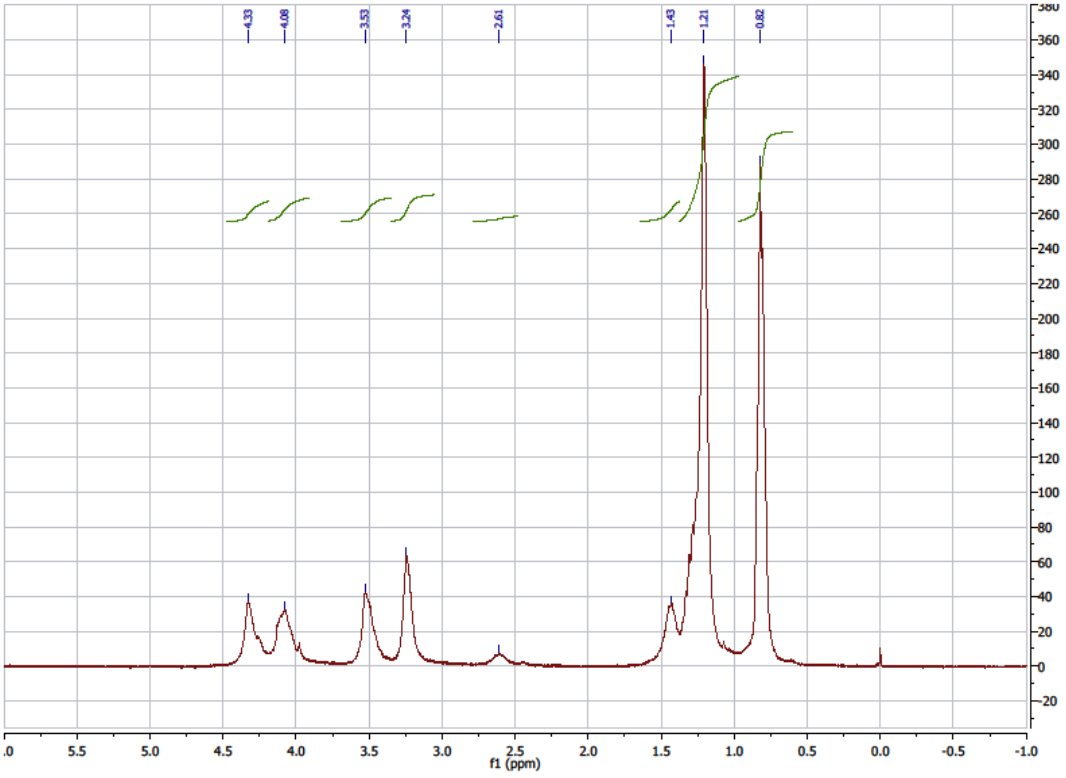

^{1}H NMR for **RC131**

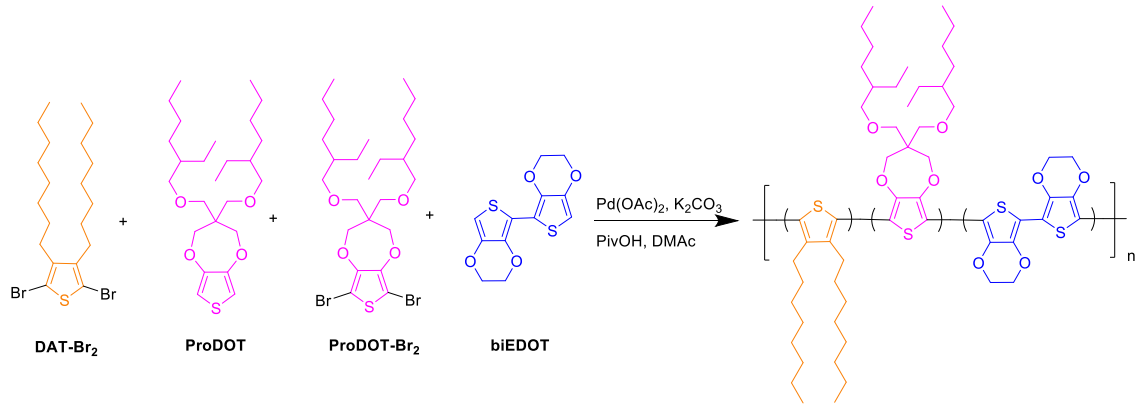

RC122: Dark purple solid in 67% yield (251 mg). ^{1}H NMR (300 MHz, $CDCl_3$) δ 4.48-4.22 (br, 16H), 4.19-3.99 (br, 8H), 3.64-3.40 (br, 8H), 3.36-3.18 (br, 8H), 2.82-2.50 (br, 4H), 1.67-1.14 (br, 60H), 0.98-0.72 (br, 30H). Elemental Analysis Calculated: C 64.90, H 8.06, S 12.63; Found: C 64.46, H 7.40, S 13.01. GPC: Mn: 15 kDa, Đ: 1.7, in $CHCl_3$ vs PS.

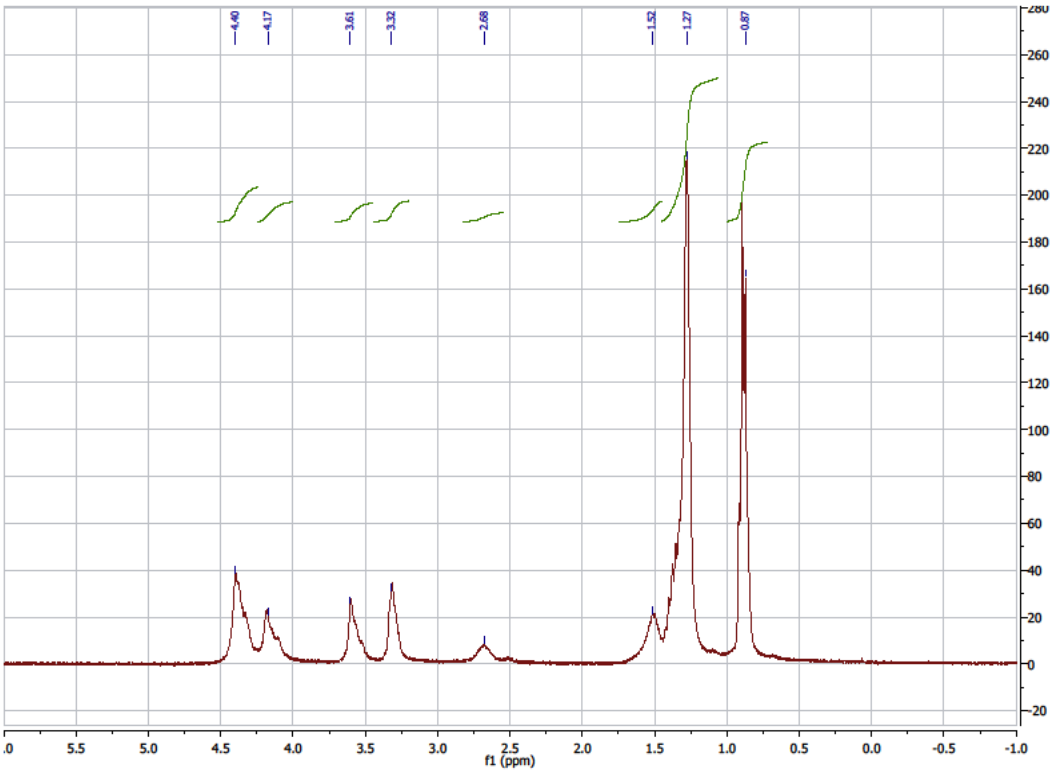

^{1}H NMR for **RC122**

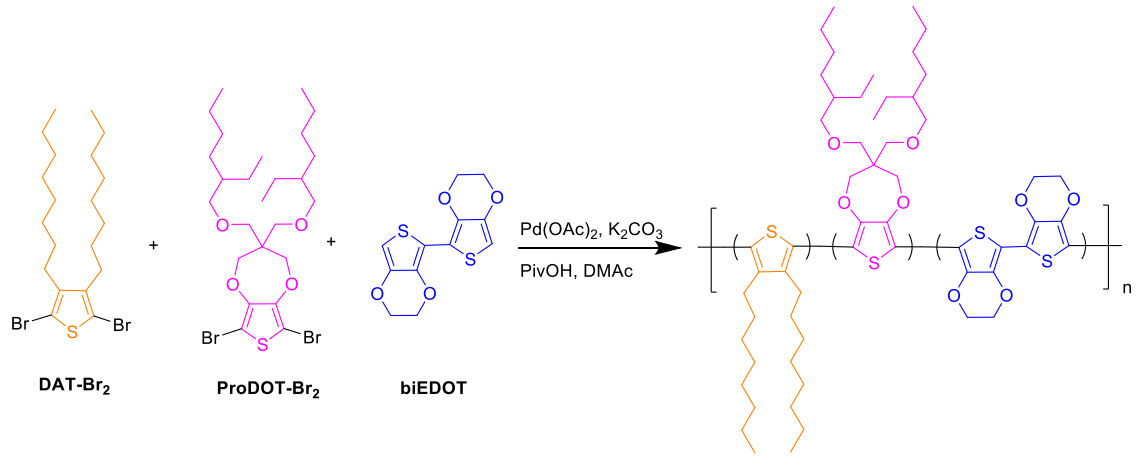

RC112: Dark blue solid in 70% yield (197 mg). ^{1}H NMR (300 MHz, $CDCl_3$) δ 4.48-4.22 (br, 16H), 4.19-3.99 (br, 4H), 3.64-3.40 (br, 4H), 3.36-3.18 (br, 4H), 2.82-2.50 (br, 4H), 1.67 -1.14 (br, 42H), 0.98-0.72 (br, 18H). Elemental

Analysis Calculated: C 63.74, H 7.53, S 14.38; Found: C 62.48, H 6.84, S 14.75. GPC: Mn: 10 kDa, Đ: 1.5, in $CHCl_3$ vs PS.

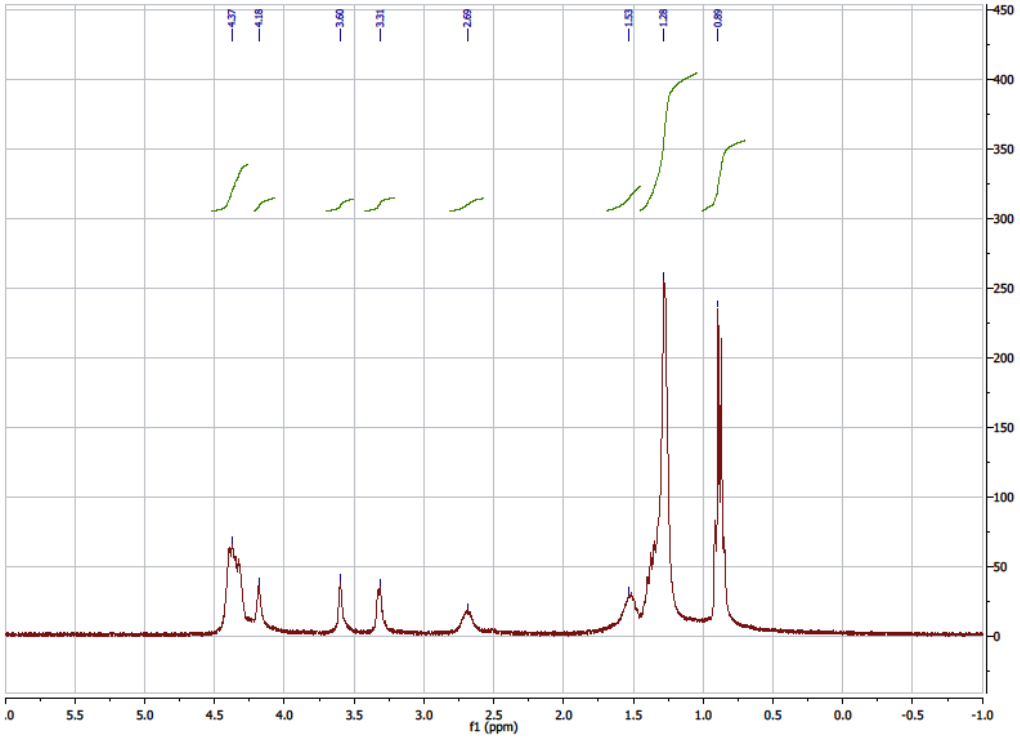

^{1}H NMR for **RC112**

Chapter 5 - Electrochromism of Alkylene-linked Discrete Chromophore Polymers with Broad Radical Cation Light Absorption

Adapted From:

Christiansen, Dylan T.; Wheeler, David L.; Tomlinson, Aimée L.; and Reynolds, John R.; Electrochromism of Alkylene-linked Discrete Chromophore Polymers with Broad Radical Cation Light Absorption; *Polymer Chemistry*; **2018**; 9, 3055-3066

This study focuses on examining the design principles of creating multi-heterocycle chromophores with a discrete conjugation length, which absorb ultraviolet light in the neutral state, and upon oxidation absorb throughout a broad spectral range in the visible. In this analysis, three discrete-length chromophore polymers with alkylene linkers were examined via time dependent DFT, synthesized via direct heteroarylation polymerization, and the electrochromic properties of their thin film characterized. Using a feedback loop of theoretical calculations with design and synthesis, it is elucidated how steric interactions can be used to control the absorption of the neutral and oxidized states of these discrete chromophore polymers. It is shown that systems with high inter-ring strain can be used to increase the molar absorptivity of the charged state by forming multiple radical cation states on a single discrete chromophore. The challenges of electrochemical

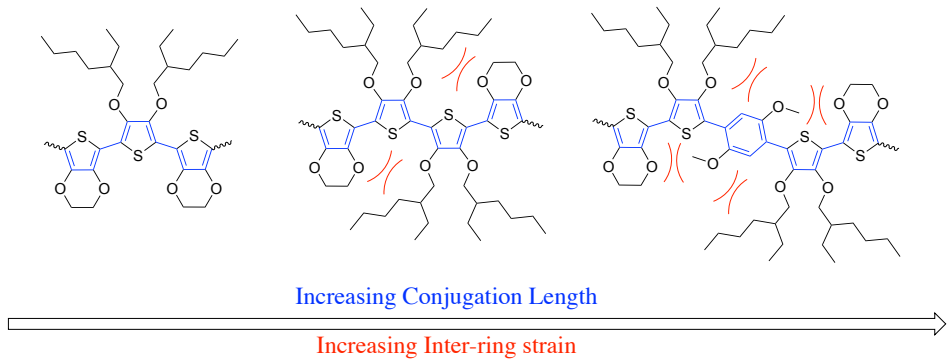

Figure 5.1. Discrete chromophores examined in computational and experimental feedback loop

redox reversibility in the solid state in these systems, while they maintain their chemical redox reversibility is also demonstrated.

5.1 Design Approach

Towards the aim of creating anodically coloring materials, a family of polymers with discrete length, π-conjugated chromophores was synthesized to give insight into these fundamental structure-property relationships (repeat unit structures in Scheme 5.1.1) with the goal of providing design characteristics for anodically coloring electrochromic polymers. This family of chromophores models the interplay between increasing chromophore conjugation length and interring steric strain and examines the absorption characteristics of both the neutral and radical cation states of the chromophores, while using electron rich moieties to maintain a low oxidation potential. Polymers containing discrete chromophores systems have been explored as an approach to electrochromics before. [158,159] In these experiments both chromophores in a polymer chain as well as conjugated chromophore side chains were examined showing electrochemical activity and optical switching upon oxidation/reduction.

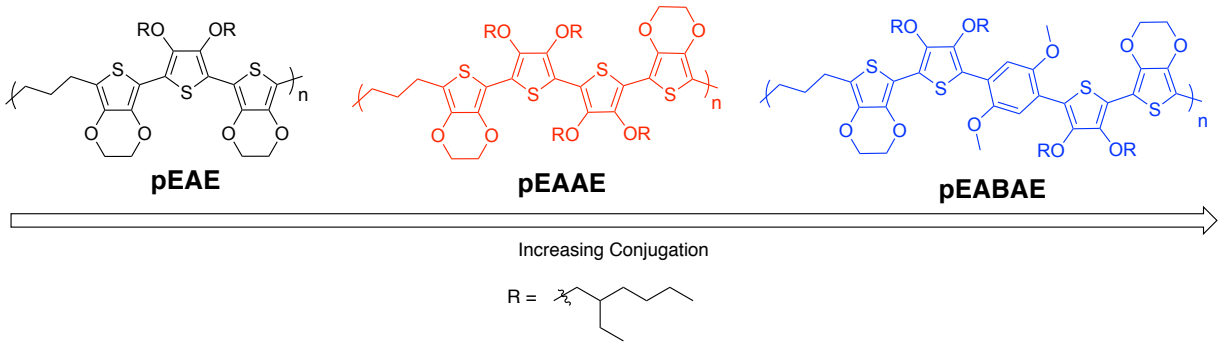

Scheme 5.1.1. Repeat unit structures for a family of dioxythiophene based discrete length chromophore polymers being investigated in order of increasing conjugation.

5.2 Quantum Chemical Calculations (David Wheeler and Dr. Aimée Tomlinson)

The quantum chemical calculations for this project were executed by David Wheeler and Dr. Aimee Tomlinson. I was involved with the design of the experiments, data processing, and writing of this section of the publication that came from this body of work.

5.2.1 Interring Strain

To elucidate the influence of structural modification on the electronic and spectral properties of the chromophores, density functional theory (DFT) was utilized. Previously, it was shown mPW1PBE functional paired with the cc-PVDZ basis set (detailed information for each included in the Supplemental Information) provides excellent correlation of optical properties to experimental spectra for dioxythiophene-containing systems.[160] To mimic the environment each system experiences during experimental data collection, all computations were performed with the incorporation of the conductor polarizable calculation model (CPCM) using dichloromethane as the applied dielectric. For each ECP, this level of theory was applied to a single chromophore in its neutral, radical cation, and dication states to predict changes in the optimized ground state geometry upon oxidation. Time-dependent DFT (TD-DFT) calculations were then performed on these geometries to simulate UV-Vis spectra, which provided insight on tuning the absorptivity of chromophores. Chromophores with high energy π-π* transitions were designed by restricting the conjugation length to three, four, and five heterocycles while also maintaining a low oxidation potential.

The impact of interring strain between neutral and oxidized states was examined utilizing the first set of ter(heterocycle) systems shown in Scheme 5.2.1.1. Each chromophore contained terminal groups of methyl-capped 3,4-ethylenedioxythiophene (E) and a distinct middle heterocycle: either a branched alkyl ether functionalized 3,4-propylenedioxythiophene (P) or a 3,4-

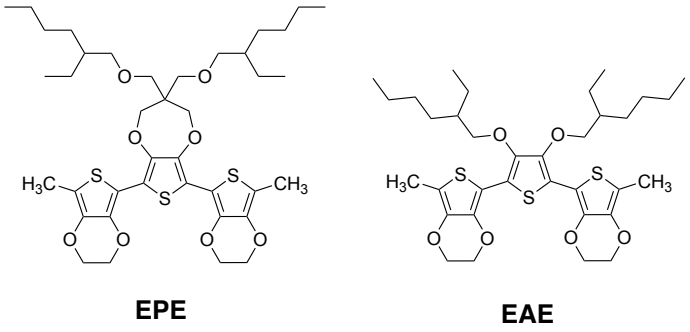

Scheme 5.2.1.1. Methyl-terminated ter(heterocycles) evaluated in the strain study.

bis(2-ethylhexyloxy)thiophene (A). By changing the identity of the middle heterocycle, the proximity of the alkoxy-chains relative to the conjugated backbone varied as a function of distance, while the number of π-electrons in the chromophore remained unchanged. The degree of interring strain was determined by observing the changes in dihedral angles between the terminal and middle heterocycles in each chromophore.

The results of the structural data for these ter(heterocycles) from the optimized geometry are collated in Table 5.2.1.1. The rings were numbered in each chromophore, and the interring bond lengths, dihedral angles, and first excited state energies (TD-DFT HOMO-LUMO gap) were measured. Examining the dihedral angle measurements, it is clear that the proximity of the 2-ethylhexyl solubilizing groups affect the degree of conjugation as the HOMO-LUMO gap for EAE is 0.68 eV higher than EPE. Since the solubilizing chains are farther from the backbone of the chromophore in EPE, all three heterocycles remain in excellent conjugation with one another, independent of the charged state. However, for the neutral EAE chromophore, only two of the three heterocycles are found to be exceptionally planar (175.2°) while the third heterocycle remains orthogonal (91.5°). Upon oxidation, the EAE chromophore becomes increasingly planar,

Table 5.2.1.1. Structural Data for Discrete Chromophore Oligomers. The figure key shows how rings and dihedral angles are numbered and symbolized in the table.

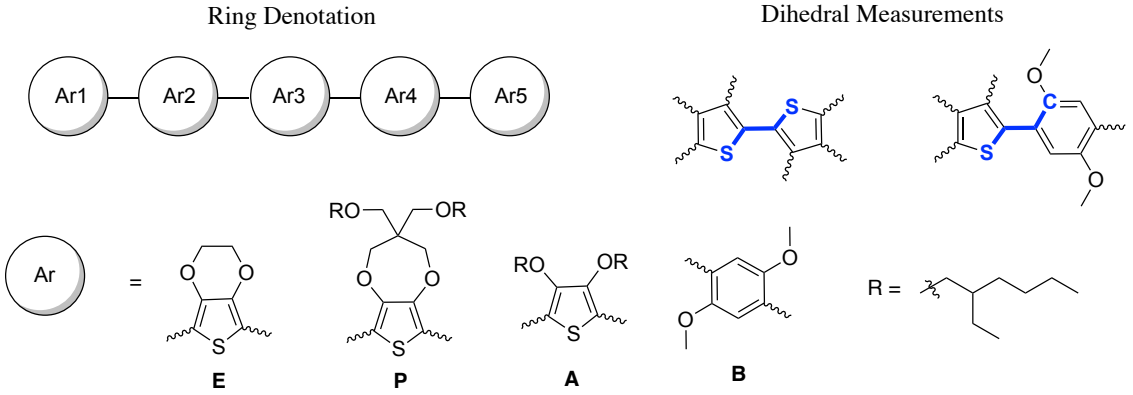

Calculation	EPE		EAE		EAAE		EABAE	
	neutral	polaron	neutral	polaron	neutral	polaron	neutral	polaron
First-Excited State Energy (eV)	3.00	-	3.68	-	3.15	-	3.64	-
Ar1-Ar2 (Å)	1.44	1.41	1.46	1.41	1.44	1.41	1.46	1.41
Ar2-Ar3 (Å)	1.44	1.41	1.44	1.41	1.46	1.41	1.47	1.44
Ar3-Ar4 (Å)	-	-	-	-	1.45	1.41	1.47	1.44
Ar4-Ar5 (Å)	-	-	-	-	-	-	1.46	1.42
Ar1-Ar2 Dihedral	177.2	178.3	91.5	164.4	174.8	179.7	86.8	167.3
Ar2-Ar3 Dihedral	177.2	178.3	175.2	178.8	111.6	151.4	121.5	137.7
Ar3-Ar4 Dihedral	-	-	-	-	174.8	179.7	125.6	132.5
Ar4-Ar5 Dihedral	-	-	-	-	-	-	83.7	169.1

reducing the orthogonal character (178.8° and 164.4°). The oxidized chromophores exhibit more quinoidal character as the bond length between heterocycles decrease by ~0.03 Å.

The structural models for the ter(heterocycles) are corroborated with the analysis of the calculated UV-Vis spectra as depicted in Figure 5.2.1.1. The absorption of EPE (λ_{max} = 413 nm) occurs extensively throughout the visible due to a lack of interring strain, while the converse is observed for EAE (λ_{max} = 337 nm). This comparative blue shift is attributed to the effective

conjugation between only two of the three heterocycles in EAE (Figure 5.2.2.1). While the neutral spectra for each chromophore are unique, the radical cation spectra have surprisingly similar characteristics (energies and band widths). As predicted from Figure 1, there are two peaks in the radical cation spectra for each chromophore, the higher energy peak indicative of the singly occupied molecular orbital (SOMO) to LUMO transition (b) and the lower for SOMO-n to SOMO (c) (note only the high energy radical cation peak is shown in Figure 5.2.1.1). For the SOMO to LUMO transitions, there is only a 7 nm difference between the peak maxima of each chromophore. In the case of the lower energy transitions (refer to Supplementary Figure 5.8.1), the peak maxima occur at 831 nm (EPE) and 809 nm (EAE) with similar oscillator strengths. These spectra demonstrate the ability to control the neutral state absorbance while producing nearly the same oxidized spectra. Thus, this theoretical experiment guides the focus of synthetic efforts towards highly strained acyclic systems to produce colorless neutral chromophores.

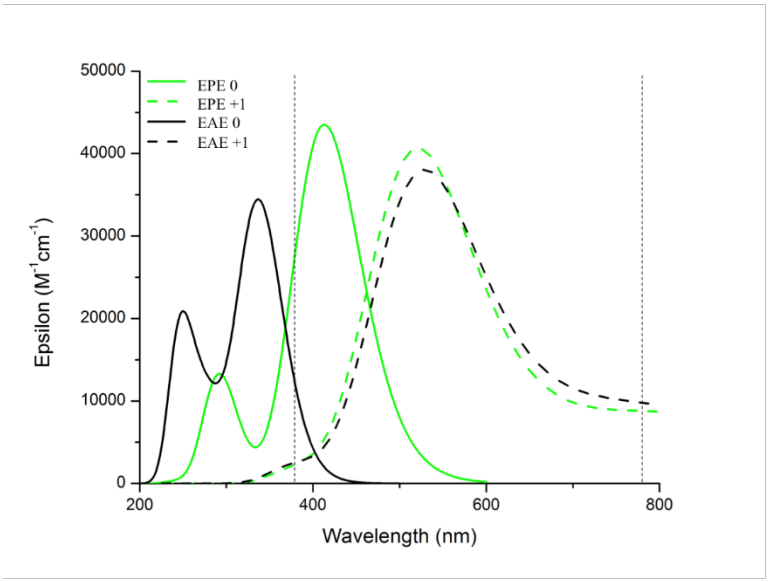

Figure 5.2.1.1. UV-Vis spectra of EPE and EAE in the neutral (solid) and radical cation (dashed) states. Vertical dotted lines indicate the visible range of 380-780 nm.

5.2.2 Conjugation vs. Strain

Next attention was focused on designing materials that absorb little to no visible light in the neutral state but exhibit broad absorbance upon oxidation. Through the incorporation of excess strain, the absorption of a chromophore is driven into the UV-region. Additionally, increasing the conjugation by utilizing more aromatic systems in a single chromophore facilitates the polaronic spectrum to absorb broadly in the visible. To this end, the methyl-capped four and five ring chromophores shown in Scheme 5.2.2.1 were explored where the latter included dimethoxybenzene (B), which offers a high degree of strain and an inherently wider optical gap than thiophene-based systems due to an increased aromaticity.

Examining the neutral structural data in Table 5.2.1.1, it is evident that the EABAE system contains a significant amount of strain as the dihedral angles between each chromophore ranges between 83.7° - 125.6°, limiting the conjugation along the backbone. For EAAE, the dihedral angles between each E and Ac heterocycles are exceptionally planar (174.8°) while the dihedral angle between the two Ac units exhibit considerable strain (111.6°). These effects are further reflected in the calculated UV-Vis spectra (Figure 5.2.2.2). In comparison to the neutral, low-energy peak of EAE, the peak for EAAE is red-shifted by 133 nm into the visible region making this chromophore undesirable. However, in the case of the EABAE, the simulated spectrum

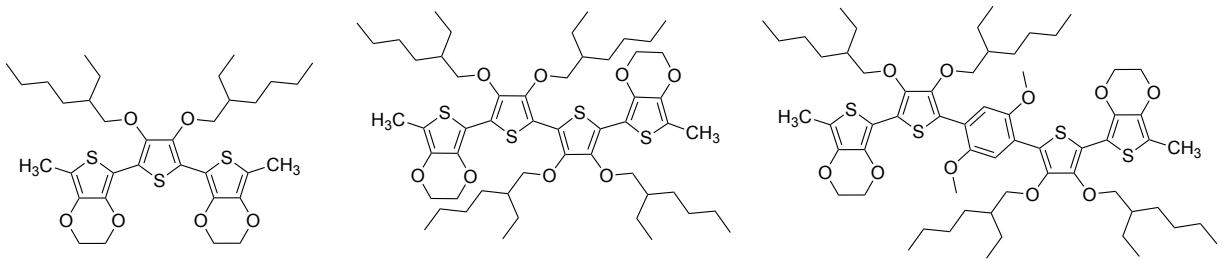

Scheme 5.2.2.1. Structural scheme depicting the chromophores evaluated in the conjugation study.

produces a single peak, which aligns with the low energy peak of EAE. The calculations for EABAE showed the primary transition occurs from HOMO → LUMO with an oscillator strength of 0.95. All other transitions had oscillator strengths less than 0.11 and were therefore negligible in the absorption spectrum. Upon closer analysis of the frontier molecular orbitals (Figure 5.2.2.1), the majority of electron density in the ground-state is delocalized on the EAB portion of the chromophore; in essence half of the molecule. Due to the increased strain along the backbone, the effective conjugation along the chromophore is compromised, producing an optical gap comparable to that observed in EAE.

Upon oxidation, all three chromophores become dramatically planar. For the EAAE chromophore, the E-A dihedrals planarize to 179.7° and the A-A dihedral shifts to 151.4°. Similarly, for EABAE, the range of dihedral angles decreases to 132.5° to 169.1°. Each oxidized

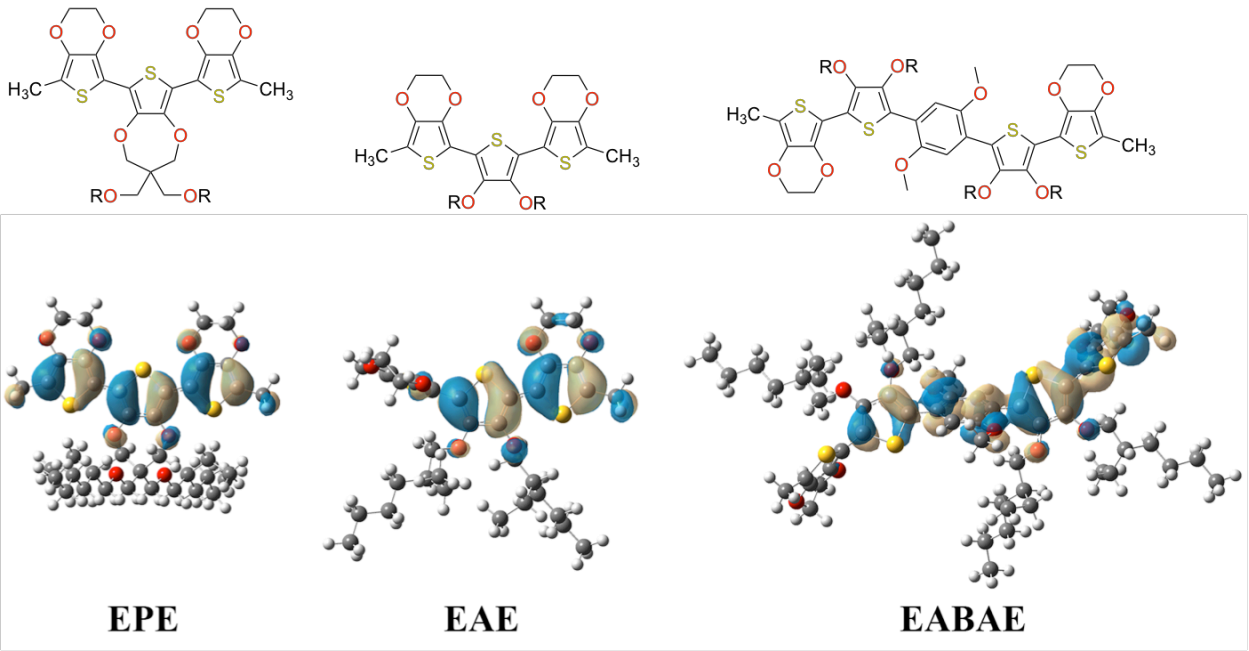

Figure 5.2.2.1. Frontier molecular orbital diagrams detailing the HOMO of the neutral, ground-state energy of EPE, EAE, and EABAE.

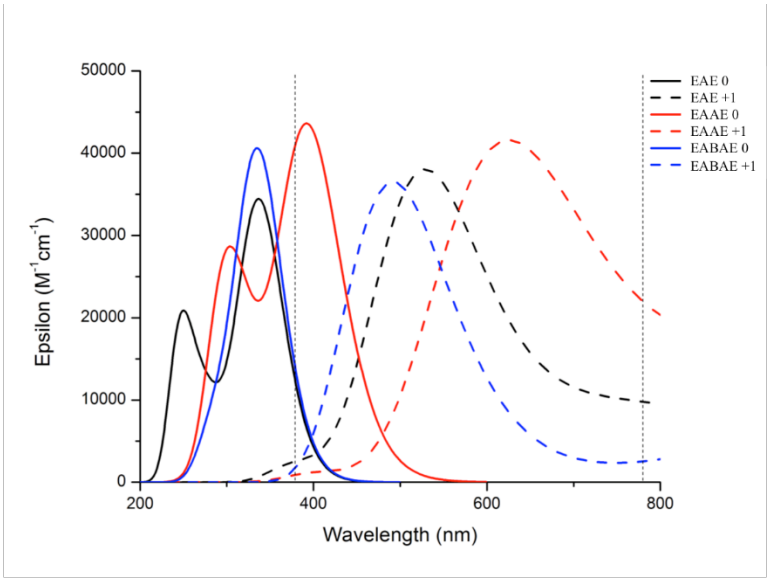

Figure 5.2.2.2. Calculated UV-Vis spectra of the neutral (solid) and radical cation (dashed) states of EAcE, EAAE, and EABAE. Vertical dotted lines indicate the visible range of 380-780 nm.

chromophore is found to absorb significantly in the visible, particularly EAE with a peak maximum at 527 nm and broad absorption leading into the near IR. EAAE exhibits a broad absorption leading into the near IR due to a prominent red-shift of 118 nm. Finally, EABAE has a single visible peak comprised of two excited states (474 nm and 514 nm, Figure S3k), which is blue-shifted to EAE. Upon closer examination of all spectra, EAE and EABAE are the most promising electrochromic materials due to their high transmissivity coupled with visible absorption in their neutral and radical cation states, respectively.

5.3 Synthesis of Discrete Chromophore Polymers *via* Direct Arylation

The target polymers in Scheme 5.1.1 were synthesized as described in Scheme 5.3.1. By lithiation of 3,4-ethylenedioxythiophene (EDOT) and subsequent quenching with propylene-1,3-

ditosylate the dihydrin monomer (E~E) was synthesized. The polymerizations were carried out via a direct heteroarylation mechanism with the respective dibromo monomers to create the family of polymers with discrete chromophores. The polymers were purified via Soxhlet extraction and the repeat unit structure confirmed using ^{1}H and $^{13}C\{^{1}H\}$ NMR and elemental analysis. Polymer molecular weights were analyzed with gel-permeation chromatography (GPC) in $CHCl_3$ at 40°C and the number average molecular weights and dispersity (M_n, Đ) relative to polystyrene standards are as follows: pEAE (14.8 kDa, 2.0), pEAAE (18.5 kDa, 1.8), pEABAE (9.7 kDa, 2.0) (Supplementary Figure 5.8.2). Synthetic procedures for E~E can be found in the Section 5.9 along with characterization results on ^{1}H NMR, $^{13}C\{^{1}H\}$ NMR, mass spectrometry, and elemental analysis.

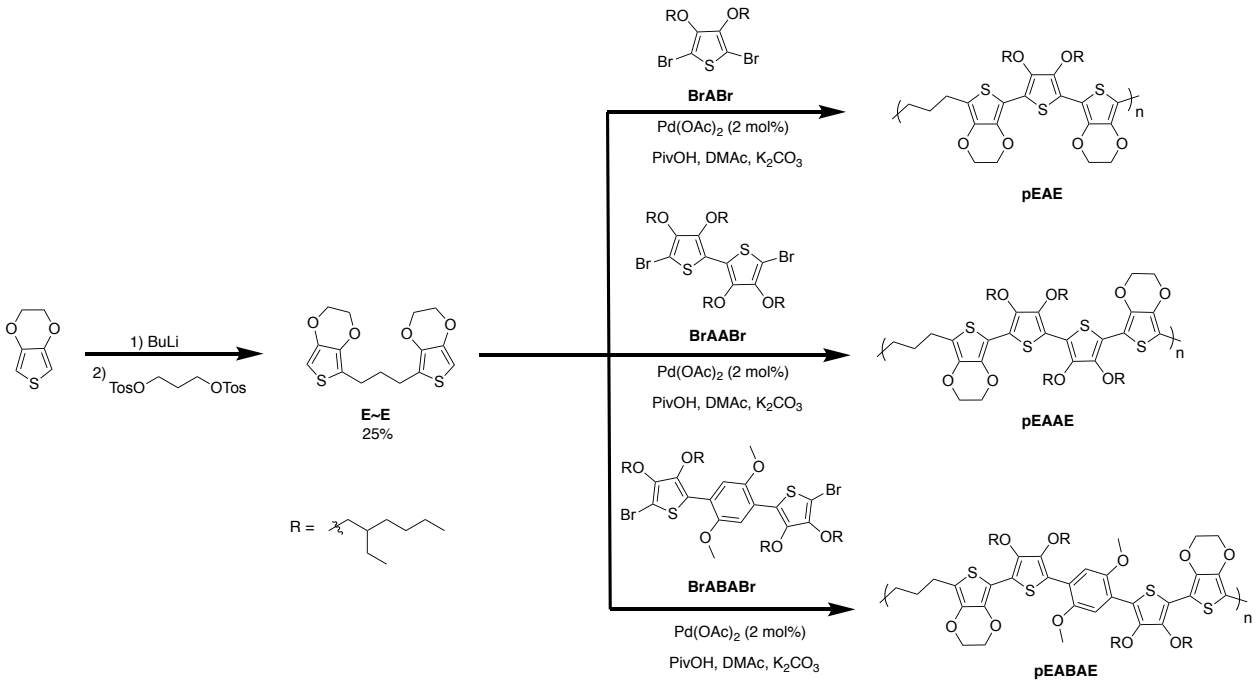

Scheme 5.3.1. Synthetic scheme outlining the synthesis of the target polymers. (PivOH = pivalic acid and DMAc = *N,N*-dimethylacetamide)

5.4 Electrochemical and Optical Properties

All electrochemical measurements were performed on films that were drop cast (3 µL of 2 mg/mL solutions in $CHCl_3$) on glassy carbon electrodes in 0.5 M tetrabutylammonium hexafluorophosphate ($TBAPF_6$). Cyclic voltammetry (CV) and differential pulse voltammetry (DPV) were used to probe the redox properties of the target polymers as illustrated by the results in Figure 5.4.1. The onsets of oxidation measured via DPV were 0.13 V, 0.16 V, and 0.25 V for pEAE, pEAAE, and pEABAE, respectively. This is counter-intuitive to the idea that increasing conjugation causes a raising of the HOMO and thus lower ionization potential, but is corroborated by the DFT calculations predicting this larger energy barrier to planarize for the A-A bond (Table 5.2.1.1). The strong A-A steric interaction in pEAAE leads to a large planarization energy, which leads to a similar oxidation potential despite the increase in conjugation length. As predicted by the DFT calculations this steric effect is even more intense in the case of the pEABAE leading to an even higher oxidation potential.

Upon examination of the CVs in Figure 5.4.1b, it becomes evident how similar pEAE and pEAAE behave electrochemically with one distinct oxidation. pEABAE, on the other hand, has two distinct oxidations, suggesting further oxidation to a dication. Examination of the charge

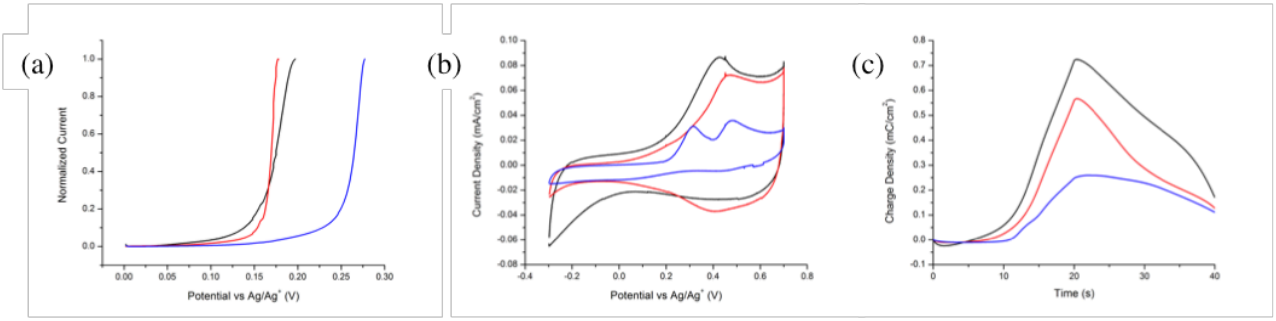

Figure 5.4.1. (a) DPV of thin films measured at 5mV/sec. (b) CV (30th scan) of the polymer films from 0-0.7V vs. Ag/Ag^+. (c) Charge passed through the film over the course of the 30th CV scan showing slow/incomplete reduction. (pEAE-black, pEAAE-red, pEABAE-blue).

accumulation results in Figure 5.4.1c, show both processes through a cycle of the CV to be partially irreversible for all polymers. This finding suggests trapped radical cation states in the film that cannot be fully reduced through electrochemical means. In order to ensure that the materials were not irreversibly degrading with the redox chemistry, the films were treated with hydrazine to successfully return them to their original oxidation state and color (Figure 5.4.2). Figure 5.4.2a shows the absorption of pEAAE as a pristine film and the formation of a broad absorption upon oxidation at +750 mV. Upon the application of a reducing potential of -500 mV for 5 minutes, only some of the original absorption is regained. This can be seen in Figure 5.4.2b as the material changes from a deep blue to a green in color as some low wavelength absorption returns. Upon removal of the electrodes and subsequent addition of hydrazine it can be seen from the photographs that the original color of the charge neutral state is returned.

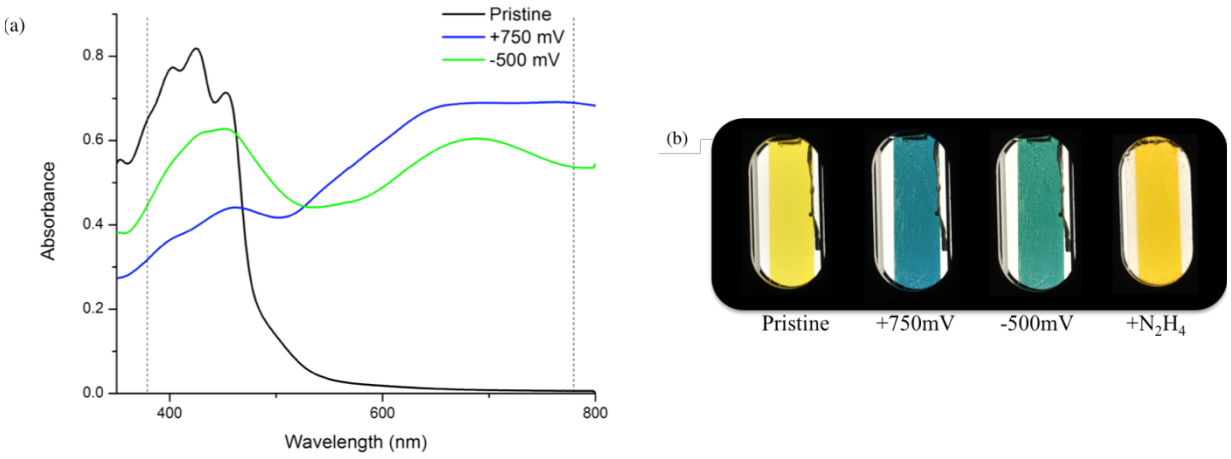

Figure 5.4.2. (a) Spectra of pEAAE showing the electrochemical irreversibility of the material upon oxidation. (b) Photographs of the same film showing the chemical reversibility of the system upon hydrazine reduction.

This irreversible electrochemical response is a surprising observation based on the high electroactivity of multi-heterocycle, broken conjugation linear polymers and acrylate coatings.[158,161–163] Figure 5.4.3 schematically shows a cross-sectional representation of the polymer at the interface of the electrode. It is speculated that, as the polymer film is being oxidized, the chromophore layer closest to the electrode is oxidized first, elevating its conductivity (Figure 5.4.3a). This increase in conductivity facilitates charge hopping between chromophores through the film, thus oxidizing the bulk (Figure 5.4.3b). Application of a reducing potential causes this first layer of chromophores to reduce to their neutral, insulating states (Figure 5.4.3c). This neutral layer acts as an insulating barrier preventing reduction of the remaining charged states in the polymer (Figure 5.4.3d). These films can be fully reduced back to the neutral with the addition of a chemical reductant, but the fully neutral form cannot be re-obtained based purely on

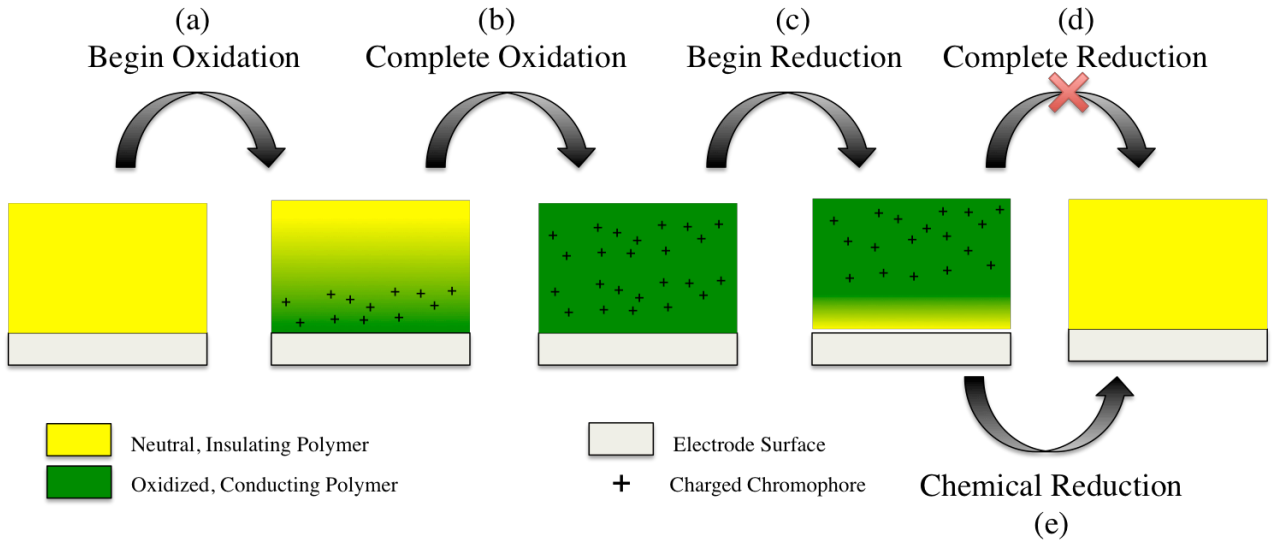

Figure 5.4.3. Cross sectional representation of broken conjugation ECP on an ITO glass substrate depicting the charge flow and postulated cause of electrochemical irreversibility. Note the ECP is immersed in electrolyte solution and each charge on the polymer is balanced by an electrolyte anion (PF_6^-).

electrochemical reduction (Figure 5.4.3e). This type of behavior is not useful for typical electrochromic applications, but could have potential use as a visual fuse that switches upon reaching an overpotential.[164–167] This fuse would remain in the new colored state until chemically reduced to the neutral state.

The energy and width of the radical cation absorption spectra and how the switching potentials can be tuned as they relate to the chromophores' structures are important in understanding these types of systems. To this end, the absorption properties of these polymers were examined. The UV/Vis spectra of the polymers were measured in a solution of 40 μg/ml in dichloromethane (DCM), normalized for Figure 5.4.4a. Contrary to the DFT calculations there is a red-shifting of the chromophores' absorbances increasing the conjugation of the dioxythiophene chromophores with λ_{max} for pEAE and pEAAE being 386nm and 424nm, respectively. However, due to the large steric strain between the AcDOTs and dimethoxybenzene in pEABAE, the

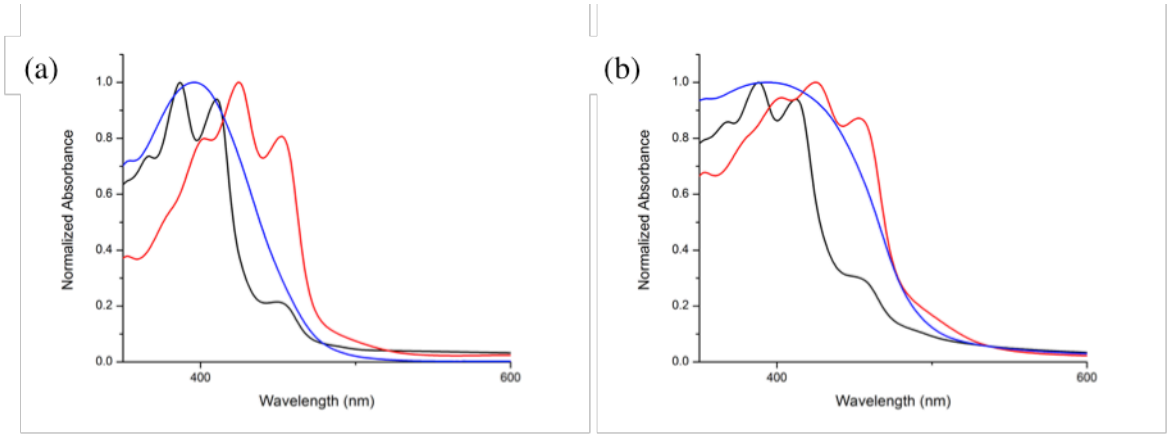

Figure 5.4.4. (a) Normalized solution UV/Vis absorbances of the polymers. (b) Normalized thin film absorbances of the polymers. (pEAE-black, pEAAE-red, pEABAE-blue). It can be seen that the absorption onset for these materials is redshifted moving to the solid state with a greater degree of broadening for pEABAE indicative of more chromophore-chromophore aggregation.

chromophore is twisted thereby lowering the extent of conjugation and a lower λ_{max} of 395nm.

To probe the spectral changes of the polymers during oxidation, films were spray coated onto ITO/glass using a hand-held airbrush from 3 mg/mL polymer-toluene solutions to an absorbance of 0.8-1.0 AU. As can be seen in Figure 5.4.4b, the normalized absorbance for the all of the polymers is largely unchanged relative to the solution spectra, other than peak broadening. This broadening is more significant in the case of pEABAE causing it to adopt an absorption onset closer to that of pEAAE.

5.5 Film Spectroelectrochemistry and Colorimetry

Spectroelectrochemical measurements were performed in 0.5 M $TBAPF_6$ in propylene carbonate with a platinum counter electrode and a Ag/Ag^+ reference electrode as shown in Figure 10 along with photographs of the films held at potential extremes dictated by the CVs results. As a pristine film, pEAE shown in Figure 5.5.1a absorbs at a λ_{max} of 386 nm (i) capturing only a small portion of the visible giving a pale-yellow color. Oxidation of pEAE to the radical cation state reduces the intensity of peak 'i' and gives rise to a sharp absorbance with at λ_{max} 582 nm (ii) centered in the visible with a less intense peak in the near IR at 935 nm (iii). This new oxidation state is perceived as blue as the lower energy red and green light is absorbed and blue is transmitted.

Turning attention to Figure 5.5.1b the neutral absorbance of pEAAE is redshifted compared to pEAE with a λ_{max} at 424 nm (iv), thus absorbing more blue light and creating a deeper yellow color. Upon oxidation of pEAAE, the neutral peak 'iv' reduces in intensity and the polymer radical cation begins to absorb in the visible at λ_{max} at 687 nm (v) and in the near IR at 1050 nm (vi), both redshifted compared to pEAE as predicted by calculations. Upon further oxidation, peak 'v' begins to decrease in intensity with the continued growth of a broadly absorbing peak 'vi' in the near-IR

indicative of a dication species. This charged state has some absorbance of lower energy red light, allowing more green and blue light to transmit, and is perceived as a teal-turquoise color.

With increasing conjugation, it was expected that pEABAE would have a neutral peak red-shifted compared to the two shorter chromophores, but the steric repulsion between the dimethoxybenzene and AcDOTs cause a decrease of π overlap in the center of the chromophore, widening the optical gap, and giving rise to an absorption with λ_{max} at 395 nm (vii). This

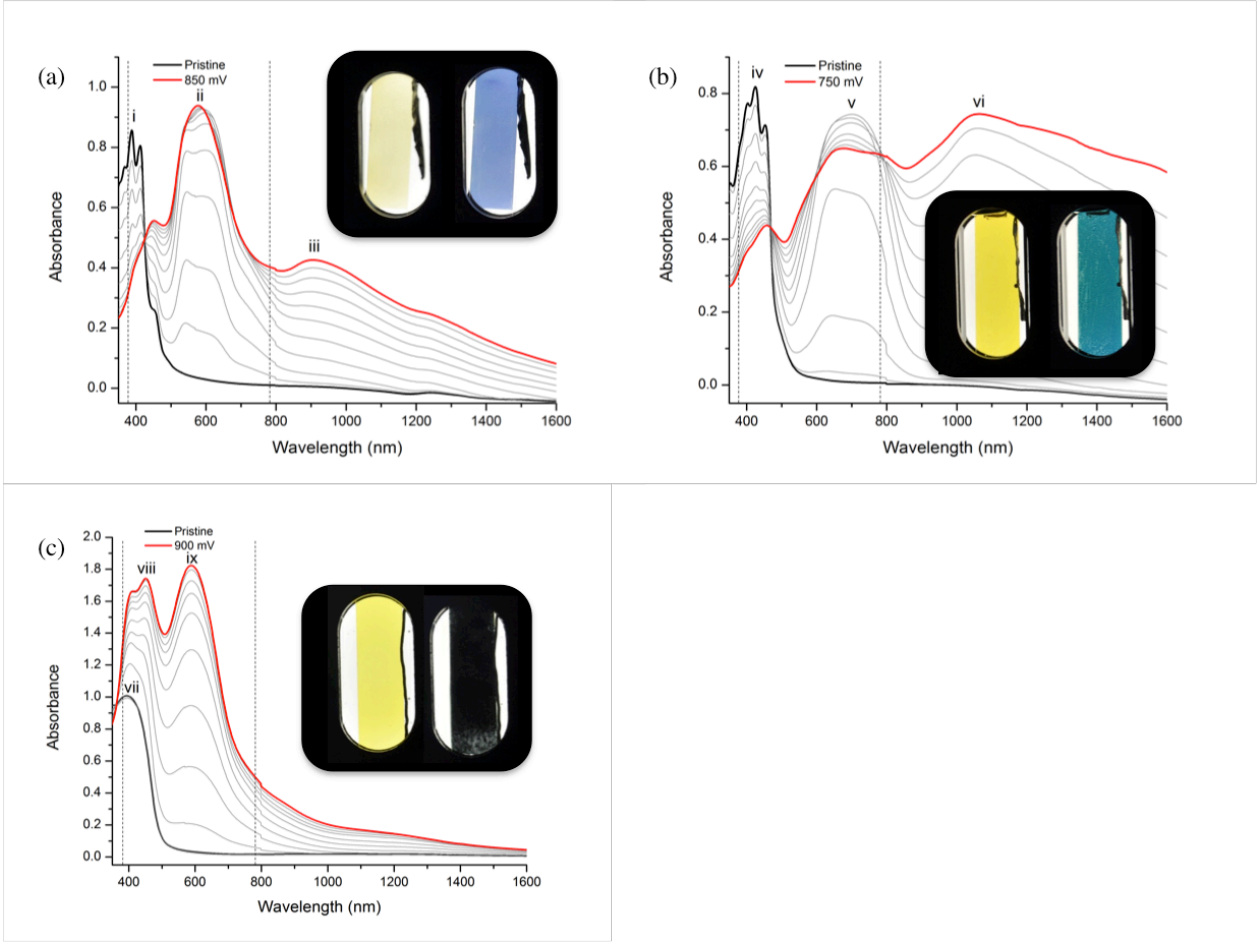

Figure 5.5.1. Spectroelectrochemistry of polymer films on ITO-glass in 0.5 M $TBAPF_6$-PC with potential steps of 50 mV from the pristine (black trace) to the fully oxidized form (red trace). Photographs of each polymer (left – as cast, right – oxidized) are in the insets of each representative spectrum (pEAE (a), pEAAE (b), pEABAE (c))

absorbance profile yields a film that is similar in appearance to that of pEAAE. Upon oxidation of pEABAE there is the growth of two sharp and intense peaks with λ_{max} at 450 nm (viii) and 587 nm (ix). The combined absorbance of these peaks allows for this charged state absorption to encompass a large portion of the visible range causing the film to appear as a dark black. Note that the intensity of the absorbance in this material's oxidized state is much higher than that of the neutral state. This large increase in intensity and the high energy of the absorptions compared to the all dioxythiophene chromophores are likely from two different radical cation species or the formation of radical cation aggregates.

The L*a*b* color space results for the polymers under study are presented graphically in Figure 5.5.2 with the values collated in Table 5.5.1. In this color space, positive a*and b* represents red and yellow while the negative values indicate blue and green, respectively. As the magnitudes of a* and b* increase, the color becomes more saturated, and as one traverses between color points, the hue changes. L* depicts the lightness: a value of 0 would be black and 100 would be white.

In the neutral state, pEAE is a low saturation yellow (b* = 26) with a high lightness value (L* = 96), due to the minimal absorbance tailing into the high-energy side of the visible spectrum. Comparatively, pEAAE and pEABAE have L* and a* values similar to pEAE, but are much more saturated (higher b*) observed by their more intense yellow color. Upon oxidation, pEAE passes through the origin along the b* axis to create a blue radical cation state with a similar saturation to that of the neutral form with a much lower L* value, 45. pEAAE follows the formation of a green radical cation state with a largely negative a* value, and upon further oxidation the color coordinates move towards the origin to make a low saturation blue-green color at 750mV. For pEABAE the formation of the two radical species causes the loss of color saturation and an

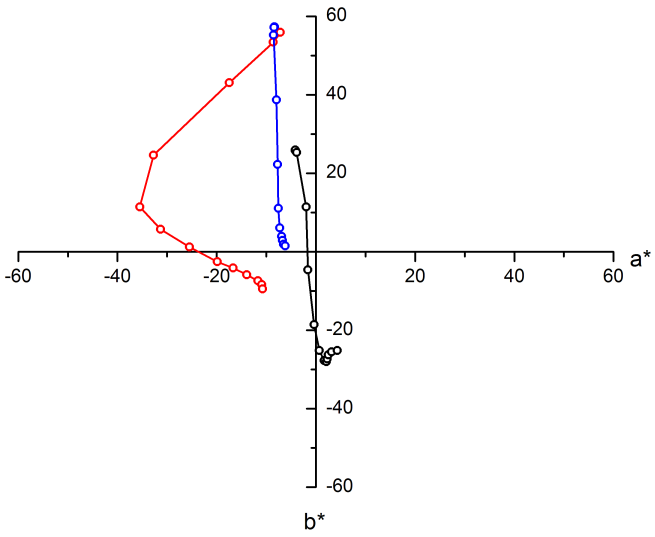

Figure 5.5.2. Progression of L*a*b* color coordinates of polymer films from pristine to oxidized (pEAE-black, pEAAE-red, pEABAE-blue).

oxidized state with color coordinates close to the origin (colorless). The L* value dropping to 18 indicates a low percentage of light transmitting across the visible. This appears to the eye as a dark, black film.

Table 5.5.1. Color Coordinate Values for the Pristine and Oxidized States of Discrete-Chromophore Polymers

	Pristine	Radical Cation
Polymer	L*, a*, b*	L*, a*, b*
pEAE	96, -4, 26	45, 4, -25
pEAAE	96, -7, 56	64, -12, -7
pEABAE	95, -8, 57	18, -6, 1

5.6 Charge State Elucidation of pEABAE

In the spectroelectrochemistry for pEABAE the charged state exhibited an unusually high-energy absorption characteristic compared to what was calculated. To elucidate the unusual charge state for this chromophore, computational methods were utilized. For this calculation, the chromophore is broken into pieces with the idea that the dimethoxybenzene would act as a steric block in the conjugation of the radical cation. Figure 5.6.1 shows calculated radical cation state absorptions of segmented portions of the EABAE chromophore overlaid with the experimental spectroelectrochemistry. These calculations suggest that there are two main phenomena contributing to the radical cation spectra: twisted/conjugation broken chromophores and π-π

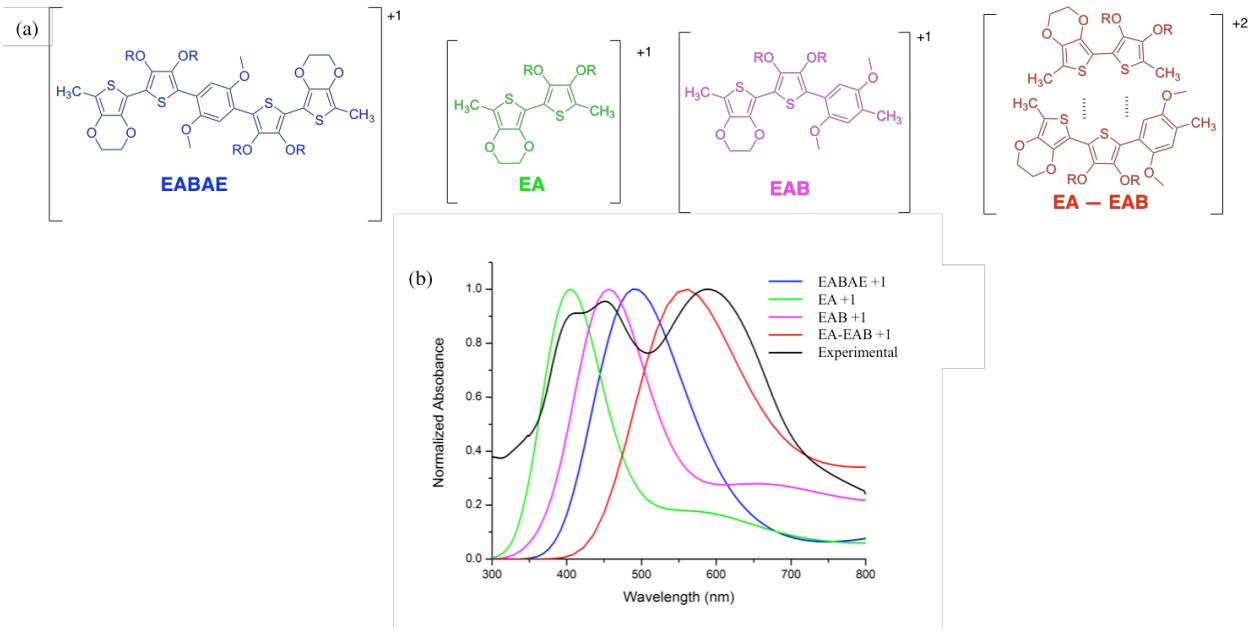

Figure 5.6.1. (a) Structures indicating where the steric blocks in the structure may occur for limiting the radical cation delocalization. These structures' absorptions were calculated to simulate a radical that is localized. EA-EAB is the π face interaction of the radical cation state of two portions of separate molecules (b) Calculated radical cation state absorptions of the segmented portions of the EABAE chromophore compared to the experimental data.

stacking. As demonstrated by the frontier molecular orbitals in Figure 5.2.2.1, the computations strongly support that the two experimental peaks at 412 nm and 452 nm are contributions from the two-ring dioxythiophene portions of the chromophore (EA, 405 nm) and the three-ring fraction (EAB, 456 nm), respectively. Surprisingly, the results did not support any major influences from the full chromophore (EABAE, 496 nm). In an effort to identify the contributor(s) to the 587 nm peak, a radical cation π-dimer comprised of EA and EAB units was generated. This aggregate, producing a 562 nm peak, provides strong support that intermolecular π-π stacking is likely responsible for the low energy peak.[168–171] Other combinations were also examined, but were unable to produce optimized aggregates and therefore require further studies.

5.7 Conclusions and Perspective

The contrast challenge for cathodically coloring electrochromics is examined from a fundamental standpoint leading to the determination that anodically coloring materials provide a means to conquer the issue. Focus was on examining the design principles of creating chromophores with discrete lengths and varying amounts of strain. Theoretical calculations, coupled with design and synthesis, helped to elucidate the interplay between sterics and chromophore size. Inter-ring steric interactions, leading to large dihedral angles, can be used as a conjugation wedge to limit, not only the neutral absorption, but also the delocalization of charged states creating radical cations that absorb at high energies compared to chromophores of similar size, but less steric encumbrance. The use of steric interactions as a conjugation block also gives the advantage of forming multiple and different high-energy light absorbing charged states. Considering the broad absorption achieved by the apparent dimerization of the EABAE chromophore attention should be shifted towards designing molecules for this purpose. The electrochemical irreversibility does appear to be a problem for purely electrochromic applications,

but it does however appear to offer an interesting approach toward making materials that could be used as overpotential fuses.

5.8 Supplementary Figures

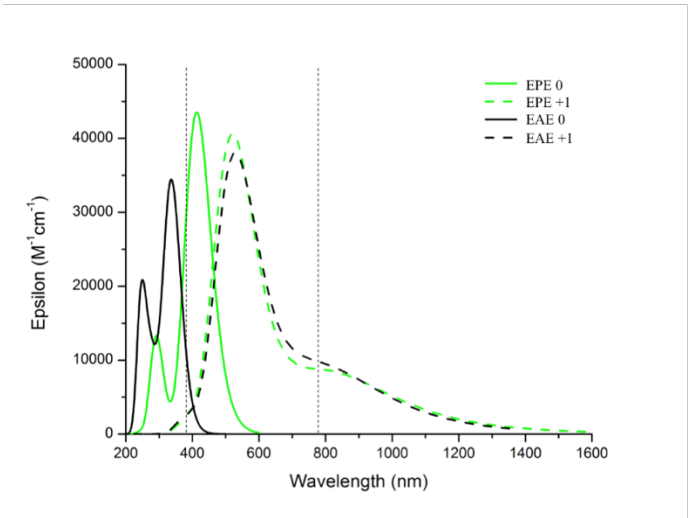

Figure 5.8.1. UV-Vis-NIR calculated spectra of EPE and EAE in the neutral (solid) and radical cation (dashed) states. Vertical dotted lines indicate the visible range of 380-780 nm

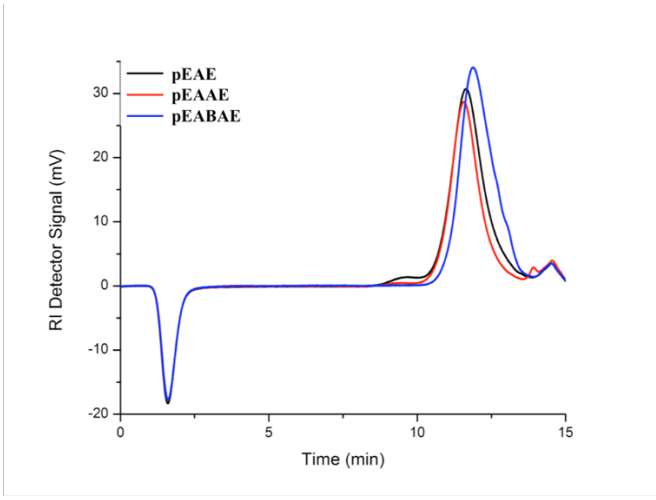

Figure 5.8.2. Gel permeation chromatography (GPC) results of the family of polymers in $CHCl_3$ at 40°C

5.9 Synthetic Procedures

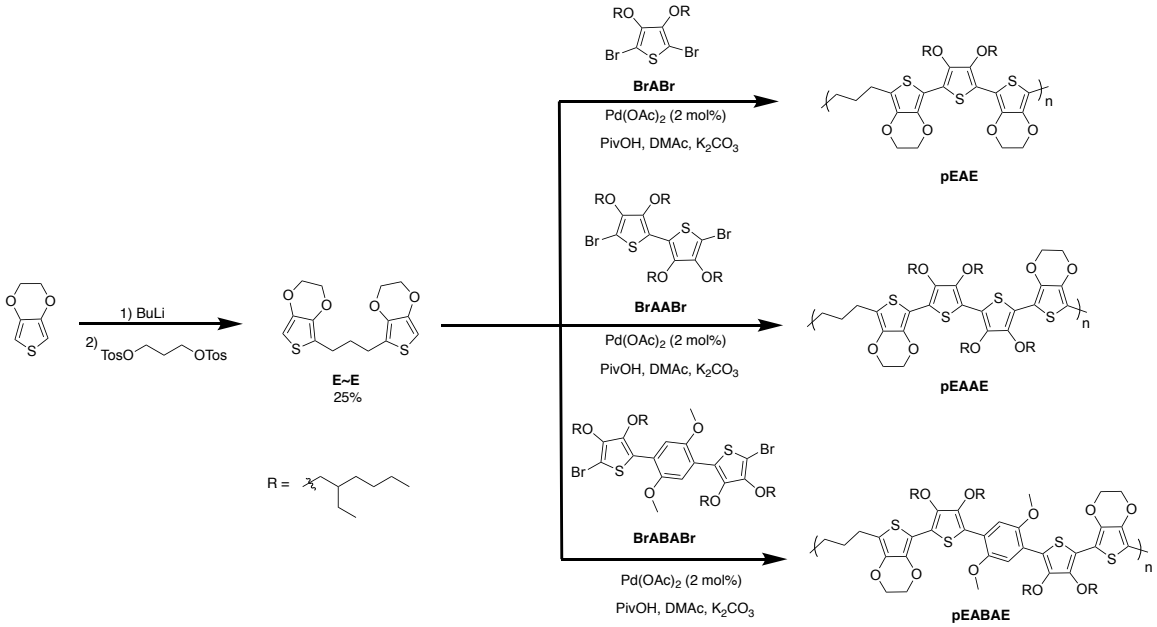

Scheme 5.9.1. Polymer synthetic routes for conjugation broken polymers.

E~E. Into a flame dried 50 mL schlenk flask with a magnetic stir bar was added freshly distilled 3,4-ethylenedioxythiophene (5.007 g, 35.17 mmol) and 30 mL of dry THF. The flask was purged with Ar and the mixture was cooled to -78ºC in a dry ice-acetone bath. To the flask was added nBuLi (2.5 M, 14.06 mL, 35.15 mmol) drop wise over 1 hour. The solution stirred for 1 additional hour at -78ºC and 1,3-propyleneditosylate (6.59 g, 17.16 mmol) was added all at once. The solution was allowed to warm to room temperature as it stirred for 12 hours. The reaction mixture was slowly quenched with 100 mL of DI water and extracted with diethyl ether (3 x 100 mL). The organic fractions were washed with water (2x 100), dried over $MgSO_4$, and solvent removed under reduced pressure. The compound was purified via fractional vacuum distillation using a kugelrhor (bp ~150ºC at 10 mbar) to give a clear oil. ^{1}H NMR ($CDCl_3$, ppm): δ 6.12 (s, 2H), 4.17 (s, 8H), 2.72-2.27 (t, 4H, J=7.5 Hz), 1.97-1.86 (q, 2H, J=7.8 Hz); $^{13}C\{^1H\}$ NMR ($CDCl_3$, ppm): δ 141.5,

137.6, 117.5, 95.3, 65.0, 65.5, 31.0, 25.5. HRMS: Calculated Mass = 324.0489 Da, Measured Mass = 324.0490 Da.

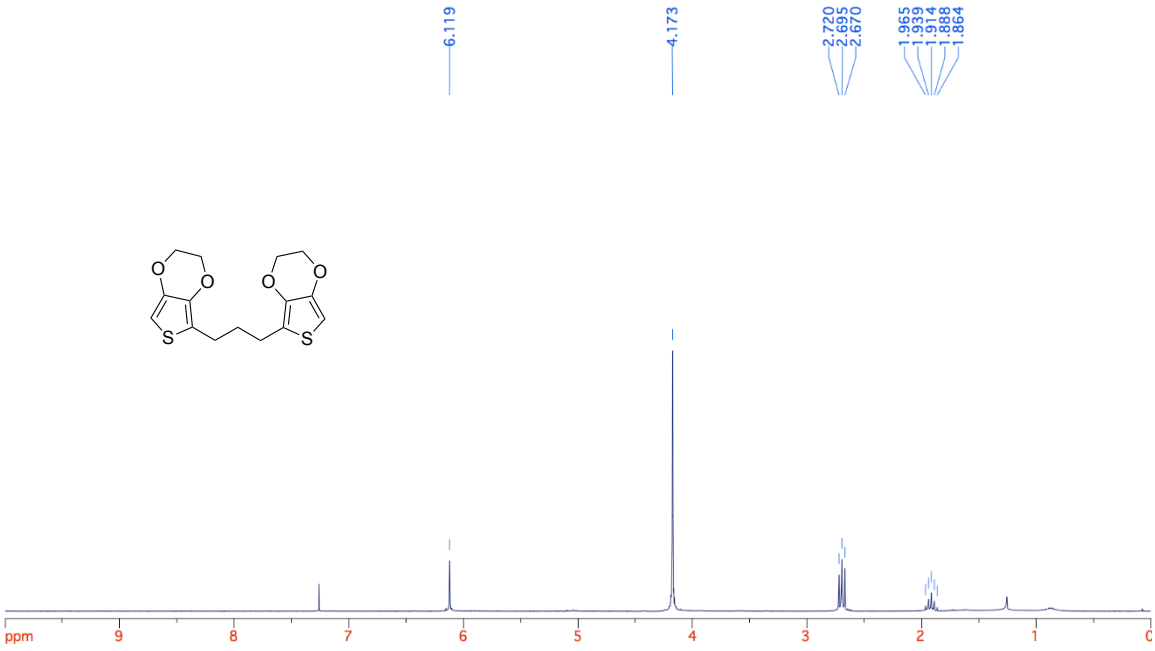

^{1}H NMR of **E~E**

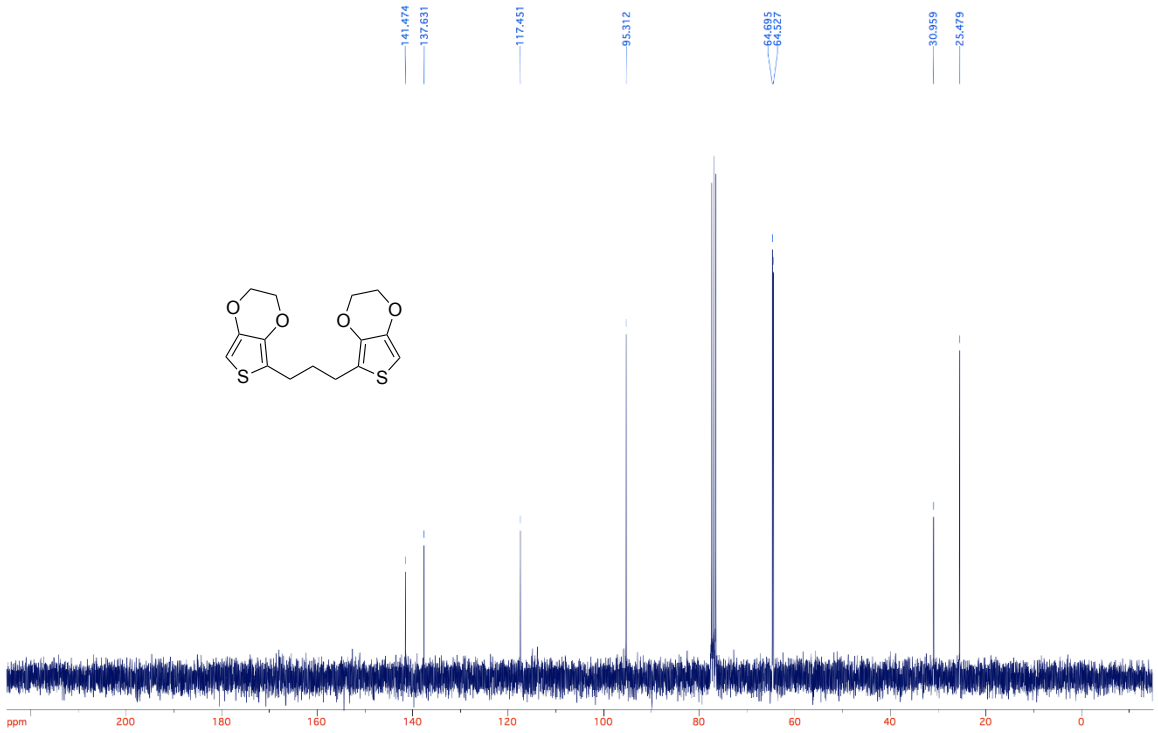

$^{13}C\{^{1}H\}$ NMR of **E~E**

pEAE. Into a dry 25 mL schlenk tube with magnetic stirring was added the dibromide monomer **BrABr** (0.154 g, 0.308 mmol), the dihydrin monomer **E~E** (0.100g, 0.308 mmol), 2 mol% palladium acetate (1.5 mg, 0.007 mmol), pivalic acid (0.031 g, 0.304 mmol), potassium carbonate (0.138 g, 0.997 mmol), and 3.1 mL of DMAc. The reaction mixture was purged with Ar, placed in an oil bath at 130ºC, and stirred for 24 hours under positive Ar pressure. The mixture was cooled to room temperature and added drop wise to 100 mL of methanol. The precipitate was filtered through a Soxhlet thimble, and washed with methanol, acetone, hexanes, and chloroform respectively. The washings were conducted until color was no longer observed during extraction. The solvent was evaporated from the fraction and a pale-yellow solid was collected (0.1004g, 49.3%). ^{1}H NMR ($CDCl_3$, ppm): δ 4.29-4.20 (d, 8H), 3.93-3.90 (d, 4H), 2.72 (t, 4H), 1.96-1.84 (bm, 4H), 1.59~1.25 (bm, 16H), 0.91~0.87 (bm, 12H). Elemental analysis: Theory: C= 63.60%,

H=7.32%, S=14.55%, Found: C= 63.38%, H=7.37%, S=14.28%. GPC analysis: M_n= 14.8 kDa, Đ = 2.0.

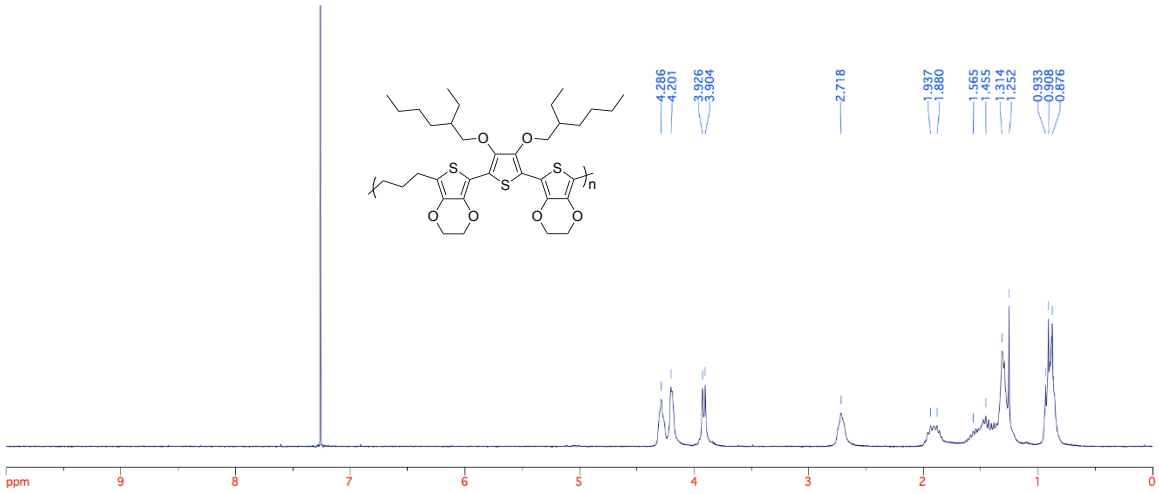

^{1}H NMR of **pEAE**

pEAAE. The polymer was synthesized using the same procedure as **pEAE**, but with the dibromide monomer **BrAABr** (0.258 g, 0.308 mmol). The polymer was collected as a yellow solid (0.1638 g, 53.2%). ^{1}H NMR ($CDCl_3$, ppm): δ 4.20-4.14 (d, 8H), 3.87-3.85 (d, 8H), 2.66 (t, 4H), 1.85 (m, 6H), 1.64-1.02 (bm, 32H), 0.98~0.58 (bm, 24H). Elemental analysis: Theory: C= 66.09%, H=8.27%, S=12.83%, Found: C= 65.63%, H=8.29%, S=12.50%. GPC analysis: M_n= 18.5 kDa, Đ = 1.8.

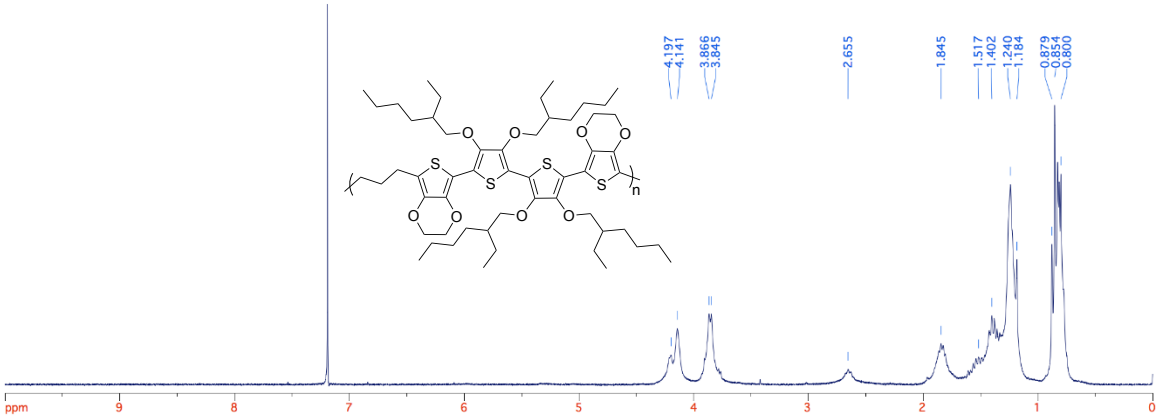

^{1}H NMR of **pEAAE**

pEABAE. The polymer was synthesized using the same procedure as **pEAE**, but with the dibromide monomer **BrABABr** (0.300 g, 0.308 mmol). The polymer was collected as a yellow solid (0.1705 g, 48.7%). ^{1}H NMR ($CDCl_3$, ppm): δ 7.37 (s, 2H), 4.29-4.22 (d, 8H), 3.97 (d, 4H), 3.84 (bm, 10H), 2.75-2.72 (q, 4H), 1.64-1.02 (bm, 32H), 0.98~0.58 (bm, 24H). Elemental analysis: Theory: C= 66.63%, H=7.99%, S=11.29%, Found: C= 66.40%, H=7.99%, S=11.05%. GPC analysis: M_n= 9.7 kDa, Đ = 2.0.

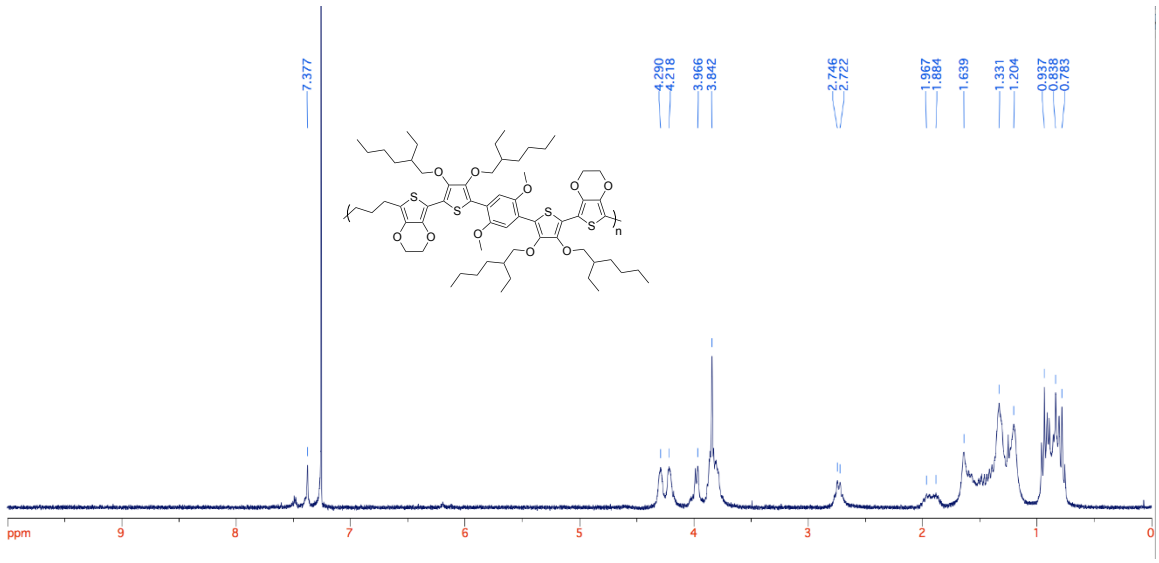

^{1}H NMR of pEABAE

Chapter 6 - Color Control in Anodically Coloring Electrochromic Molecules

Adapted From:

Christiansen, Dylan T.; Tomlinson, Aimée L.; and Reynolds, John R.; New Design Paradigm for Color Control in Anodically Coloring Electrochromic Molecules *Journal of the American Chemical Society*; **2019**, 141, 9, 3859-3862

A new paradigm is established for the design of conjugated anodically coloring electrochromic molecules where the electronic energy levels of the radical cation state are controllably tuned independent of the neutral state. It is shown how cross-conjugation can be used to tune the radical cation state independent of the neutral state. Manipulating the oscillator strengths of radical cation transitions allows for tuning of the color by shifting the λ_{max} of the low energy absorption by over 400 nm. The neutral states of these molecules are UV absorbing, providing solutions that are colorless with L*a*b* values of 100,0,0. They are oxidized to vibrantly colored radical cations with absorptions that span the visible spectrum creating green, yellow, and red chromophores. These molecules are then mixed to create transmissive, colorless blends that switch to opaque black solutions.

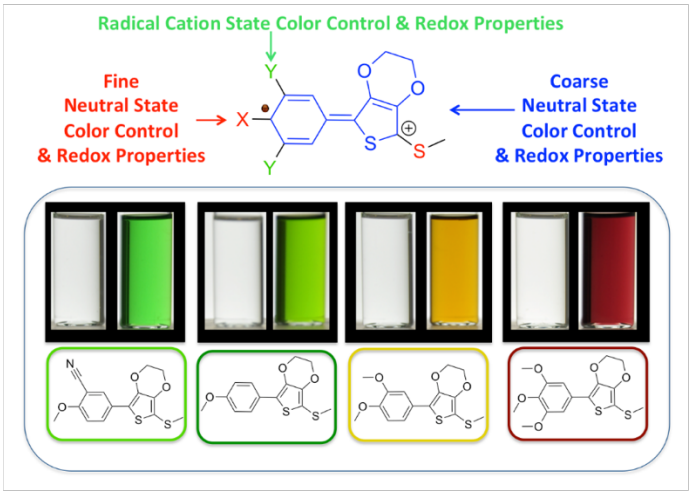

Figure 6.1. Absorption and oxidation control scheme for anodically coloring molecules

6.1 Design Approach

In contrast to cathodically coloring polymers, anodically coloring electrochromics are colorless in the neutral state and oxidize to colored species. In the field of anodically coloring organic electrochromics there is a knowledge gap on how absorption in the charged state is fundamentally controlled. [67,75,82–85] This work demonstrates how to bridge this gap with a fundamental approach to manipulating the electronic energy levels of odd-electron organic systems.[31,32] In this work, it is shown that electron rich/deficient moieties cross-conjugated into the chromophore can be utilized for manipulating radical cation energy levels and ultimately controlling absorption and color.

Figure 6.1.1 details the structures designed to create a set of anodically coloring electrochromes where the neutral and radical cation states' optical gaps are controlled independently. Here, novel UV absorbing discrete chromophores based on a 2-thiomethyl-ethylenedioxythiophene coupled to a 4-methoxybenzene derivative are introduced giving anodically coloring electrochromes (ACEs). Color control is achieved by altering the substitution on the benzene moiety, leading to radical cations that absorb across the visible spectrum. While the absorption of the neutral state can be tuned through manipulating the electron donating/withdrawing character of the substituent in the *para*-position (red), it is largely unaffected

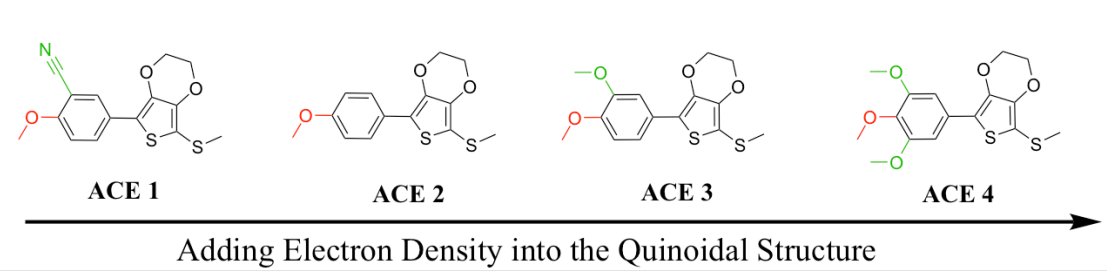

Figure 6.1.1. The key molecules are listed in order of increasing electron donating character of the moieties in the *meta*-position.

by the substituents in the *meta*-position (green). The chromophores examined in this study increase in electron density donated in the *meta*-position of the benzene from ACE1 to ACE4. The *para*-position moiety remains constant to add electron density, cap reactive ends, and maintain a neutral state with a similar optical gap. This study examines the effectiveness of altering the radical cation absorption independent of the neutral absorption through tailoring the electron richness in the *meta*-positions.

6.2 Quantum Chemical Calculations (Dr. Aimee Tomlinson)

The quantum chemical calculations for this project were executed by Dr. Aimee Tomlinson. I was involved with the design of the experiments, data processing, and writing of this section of the publication that came from this body of work.

In order to guide experiment and probe the design paradigm from a molecular orbital perspective, time dependent density functional theory (TDDFT) calculations were performed on these molecules and theoretical spectra were generated for the neutral and radical cation states of the molecules (see Figure 6.2.1). As can be seen in comparing the solid curves, there is minimal

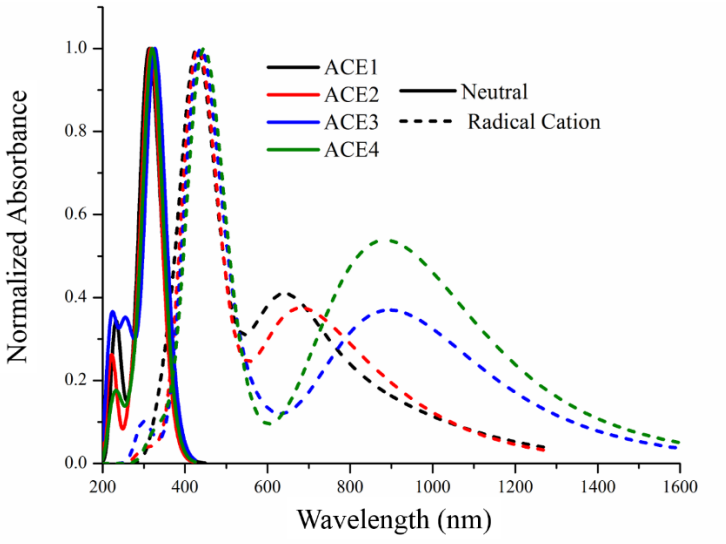

Figure 6.2.1. TDDFT calculated spectra for the neutral and radical cation states for the molecules in this study.

change in the absorbance of the neutral molecules upon the addition of electron rich moieties at the *meta*-position. All of the spectra have a λ_{max} in the UV with absorption onsets ~400 nm. However, when examining the radical cation spectra there are stark differences. While the high-energy absorption appears to be consistent between these molecules, there is a significant alteration in energies between the long wavelength transitions as evidenced by a red-shifting of this peak. There is a particularly large red-shift going from ACE2 to ACE3, upon addition of a methoxy group to the *meta*-position, which is consistent with the energy levels, oscillator strengths, and frontier molecular orbitals (FMOs), Figure 6.2.2, Table 6.2.1, and Figure 6.2.3.

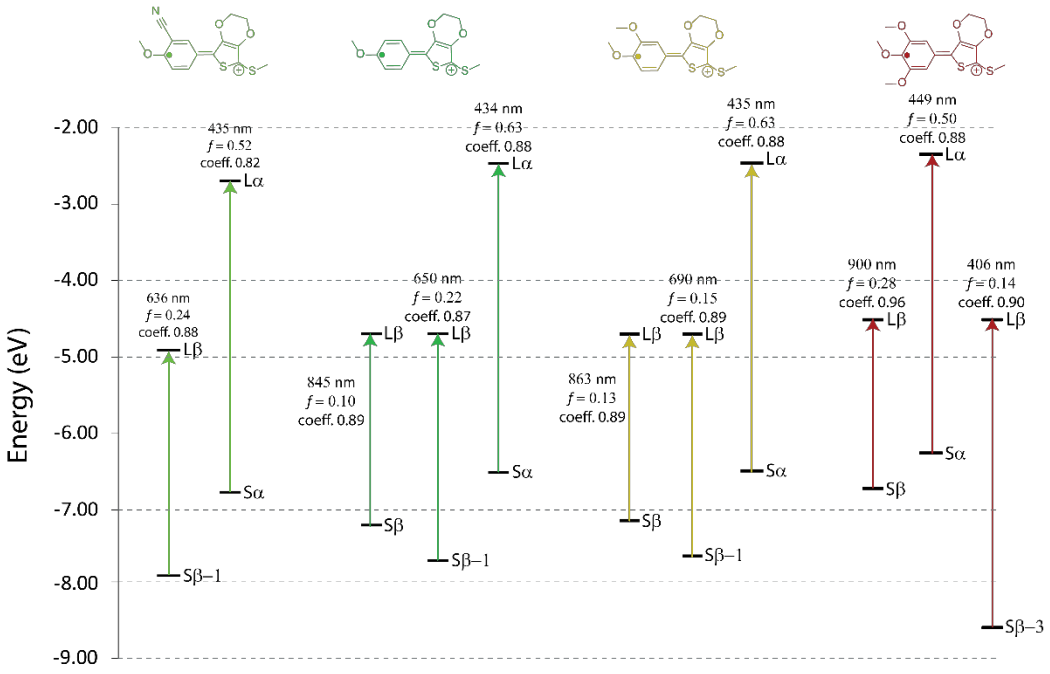

Figure 6.2.2. Calculated FMO energy levels of the radical cation state through TDDFT with optical transitions with oscillator strengths (*f*) of greater than 0.1. For each molecule, the wavelength, oscillator strength and coefficient for the transition are shown. The type of transition (spin up α or spin down β) are indicated for each. All transitions corresponding to these *f* values are given in Table 6.2.1.

A detailed analysis of the TDDFT oscillator strengths provides some insight into the absorption differences for these radical cations, as seen in Figure 6.2.2 and Table 6.2.1 In all cases, the transition which carries the largest oscillator strength (*f*) is the SOMOα→LUMOα (Sα→Lα) which remains relatively unchanged (434-435 nm) until ACE4 (449 nm). It is the remaining significant transitions (those possessing $f \geq 0.1$) which are believed to control the color. For ACE1, there was a transition found for the SOMO-1β→LUMOβ (S-1β→Lβ) corresponding to 636 nm. In the case of ACE2, the Sβ−1→Lβ transition was slightly red-shifted at 650 nm peak and the appearance of a SOMOβ→LUMOβ (Sβ→Lβ) at 846 nm with a lower oscillator strength. The oscillator strength for the Sβ→Lβ transition for ACE3 increases relative to the S-1β→Lβ transition and red-shifts to 863 nm. Finally, ACE4 indicated the largest red-shift for the Sβ→Lβ transition at 900 nm and a further decrease in the oscillator strength associated with the S-1β→Lβ transition. Interestingly, ACE4 has a second high-energy transition of significant oscillator strength in the visible at 406 nm associated with the S-3β→Lβ transition.

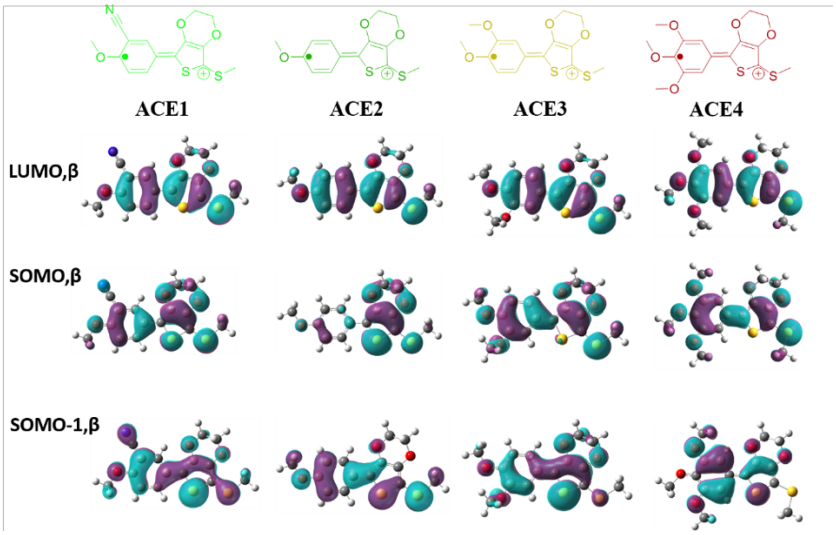

Figure 6.2.3. Frontier molecular orbitals of the beta-radical cation states of each ACE molecule.

Table 6.2.1. Oscillator Strengths and Transitions of Radical Cations of ACE Molecules

Molecule	λ (nm)	f	Dominant Transtion
ACE1	636	0.24	S-1β→Lβ
ACE1	435	0.52	Sα→Lα
ACE2	847	0.10	Sβ→Lβ
ACE2	650	0.22	S-1β→Lβ
ACE2	434	0.63	Sα→Lα
ACE3	863	0.13	Sβ→Lβ
ACE3	690	0.15	S-1β→Lβ
ACE3	434	0.63	Sα→Lα
ACE4	900	0.28	Sβ→Lβ
ACE4	449	0.50	Sα→Lα
ACE4	406	0.14	Sβ-3→Lβ

6.3 Manipulating the Dominant Absorption for Control Color

Figure 6.3.1 describes electronic structures and representative spectra for a pair of ideal anodically coloring molecules in the radical cation state. In both cases the highest oscillator strength transitions corresponds most strongly with the Sα→Lα excitation (a and c). As there is a minimal energy difference in this transition between the molecules, minimal red-shifting of this absorption peak is observed. For an electron poor system, the low energy absorption is dominated by the Sβ−1→Lβ excitation (b). As electron density is added to the chromophore, the Sβ→Lβ excitation takes over as the dominate contributor to the transition leading to a red-shift in absorption (d).

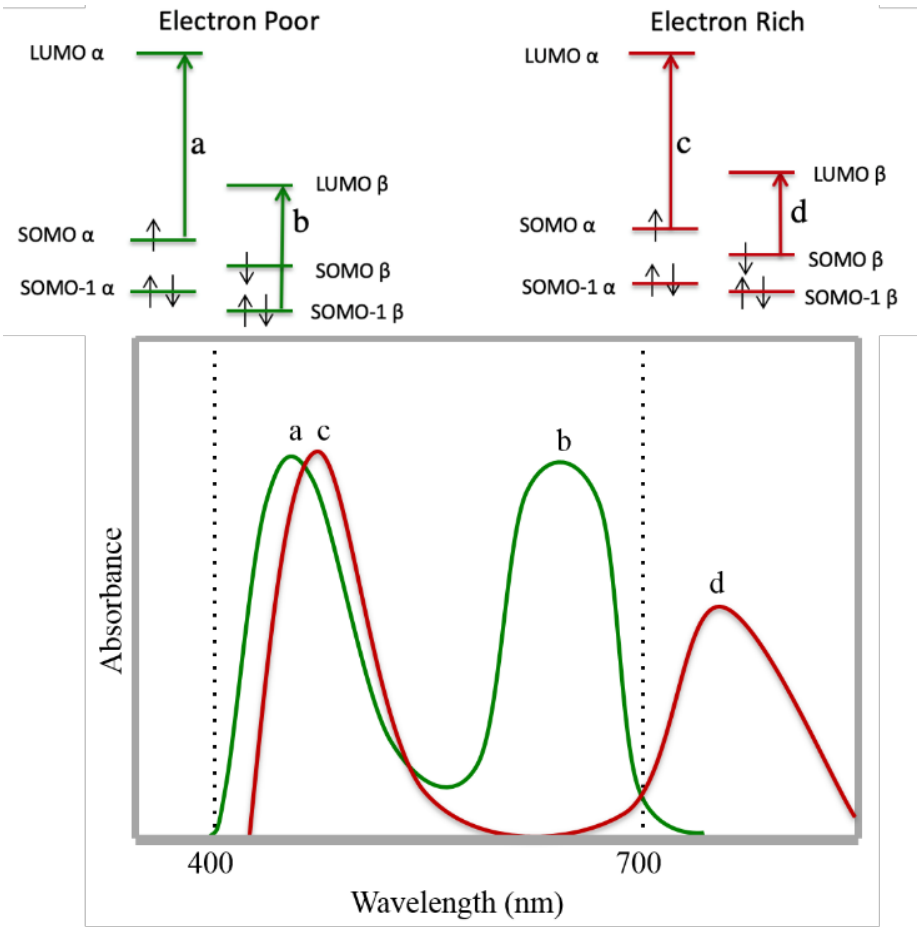

Figure 6.3.1. Concept diagram showing electronic structures and representative spectra of allowed transitions in ideal conjugated molecular electrochromes in the radical cation state.

6.3.1 Synthesis of Anodically Coloring Molecules via Stille Coupling

The synthetic approach to the monomer and polymer syntheses is shown in Scheme 6.3.1. Starting with commercially available 3,4-ehtylenedioxythiophene a lithiation followed by addition of dimethyldisulfide formed 2. Subsequent lithiation and transmetalation with trimethyltin chloride forms the desired compound, 3. The synthetic scheme diverges from here where 3 can be used for Stille coupling with a bromo-substituted benzene derivative (4, 5, 6, and 7) to prepare the target compounds ACE1, ACE2, ACE3, and ACE4.

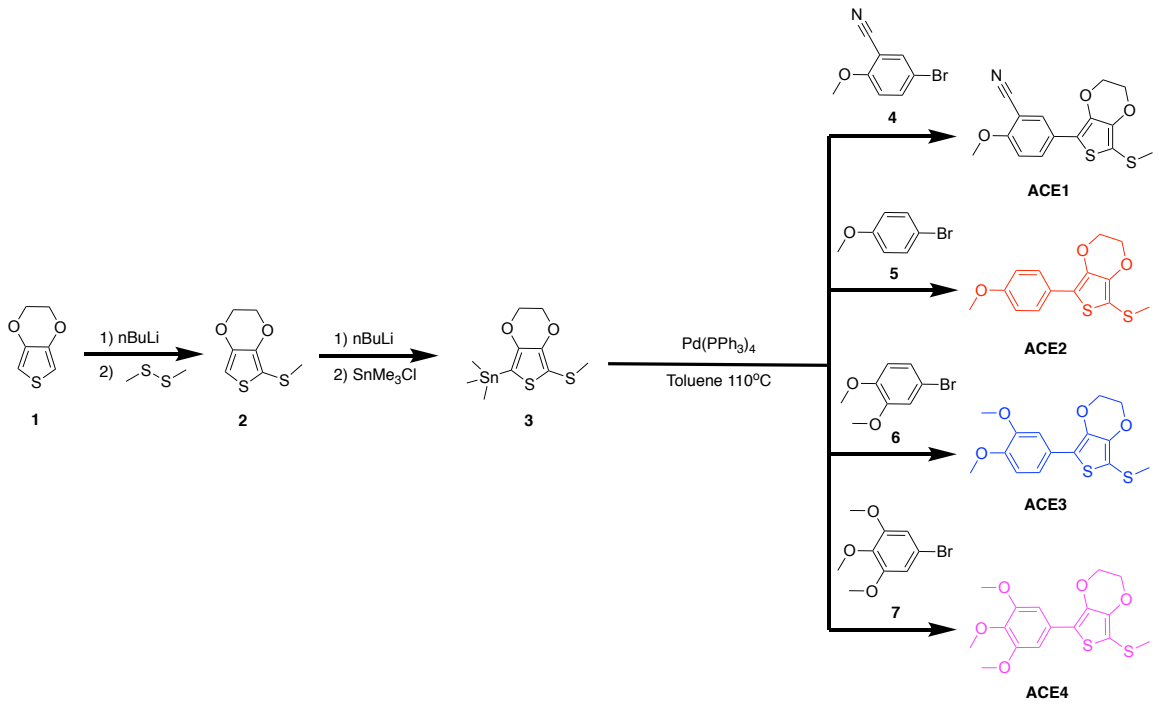

Scheme 6.3.1. Synthetic approach for anodically coloring molecules

6.3.2 Electrochemical Properties

Cyclic voltammetry (CV) and differential pulse voltammetry (DPV) were used to probe cation-radical formation and the results are shown in Figure 6.3.2.1. All molecules show quasi-reversible radical cation oxidations, but Figure 6.3.2.1c shows that ACE4 has two peaks indicative of the formation of a dication. This oxidation renders the electrochemistry irreversible and causes the formation of a new electroactive species, although it can be reduced back to neutral/colorless on the OTTLE when applying a reducing potential for an extended period. Formation of the dication would also corroborate with the apparent red-shift and broadening observed for the high-energy radical cation peak, as it is a combination of absorption from radical cations and dications.

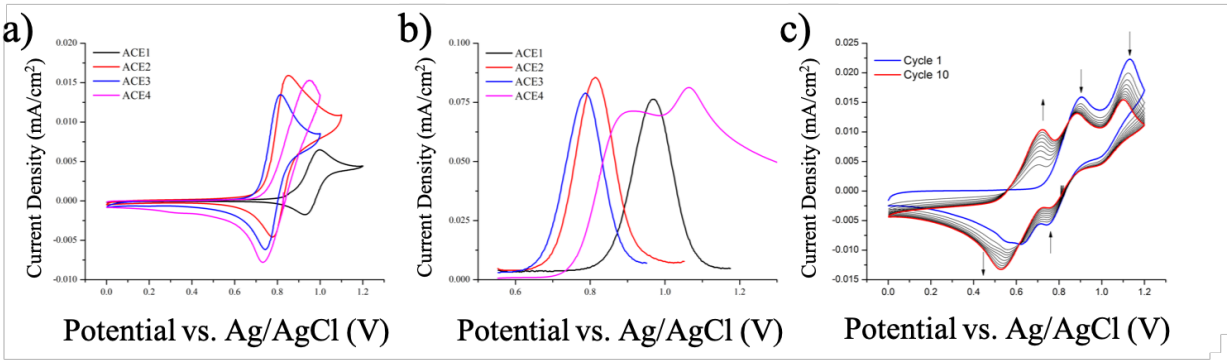

Figure 6.3.2.1. Cyclic (a) and differential pulse (b) voltammograms of 250 µM of the respective ACE molecule in 0.5M $TBAPF_6$/DCM solution. (c) 10 CV cycles of ACE4 with a range of 0-1.2 V showing the formation of a new species after the first cycle.

6.3.3 OTTLE Spectroelectrochemistry

When probing these molecules experimentally, the observations are consistent with the trends seen in the calculations. Figure 6.3.3.1 details the differential spectroelectrochemistry results performed in electrolyte solution using an optically transparent thin layer electrode (OTTLE), where a platinum screen is used as a working electrode to allow light to pass through the cell. In this experiment the neutral spectrum is subtracted as a baseline in order to remove the noise caused by the screen. Comparisons of the calculated and experimental spectra are available in Figure 6.3.3.2. It is evident that the calculations accurately depicted the location of the peaks and the red-shifting trend seen in the low energy absorption upon the incorporation of electron rich substituents. This ability to rationally shift the low energy absorbance allows access to a large variety of colors through minimal changes in chemical structure. The bright green of the cyano-containing ACE1 is due to the combination of two peaks in the visible with λ_{max} at 461 nm and 653 nm and a transmission window between 500-570 nm. Upon removing the electron-withdrawing group, there is a small shift in absorbance of the radical cation peaks for ACE2 with

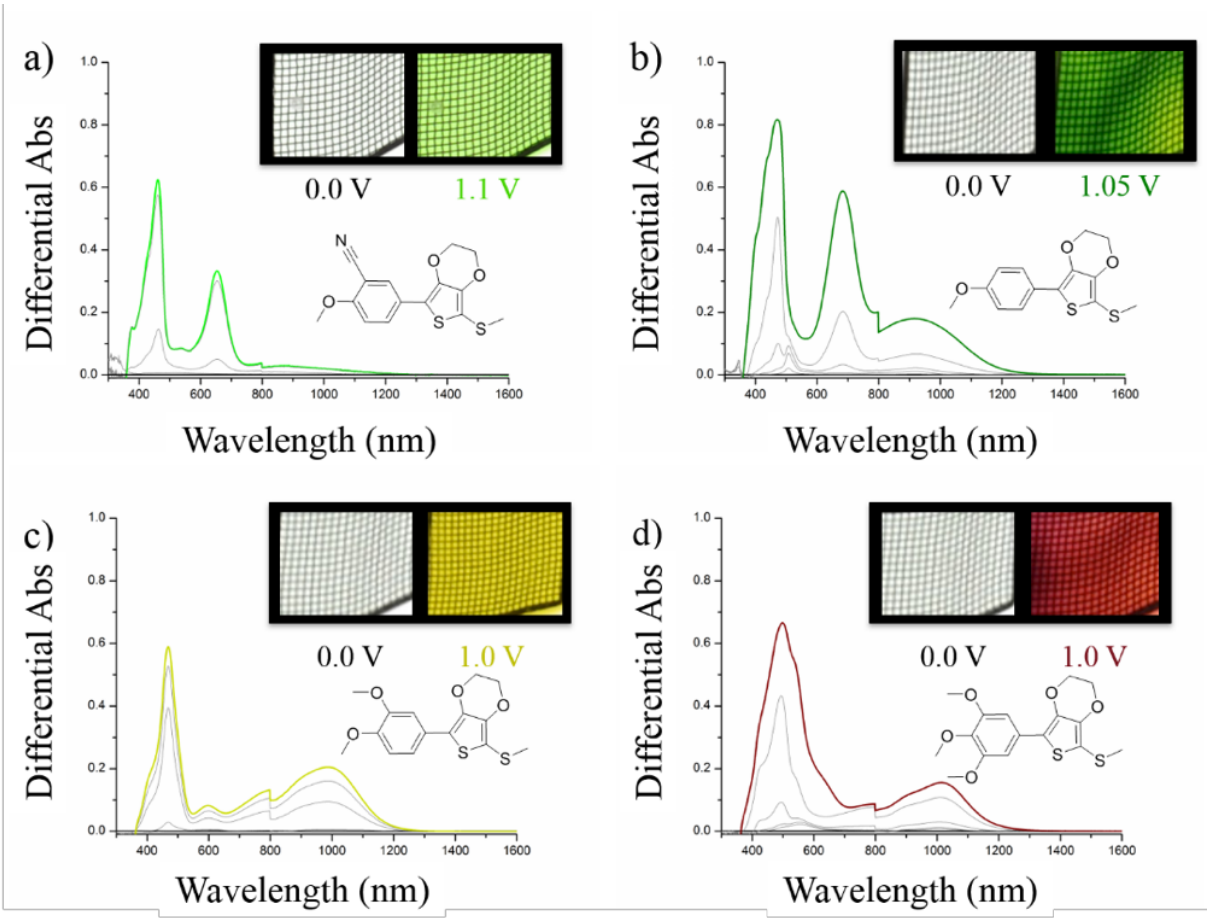

Figure 6.3.3.1. Differential spectroelectrochemistry performed with an OTTLE with photographs in the insets. (a) ACE1 (b) ACE2 (c) ACE3 (d) ACE4

λ_{max} at 471 nm and 683 nm and a more red-shifted window of transmission at 520-690 nm, yielding a more saturated green color. The formation of the shoulder in the NIR for ACE2 at 915 nm is the first evidence of contribution from the Sβ→Lβ transition. As more electron density is added to the chromophore for ACE3, the contribution from the Sβ-1→Lβ becomes suppressed with only a small absorbance observed at 597 nm. Large absorbances at 469 nm and 986 nm give a bright yellow color, with only one strong transition being in the visible. When examining the most electron rich system, ACE4, the low energy peak red-shifts to 1013 nm as predicted, and there is

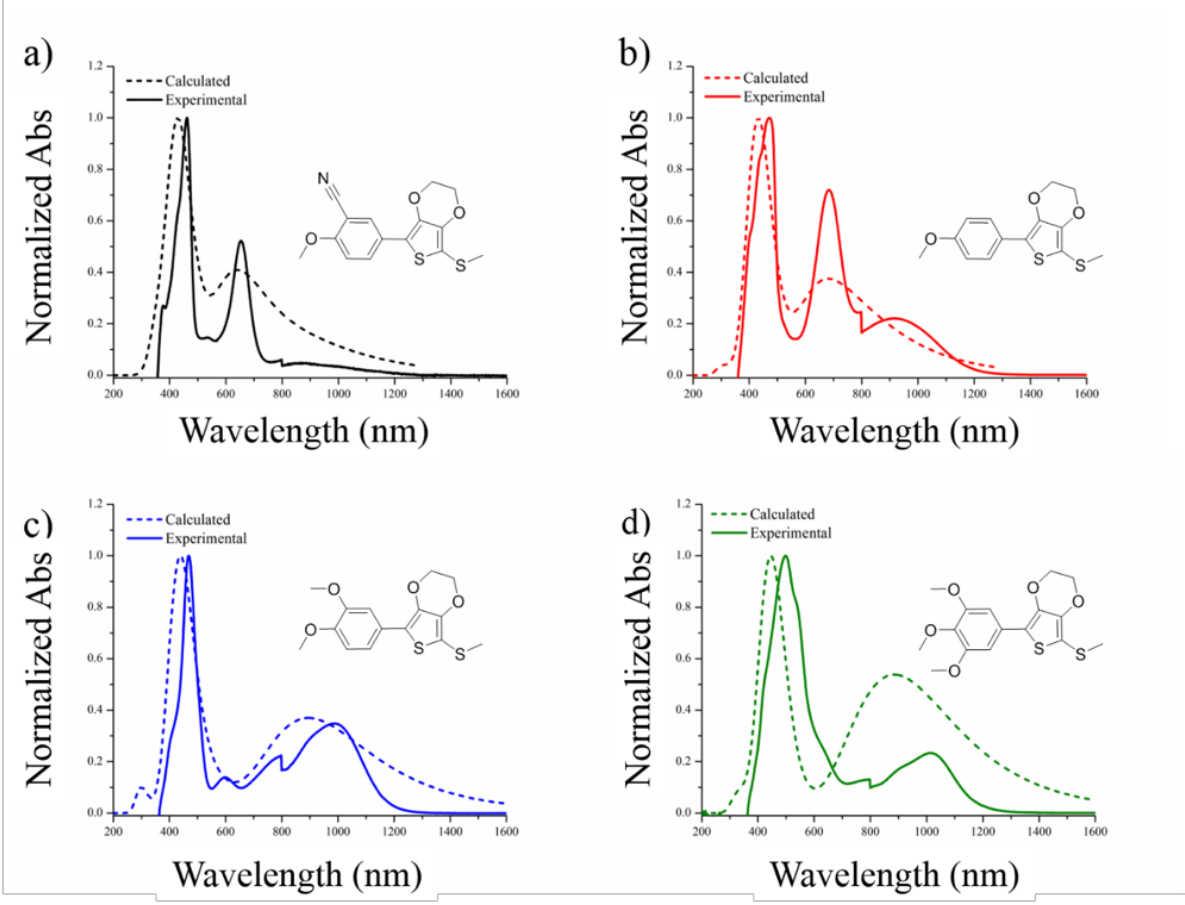

Figure 6.3.3.2. Comparison of calculated and experimental radical cation spectra. (a) ACE1 (b) ACE2 (c) ACE3 (d) ACE4

an observed red-shift and broadening of the high-energy peak at 496 nm. The increased breadth of the high-energy radical cation peak when comparing ACE3 with ACE4 causes a color change from a vibrant yellow to a deep red. This broadening can be attributed to the combination of the S-1β→Lβ and S-3β→Lβ transitions. The calculated and experimental data comparisons are collated in Table 6.3.3.1.

Table 6.3.3.1. Calculated and Experimental UV-Vis and Electrochemical Data for ACE Molecules

Molecule	λ_{max} (nm) Neutral Calculated	λ_{max} (nm) Neutral Experimental	λ_{max} (nm) Radical Cation Calculated	λ_{max} (nm) Radical Cation Experimental	E_{ox}[a] (mV) vs Ag/AgCl
ACE1	312	317	429, 641	416, 653	969
ACE2	316	312	432, 680	471, 683, 915	814
ACE3	326	326	439, 895	469, 986	787
ACE4	320	318	445, 884	496, 1013	916, 1063

[a] As determined by DPV as the peak of the current for oxidation.

6.3.4 Solution Oxidative Doping and Colorimetry

The color neutrality and transmissivity of the neutral state and the color vibrancy obtained through chemical oxidative doping is shown in Figure 6.3.4.1. This experiment was performed in 250 μM solutions with $Fe(OTf)_3$ as the oxidizing dopant. Photographs are taken in borosilicate vials before exposure to air. Color for these materials was quantified using the CIELAB color space.[21] The a*b* plot shows the quantitative change in color upon sequential oxidative doping as calculated from the UV-Vis absorbance spectra of neutral and doped solutions. All calculated L*a*b* values for the neutral compounds are (100, 0, 0), which can be observed in the photographs as being completely color neutral and transmissive. Each of these compounds is oxidized to a vivid color that, in combination, cover a wide area in the color space. From the spectra in Figure 6.3.4.2, it can be noted that the absorptions generated with chemical oxidation are similar to what is seen on the OTTLE, with the exception of ACE4. This molecule has a single peak upon oxidation with

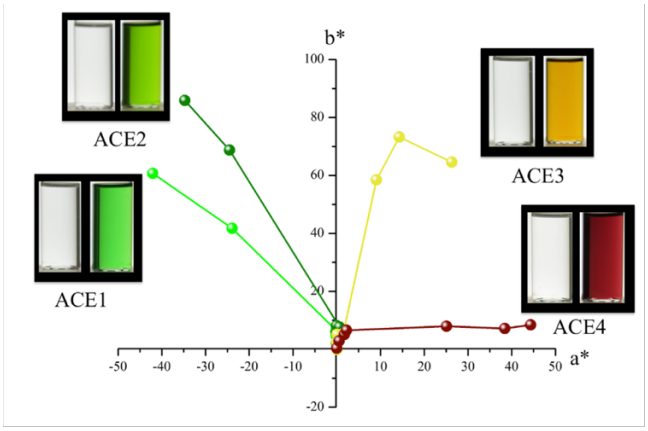

Figure 6.3.4.1. Evolution of colorimetry of oxidatively doped solutions of the ACE molecules. The solutions are 250 µM of each compound and $Fe(OTf)_3$ is the dopant.

a λ_{max} at 496 nm. This observation is indicative of the molecule oxidizing directly to the dication upon chemical doping, as there is no spectral evidence of radical cation formation. This result is not unexpected due to how close the electrochemical peaks in the DPV are measured to be.

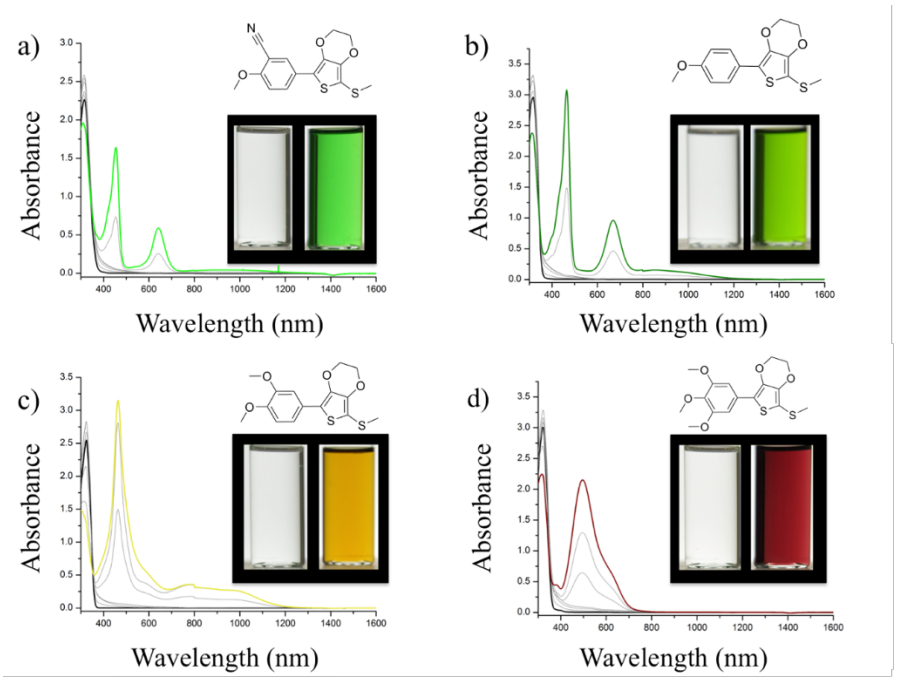

Figure 6.3.4.2. Evolution of UV-Vis spectra of oxidatively doped solutions of the ACE molecules. The solutions are 250 µM of each compound and $Fe(OTf)_3$ is the dopant.

6.4 Conclusions and Perspective

A 1:1 mixture of ACE2 and ACE4 was created and the differential spectroelectrochemistry and photography is detailed in Figure 6.4.1. As can be seen from the photography, the mixture changes from a color neutral, transmissive solution to an opaque black. One can imagine that the blends can be adjusted to create browns and other secondary colors from only a few molecules, as the library of ACE molecules is expanded.

In conclusion, a new design paradigm is introduced for making anodically coloring molecules where there is synthetic control on the absorption of the oxidized state. Radical cation absorption is tailored independent of the neutral absorption using electron donating/withdrawing moieties cross-conjugated into the chromophore structure. Quantum chemical calculations give insight into how energy levels are manipulated to control transition dominance in odd-electron systems and guide molecular design to create new anodically coloring electrochromic molecules.

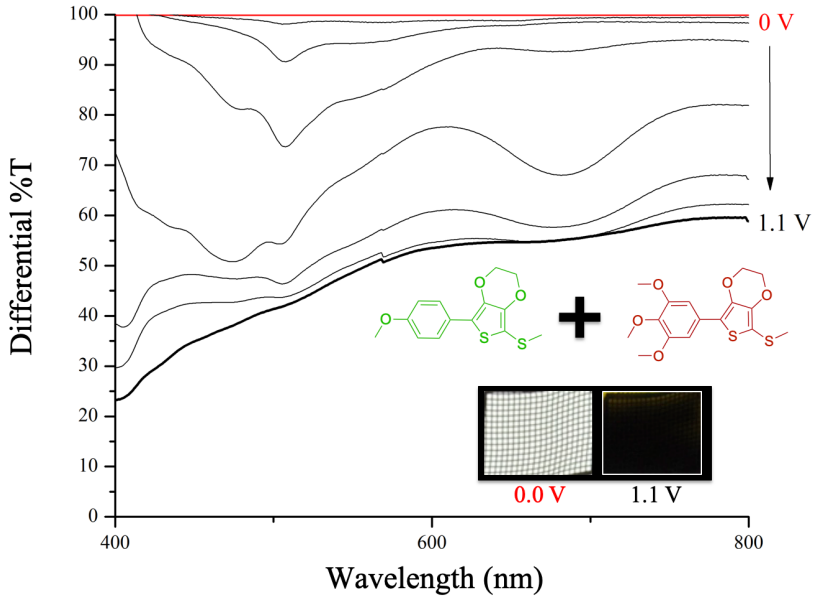

Figure 6.4.1. Differential spectroelectrochemistry performed with an OTTLE of a 1:1 mixture of ACE2 and ACE4 with photographs in the inset at the extreme potentials as noted.

It has been shown that these molecules have overcome the contrast barrier present in the field of organic electrochromism while maintaining a wide variety of tunable colors and secondary blends. As the collection of available ACE compounds expands, these materials have prospects towards moving to solid state devices by incorporation into polymers or adding cross-linkable moieties to create an insoluble network. Additionally, these molecular design principles can be used in other conjugated organic systems for tuning radical cation electronic structures.

6.5 Synthetic Procedures

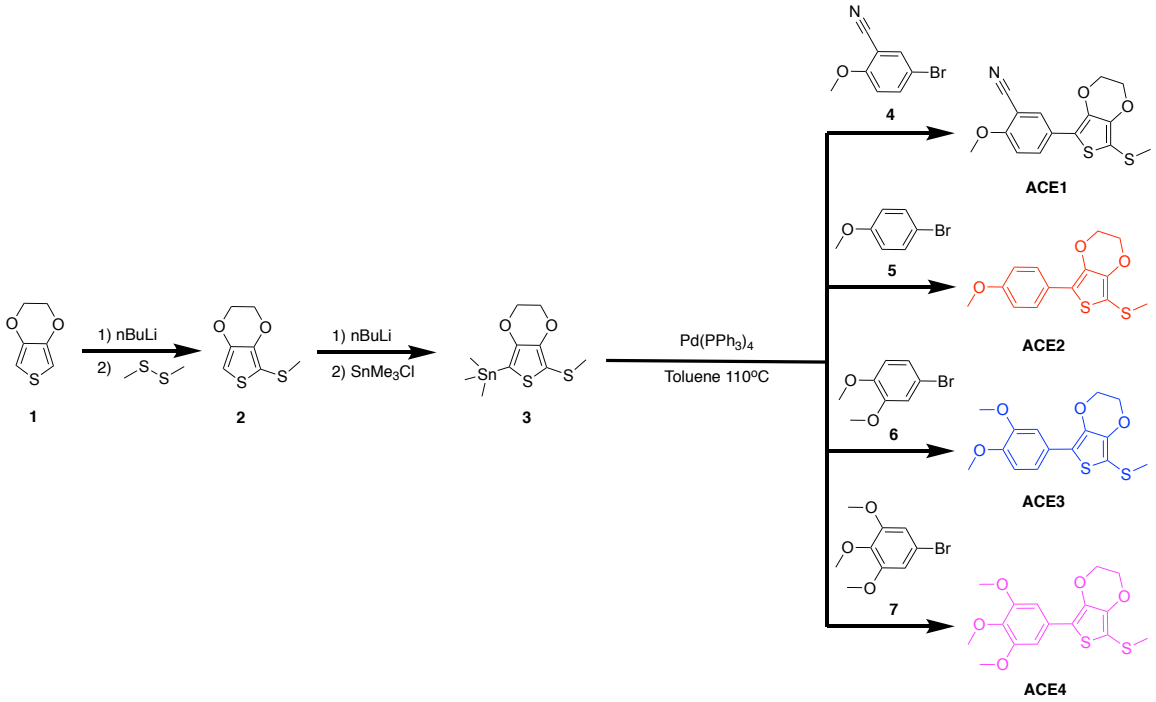

Scheme 6.5.1. Synthetic outline for creating the ACE molecules

2-thiomethyl-3,4-ethylenedioxythiophene (2): Into a dry 250 mL schlenk flask with an argon atmosphere and a magnetic stir bar was added **1** (10.00g, 70.34 mmol) and THF (100 mL). The solution was cooled to -78 °C and 2.5 M BuLi (28.2 mL, 70.5 mmol) was added drop wise via

syringe pump over 1 hour. The solution was stirred for 1 hour at -78 °C and dimethyldisulfide (10.0 g, 106 mmol) was added in one dose. The solution stirred over 12 hours as it warmed to room temperature. The reaction mixture was poured over ice (100 g) and 0.1M HCl (100 mL). The mixture was extracted with DCM (3 x 50 mL), the organic extracts were dried over anhydrous $MgSO_4$, and the solvent was removed under vacuum. The resulting clear oil was used without further purification. The yield was 11.92 g (90%). ^{1}H NMR ($CDCl_3$, ppm): δ 6.41-6.28 (s, 1H), 4.29-4.24 (m, 2H), 4.20-4.14 (m, 2H), 2.40-2.26 (s, 3H). $^{13}C\{^1H\}$ NMR ($CDCl_3$, ppm): δ 143.3, 141.4, 108.7, 102.0, 65.0, 64.3, 21.3.

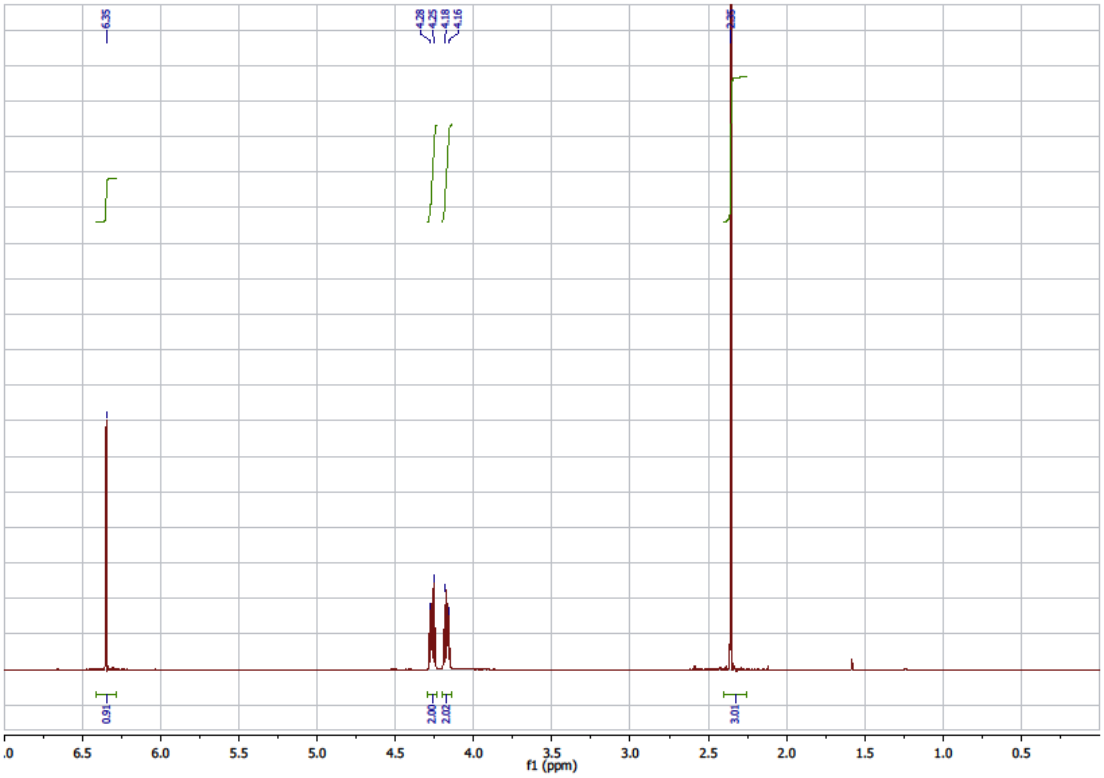

^{1}H NMR for 2-thiomethyl-3,4-ethylenedioxythiophene (2)

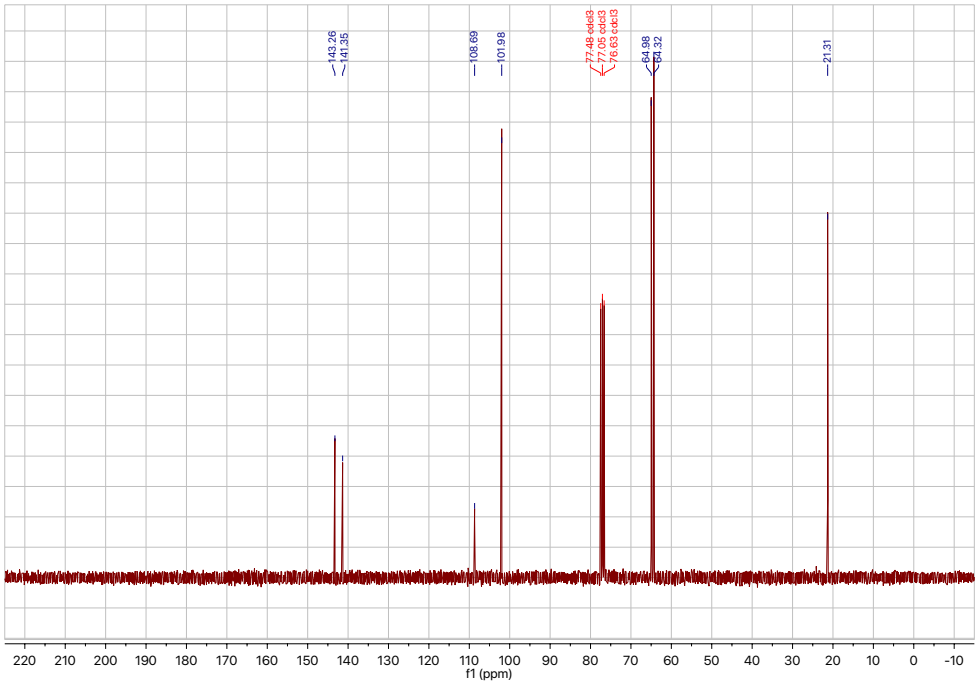

$^{13}C\{^{1}H\}$ NMR for 2-thiomethyl-3,4-ethylenedioxythiophene (2)

2-thiomethyl-3,4-ethylenedioxy-5-trimethyltin-thiophene (3): Into a dry 250 mL Schlenk flask under an argon atmosphere and with magnetic stir bar was added **2** (5.00g, 26.6 mmol) and THF (50 mL). The solution was cooled to -78 °C and 2.5 M BuLi (10.7 mL, 26.8 mmol) was added drop wise via syringe pump over 1 hour. The solution was stirred for 1 hour at -78 °C and trimethyltinchloride (5.34 g, 26.8 mmol) was added in one dose. The solution stirred over 12 hours as it warmed to room temperature. The reaction mixture was poured over ice (100 g). The mixture was extracted with DCM (3 x 50 mL), the organic extracts were dried over anhydrous $MgSO_4$, and the solvent was removed under vacuum. The resulting white crystalline solid was used without further purification. The yield was 9.25 g (99%). ^{1}H NMR ($CDCl_3$, ppm): δ 4.27-4.22 (m, 2H), 4.18-4.13 (m, 2H), 2.41-2.31 (s, 3H), 0.58-0.02 (t, 9H, J=29.1 Hz). $^{13}C\{^{1}H\}$ NMR ($CDCl_3$, ppm): δ 147.3, 1143.6, 114.0, 112.6, 65.0, 64.3, 21.3, -8.5.

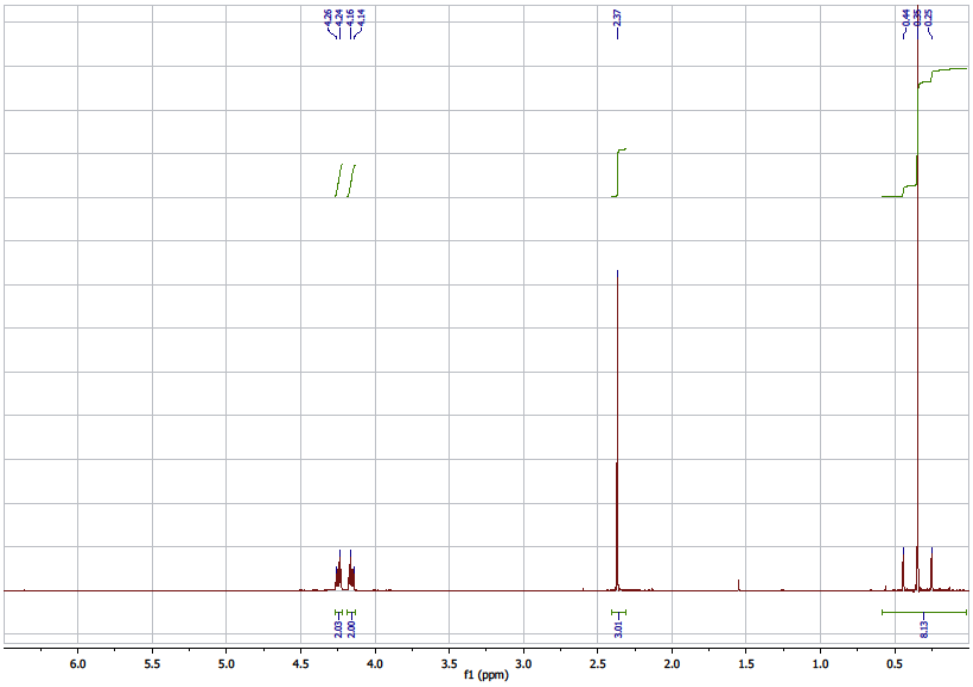

^{1}H NMR for 2-thiomethyl-3,4-ethylenedioxy-5-trimethyltin-thiophene (3)

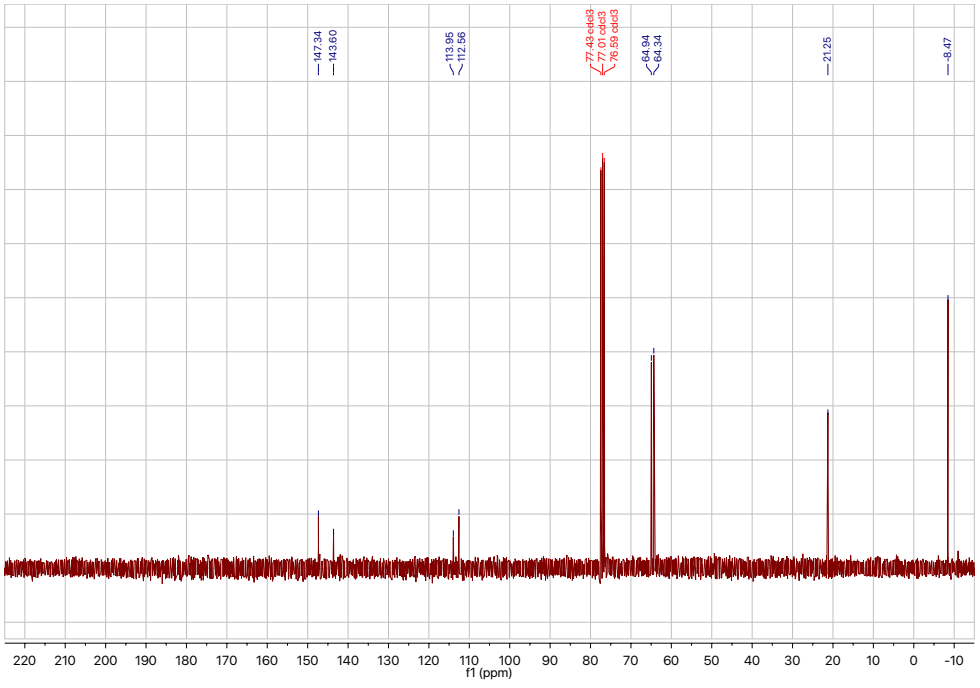

^{13}C{^{1}H} NMR for 2-thiomethyl-3,4-ethylenedioxy-5-trimethyltin-thiophene (3)

General Stille coupling procedure: Into a dry 100 mL Schlenk flask under an argon atmosphere and with a magnetic stir bar was added **3** (0.50 g, 1.42 mmol), aryl bromide **4**, **5**, **6** or **7** (1.42 mmol), $Pd(PPh_3)_4$ (0.08 g, 0.07 mmol), and toluene (50 mL). The reaction was stirred at 100 °C for 12 hours and cooled to room temperature. The reaction was washed with water (3 x 50 mL), saturated $NaHSO_3$ (2 x 50 mL), and brine (1 x 50 mL). The organic layer was dried over $MgSO_4$ and solvent was removed under vacuum. The resulting compounds were purified by column chromatography with EtOAc/hexanes (1:9) as the eluent.

ACE1: Pale yellow fluffy solid in 89% yield (405 mg). Melt point: 192-193 °C. ^{1}H NMR ($CDCl_3$, ppm): δ 8.00-7.94 (s, 1H), 7.78-7.71 (d, 1H, *J*=9.0 Hz), 6.98-6.91 (d, 1H, *J*=9.0 Hz), 4.36-4.28 (m, 4H), 3.96-3.92 (s, 3H), 2.42-2.39 (s, 3H). ^{13}C{^{1}H} NMR ($CDCl_3$, ppm): δ 159.7, 143.6, 137.8, 131.6, 131.2, 126.0, 116.7, 116.3, 111.5, 107.2, 102.1, 64.8, 64.5, 56.2, 21.3. HRMS, $C_{15}H_{13}O_3NS_2$ Calculated m/z: 319.0331, Measured m/z: 319.0331

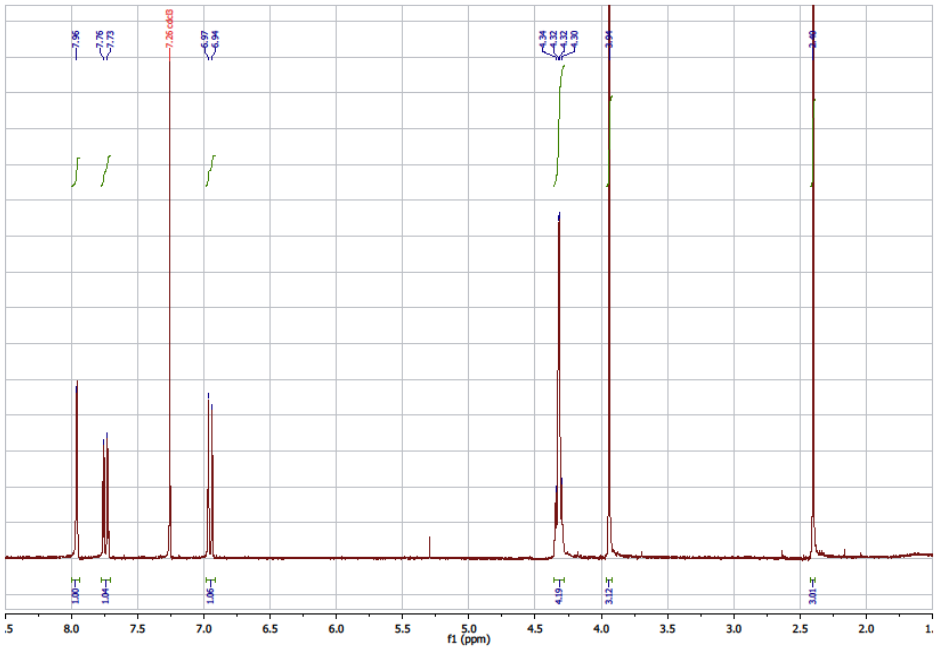

^{1}H NMR for ACE1

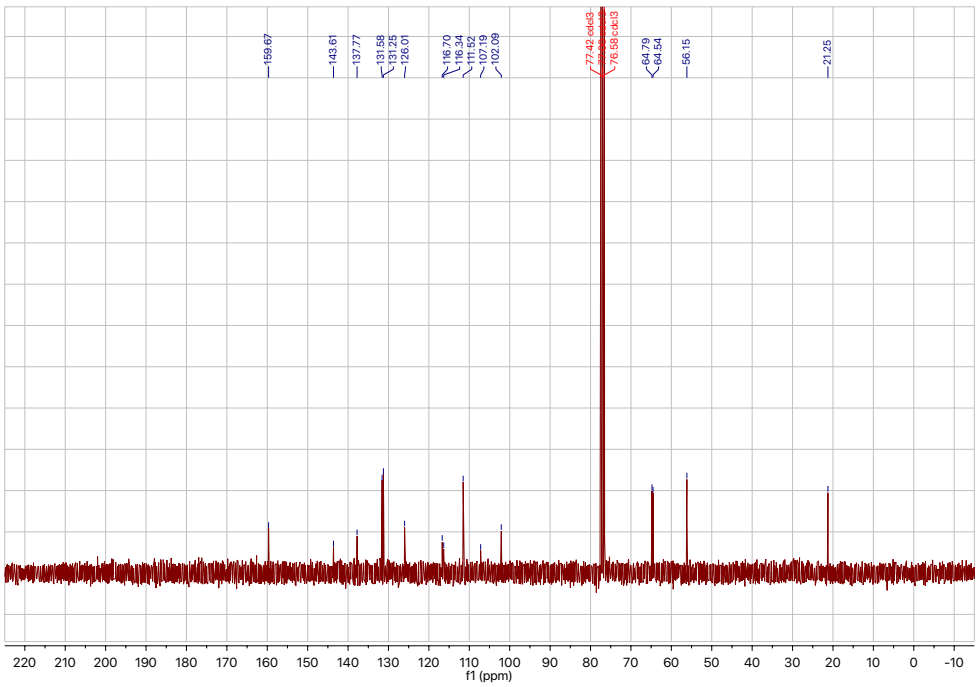

$^{13}C\{^{1}H\}$ NMR for ACE1

ACE2: White crystalline solid in 83% yield (348 mg). Melt point: 90-91 °C. ^{1}H NMR ($CDCl_3$, ppm): δ 7.69-7.54 (d, 2H, *J*=9.0 Hz), 6.96-6.81 (d, 2H, *J*=9.0 Hz), 4.37-4.22 (m, 4H), 3.86-3.76 (s, 3H), 2.47-2.32 (s, 3H). $^{13}C\{^{1}H\}$ NMR ($CDCl_3$, ppm): δ 158.6, 143.7, 136.7, 127.5, 125.4, 119.7, 114.1 105.4, 64.9, 64.4, 55.3, 21.5. HRMS, $C_{14}H_{14}O_3S_2$ Calculated m/z: 294.0379, Measured m/z: 294.0379

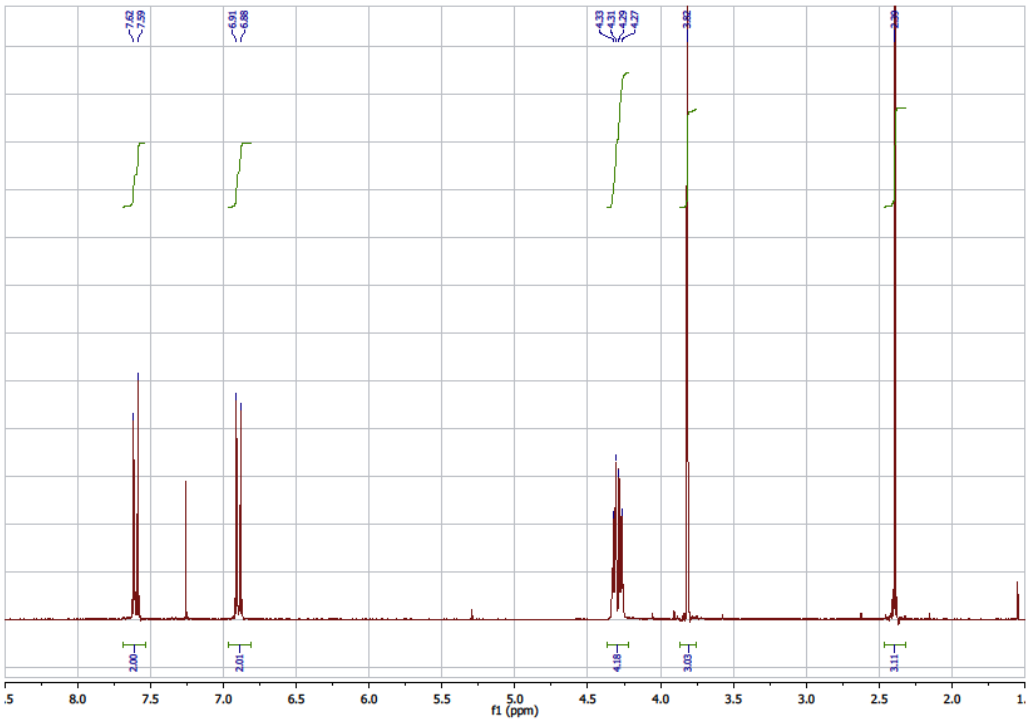

^{1}H NMR for ACE2

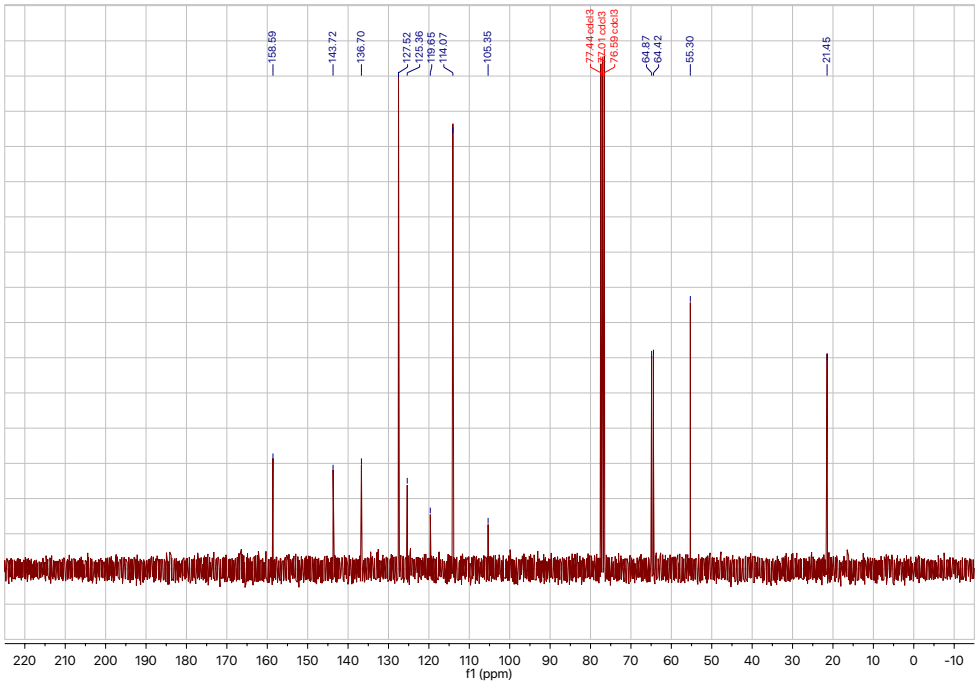

^{13}C{^{1}H} NMR for ACE2

ACE3: White crystalline solid in 69% yield (319 mg). Melt point: 107-108 °C. ^{1}H NMR ($CDCl_3$, ppm): δ 7.25-7.23 (d, 1H, *J*=2.1Hz), 7.23-7.21 (d, 1H, *J*=2.1Hz), 6.89-6.83 (dd, 1H, *J*=6.9 Hz, 2.1Hz), 4.38-4.24 (m, 4H), 3.95-3.90 (s, 3H), 3.90-3.86 (s, 3H), 2.44-2.36 (s, 3H). ^{13}C{^{1}H} NMR ($CDCl_3$, ppm): δ 148.9, 148.2, 143.7, 136.8, 125.6, 119.7, 118.9, 111.3, 109.8, 105.6, 64.9, 64.5, 55.9, 55.9, 21.4. HRMS, $C_{15}H_{16}O_4S_2$ Calculated m/z: 324.0485, Measured m/z: 324.0484

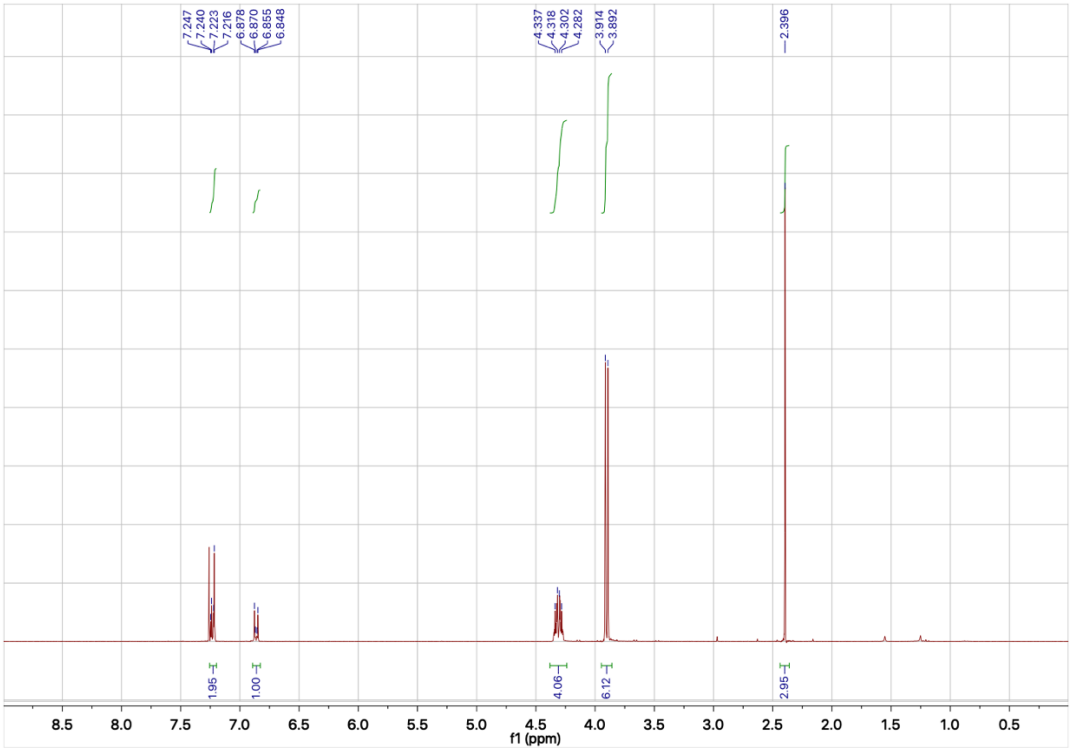

^{1}H NMR for ACE3

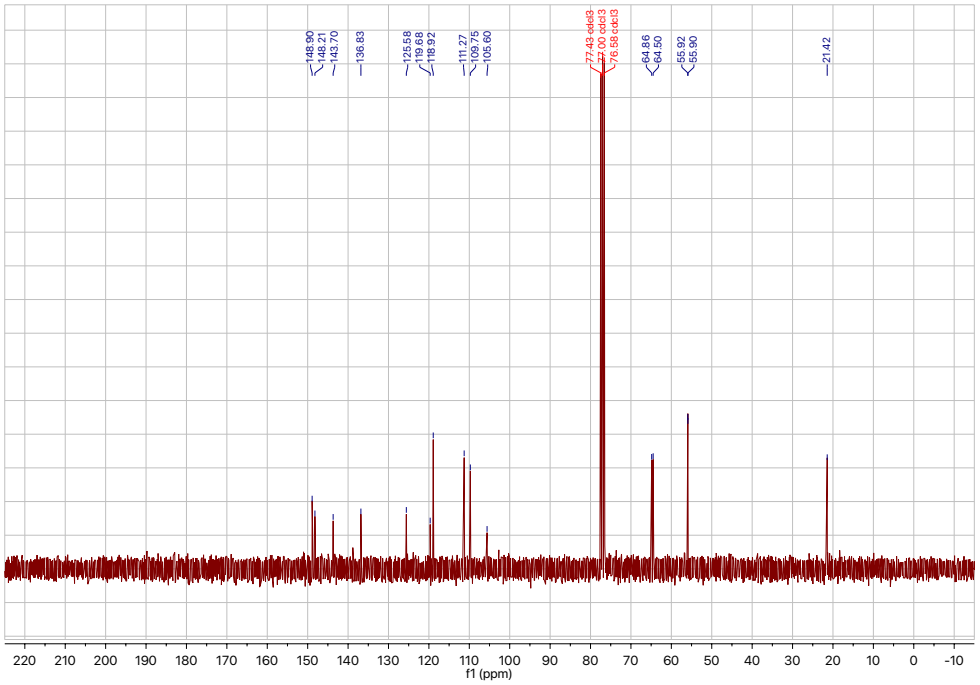

$^{13}C\{^{1}H\}$ NMR for ACE3

ACE4: Pale brown crystalline solid in 74% yield (374 mg). Melt point: 120-121°C. ^{1}H NMR ($CDCl_3$, ppm): δ 6.93-6.86 (s, 2H), 4.36-4.27 (m, 4H), 3.90-3.87 (s, 6H), 3.86-3.84 (s, 3H), 2.43-2.34 (s, 3H). $^{13}C\{^{1}H\}$ NMR ($CDCl_3$, ppm): δ 153.3, 143.6, 137.3, 128.1, 119.5, 106.5, 103.8, 64.8, 64.6, 60.9, 56.2, 21.3. HRMS, $C_{16}H_{18}O_5S_2$ Calculated m/z: 354.0590, Measured m/z: 354.0589

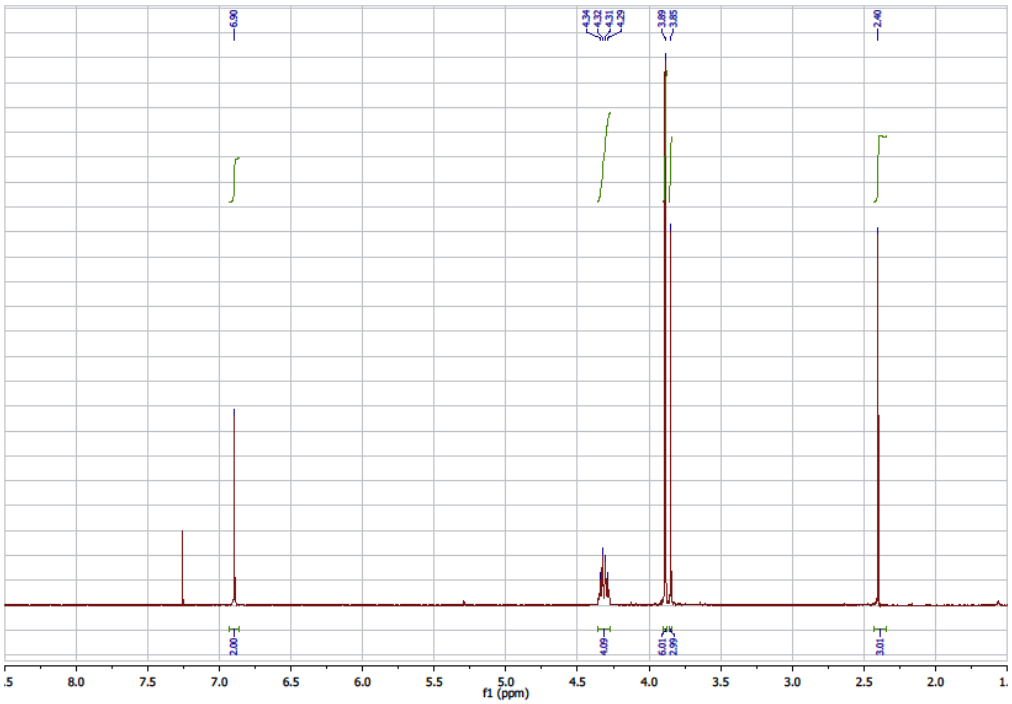

^{1}H NMR for ACE4

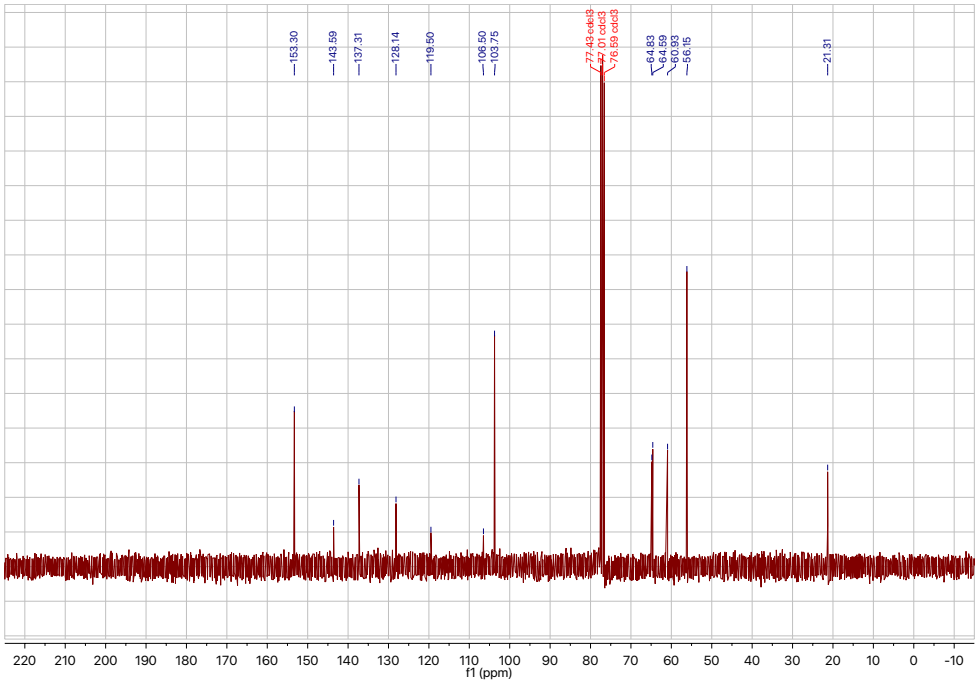

^{13}C{^{1}H} NMR for ACE4

Chapter 7 - Path Forward

The research presented in this thesis has created state of the art electrochromic polymers and molecules that possess higher redox stability, color tunability, and contrast than previously explored materials. A new approach to creating wide-gap electrochromic systems allows for access to red, orange, and yellow electrochromic polymers with improved redox stability. The use of a random copolymerization approach has led to materials that are tunable across the visible spectrum with only three repeat units added in different ratios. A detailed analysis on interring strain and conjugation length laid the framework for introducing conjugation broken, anodically coloring electrochromic polymers and showed the limitations of this approach. A fundamental look at the radical cation state in molecular systems has led to a new paradigm of color control in anodically coloring electrochromic molecules, which has created electrochromes of exceptional contrast. This chapter serves to put these accomplishments into perspective and to propose paths forward to answer the question left unanswered.

7.1 Cathodically Coloring Electrochromism

7.1.1 A New Monomer for Redox Stable Wide Gap Electrochromic Polymers

While Chapter 3 detailed one approach to creating new redox stable systems, there is a limitation in the approach of using interring strain to widen the gap. As too much interring strain is added to a conjugated polymer system, the oxidation potential gets to a point where the material switches slowly or may even oxidize irreversibly. The approach outlined in this section uses a monomer that has an inherently wider gap than DOTs but offers electron more richness than DATs, which helps to drive the oxidation potential down, Figure 7.1.1.1.

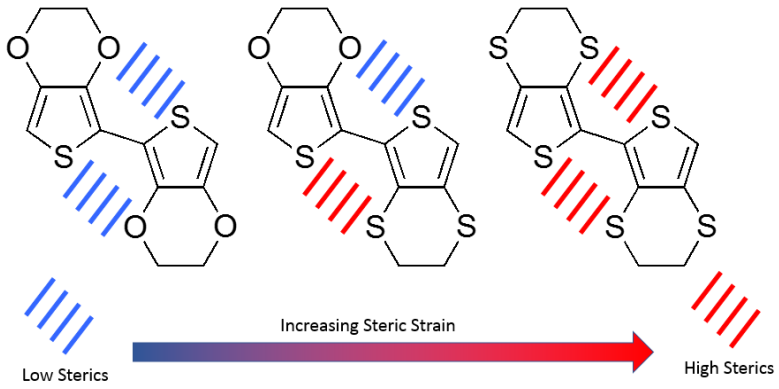

Figure 7.1.1.1. Alternating S-S and S-O interactions allowing for optical gap control with electron rich monomers

The use of 3,4-dithiothiophenes (DTTs) as comonomers has been limited to electropolymerization. They have been shown to have significantly wider gaps than DOTs due to the repulsive sulfur-sulfur interaction between rings. Figure 7.1.1.1 shows an example of dimers of biEDOT, EDOT-EDTT, and biEDTT showing the steric interactions that cause interring torsion. This S-S interaction causes a twisting between rings similar to the what was discussed throughout this dissertation, but the DTT monomer brings considerably more electron richness than DAT. Examinations of electropolymerized copolymers of these materials show that both the optical gap and oxidation potential can be tuned through manipulating the EDOT:EDTT ratio in the starting monomers.

Bringing DTT monomers into polymers with well examined soluble DOTs would allow for examining them as processable, wide gap electrochromic materials, Figure7.1.1.2. Since the materials have not been thoroughly optimized for direct arylation, Stille polymerization is outlined as the inital approach to reach high molecular weight polymers. The DOTs chosen for the polymerizations have solubilizing side chains that allow for bringing solution processability to these systems. The DTTs chosen give a range of interring strain to allow for color tuning of the neutral state.

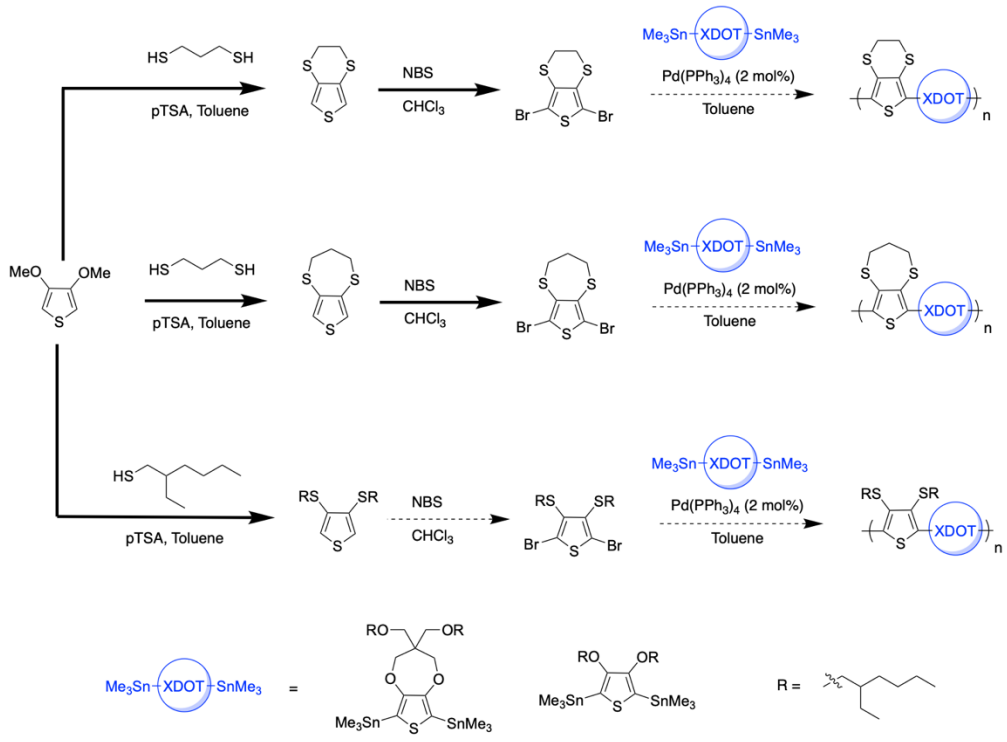

Scheme 7.1.1.1. Synthetic approach to incorporating DTTs into copolymers with DOTs

Can these copolymers be synthesized? Will these materials switch? What is the effect of the DTTs on the transmissivity of the oxidized state (where do the charge carrier bands absorb?)?

7.1.2 Further Broadening through Random Copolymerization

Chapter 4 presented on an approach to create broadly color tunable systems with the use of only three monomers. This approach gave access to a wide array of color with low oxidation potentials, but the polymers' individual absorbances did not offer the breadth necessary to access materials that are brown with only three monomers. More monomers should can be used in order to access broader absorbances in these polymers without increasing the oxidation potential, Figure 7.1.2.1. The monomers in this figure are in order of decreasing optical gap. The increase in the amount of comonomers leads to an increase in the number of potential chromophore possibilities.

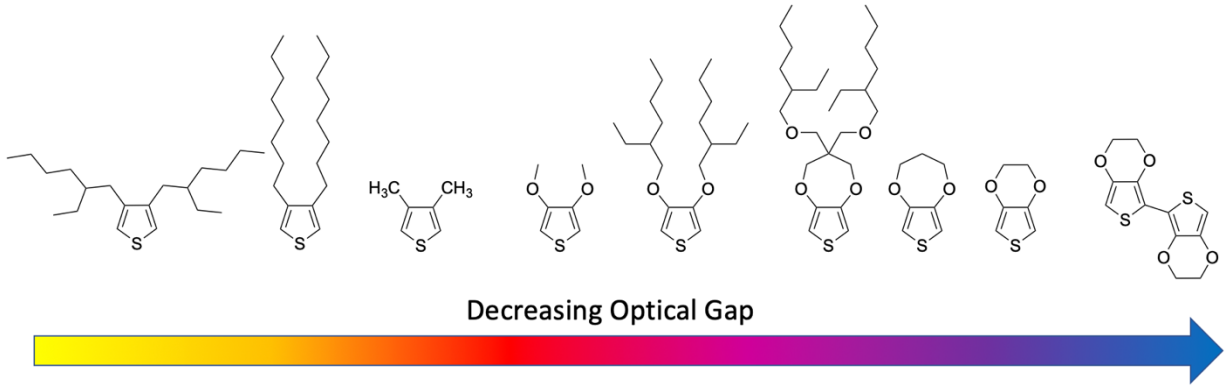

Figure 7.1.2.1. Potential repeat unit structures for use in random copolymerization to access broadly absorbing materials with muted colors.

How broad can the absorbance of a single random copolymer get without acceptors? Will these materials allow access to a brown electrochromic polymer? How large of an affect does copolymer drift on the produced polymer? Can synthetic control on the feeding times and ratios broaden the absorbance further?

7.2 Anodically Coloring Electrochromism

7.2.1 Challenges of Discrete Chromophore Polymer Systems

Chapter 5 detailed an approach to incorporating discrete chromophores into a polymer chain as a means of creating anodically coloring electrochromic polymers. When examining the switching of these materials, there are issues with charge transport causing slow switching and charge trapping in the films. The alkylene portion of the polymer backbone acts to insulate the redox active portion of the polymers and prevents charge hopping between chromophores. One way to potentially circumvent this challenge is to remove as much alkyl moieties as possible and replace them with side chains and/or linkers that could facilitate charge transport, such as glycols.

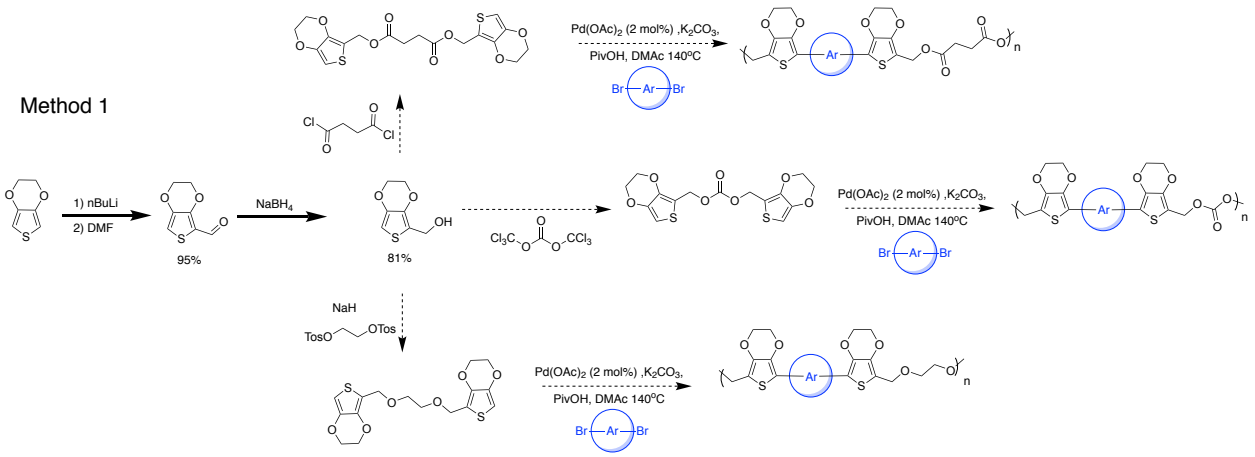

Scheme 7.2.1.1. Synthetic approach to creating high dielectric discrete chromophore systems

Scheme 7.2.1.1 details a synthetic approach to bring glycols, esters, and carbonates into discrete chromophore polymers. While this approach attempts to address the charge transport issues in these systems, there are still challenges to this synthetic method. Chromophores in this type of system would likely be colored to colored switching due to them being limited to three or more rings. The conditions for the polymerization also have the potential of oligomers precipitating out before reaching high molecular weight, as there is low alkyl content for solubility. This would lead to the need to reoptimize polymerization conditions. These challenges are why there was a shift towards using discrete molecules as electrochromes.

Do these new linkers lead to electrochemically switchable systems? Can these polymers be blended with a fully conjugated system to aid in charge transport for switching?

7.2.2 Color Control in Anodically Coloring Electrochromic Molecules

Chapter 6 delved into how color is controlled in the radical cation state of conjugated molecular systems, but there are still structure-property relationships to examine. Figure 7.2.2.1a shows the study outlined in Chapter 6. This study detailed how the neutral and radical cation state

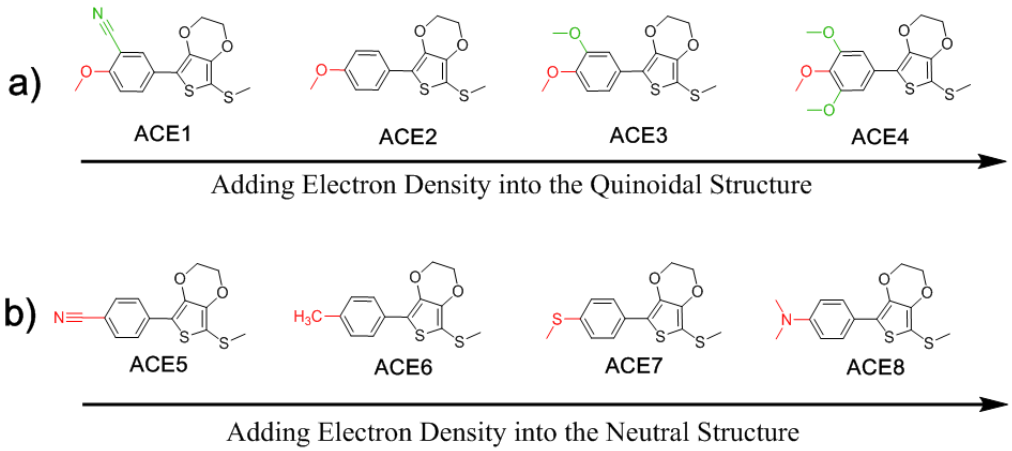

Figure 7.2.2.1. Complete set of molecules in the broader study of ACE molecules: (a) electron donation in the meta position (b) electron donation in the para position

absorbances can be decoupled to control color by manipulating the electron donating/withdrawing character of moieties cross conjugated into the chromophore. The path forward for this project involves comparing this approach to changing the electron donation/withdrawal nature of moieties directly conjugated into the chromophore via the para position of the benzene, Figure 7.2.2.1b. Here it is hypothesized that adding electron density in this position will red-shift both the neutral and radical cation state absorptions. Specifically, the effect on the radical cation state should be analogous to the previous study.

Will the para donation effect the radical cation state in an analogous way? How will the magnitude of these effects compare?

7.2.3 Phosphonic Acids and High Surface Area Electrodes

In addition to expanding the ACE color palette, these materials have potential to be moved into the solid state for improving switching speed. Phosphonic acid functionalized organic materials have been shown to noncovalently bind to ITO, which in this case would act to

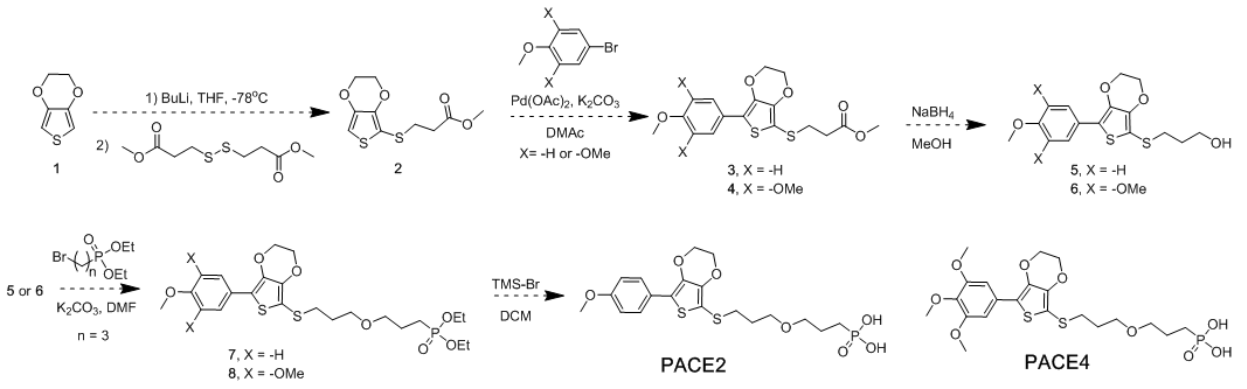

Scheme 7.2.3.1. Proposed synthetic route for making PACE2 and PACE4.

remove/reduce the diffusion of the active materials from the electrode. Figure 7.2.3.1 details the synthetic path forward to create phosphonic acid modified ACE molecules, PACE2 and PACE4. Starting with EDOT there is a lithiation and quenching with a ester functionalized disulfide to afford the asymmetric molecule 2. Here the synthesis diverges with a direct arylation reaction with an aryl bromide to obtain 3 or 4. Subsequent reduction with $NaBH_4$ affords the primary alcohols 5 and 6. These materials can react with diethyl(3-bromopropyl)phosphonate to create the respective phosphonate esters 7 and 8.[177,178] Deprotection of the esters with TMS-Br yields the desired products PACE2 and PACE4.

In addition to making materials that bind to ITO, this project can move towards making mesoporous ITO/glass for making high surface area electrodes and devices. This type of modification to ITO has been done in the solar fuels and dye sensitized solar cell fields for making high surface area electrodes.[179–182] Figure 7.2.4.2 details a blade coating procedure followed by low temperature sintering for mesoporous ITO fabrication. The procedure involves acquiring a solution 30 wt% nanoITO in ethanol, with 5-10% SnO_2. The solution is usually blue. You make a 10 wt% solution of hydroxypropylcellulose (HPC) in ethanol and mix in the nanoITO at a 1:1 v:v ratio and stir overnight. While this solution is stirring the clean conducting glass is masked with

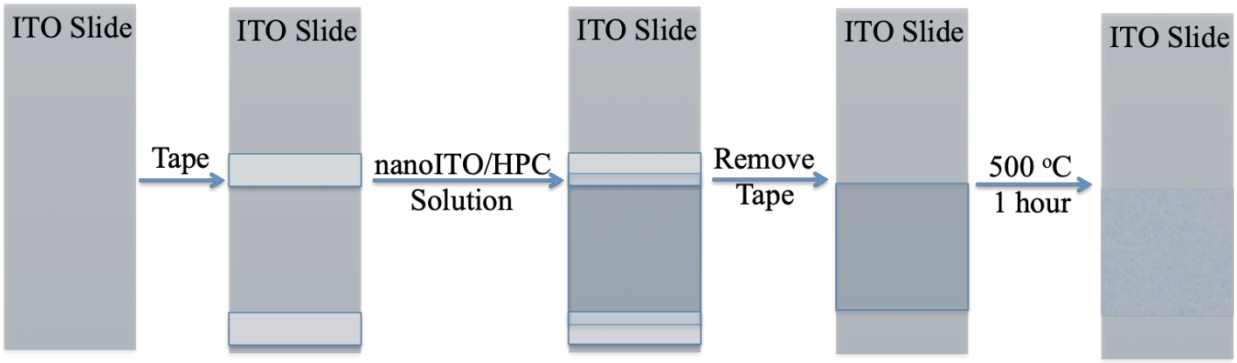

Figure 7.2.4.2. Outline of mesoporous ITO fabrication through blade coating and sintering.

scotch tape. The solution is now blade coated and allowed to sit for 10 minutes before tape is removed. The slides are now placed in an oven at 500 °C for one hour to sinter the HPC and cooled to yield mesoporous ITO. The downside to these mesoporous ITO/glass slides is that they tend to have a slightly yellow tint. While it will lower the contrast in the visible, it can function as a proof of concept for devices.

Will the phosphonic acid functionalized materials behave similarly as the parent molecules, with respect to absorption? How well will the PACE molecules bind to the ITO (particularly under the coulombic repulsive forces of the working electrode)? How much more current can be passed through the mesoporous ITO/glass? What is the tradeoff between a thicker mesoporous layer and loss of contrast in the visible?

References

(1) Tipler, P. A.; Mosca, G. P. *Physics for Scientists and Engineers.*, 5th ed.; W.H. Freeman: New York, 2003.

(2) Lekner, J. Theory of Reflection of Electromagnetic and Particle Waves, Martinus Nijhoff. Dordrecht 1987.

(3) Bohren, C. F.; Huffman, D. R. *Absorption and Scattering of Light by Small Particles*; John Wiley & Sons, 2008.

(4) Berns, R. S. Billmeyer and Saltzman's Principles of Color Technology. In *Billmeyer and Saltzman's Principles of Color Technology*; John Wiley & Sons, 2000.

(5) Ohta, N.; Robertson, A. *Colorimetry: Fundamentals and Applications*; John Wiley & Sons, 2006.

(6) Wald, G. The Receptors of Human Color Vision. *Science (80-.).* **1964**, *145* (3636), 1007–1016.

(7) Wald, G.; Brown, P. K. Human Color Vision and Color Blindness. In *Cold Spring Harbor symposia on quantitative biology*; Cold Spring Harbor Laboratory Press, 1965; Vol. 30, pp 345–361.

(8) Deeb, S. S. The Molecular Basis of Variation in Human Color Vision. *Clin. Genet.* **2005**, *67* (5), 369–377.

(9) McLaren, K. XIII—The Development of the CIE 1976 (L* A* B*) Uniform Colour Space and Colour-difference Formula. *J. Soc. Dye. Colour.* **1976**, *92* (9), 338–341.

(10) Robertson, A. R. The CIE 1976 Color-difference Formulae. *Color Res. Appl.* **1977**, *2* (1), 7–11.

(11) Chiang, C.-Y.; Chen, K.-S.; Chu, C.-Y.; Chang, Y.-L.; Fan, K.-C. Color Enhancement for Four-Component Decomposed Polarimetric SAR Image Based on a CIE-Lab Encoding. *Remote Sens.* **2018**, *10* (4), 545.

(12) Reddinger, J. L.; Reynolds, J. R. Molecular Engineering of π-Conjugated Polymers. In *Radical Polymerisation Polyelectrolytes*; Springer, 1999; pp 57–122.

(13) McCullough, R. D. The Chemistry of Conducting Polythiophenes. *Adv. Mater.* **1998**, *10* (2), 93–116.

(14) Moliton, A.; Hiorns, R. C. Review of Electronic and Optical Properties of Semiconducting Π-conjugated Polymers: Applications in Optoelectronics. *Polym. Int.* **2004**, *53* (10), 1397–1412.

(15) Schultze, J. W.; Karabulut, H. Application Potential of Conducting Polymers. *Electrochim. Acta* **2005**, *50* (7–8), 1739–1745.

(16) Groenendaal, L.; Zotti, G.; Aubert, P.; Waybright, S. M.; Reynolds, J. R. Electrochemistry of Poly (3, 4-alkylenedioxythiophene) Derivatives. *Adv. Mater.* **2003**, *15* (11), 855–879.

(17) Cirpan, A.; Argun, A. A.; Grenier, C. R. G.; Reeves, B. D.; Reynolds, J. R. Electrochromic Devices Based on Soluble and Processable Dioxythiophene Polymers. *J. Mater. Chem.* **2003**, *13* (10), 2422–2428.

(18) Argun, A. A.; Aubert, P.-H.; Thompson, B. C.; Schwendeman, I.; Gaupp, C. L.; Hwang, J.; Pinto, N. J.; Tanner, D. B.; MacDiarmid, A. G.; Reynolds, J. R. Multicolored Electrochromism in Polymers: Structures and Devices. *Chem. Mater.* **2004**, *16* (23), 4401–4412. https://doi.org/10.1021/cm049669l.

(19) Gigli, G.; Inganäs, O.; Anni, M.; De Vittorio, M.; Cingolani, R.; Barbarella, G.; Favaretto, L. Multicolor Oligothiophene-Based Light-Emitting Diodes. *Appl. Phys. Lett.* **2001**, *78* (11), 1493–1495.

(20) Perepichka, I. F.; Perepichka, D. F.; Meng, H.; Wudl, F. Light-emitting Polythiophenes. *Adv. Mater.* **2005**, *17* (19), 2281–2305.

(21) Groenendaal, L.; Jonas, F.; Freitag, D.; Pielartzik, H.; Reynolds, J. R. Poly (3, 4-ethylenedioxythiophene) and Its Derivatives: Past, Present, and Future. *Adv. Mater.* **2000**, *12* (7), 481–494.

(22) Brabec, C. J.; Sariciftci, N. S.; Hummelen, J. C. Plastic Solar Cells. *Adv. Funct. Mater.* **2001**, *11* (1), 15–26.

(23) McQuade, D. T.; Pullen, A. E.; Swager, T. M. Conjugated Polymer-Based Chemical Sensors. *Chem. Rev.* **2000**, *100* (7), 2537–2574.

(24) Reddinger, J. L.; Reynolds, J. R. A Novel Polymeric Metallomacrocycle Sensor Capable of Dual-Ion Cocomplexation. *Chem. Mater.* **1998**, *10* (1), 3–5.

(25) Reddinger, J. L.; Reynolds, J. R. Tunable Redox and Optical Properties Using Transition Metal-Complexed Polythiophenes. *Macromolecules* **1997**, *30* (3), 673–675.

(26) Roncali, J. Electrogenerated Functional Conjugated Polymers as Advanced Electrode Materials. *J. Mater. Chem.* **1999**, *9* (9), 1875–1893.

(27) Smela, E. Conjugated Polymer Actuators for Biomedical Applications. *Adv. Mater.* **2003**, *15* (6), 481–494.

(28) Pernaut, J.-M.; Reynolds, J. R. Use of Conducting Electroactive Polymers for Drug Delivery and Sensing of Bioactive Molecules. A Redox Chemistry Approach. *J. Phys. Chem. B* **2000**, *104* (17), 4080–4090.

(29) Bredas, J.-L. Mind the Gap! *Mater. Horizons* **2014**, *1* (1), 17–19.

(30) Salzner, U.; Lagowski, J. B.; Pickup, P. G.; Poirier, R. A. Comparison of Geometries and Electronic Structures of Polyacetylene, Polyborole, Polycyclopentadiene, Polypyrrole, Polyfuran, Polysilole, Polyphosphole, Polythiophene, Polyselenophene and Polytellurophene. *Synth. Met.* **1998**, *96* (3), 177–189.

(31) Winkler, S.; Amsalem, P.; Frisch, J.; Oehzelt, M.; Heimel, G.; Koch, N. Probing the Energy Levels in Hole-Doped Molecular Semiconductors. *Mater. Horizons* **2015**, *2* (4), 427–433. https://doi.org/10.1039/c5mh00023h.

(32) Png, R. Q.; Ang, M. C. Y.; Teo, M. H.; Choo, K. K.; Tang, C. G.; Belaineh, D.; Chua, L. L.; Ho, P. K. H. Madelung and Hubbard Interactions in Polaron Band Model of Doped Organic Semiconductors. *Nat. Commun.* **2016**, *7* (May), 1–9. https://doi.org/10.1038/ncomms11948.

(33) Coropceanu, V.; Cornil, J.; Silva, D.; A, D.; Olivier, Y.; Silbey, R.; Bredas, J. L.; da Silva Filho, D. A.; Brédas, J.-L. J.-L.; Olivier, Y.; et al. Charge Transport in Organic Semiconductors. *Chem. Rev.* **2007**, *107* (4), 926–952. https://doi.org/10.1007/128_2011_218.

(34) Bredas, J. L.; Street, G. B. Polarons, Bipolarons, and Solitons in Conducting Polymers. *Acc. Chem. Res.* **1985**, *18* (10), 309–315.

(35) Hubbard, J. Electron Correlations in Narrow Energy Bands. *Proc. R. Soc. London. Ser. A. Math. Phys. Sci.* **1963**, *276* (1365), 238–257.

(36) Schwedhelm, R.; Kipp, L.; Dallmeyer, A.; Skibowski, M. Experimental Band Gap and Core-Hole Electron Interaction in Epitaxial C60 Films. *Phys. Rev. B* **1998**, *58* (19), 13176–13180. https://doi.org/10.1103/PhysRevB.58.13176.

(37) Hansmann, P.; Vaugier, L.; Jiang, H.; Biermann, S. What AboutUon Surfaces? Extended Hubbard Models for Adatom Systems from First Principles. *J. Phys. Condens. Matter* **2013**, *25* (9), 94005. https://doi.org/10.1088/0953-8984/25/9/094005.

(38) Bubnova, O.; Crispin, X. Towards Polymer-Based Organic Thermoelectric Generators. *Energy Environ. Sci.* **2012**, *5* (11), 9345–9362. https://doi.org/10.1039/c2ee22777k.

(39) Beaujuge, P. M.; Amb, C. M.; Reynolds, J. R. Color Control in π-Conjugated Organic Polymers for Use in Electrochromic Devices. *Chem. Rev.* **2010**, *110* (1), 268–320. https://doi.org/10.1021/cr900129a.

(40) Müller, H. K.; Hocker, J.; Menke, K.; Ehinger, K.; Roth, S. Long-Term Conductivity Decrease in Polyacetylene Samples. *Synth. Met.* **1985**, *10* (4), 273–280.

(41) Elschner, A.; Kirchmeyer, S.; Lovenich, W.; Merker, U.; Reuter, K. *PEDOT: Principles and Applications of an Intrinsically Conductive Polymer*; CRC Press, 2010.

(42) Jonas, F.; Heywang, G.; Schmidtberg, W.; Heinze, J.; Dietrich, M. Polythiophenes, Process for Their Preparation and Their Use. Google Patents September 25, 1990.

(43) Jonas, F.; Heywang, G.; Schmidtberg, W. Solid Electrolytes, and Electrolyte Capacitors Containing Same. Google Patents March 20, 1990.

(44) Jonas, F.; Heywang, G.; Schmidtberg, W.; Heinze, J.; Dietrich, M. Method of Imparting Antistatic Properties to a Substrate by Coating the Substrate with a Novel Polythiophene. Google Patents July 30, 1991.

(45) Jonas, F.; Heywang, G.; Schmidtberg, W.; Heinze, J.; Dietrich, M. Polythiophenes, Process for Their Preparation and Their Use. Google Patents January 22, 1991.

(46) Heywang, G.; Jonas, F. Poly (Alkylenedioxythiophene) S—new, Very Stable Conducting Polymers. *Adv. Mater.* **1992**, *4* (2), 116–118.

(47) Merz, A.; Rehm, C. Improved Preparation of 3, 4-Dimethoxythiophene. *J. für Prakt. Chemie/Chemiker-Zeitung* **1996**, *338* (1), 672–674.

(48) Janda, M.; Šrogl, J.; Stibor, I.; Němec, M.; Vopatrna, P. Polylithiothiophenes and a Convenient Synthesis of Polymethylthiophenes. *Synthesis (Stuttg).* **1972**, *1972* (10), 545–547.

(49) Granowitz, S. New Syntheses of 3-Bromothiophene and 3, 4-Dibromothiophene. *Acta Chemica Scandinavica*. MUNKSGAARD INT PUBL LTD 35 NORRE SOGADE, PO BOX 2148, DK-1016 COPENHAGEN … 1959, pp 1045–1046.

(50) Keegstra, M. A.; Peters, T. H. A.; Brandsma, L. Copper (I) Halide Catalysed Synthesis of Alkyl Aryl and Alkyl Heteroaryl Ethers. *Tetrahedron* **1992**, *48* (17), 3633–3652.

(51) Welsh, D. M.; Kumar, A.; Morvant, M. C.; Reynolds, J. R. Fast Electrochromic Polymers Based on New Poly (3, 4-Alkylenedioxythiophene) Derivatives. *Synth. Met.* **1999**, *102* (1–3), 967–968.

(52) Kumar, A.; Reynolds, J. R. Soluble Alkyl-Substituted Poly (Ethylenedioxythiophenes) as Electrochromic Materials. *Macromolecules* **1996**, *29* (23), 7629–7630.

(53) Reeves, B. D.; Grenier, C. R. G.; Argun, A. A.; Cirpan, A.; McCarley, T. D.; Reynolds, J. R. Spray Coatable Electrochromic Dioxythiophene Polymers with High Coloration Efficiencies. *Macromolecules* **2004**, *37* (20), 7559–7569.

(54) Dyer, A. L.; Thompson, E. J.; Reynolds, J. R. Completing the Color Palette with Spray-Processable Polymer Electrochromics. *ACS Appl. Mater. Interfaces* **2011**, *3* (6), 1787–1795. https://doi.org/10.1021/am200040p.

(55) Dyer, A. L.; Craig, M. R.; Babiarz, J. E.; Kiyak, K.; Reynolds, J. R. Orange and Red to Transmissive Electrochromic Polymers Based on Electron-Rich Dioxythiophenes. *Macromolecules* **2010**, *43* (10), 4460–4467.

(56) Kerszulis, J. A.; Amb, C. M.; Dyer, A. L.; Reynolds, J. R. Follow the Yellow Brick Road: Structural Optimization of Vibrant Yellow-to-Transmissive Electrochromic Conjugated Polymers. *Macromolecules* **2014**, *47* (16), 5462–5469. https://doi.org/10.1021/ma501080u.

(57) Beaujuge, P. M.; Ellinger, S.; Reynolds, J. R. Spray Processable Green to Highly Transmissive Electrochromics via Chemically Polymerizable Donor–acceptor Heterocyclic Pentamers. *Adv. Mater.* **2008**, *20* (14), 2772–2776.

(58) Cao, K.; Shen, D. E.; Österholm, A. M.; Kerszulis, J. A.; Reynolds, J. R. Tuning Color, Contrast, and Redox Stability in High Gap Cathodically Coloring Electrochromic Polymers. *Macromolecules* **2016**, *49* (22), 8498–8507. https://doi.org/10.1021/acs.macromol.6b01763.

(59) Oguzhan, E.; Bilgili, H.; Koyuncu, F. B.; Ozdemir, E.; Koyuncu, S. A New Processable Donor–acceptor Polymer Displaying Neutral State Yellow Electrochromism. *Polymer (Guildf).* **2013**, *54* (23), 6283–6292.

(60) İçli-Özkut, M.; Öztaş, Z.; Algi, F.; Cihaner, A. A Neutral State Yellow to Navy Polymer Electrochrome with Pyrene Scaffold. *Org. Electron.* **2011**, *12* (9), 1505–1511.

(61) Österholm, A. M.; Shen, D. E.; Gottfried, D. S.; Reynolds, J. R. Full Color Control and High-Resolution Patterning from Inkjet Printable Cyan/Magenta/Yellow Colored-to-Colorless Electrochromic Polymer Inks. *Adv. Mater. Technol.* **2016**, *1* (4), 1600063–n/a. https://doi.org/10.1002/admt.201600063.

(62) Guan, S.; Elmezayyen, A. S.; Zhang, F.; Zheng, J.; Xu, C. Deterioration Mechanism of Electrochromic Poly (3, 4-(2, 2-Dimethylpropylenedioxy) Thiophene) Thin Films. *J. Mater. Chem. C* **2016**, *4* (20), 4584–4591.

(63) Li, Y.; Michinobu, T. Click Synthesis and Reversible Electrochromic Behaviors of Novel Polystyrenes Bearing Aromatic Amine Units. *J. Polym. Sci. Part A Polym. Chem.* **2012**, *50* (11), 2111–2120. https://doi.org/10.1002/pola.25990.

(64) Nguyen, W. H.; Barile, C. J.; McGehee, M. D. Small Molecule Anchored to Mesoporous ITO for High-Contrast Black Electrochromics. *J. Phys. Chem. C* **2016**, *120* (46), 26336–26341. https://doi.org/10.1021/acs.jpcc.6b08820.

(65) Granqvist, C. G. Electrochromics for Smart Windows: Oxide-Based Thin Films and Devices. *Thin Solid Films* **2014**, *564*, 1–38. https://doi.org/10.1016/j.tsf.2014.02.002.

(66) Mortimer, R. J.; Dyer, A. L.; Reynolds, J. R. Electrochromic Organic and Polymeric Materials for Display Applications. *Displays* **2006**, *27* (1), 2–18. https://doi.org/10.1016/j.displa.2005.03.003.

(67) Sezgin, M.; Ozay, O.; Koyuncu, S.; Ozay, H.; Baycan Koyuncu, F. A Neutral State Colorless Phosphazene/Carbazole Hybride Dendron and Its Electrochromic Device Application. *Chem. Eng. J.* **2015**, *274*, 282–289. https://doi.org/10.1016/j.cej.2015.03.134.

(68) Camurlu, P. Polypyrrole Derivatives for Electrochromic Applications. *RSC Adv.* **2014**, *4*, 55832–55845. https://doi.org/10.1039/C4RA11827H.

(69) Wu, J.-T.; Liou, G.-S. A Novel Panchromatic Shutter Based on an Ambipolar Electrochromic System without Supporting Electrolyte. *Chem. Commun.* **2018**, *54* (21), 2619–2622.

(70) Liu, H.-S.; Pan, B.-C.; Huang, D.-C.; Kung, Y.-R.; Leu, C.-M.; Liou, G.-S. Highly Transparent to Truly Black Electrochromic Devices Based on an Ambipolar System of Polyamides and Viologen. *NPG Asia Mater.* **2017**, *9* (6), e388.

(71) Weng, D.; Shi, Y.; Zheng, J.; Xu, C. High Performance Black-to-Transmissive Electrochromic Device with Panchromatic Absorption Based on TiO2-Supported Viologen and Triphenylamine Derivatives. *Org. Electron.* **2016**, *34*, 139–145.

(72) Tahtali, G.; Has, Z.; Doyranli, C.; Varlikli, C.; Koyuncu, S. Solution Processable Neutral State Colourless Electrochromic Devices: Effect of the Layer Thickness on the Electrochromic Performance. *J. Mater. Chem. C* **2016**, *4* (42), 10090–10094.

(73) Hsiao, S.-H.; Liou, G.-S.; Kung, Y.-C.; Yen, H.-J. High Contrast Ratio and Rapid Switching Electrochromic Polymeric Films Based on 4-(Dimethylamino)Triphenylamine-Functionalized Aromatic Polyamides. *Macromolecules* **2008**, *41* (8), 2800–2808. https://doi.org/10.1021/ma702426z.

(74) Sönmez, G.; Schwendeman, I.; Schottland, P.; Zong, K.; Reynolds, J. R. N-Substituted Poly(3,4-Propylenedioxypyrrole)s: High Gap and Low Redox Potential Switching Electroactive and Electrochromic Polymers. *Macromolecules* **2003**, *36* (3), 639–647. https://doi.org/10.1021/ma021108x.

(75) Walczak, R. M.; Reynolds, J. R. Poly(3,4-Alkylenedioxypyrroles): The PXDOPs as Versatile yet Underutilized Electroactive and Conducting Polymers. *Adv. Mater.* **2006**, *18* (9), 1121–1131. https://doi.org/10.1002/adma.200502312.

(76) Mortier, C.; Darmanin, T.; Guittard, F. 3,4-Ethylenedioxypyrrole (EDOP) Monomers with Aromatic Substituents for Parahydrophobic Surfaces by Electropolymerization. *Macromolecules* **2015**, *48* (15), 5188–5195. https://doi.org/10.1021/acs.macromol.5b01054.

(77) Kurtay, G.; Soganci, T.; Ak, M.; Gullu, M. Synthesis and Computational Bandgap Engineering of New 3,4-Alkylenedioxypyrrole (ADOP) Derivatives and Investigation of Their Electrochromic Properties. *J. Electrochem. Soc.* **2016**, *163* (10), 896–905. https://doi.org/10.1149/2.0131610jes.

(78) Knott, E. P.; Craig, M. R.; Liu, D. Y.; Babiarz, J. E.; Dyer, A. L.; Reynolds, J. R. A Minimally Coloured Dioxypyrrole Polymer as a Counter Electrode Material in Polymeric Electrochromic Window Devices. *J. Mater. Chem.* **2012**, *22* (11), 4953–4962. https://doi.org/10.1039/C2JM15057C.

(79) Arroyave, F. A.; Reynolds, J. R. Dioxypyrrole-Based Polymers via Dehalogenation Polycondensation Using Various Electrophilic Halogen Sources. *Macromolecules* **2012**, *45* (15), 5842–5849. https://doi.org/10.1021/ma300684t.

(80) Yen, H.-J.; Liou, G.-S. Solution-Processable Triarylamine-Based Electroactive High Performance Polymers for Anodically Electrochromic Applications. *Polym. Chem.* **2012**, *3* (2), 255–264. https://doi.org/10.1039/c1py00346a.

(81) Yen, H. J.; Chen, C. J.; Liou, G. S. Flexible Multi-Colored Electrochromic and Volatile Polymer Memory Devices Derived from Starburst Triarylamine-Based Electroactive Polyimide. *Adv. Funct. Mater.* **2013**, *23* (42), 5307–5316. https://doi.org/10.1002/adfm.201300569.

(82) Yen, H.-J.; Liou, G.-S. Solution-Processable Triarylamine-Based Electroactive High Performance Polymers for Anodically Electrochromic Applications. *Polym. Chem.* **2012**, *3* (2), 255–264.

(83) Liou, G.-S.; Lin, H.-Y. Synthesis and Electrochemical Properties of Novel Aromatic Poly (Amine− Amide) s with Anodically Highly Stable Yellow and Blue Electrochromic Behaviors. *Macromolecules* **2008**, *42* (1), 125–134.

(84) Yen, H.-J.; Lin, K.-Y.; Liou, G.-S. Transmissive to Black Electrochromic Aramids with High Near-Infrared and Multicolor Electrochromism Based on Electroactive Tetraphenylbenzidine Units. *J. Mater. Chem.* **2011**, *21* (17), 6230–6237. https://doi.org/10.1039/C1JM10210A.

(85) Chang, T.-H.; Lu, H.-C.; Lee, M.-H.; Kao, S.-Y.; Ho, K.-C. Multi-Color Electrochromic Devices Based on Phenyl and Heptyl Viologens Immobilized with Uv-Cured Polymer Electrolyte. *Sol. Energy Mater. Sol. Cells* **2018**, *177*, 75–81.

(86) Granqvist, C. G. Transparent Conductive Electrodes for Electrochromic Devices: A Review. *Appl. Phys. A* **1993**, *57* (1), 19–24.

(87) Sapp, S. A.; Sotzing, G. A.; Reynolds, J. R. High Contrast Ratio and Fast-Switching Dual Polymer Electrochromic Devices. *Chem. Mater.* **1998**, *10* (8), 2101–2108.

(88) Bange, K.; Gambke, T. Electrochromic Materials for Optical Switching Devices. *Adv. Mater.* **1990**, *2* (1), 10–16.

(89) Mortimer, R. J. Organic Electrochromic Materials. *Electrochim. Acta* **1999**, *44* (18), 2971–2981.

(90) Byker, H. J. Single-Compartment, Self-Erasing, Solution-Phase Electrochromic Devices, Solutions for Use Therein, and Uses Thereof. Google Patents February 20, 1990.

(91) Byker, H. J. Electrochromic Devices with Bipyridinium Salt Solutions. Google Patents August 9, 1994.

(92) Theiste, D. A.; Byker, H. J. Tinted Solution-Phase Electrochromic Devices. Google Patents January 11, 1994.

(93) Hoekstra, E. J.; Schierbeek, K. L. Digital Electrochromic Mirror System. Google Patents May 2, 2000.

(94) Gesheva, K. A.; Ivanova, T.; Hamelmann, F. Optical Coatings of CVD-Transition Metal Oxides as Functional Layers in "SMART WINDOWS" and X-Ray Mirrors. *J. Optoelectron. Adv. Mater.* **2005**, *7* (3), 1243–1252.

(95) Byker, H. J. Electrochromics and Polymers. *Electrochim. Acta* **2001**, *46* (13–14), 2015–2022.

(96) Möller, M.; Leyland, N.; Copeland, G.; Cassidy, M. Self-Powered Electrochromic Display as an Example for Integrated Modules in Printed Electronics Applications. *Eur. Phys. J. Appl. Phys.* **2010**, *51* (3), 33205.

(97) Corr, D.; Bach, U.; Fay, D.; Kinsella, M.; McAtamney, C.; O'Reilly, F.; Rao, S. N.; Stobie, N. Coloured Electrochromic "Paper-Quality" Displays Based on Modified Mesoporous Electrodes. *Solid State Ionics* **2003**, *165* (1–4), 315–321.

(98) Bulloch, R. H.; Kerszulis, J. A.; Dyer, A. L.; Reynolds, J. R. Mapping the Broad CMY Subtractive Primary Color Gamut Using a Dual-Active Electrochromic Device. *ACS Appl. Mater. Interfaces* **2014**, *6* (9), 6623–6630.

(99) Watanabe, Y.; Nagashima, T.; Nakamura, K.; Kobayashi, N. Continuous-Tone Images Obtained Using Three Primary-Color Electrochromic Cells Containing Gel Electrolyte. *Sol. Energy Mater. Sol. Cells* **2012**, *104*, 140–145.

(100) Kondo, Y.; Tanabe, H.; Kudo, H.; Nakano, K.; Otake, T. Electrochromic Type E-Paper Using Poly (1H-Thieno [3, 4-d] Imidazol-2 (3H)-One) Derivatives by a Novel Printing Fabrication Process. *Materials (Basel).* **2011**, *4* (12), 2171–2182.

(101) Schoot, C. J.; Ponjee, J. J.; Van Dam, H. T.; Van Doorn, R. A.; Bolwijn, P. T. New Electrochromic Memory Display. *Appl. Phys. Lett.* **1973**, *23* (2), 64–65.

(102) Baloukas, B.; Lamarre, J.-M.; Martinu, L. Active Metameric Security Devices Using an Electrochromic Material. *Appl. Opt.* **2011**, *50* (9), C41–C49.

(103) Schwendeman, I.; Hickman, R.; Sönmez, G.; Schottland, P.; Zong, K.; Welsh, D. M.; Reynolds, J. R. Enhanced Contrast Dual Polymer Electrochromic Devices. *Chem. Mater.* **2002**, *14* (7), 3118–3122.

(104) Puodziukynaite, E.; Oberst, J. L.; Dyer, A. L.; Reynolds, J. R. Establishing Dual Electrogenerated Chemiluminescence and Multicolor Electrochromism in Functional Ionic Transition-Metal Complexes. *J. Am. Chem. Soc.* **2011**, *134* (2), 968–978.

(105) Reynolds, J. R.; Dyer, A. L. Interdigitated Electrode Dual Electroemissive/Electrochromic

Devices. Google Patents February 21, 2012.

(106) Ding, Y.; Invernale, M. A.; Sotzing, G. A. Conductivity Trends of PEDOT-PSS Impregnated Fabric and the Effect of Conductivity on Electrochromic Textile. *ACS Appl. Mater. Interfaces* **2010**, *2* (6), 1588–1593.

(107) Tehrani, P.; Hennerdal, L.-O.; Dyer, A. L.; Reynolds, J. R.; Berggren, M. Improving the Contrast of All-Printed Electrochromic Polymer on Paper Displays. *J. Mater. Chem.* **2009**, *19* (13), 1799–1802.

(108) Imamura, A.; Kimura, M.; Kon, T.; Sunohara, S.; Kobayashi, N. Bi-Based Electrochromic Cell with Mediator for White/Black Imaging. *Sol. Energy Mater. Sol. Cells* **2009**, *93* (12), 2079–2082.

(109) Liu, H.; Crooks, R. M. Based Electrochemical Sensing Platform with Integral Battery and Electrochromic Read-Out. *Anal. Chem.* **2012**, *84* (5), 2528–2532.

(110) Monk, P.; Mortimer, R.; Rosseinsky, D. *Electrochromism and Electrochromic Devices*; Cambridge University Press, 2007.

(111) Svensson, J.; Granqvist, C. G. Electrochromic Coatings for "Smart Windows." *Sol. energy Mater.* **1985**, *12* (6), 391–402.

(112) Rauh, R. D. Electrochromic Windows: An Overview. *Electrochim. Acta* **1999**, *44* (18), 3165–3176.

(113) Lee, E. S.; DiBartolomeo, D. L. Application Issues for Large-Area Electrochromic Windows in Commercial Buildings. *Sol. Energy Mater. Sol. Cells* **2002**, *71* (4), 465–491.

(114) Azens, A.; Granqvist, C. Electrochromic Smart Windows: Energy Efficiency and Device Aspects. *J. Solid State Electrochem.* **2003**, *7* (2), 64–68.

(115) Zinzi, M. Office Worker Preferences of Electrochromic Windows: A Pilot Study. *Build. Environ.* **2006**, *41* (9), 1262–1273.

(116) Baetens, R.; Jelle, B. P.; Gustavsen, A. Properties, Requirements and Possibilities of Smart Windows for Dynamic Daylight and Solar Energy Control in Buildings: A State-of-the-Art Review. *Sol. energy Mater. Sol. cells* **2010**, *94* (2), 87–105.

(117) Barratt, J.; Dowd, K. A New Airplane for a New World: The Boeing 787 Dreamliner. *Des. Manag. Rev.* **2006**, *17* (4), 25–30.

(118) Xu, C.; Ma, C.; Taya, M. Smart Sunglasses, Helmet Faceshields and Goggles Based on Electrochromic Polymers. Google Patents January 25, 2011.

(119) Kallman, W. R.; Roberts, M. B.; Baretich, D. F.; Dorfman, L. M.; Ahern, J. F. Electrochromic Eyewear System, Rechargeable Eyewear and External Charger Therefor. Google Patents October 3, 1995.

(120) Poverenov, E.; Li, M.; Bitler, A.; Bendikov, M. Major Effect of Electropolymerization Solvent on Morphology and Electrochromic Properties of PEDOT Films. *Chem. Mater.* **2010**, *22* (13), 4019–4025.

(121) Diaz, A. F.; Kanazawa, K. K.; Gardini, G. P. Electrochemical Polymerization of Pyrrole. *J. Chem. Soc. Chem. Commun.* **1979**, No. 14, 635–636.

(122) King, A. O.; Okukado, N.; Negishi, E. Highly General Stereo-, Regio-, and Chemo-Selective Synthesis of Terminal and Internal Conjugated Enynes by the Pd-Catalysed Reaction of Alkynylzinc Reagents with Alkenyl Halides. *J. Chem. Soc. Chem. Commun.* **1977**, No. 19, 683–684.

(123) Miyaura, N.; Yanagi, T.; Suzuki, A. The Palladium-Catalyzed Cross-Coupling Reaction of Phenylboronic Acid with Haloarenes in the Presence of Bases. *Synth. Commun.* **1981**, *11* (7), 513–519.

(124) Milstein, D.; Stille, J. K. A General, Selective, and Facile Method for Ketone Synthesis from Acid Chlorides and Organotin Compounds Catalyzed by Palladium. *J. Am. Chem. Soc.* **1978**, *100* (11), 3636–3638.

(125) Kosugi, M.; Sasazawa, K.; Shimizu, Y.; Migita, T. Reactions of Allyltin Compounds Iii. Allylation of Aromatic Halides With Allyltributyltin in the Presence of Tetrakis (Triphenylphosphine) Palladium (O). *Chem. Lett.* **1977**, *6* (3), 301–302.

(126) Azarian, D.; Dua, S. S.; Eaborn, C.; Walton, D. R. M. Reactions of Organic Halides with R3 MMR3 Compounds (M= Si, Ge, Sn) in the Presence of Tetrakis (Triarylphosphine) Palladium. *J. Organomet. Chem.* **1976**, *117* (3), C55–C57.

(127) Satoh, T.; Miura, M. Catalytic Direct Arylation of Heteroaromatic Compounds. *Chem. Lett.* **2006**, *36* (2), 200–205.

(128) Alberico, D.; Scott, M. E.; Lautens, M. Aryl− Aryl Bond Formation by Transition-Metal-Catalyzed Direct Arylation. *Chem. Rev.* **2007**, *107* (1), 174–238.

(129) Kasahara, A.; Izumi, T.; Yodono, M.; Saito, R.; Takeda, T.; Sugawara, T. Arylation and Vinylation Reactions of Benzo [b] Furan via Organopalladium Intermediates. *Bull. Chem. Soc. Jpn.* **1973**, *46* (4), 1220–1225.

(130) Jafarpour, F.; Rahiminejadan, S.; Hazrati, H. Triethanolamine-Mediated Palladium-Catalyzed Regioselective C-2 Direct Arylation of Free NH-Pyrroles. *J. Org. Chem.* **2010**, *75* (9), 3109–3112. https://doi.org/10.1021/jo902739n.

(131) Ueda, K.; Amaike, K.; Maceiczyk, R. M.; Itami, K.; Yamaguchi, J. β-Selective C–H Arylation of Pyrroles Leading to Concise Syntheses of Lamellarins C and I. *J. Am. Chem. Soc.* **2014**, *136* (38), 13226–13232.

(132) Ackermann, L.; Lygin, A. V. Ruthenium-Catalyzed Direct C–H Bond Arylations of Heteroarenes. *Org. Lett.* **2011**, *13* (13), 3332–3335.

(133) Ishiyama, T.; Takagi, J.; Yonekawa, Y.; Hartwig, J. F.; Miyaura, N. Iridium-Catalyzed Direct Borylation of Five-Membered Heteroarenes by Bis (Pinacolato) Diboron: Regioselective, Stoichiometric, and Room Temperature Reactions. *Adv. Synth. Catal.* **2003**, *345* (9-10), 1103–1106.

(134) Okamoto, K.; Zhang, J.; Housekeeper, J. B.; Marder, S. R.; Luscombe, C. K. C–H Arylation Reaction: Atom Efficient and Greener Syntheses of π-Conjugated Small Molecules and Macromolecules for Organic Electronic Materials. *Macromolecules* **2013**, *46* (20), 8059–8078.

(135) Wang, Q.; Takita, R.; Kikuzaki, Y.; Ozawa, F. Palladium-Catalyzed Dehydrohalogenative Polycondensation of 2-Bromo-3-Hexylthiophene: An Efficient Approach to Head-to-Tail Poly (3-Hexylthiophene). *J. Am. Chem. Soc.* **2010**, *132* (33), 11420–11421.

(136) Matsidik, R.; Komber, H.; Sommer, M. Rational Use of Aromatic Solvents for Direct Arylation Polycondensation: C–H Reactivity versus Solvent Quality. *ACS Macro Lett.* **2015**, *4* (12), 1346–1350.

(137) Broll, S.; Nübling, F.; Luzio, A.; Lentzas, D.; Komber, H.; Caironi, M.; Sommer, M. Defect Analysis of High Electron Mobility Diketopyrrolopyrrole Copolymers Made by Direct Arylation Polycondensation. *Macromolecules* **2015**, *48* (20), 7481–7488.

(138) Kuwabara, J.; Yamazaki, K.; Yamagata, T.; Tsuchida, W.; Kanbara, T. The Effect of a Solvent on Direct Arylation Polycondensation of Substituted Thiophenes. *Polym. Chem.* **2015**, *6* (6), 891–895.

(139) Kuwabara, J.; Yasuda, T.; Choi, S. J.; Lu, W.; Yamazaki, K.; Kagaya, S.; Han, L.; Kanbara, T. Direct Arylation Polycondensation: A Promising Method for the Synthesis of Highly Pure, High-Molecular-Weight Conjugated Polymers Needed for Improving the Performance of Organic Photovoltaics. *Adv. Funct. Mater.* **2014**, *24* (21), 3226–3233.

(140) Rudenko, A. E.; Thompson, B. C. Influence of the Carboxylic Acid Additive Structure on the Properties of Poly (3-Hexylthiophene) Prepared via Direct Arylation Polymerization (DArP). *Macromolecules* **2015**, *48* (3), 569–575.

(141) Rudenko, A. E.; Thompson, B. C. Optimization of Direct Arylation Polymerization (DArP) through the Identification and Control of Defects in Polymer Structure. *J. Polym. Sci. Part A Polym. Chem.* **2015**, *53* (2), 135–147.

(142) Pouliot, J.-R.; Grenier, F.; Blaskovits, J. T.; Beaupré, S.; Leclerc, M. Direct (Hetero) Arylation Polymerization: Simplicity for Conjugated Polymer Synthesis. *Chem. Rev.* **2016**, *116* (22), 14225–14274.

(143) Morin, P.-O.; Bura, T.; Sun, B.; Gorelsky, S. I.; Li, Y.; Leclerc, M. Conjugated Polymers a La Carte from Time-Controlled Direct (Hetero) Arylation Polymerization. *ACS Macro Lett.* **2014**, *4* (1), 21–24.

(144) Estrada, L. A.; Deininger, J. J.; Kamenov, G. D.; Reynolds, J. R. Direct (Hetero) Arylation

Polymerization: An Effective Route to 3, 4-Propylenedioxythiophene-Based Polymers with Low Residual Metal Content. *ACS Macro Lett.* **2013**, *2* (10), 869–873.

(145) Bura, T.; Blaskovits, J. T.; Leclerc, M. Direct (Hetero) Arylation Polymerization: Trends and Perspectives. *J. Am. Chem. Soc.* **2016**, *138* (32), 10056–10071.

(146) Bulloch, R. H.; Reynolds, J. R. Photostability in Dioxyheterocycle Electrochromic Polymers. *J. Mater. Chem. C* **2016**, *4* (3), 603–610.

(147) Odin, C.; Nechtschein, M. Slow Relaxation in Conducting Polymers: The Case of Poly (3-Methylthiophene). *Synth. Met.* **1991**, *44* (2), 177–188.

(148) Odin, C.; Nechtschein, M.; Hapiot, P. Kinetics of the Charge-Discharge Process in Conducting Polymers: Slow Relaxation and Hysteresis Effects. Investigations on Polyaniline by Millimetric and Ultramicroelectrodes. *Synth. Met.* **1992**, *47* (3), 329–350.

(149) Inzelt, G. Charge Transport in Conducting Polymer Film Electrodes. *Chem. Biochem. Eng. Q.* **2007**, *21* (1), 1–14.

(150) Hassab, S.; Shen, D. E.; Österholm, A. M.; Reynolds, J. R.; Padilla, J. Exploring Unbalanced Electrode Configurations for Electrochromic Devices. *J. Mater. Chem. C* **2018**, *6* (2), 393–400.

(151) Amb, C. M.; Kerszulis, J. A.; Thompson, E. J.; Dyer, A. L.; Reynolds, J. R. Propylenedioxythiophene (ProDOT)-Phenylene Copolymers Allow a Yellow-to-Transmissive Electrochrome. *Polym. Chem.* **2011**, *2* (4), 812–814. https://doi.org/10.1039/C0PY00405G.

(152) Mercier, L. G.; Leclerc, M. Direct (Hetero) Arylation: A New Tool for Polymer Chemists. *Acc. Chem. Res.* **2013**, *46* (7), 1597–1605.

(153) Facchetti, A.; Vaccaro, L.; Marrocchi, A. Semiconducting Polymers Prepared by Direct Arylation Polycondensation. *Angew. Chemie Int. Ed.* **2012**, *51* (15), 3520–3523.

(154) Padilla, J.; Österholm, A. M.; Dyer, A. L.; Reynolds, J. R. Process Controlled Performance for Soluble Electrochromic Polymers. *Sol. Energy Mater. Sol. Cells* **2015**, *140*, 54–60.

(155) Hassab, S.; Shen, D. E.; Österholm, A. M.; Da Rocha, M.; Song, G.; Alesanco, Y.; Viñuales, A.; Rougier, A.; Reynolds, J. R.; Padilla, J. A New Standard Method to Calculate Electrochromic Switching Time. *Sol. Energy Mater. Sol. Cells* **2018**, *185*, 54–60.

(156) Savagian, L. R.; Österholm, A. M.; Shen, D. E.; Christiansen, D. T.; Kuepfert, M.; Reynolds, J. R. Conjugated Polymer Blends for High Contrast Black-to-Transmissive Electrochromism. *Adv. Opt. Mater.* **2018**, 1800594.

(157) Ponder Jr, J. F.; Österholm, A. M.; Reynolds, J. R. Designing a Soluble PEDOT Analogue without Surfactants or Dispersants. *Macromolecules* **2016**, *49* (6), 2106–2111.

(158) Stalder, R.; Mavrinskiy, A.; Grand, C.; Imaram, W.; Angerhofer, A.; Pisula, W.; Müllen, K.; Reynolds, J. R. Electrochromic and Liquid Crystalline Polycarbonates Based on Telechelic Oligothiophenes. *Polym. Chem.* **2015**, *6* (8), 1230–1235.

(159) Nawa, K.; Imae, I.; Noma, N.; Shirota, Y. Synthesis of a Novel Type of Electrochemically Doped Vinyl Polymer Containing Pendant Terthiophene and Its Electrical and Electrochromic Properties. *Macromolecules* **1995**, *28* (3), 723–729.

(160) Wheeler, D. L.; Rainwater, L. E.; Green, A. R.; Tomlinson, A. L. Modeling Electrochromic Poly-Dioxythiophene-Containing Materials through TDDFT. *Phys. Chem. Chem. Phys.* **2017**, *19* (30), 20251–20258. https://doi.org/10.1039/C7CP04130F.

(161) Nielsen, C. B.; Angerhofer, A.; Abboud, K. A.; Reynolds, J. R. Discrete Photopatternable π-Conjugated Oligomers for Electrochromic Devices. *J. Am. Chem. Soc.* **2008**, *130* (30), 9734–9746. https://doi.org/10.1021/ja7112273.

(162) Oh, J. Y.; Rondeau-Gagné, S.; Chiu, Y.-C.; Chortos, A.; Lissel, F.; Wang, G.-J. N.; Schroeder, B. C.; Kurosawa, T.; Lopez, J.; Katsumata, T.; et al. Intrinsically Stretchable and Healable Semiconducting Polymer for Organic Transistors. *Nature* **2016**, *539*, 411–415.

(163) Savagatrup, S.; Zhao, X.; Chan, E.; Mei, J.; Lipomi, D. J. Effect of Broken Conjugation on the Stretchability of Semiconducting Polymers. *Macromol. Rapid Commun.* **2016**, *37* (19), 1623–1628. https://doi.org/10.1002/marc.201600377.

(164) Janata, J. *Principles of Chemical Sensors*; Springer Science & Business Media, 2010.

(165) Gallazzi, M. C.; Tassoni, L.; Bertarelli, C.; Pioggia, G.; Di Francesco, F.; Montoneri, E. Poly(Alkoxy-Bithiophenes) Sensors for Organic Vapours. *Sensors Actuators B Chem.* **2003**, *88* (2), 178–189. https://doi.org/https://doi.org/10.1016/S0925-4005(02)00323-4.

(166) Rella, R.; Siciliano, P.; Quaranta, F.; Primo, T.; Valli, L.; Schenetti, L. Poly[3-(Butylthio)Thiophene] Langmuir–Blodgett Films as Selective Solid State Chemiresistors for Nitrogen Dioxide. *Colloids Surfaces A Physicochem. Eng. Asp.* **2002**, *198–200* (Supplement C), 829–833. https://doi.org/https://doi.org/10.1016/S0927-7757(01)01008-1.

(167) Mabrook, M. F.; Pearson, C.; Petty, M. C. An Inkjet-Printed Chemical Fuse. *Appl. Phys. Lett.* **2004**, *86* (1), 13507. https://doi.org/10.1063/1.1846950.

(168) Scherlis, D. A.; Marzari, N. π-Stacking in Charged Thiophene Oligomers. *J. Phys. Chem. B* **2004**, *108* (46), 17791–17795.

(169) Hill, M. G.; Penneau, J. F.; Zinger, B.; Mann, K. R.; Miller, L. L. Oligothiophene Cation Radicals.. Pi.-Dimers as Alternatives to Bipolarons in Oxidized Polythiophenes. *Chem. Mater.* **1992**, *4* (5), 1106–1113.

(170) Hapiot, P.; Audebert, P.; Monnier, K.; Pernaut, J.-M.; Garcia, P. Electrochemical Evidence of. Pi.-Dimerization with Short Thiophene Oligomers. *Chem. Mater.* **1994**, *6* (9), 1549–1555.

(171) Zotti, G.; Schiavon, G.; Berlin, A.; Pagani, G. Thiophene Oligomers as Polythiophene Models. 2. Electrochemistry and in Situ ESR of End-Capped Oligothienyls in the Solid State. Evidence for. Pi.-Dimerization of Hexameric Polarons in Polythiophene. *Chem. Mater.* **1993**, *5* (5), 620–624.

(172) Kerszulis, J. A.; Bulloch, R. H.; Teran, N. B.; Wolfe, R. M. W.; Reynolds, J. R. Relax: A Sterically Relaxed Donor–Acceptor Approach for Color Tuning in Broadly Absorbing, High Contrast Electrochromic Polymers. *Macromolecules* **2016**, *49* (17), 6350–6359. https://doi.org/10.1021/acs.macromol.6b01114.

(173) İçli, M.; Pamuk, M.; Algi, F.; Önal, A. M.; Cihaner, A. Donor− Acceptor Polymer Electrochromes with Tunable Colors and Performance. *Chem. Mater.* **2010**, *22* (13), 4034–4044.

(174) Dey, T.; Invernale, M. A.; Ding, Y.; Buyukmumcu, Z.; Sotzing, G. A. Poly (3, 4-Propylenedioxythiophene) s as a Single Platform for Full Color Realization. *Macromolecules* **2011**, *44* (8), 2415–2417.

(175) Zhang, Y.-M.; Xie, F.; Li, W.; Wang, Y.; Zhang, W.; Wang, X.; Li, M.; Zhang, X.-A. A Methyl Ketone Bridged Molecule as a Multi- Stimuli-Responsive Color Switch for Electrochromic Devices. *J. Mater. Chem. C.* *4*, 4662–4667. https://doi.org/10.1039/c5tc04236d.

(176) Christiansen, D. T.; Wheeler, D. L.; Tomlinson, A. L.; Reynolds, J. R. Electrochromism of Alkylene-Linked Discrete Chromophore Polymers with Broad Radical Cation Light Absorption. *Polym. Chem.* **2018**, *9*, 3055–3066.

(177) Paniagua, S. A.; Giordano, A. J.; Smith, O. L.; Barlow, S.; Li, H.; Armstrong, N. R.; Pemberton, J. E.; Brédas, J. L.; Ginger, D.; Marder, S. R. Phosphonic Acids for Interfacial Engineering of Transparent Conductive Oxides. *Chem. Rev.* **2016**, *116* (12), 7117–7158. https://doi.org/10.1021/acs.chemrev.6b00061.

(178) Polaske, N. W.; Lin, H. C.; Tang, A.; Mayukh, M.; Oquendo, L. E.; Green, J. T.; Ratcliff, E. L.; Armstrong, N. R.; Saavedra, S. S.; McGrath, D. V. Phosphonic Acid Functionalized Asymmetric Phthalocyanines: Synthesis, Modification of Indium Tin Oxide, and Charge Transfer. *Langmuir* **2011**, *27* (24), 14900–14909. https://doi.org/10.1021/la203126c.

(179) Ito, S.; Kitamura, T.; Wada, Y.; Yanagida, S. Facile Fabrication of Mesoporous TiO2 Electrodes for Dye Solar Cells: Chemical Modification and Repetitive Coating. *Sol. energy Mater. Sol. cells* **2003**, *76* (1), 3–13.

(180) Ito, S.; Takeuchi, T.; Katayama, T.; Sugiyama, M.; Matsuda, M.; Kitamura, T.; Wada, Y.; Yanagida, S. Conductive and Transparent Multilayer Films for Low-Temperature-Sintered Mesoporous TiO2 Electrodes of Dye-Sensitized Solar Cells. *Chem. Mater.* **2003**, *15* (14), 2824–2828.

(181) Pohl, A.; Dunn, B. Mesoporous Indium Tin Oxide (ITO) Films. *Thin Solid Films* **2006**, *515* (2), 790–792.

(182) Lian, Z.; Wang, W.; Li, G.; Tian, F.; Schanze, K. S.; Li, H. Pt-Enhanced Mesoporous Ti3+/TiO2 with Rapid Bulk to Surface Electron Transfer for Photocatalytic Hydrogen Evolution. *ACS Appl. Mater. Interfaces* **2017**, *9* (20), 16959–16966.